

# How Well Do We Understand the Land-Ocean-Atmosphere Carbon Cycle?

David Crisp<sup>1,1,1</sup>, Han Dolman<sup>2,3,3</sup>, Toste Tanhua<sup>4,4,4</sup>, Galen A McKinley<sup>5,5,5</sup>, Judith Hauck<sup>6,6,6</sup>, Simon Eggleston<sup>7,7,7</sup>, Valentin Aich<sup>7,8,8</sup>, Ana Bastos<sup>9,9</sup>, and Stephen Sitch<sup>10,10</sup>

<sup>1</sup>Jet Propulsion Laboratory, California Institute of Technology

<sup>2</sup>Vrije Universiteit

<sup>3</sup>Royal NIOZ, Texel, Netherlands and Department of Earth Sciences, Vrije Universiteit Amsterdam, Amsterdam, The Netherlands

<sup>4</sup>GEOMAR Helmholtz Centre for Ocean Research

<sup>5</sup>Lamont Doherty Earth Observatory of Columbia University

<sup>6</sup>Alfred Wegener Institute Helmholtz Centre for Polar and Marine Research

<sup>7</sup>World Meteorological Organization

<sup>8</sup>Global Climate Observing System, World Meteorological Organization, Geneva, Switzerland

<sup>9</sup>Max Planck Institute for Biogeochemistry Department Biogeochemical Integration

<sup>10</sup>College of Life and Environmental Sciences

November 30, 2022

## Abstract

Fossil fuel combustion, land use change and other human activities have increased the atmospheric carbon dioxide (CO<sub>2</sub>) abundance by almost 50% since the beginning of the industrial age. These changes would have been much larger if natural sinks in the land biosphere and ocean had not removed over half of this anthropogenic CO<sub>2</sub>. Here, we review the current state of knowledge of the ocean, land and atmospheric carbon cycles, identify emerging measurement and modeling capabilities, and gaps that must be addressed to diagnose the processes driving the carbon cycle and predict their response to human activities and a changing climate. The anthropogenic CO<sub>2</sub> uptake by the ocean has increased over this period, as the atmospheric CO<sub>2</sub> partial pressure (pCO<sub>2</sub>) has increased. For the land carbon cycle, the emerging picture is more complicated. Over the past three decades, the uptake of CO<sub>2</sub> by intact tropical humid forests appears to be declining, but these effects are offset by a net greening across mid- and high-latitudes associated with afforestation, agricultural, and longer growing seasons. These studies have also revealed measurement gaps and other limitations in our understanding of the evolving carbon cycle. They show that continued ship-based observations combined with expanded deployments of autonomous platforms are needed to quantify ocean-atmosphere fluxes on policy relevant spatial and temporal scales. They also reinforce the urgent need for more comprehensive measurements of stocks, fluxes and atmospheric CO<sub>2</sub> in humid tropical forests and across the Arctic and boreal regions, which appear to be experiencing rapid change.

## How Well Do We Understand the Land-Ocean-Atmosphere Carbon Cycle?

David Crisp<sup>1</sup>, Han Dolman<sup>2</sup>, Toste Tanhua<sup>3</sup>, Galen A. McKinley<sup>4</sup>, Judith Hauck<sup>5</sup>, Ana Bastos<sup>6</sup>, Stephen Sitch<sup>7</sup>, Simon Eggleston<sup>8</sup>, Valentin Aich<sup>8</sup>

<sup>1</sup>Jet Propulsion Laboratory, California Institute of Technology, Pasadena, CA, USA.

<sup>2</sup>Royal NIOZ, Texel, Netherlands and Department of Earth Sciences, Vrije Universiteit Amsterdam, Amsterdam, The Netherlands.

<sup>3</sup>GEOMAR Helmholtz Centre for Ocean Research Kiel, Marine Biogeochemistry, Kiel, Germany.

<sup>4</sup>Columbia University and Lamont Doherty Earth Observatory, Palisades, NY, USA.

<sup>5</sup>Alfred-Wegener-Institut, Helmholtz-Zentrum für Polar und Meeresforschung, Bremerhaven, Germany.

<sup>6</sup>Max Planck Institute for Biogeochemistry Department Biogeochemical Integration, Jena, Germany

<sup>7</sup>College of Life and Environmental Sciences, University of Exeter, Exeter, EX4 4RJ, UK.

<sup>8</sup>Global Climate Observing System, World Meteorological Organization, Geneva, Switzerland.

Corresponding author: first and last name (David Crisp davidcri@gmail.com)

### Key Points:

- Anthropogenic CO<sub>2</sub> emissions would have produced larger atmospheric increases if ocean and land sinks had not removed over half of this CO<sub>2</sub>.
- Uptake by both ocean and land sinks increased in response to rising atmospheric CO<sub>2</sub> levels, maintaining the airborne fraction near 45%.
- Improved and sustained measurements and models are needed to track changes in sinks and enhance the scientific basis for carbon management.

## Abstract

Fossil fuel combustion, land use change and other human activities have increased the atmospheric carbon dioxide ( $\text{CO}_2$ ) abundance by about 50% since the beginning of the industrial age. The atmospheric  $\text{CO}_2$  growth rates would have been much larger if natural sinks in the land biosphere and ocean had not removed over half of this anthropogenic  $\text{CO}_2$ . As these  $\text{CO}_2$  emissions grew, uptake by the ocean increased in response to increases in atmospheric  $\text{CO}_2$  partial pressure ( $\text{pCO}_2$ ). On land, gross primary production (GPP) also increased, but the dynamics of other key aspects of the land carbon cycle varied regionally. Over the past three decades,  $\text{CO}_2$  uptake by intact tropical humid forests declined, but these changes are offset by increased uptake across mid- and high-latitudes. While there have been substantial improvements in our ability to study the carbon cycle, measurement and modeling gaps still limit our understanding of the processes driving its evolution. Continued ship-based observations combined with expanded deployments of autonomous platforms are needed to quantify ocean-atmosphere fluxes and interior ocean carbon storage on policy-relevant spatial and temporal scales. There is also an urgent need for more comprehensive measurements of stocks, fluxes and atmospheric  $\text{CO}_2$  in humid tropical forests and across the Arctic and boreal regions, which are experiencing rapid change. Here, we review our understanding of the atmosphere, ocean, and land carbon cycles and their interactions, identify emerging measurement and modeling capabilities and gaps and the need for a sustainable, operational framework to ensure a scientific basis for carbon management.

## Plain Language Summary

Since the beginning of the industrial age in the mid-1700s, fossil fuel combustion, land use change and other human activities have increased the atmospheric carbon dioxide ( $\text{CO}_2$ ) concentration to levels never seen before in human history. The atmospheric  $\text{CO}_2$  growth rate would have been much larger if natural sinks in the ocean and on land carbon cycle had not removed over half of the  $\text{CO}_2$  emitted by human activities. While the uptake of anthropogenic  $\text{CO}_2$  by the ocean has increased with the increasing atmospheric  $\text{CO}_2$  partial pressure, the land biosphere response has varied spatially and with time. Over the industrial age,  $\text{CO}_2$  uptake by intact forests and other natural parts of the land biosphere has roughly balanced emissions from land use change. Since the 1990s, the tropical land sink has diminished while the high latitude land sink has increased. Here, we review our understanding of the natural carbon cycle and the processes controlling its response to human activities and climate change and identify measurement and knowledge gaps.

## 1 Introduction

Since the beginning of the industrial age, human activities have increased the atmospheric concentrations of carbon dioxide ( $\text{CO}_2$ ) and other greenhouse gases (GHGs) to levels never before seen in human history. These large increases are driving climate change because  $\text{CO}_2$  is an efficient greenhouse gas with atmospheric residence times spanning years to millennia (see Box 6.1 of Ciais et al., 2013). Bottom-up statistical inventories indicate that fossil fuel combustion, industry, agriculture, forestry, and other human activities are now adding more than 11.5 petagrams of carbon ( $\text{Pg C}$ ) to the atmosphere each year (Friedlingstein et al., 2019; 2020; 2021). Direct measurements of  $\text{CO}_2$  in the atmosphere and in air bubbles in ice cores (Etheridge et al., 1996) indicate that human activities have increased the globally averaged

atmospheric CO<sub>2</sub> dry air mole fraction from less than 277 parts per million (ppm) in 1750 (e.g., Joos and Spahni, 2008) to more than 412 ppm in 2020 (Dlugokencky et al., 2018; Rubino et al., 2019). Over half of this increase has been added since 1985 and over a quarter has been added since 2000.

These increases would be much larger if natural processes operating in the land and ocean had not removed over half of these anthropogenic CO<sub>2</sub> emissions. Carbon cycle measurements and modeling studies show that these anthropogenic CO<sub>2</sub> emissions are superimposed on an active natural carbon cycle that regulates CO<sub>2</sub> through photosynthesis and respiration on land and in the ocean (Beer et al., 2010), as well as temperature-driven solubility and carbonate chemistry coupled with the ocean circulation (Takahashi et al., 2002; 2009; Sabine et al., 2004; Gruber et al., 2019a). In pre-industrial times, these processes were roughly in balance, with the land biosphere and ocean emitting gross CO<sub>2</sub> fluxes of ~120 and ~90 Pg C yr<sup>-1</sup> into the atmosphere, respectively, then removing a comparable amount. Today, these natural fluxes have comparable amplitudes, but now, CO<sub>2</sub> “sinks” the land biosphere and ocean also remove about half of the anthropogenic CO<sub>2</sub> emissions, reducing the atmospheric CO<sub>2</sub> growth rate and mitigating climate change (Canadell et al., 2007; Raupach et al., 2008; Knorr 2009; Bennedsen et al., 2019, Friedlingstein et al., 2020).

While the fraction of the anthropogenic CO<sub>2</sub> that stays in the atmosphere (the “airborne fraction”) has remained remarkably constant, at about 0.45 for the multi-year average for the past ~60 years (e.g., Ballantyne et al., 2012; Raupach et al., 2008; 2014; Bennedsen et al., 2019), it can change substantially from year to year (Francey et al., 1995; Keeling et al., 1995; Bousquet et al., 2000). In some years, the airborne fraction can be as high as 80%, while in others, it can be as low as 30% (Raupach et al., 2008; 2014). Some of the largest changes in this airborne fraction appear to be associated with changes in uptake of CO<sub>2</sub> by the land biosphere (the land sink) in response to large-scale temperature and precipitation anomalies, like those associated with major El Niño events or large volcanic aerosol injections into the stratosphere (Frölicher et al., 2011; 2013). The ocean sink also responds to El Niño events and large volcanic eruptions (Keeling et al., 2005; Eddebbar et al., 2019; McKinley et al., 2004; 2017; 2020), but has a smaller impact on the amplitude of variability in the airborne fraction. The relative roles of these and other processes reviewed here that link the land, ocean and atmospheric carbon cycles with the climate are less well understood, compromising our ability to predict how the atmospheric CO<sub>2</sub> growth rate might change as the carbon cycle responds to climate change (Ballantyne et al., 2012).

Over the past two decades, our understanding of the natural and anthropogenic contributions to the carbon cycle has grown steadily with the deployment of progressively more sophisticated ground-based, oceanic, airborne, and space-based measurement systems. These advances have been accompanied by the development of far more comprehensive diagnostic and prognostic carbon cycle modeling tools. For the ocean, measurements of vertical gradients in pCO<sub>2</sub> across the air-sea interface provide the best available estimates of ocean-atmosphere carbon fluxes on annual time-scales. Over land, flux towers provide estimates of carbon fluxes on local scales, while high-spatial-resolution space-based observations of solar induced chlorophyll fluorescence (SIF) and atmospheric CO<sub>2</sub> can be analyzed to constrain land carbon fluxes at regional scales and seasonal to interannual time scales (Heimann et al., 1998). On decadal time-scales, the storage of anthropogenic carbon in the interior ocean can be assessed by biogeochemical and tracer observations. On land, in situ carbon-13 ( $\delta^{13}\text{C}$ ) measurements and

estimates of above-ground biomass derived from remote sensing observations provide similar constraints on these time scales.

Both bottom-up stock and flux estimates and “top-down” atmospheric estimates are providing key insights into the carbon cycle. Bottom-up methods use empirical or process-based models to estimate fluxes, or to upscale in situ measurements of the time change of stocks or of direct flux observations of the oceans (e.g., Sabine et al., 2004; Doney et al., 2004; Rödenbeck et al., 2014; 2015; Gruber et al., 2019a; Landschützer, et al., 2013; Long et al., 2013; Hauck et al., 2020; Carroll et al., 2020; Gregor et al., 2019; Watson et al., 2020) or land biosphere (Pan et al., 2011; Sitch et al., 2015; Hubau et al., 2020; Piao et al., 2020a; Jung et al., 2020). “Top-down” models use inverse methods to estimate the surface CO<sub>2</sub> fluxes from the land or ocean needed to match the observed atmospheric or ocean CO<sub>2</sub> concentrations, within their uncertainties, in the presence of the prevailing winds and ocean circulation (e.g., Enting et al., 1995; Mikaloff-Fletcher et al., 2006; Jacobson et al., 2007; Khatiwala et al., 2009; Chevallier et al., 2010; 2019; DeVries, 2014; Crowell et al., 2019; Wu et al., 2018; Nassar et al. 2021).

Both bottom-up and top-down methods benefit from remote sensing as well as in situ data. For example, a bottom-up forest stock inventory might use in situ measurements to estimate the above ground biomass from an ensemble of specific plots and then use remote sensing measurements to upscale those measurements to larger areas. Similarly, a top-down approach might combine in situ and remote sensing observations of atmospheric CO<sub>2</sub> along with models of atmospheric transport to estimate regional-scale fluxes.

In practice, top-down and bottom-up methods are often combined. For example, top-down inverse methods for estimating net biospheric exchange (NBE) often use prior biospheric and fossil flux estimates derived from bottom-up methods (e.g., Crowell et al., 2019; Peiro et al., 2021). They are also often compared to characterize processes or identify sources of uncertainty (Kondo et al., 2020; Bastos et al. 2020). However, some caution is needed when comparing and combining results from top-down and bottom-up methods because these approaches include different processes and often use different definitions of stocks and fluxes (Ciais et al., 2022).

As the world embarks on efforts to monitor and control anthropogenic CO<sub>2</sub> emissions, there is growing evidence that the natural carbon cycle is evolving in response to human activities, severe weather, disturbances and climate change. If these changes affect the efficiency of the land or ocean CO<sub>2</sub> sinks, they could impede or confuse efforts to monitor progress toward emission reduction goals. An improved understanding of both the anthropogenic and natural processes that control the emissions and removals of atmospheric CO<sub>2</sub> by the land biosphere and ocean is critical to our ability to monitor and predict the rate of CO<sub>2</sub> increase in the atmosphere and its impact on the climate.

Anthropogenic processes emitting CO<sub>2</sub> into the atmosphere are now routinely tracked in the annual reports by the Global Carbon Project (e.g., Le Quéré et al., 2007; 2009; 2013; 2014; 2015a,b, 2016; 2018 a,b; Friedlingstein et al., 2019; 2020; 2021) and in more focused reviews by others (e.g., Andrew, 2019; 2020; Hong et al., 2021). Similarly, carbon-climate interactions on long (“slow domain”) and short (“fast domain”) timescales, their representation in state-of-the-art Earth System Models and their implications for climate change are described in J. Hansen et al. (2013) and routinely reviewed in the IPCC reports. See, for example, Chapter 6 of IPCC AR5 (IPCC, 2014; Ciais et al., 2013) and the soon to be released IPCC AR6 reports (IPCC 2021).

Here, we begin with a brief review of the atmospheric carbon cycle, including the anthropogenic drivers. We then focus on the contemporary processes controlling the fluxes of CO<sub>2</sub> between the ocean and land carbon reservoirs and the atmosphere and their implications for the evolution of the ocean and land carbon sinks. We update earlier works (e.g., Ciais et al., 2014; Ballantyne, et al., 2015) by reviewing the mean state and emerging trends in carbon stocks and fluxes revealed by various approaches, including new observing capabilities and analysis techniques. Finally, we summarize critical measurement and modeling gaps that must be addressed to produce an effective system for monitoring the carbon cycle as it continues to respond to human activities and climate change.

## 2 A Note on Units

Because the bottom-up and top-down atmospheric, ocean and land carbon communities focus on different aspects of the carbon cycle, they have developed a diverse array of units to quantify stocks and fluxes of carbon and CO<sub>2</sub>. For example, the land carbon community typically quantifies the mass of stocks and fluxes of carbon, the atmospheric remote sensing community typically measures and reports the column-averaged CO<sub>2</sub> dry air mole fraction, XCO<sub>2</sub>, and the ocean community uses the partial pressure, pCO<sub>2</sub>, fugacity, fCO<sub>2</sub>, and the air-sea carbon flux. For the atmosphere, it is useful to note that one petagram of carbon (1 Pg C) yields 3.66 petagrams of CO<sub>2</sub> and that this is equivalent to a concentration change of ~ 2.124 ppm in the atmospheric CO<sub>2</sub> (e.g., Ballantyne et al., 2012; Friedlingstein et al., 2020). Table 1 summarizes these and other commonly used quantities and units used by the carbon cycle community and describes their relationships.

## 3 The Atmospheric Carbon Cycle

The atmosphere is the smallest, but most rapidly changing component of the global carbon cycle. It also serves as the primary medium for the exchange of carbon between the land biosphere, oceans and fossil reservoirs. The vast majority of the atmospheric carbon is in the form of CO<sub>2</sub>. If we assume a total dry air mass of  $5.1352 \times 10^{18}$  kg (Trenberth and Smith, 2005), a CO<sub>2</sub> dry air mole fraction of 412 ppm, a mean CO<sub>2</sub> molecular weight of 44.01 kg/kmole, and a mean atmospheric molecular weight of 28.97 kg/kmole, the total mass of CO<sub>2</sub> in the atmosphere was ~3214 Pg (~877 Pg C) in 2020. The next largest contributor to the atmospheric carbon reservoir is methane (CH<sub>4</sub>), which is 220 times less abundant. For that reason, the atmospheric section of this carbon cycle review focuses on CO<sub>2</sub>.

The largest net sources of atmospheric CO<sub>2</sub> are fossil fuel combustion, land use change and other human activities, which have added  $700 \pm 75$  Pg C to the atmosphere between 1750 and 2019. Of that,  $41 \pm 11\%$  has remained in the atmosphere (Friedlingstein et al., 2021). Because CO<sub>2</sub> has no significant photochemical sinks in the atmosphere, the remainder has been removed by natural sinks in the land biosphere and oceans. This section reviews our current understanding of the atmospheric carbon cycle, starting with observations, and then summarizing the insights contributed by top-down models and bottom-up inventories.

**Table 1.** Quantities and units commonly used to quantify stocks and fluxes by the atmosphere (white), ocean (blue) and land (yellow) carbon cycle communities.

Quantity	Acronym	Typical units	Description
Carbon dioxide dry air mole fraction	CO <sub>2</sub> or xCO <sub>2</sub>	parts per million by volume (ppm)	Number of CO <sub>2</sub> molecules relative to each million (10 <sup>6</sup> ) molecules of dry air. If CO <sub>2</sub> is assumed to be an ideal gas and its dry air mole fraction is increased by 1 ppm at constant temperature, the CO <sub>2</sub> partial pressure will increase by one micro atmosphere (μatm).
Column-averaged carbon dioxide dry air mole fraction	XCO <sub>2</sub>	ppm	A vertically-averaged quantity used by the atmospheric remote sensing community, derived from the ratio of the CO <sub>2</sub> column abundance and the dry air column abundance. The dry air column abundance is estimated from the measured molecular oxygen (O <sub>2</sub> ) column abundance (assuming an O <sub>2</sub> dry air mole fraction of 0.20955) or from surface pressure and humidity.
partial pressure of carbon dioxide	pCO <sub>2</sub>	μatm	At sea level, $p\text{CO}_2 = (P - p\text{H}_2\text{O}) \times x\text{CO}_2$ , where P is the total atmospheric pressure and pH <sub>2</sub> O is the water vapor saturation vapor pressure (see Woolf et al., 2016). 1 μatm = 10 <sup>-6</sup> atmospheres = 0.10325 Pascals.
Carbon dioxide fugacity	fCO <sub>2</sub>	μatm	Effective partial pressure of CO <sub>2</sub> that has the same temperature and Gibbs free energy as the real gas. At the surface, $f\text{CO}_2 = x\text{CO}_2 \times \phi_{\text{CO}_2}$ , where $\phi_{\text{CO}_2} \approx 0.0002/\text{K}$ is the fugacity coefficient for CO <sub>2</sub> and K is the temperature in Kelvin.
Net Community Production	NCP	mol C m <sup>-2</sup> yr <sup>-1</sup>	The net carbon removed from the atmosphere by the ocean biological pump.
Dissolved Inorganic Carbon	DIC	μmol/kg	Total amount of inorganic carbon in water.
Carbon stock or stock change		petagrams of carbon/year (Pg C yr <sup>-1</sup> )	1 Pg C = 10 <sup>15</sup> g C. 1 Pg C = 10 <sup>12</sup> kg C = 10 <sup>9</sup> tons of carbon = 1 Gt C. When oxidized to form CO <sub>2</sub> , 1 Pg C = 3.664 Pg CO <sub>2</sub> .
Gross Primary Production	GPP	Pg C yr <sup>-1</sup>	Total flux of carbon fixed through photosynthetic reduction of CO <sub>2</sub> by plants in an ecosystem.
Net Primary Production	NPP	Pg C yr <sup>-1</sup>	Net flux of organic carbon produced by plants in an ecosystem. $\text{NPP} = \text{GPP} - R_a$ , where $R_a$ is autotrophic respiration by plants
Net Ecosystem Exchange or Net Ecosystem Production	NEE or NEP	Pg C yr <sup>-1</sup>	$\text{NPP} - R_h$ , where $R_h$ is the carbon loss by heterotrophic (non-plant) respiration. $\text{NEE} = -\text{NEP}$ but these terms are otherwise generally interchangeable, with NEE used more often to refer to fluxes measured in the atmosphere, while NEP is more often used for fluxes inferred from measurements of carbon stock changes.
Net Biospheric (Biome) Exchange	NBE	Pg C yr <sup>-1</sup>	Change in mass of carbon stocks after episodic carbon losses due to natural or anthropogenic disturbance.
Net Biome Productivity	NBP	Pg C yr <sup>-1</sup>	NEP minus disturbance emissions.

### 3.1 Observations of Atmospheric CO<sub>2</sub>

Continuous measurements of atmospheric CO<sub>2</sub> were initiated in 1958 by Charles David Keeling of the Scripps Institution of Oceanography, when he established stations at Mauna Loa, Hawaii and the South Pole. Weekly flask samples and continuous measurements are now being returned by a global network that includes the U.S. National Oceanic and Atmospheric Administration (NOAA) Global Monitoring Laboratory (GML) Global Greenhouse Gas Reference Network (GGGRN) and other stations in their Carbon Cycle Greenhouse Gas (CCGG) Cooperative Global Air Sampling Network, the European Integrated Carbon Observation System (ICOS) network and other partners of the World Meteorological Organization Global Atmospheric Watch (WMO GAW) program (Figure 1).

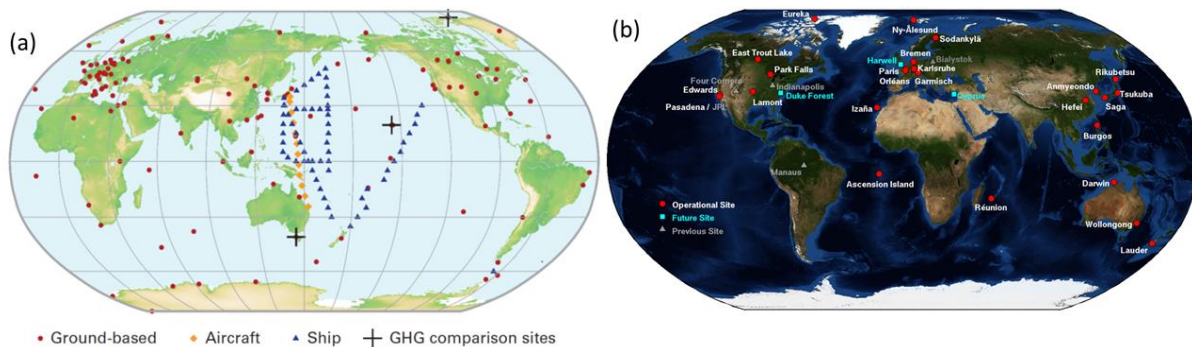


**Figure 1:** Spatial distribution of stations in the ground-based atmospheric CO<sub>2</sub> monitoring network. The vast majority of the stations are in North America and western Europe. (a) In situ CO<sub>2</sub> measurements are collected routinely at the WMO Global Atmospheric Watch Stations (from WMO Greenhouse Gas Bulletin, 25 Nov. 2019). (b) Solar-looking remote sensing observations of CO<sub>2</sub> are collected at Total Carbon Column Observing Network (TCCON) stations.

These in situ measurements provide the most accurate estimates of the CO<sub>2</sub> and CH<sub>4</sub> concentrations and their trends on global scales. The flask samples are also analyzed to quantify non-carbon greenhouse gases including nitrous oxide (N<sub>2</sub>O), halocarbons, sulfur hexafluoride (SF<sub>6</sub>), molecular hydrogen (H<sub>2</sub>) and carbon isotopes including carbon-13 (<sup>13</sup>C) and carbon-14 (<sup>14</sup>C), which help to distinguish fossil fuel from biogenic contributions to the observed CO<sub>2</sub> trends.

More recently, these ground-based in situ networks have been joined by expanding networks of airborne in situ systems and ground-based remote sensing networks. NOAA routinely collects airborne profiles of CO<sub>2</sub> and other GHGs from 17 sites across North America using fixed-wing aircraft (see <https://gml.noaa.gov/dv/data/>). Vertical profiles of CO<sub>2</sub>, CH<sub>4</sub> and other trace gases are also being returned by the balloon-borne AirCore systems (Karion et al., 2010; Baier et al., 2020), which are being deployed from an increasing number of sites. These research observations are now being augmented by GHG sensors deployed in the cargo holds of commercial aircraft as part of Japan's Comprehensive Observation Network for TRace gases by AirLiner (CONTRAIL; Umezawa et al., 2018; Müller et al., 2021; data available at <https://www.cger.nies.go.jp/contrail/protocol.html>) program and Europe's In-service Aircraft for Global Observations (IAGOS; Clark et al., 2021; data available at <https://www.iagos.org/iagos-data/>) program. So far, GHG systems have been deployed on a small number of commercial



aircraft, but that number is expected to grow as the size and operational complexity of the sensor systems is reduced.

The atmospheric CO<sub>2</sub> content can also be monitored remotely by measuring the amount of sunlight that it absorbs as it traverses the atmosphere. The Total Carbon Column Observing Network (TCCON) exploits this approach from 27 stations in 14 countries spanning latitudes between Eureka, Canada (80.05°N) and Lauder, New Zealand (45.038°S; Figure 1b). Each station collects high-resolution spectra that are analyzed to yield estimates of the column-averaged dry air mole fractions of CO<sub>2</sub>, CH<sub>4</sub>, and other trace gases. These estimates are related to the WMO standard through comparisons with in situ measurements collected by over the stations by fixed-wing aircraft and AirCore instruments (Wunch et al., 2011).

One of the most important assets of the ground-based and airborne CO<sub>2</sub> measurement time series is their length, which now extends over 60 years at Mauna Loa and 40 years for the globe (Figure 2). The Mauna Loa measurements show that the atmospheric CO<sub>2</sub> dry air mole fraction has increased by about 100 ppm over this period, from less than 316 ppm in 1959 to more than 416 ppm in 2021. Over this period, the atmospheric growth rate increased from less than 1 ppm yr<sup>-1</sup> in the 1960s to more than 2.5 ppm yr<sup>-1</sup> during the 2010s, driven primarily by steadily increasing fossil fuel emissions (IPCC, 2014; Friedlingstein et al., 2021). In addition to this long-term trend, the growth rate also varies by up to 2 ppm from year to year. Because these variations occur in the context of much more uniformly increasing anthropogenic emissions, they are attributed to interannual changes in the anthropogenic CO<sub>2</sub> airborne fraction and thus the efficiency of the land and ocean CO<sub>2</sub> sinks (Keeling et al., 1989; 1995; Francey et al., 1995).

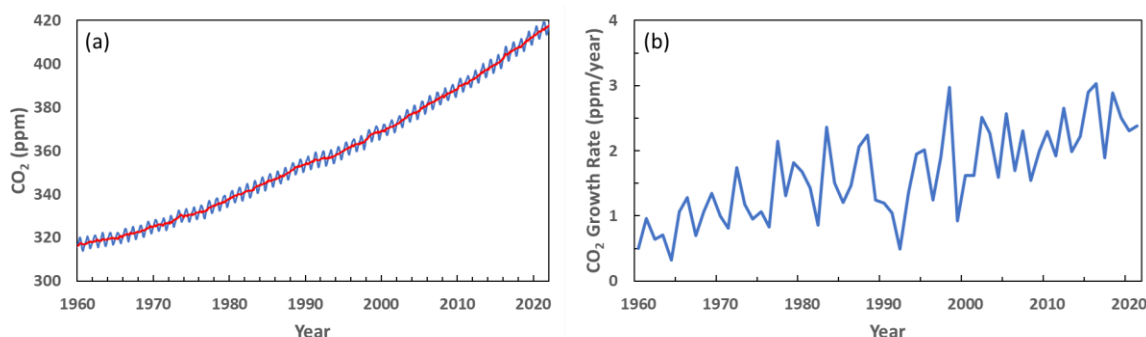


**Figure 2:** (a) Monthly mean CO<sub>2</sub> dry air mole fraction at Mauna Loa Observatory from 1960 to 2022 (blue line) and long-term trend (red line). (b) Annual growth rate in atmospheric CO<sub>2</sub> at Mauna Loa Observatory (data from NOAA GML, <https://gml.noaa.gov/ccgg/trends/data.html>).

During the first 30 years of this atmospheric CO<sub>2</sub> record, while there were still fewer than 10 stations regularly reporting data, innovative methods were already beginning to yield additional insights into the behavior of the land and ocean sinks. For example, Keeling et al. (1973; 1989; 1995) combined measurements of the atmospheric CO<sub>2</sub> growth rates from Mauna Loa and South Pole with <sup>13</sup>C/<sup>12</sup>C ratios ( $\delta^{13}\text{C}$ ) to assess the relative contributions to this variability from the land biosphere and ocean sinks. They found that the CO<sub>2</sub> growth rate anomalies were well correlated with atmospheric temperature increases during the warm phase of El Niño and decreases following the Pinatubo eruption. Their isotopic analysis suggested that

El Niño typically enhanced the efficiency of the ocean sink and decreased the uptake by the land sink. These early conclusions have been reinforced by more recent measurements and modeling studies (e.g., Bousquet et al., 2000; Canadell et al., 2007; Raupach et al., 2008; Bennedsen et al., 2019).

In addition to the global-scale perspectives, the ground-based record has provided new insights into regional-scale phenomena. For example, they not only provided the first evidence for the now well-known atmospheric CO<sub>2</sub> seasonal cycle (Keeling, 1960), they also provided the first evidence for long-term changes in the CO<sub>2</sub> seasonal cycle amplitude (SCA) across the northern hemisphere (Bacastow et al., 1985; Keeling et al., 1996). These results have also been reinforced by more recent experiments that exploit an expanded ground-based network and longer CO<sub>2</sub> data record (Graven et al., 2013; Byrne et al., 2018; 2020a; Liu et al., 2020a).

Recent advances in space-based remote sensing technologies are now providing new opportunities to dramatically improve the spatial and temporal coverage and resolution of atmospheric CO<sub>2</sub> observations. These space-based sensors collect high-resolution spectra of reflected sunlight within molecular oxygen (O<sub>2</sub>) and CO<sub>2</sub> bands that can be analyzed to yield precise, spatially resolved estimates of XCO<sub>2</sub>. The first space-based sensor to use this approach was the German-Dutch-Belgian SCanning Imaging Absorption spectroMeter for Atmospheric Cartography (SCIAMACHY) onboard the European Space Agency (ESA) Environmental Satellite (ENVISAT), which operated from 2002 to 2012. ENVISAT/SCIAMACHY was followed by Japan's Greenhouse gases Observing SATellite, GOSAT in 2009 (Kuze et al., 2009; 2016; Yoshida et al., 2011; ), and then by NASA's Orbiting Carbon Observatory-2 (OCO-2) in 2014 (Crisp et al., 2004; 2008, Eldering et al., 2017). OCO-2 returns about three million XCO<sub>2</sub> estimates over the sunlit hemisphere each month (Figure 3) with single sounding random errors of ~0.5 ppm and accuracies of ~1 ppm (Wunch et al., 2017; O'Dell et al., 2018; Müller et al., 2021). GOSAT and OCO-2 have recently been joined by their sister missions, GOSAT-2 (2018) and OCO-3 (2019), providing additional coverage and resolution.

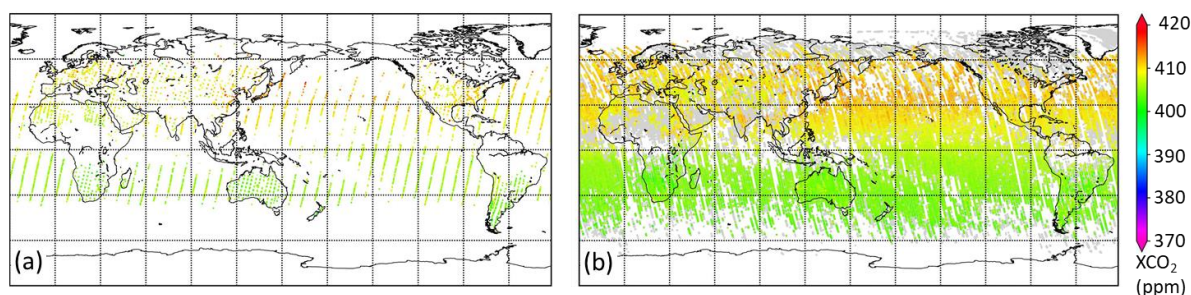


**Figure 3.** Monthly maps of XCO<sub>2</sub> estimates derived from (a) GOSAT and (b) OCO-2 measurements for April 2018. OCO-2 collects ~100 times as many samples each day as GOSAT, providing much greater data density. For both satellite products, the coverage at high latitudes varies with the availability of sunlight. Persistent optically-thick clouds and airborne dust (Sahara) limit the coverage (Images from the World Data Center for Greenhouse Gases, <https://gaw.kishou.go.jp/satellite/file/0149-9011-1001-08-08-9999> ).

These data are now providing a record of the atmospheric CO<sub>2</sub> distribution with unprecedented detail, revealing trends in atmospheric CO<sub>2</sub> concentrations that are providing new insights into atmospheric sources and sinks. For example, each month, XCO<sub>2</sub> estimates derived

from OCO-2 observations using the Atmospheric CO<sub>2</sub> Observations from Space (ACOS) algorithm (O'Dell et al., 2018) provide a global maps of CO<sub>2</sub>, reflecting the net effects of emissions, removals, and atmospheric transport. These maps provide snapshots of most robust features of the atmospheric carbon cycle. For example, during the early northern hemisphere (NH) spring, they reveal the relatively large (> 10 ppm) north-south gradient in XCO<sub>2</sub>, driven by the CO<sub>2</sub> buildup across the NH during the winter, when photosynthetic uptake by the land biosphere is suppressed. The maps also indicate enhanced values over east Asia that might be associated with intense fossil fuel combustion.

While CO<sub>2</sub> time series and XCO<sub>2</sub> maps provide some direct insight into the sources and sinks of atmospheric CO<sub>2</sub>, methods that account for atmospheric transport are needed to quantify CO<sub>2</sub> fluxes on sub-regional to continental scales. Atmospheric inverse systems address this need. Inverse systems designed to constrain fluxes on these scales typically incorporate a global chemical transport model that assimilates estimates of the atmospheric CO<sub>2</sub> dry air mole fraction with an optimization algorithm that derives estimates of the net surface CO<sub>2</sub> fluxes needed to match the observed CO<sub>2</sub> distribution to within its uncertainties in the presence of the imposed wind field (Enting et al., 1995; Bousquet et al., 2000; Enting 2002, Peters et al., 2005; Baker et al., 2006a). Studies of anthropogenic emissions from point sources or large urban areas typically employ simpler emission plume mass balance models (Nassar et al., 2017; 2021; Varon et al., 2018; Reuter et al., 2019) although some use more sophisticated inverse models with Eulerian (Ye et al., 2020; Lei et al., 2021) or Lagrangian transport schemes (Wu et al., 2018). Both types of systems are summarized here.

### 3.2 *Constraining CO<sub>2</sub> fluxes with Regional-scale Atmospheric Inverse Models*

Most inverse modeling systems use a form of Bayesian inference that adjusts surface fluxes to minimize a cost function, a mathematical expression that describes the mismatch between the observations and the simulated observations based on prior estimates of surface fluxes, accounting for their respective uncertainties (e.g., Enting, 2002). Commonly-used inverse methods include variational data assimilation (3-D and 4-D VAR), ensemble Kalman filter, and the Markov Chain Monte Carlo methods. These systems are typically initialized with “prior” CO<sub>2</sub> concentration and flux distributions derived from bottom-up inventories, climatologies and biogeochemical models. Most inverse modeling systems use precomputed (off-line) atmospheric winds fields from a meteorological reanalysis in a global, 3-dimensional chemical tracer transport models, such as the Goddard Earth Observing System (GEOS) Chemistry (GEOS-Chem) or Tracer Model 5 (TM5) (e.g., Crowell et al., 2019; Peiro et al., 2022).

#### 3.2.1 *Constraining Regional-scale CO<sub>2</sub> Sources and Sinks with Atmospheric Inverse Systems*

Historically, top-down estimates of CO<sub>2</sub> fluxes from atmospheric inverse systems have relied on *in situ* measurements collected by the surface network (Figure 1). To exploit this sparse network, CO<sub>2</sub> fluxes were derived for a small number of pre-defined continental and oceanic regions and anthropogenic emissions were prescribed from bottom-up inventories to diagnose the behavior of the ocean and land carbon cycles. For example, in early forward model studies, Tans et al. (1990) found that the observed pole-to-pole gradient in atmospheric CO<sub>2</sub> indicated the presence of a large land sink in the northern extratropics, a result that was confirmed by other studies (e.g., Ciais et al., 1995). Others used inverse models to study the variability of the airborne fraction and concluded that terrestrial carbon fluxes were roughly twice as variable as ocean fluxes during the 1980s and 1990s, and that tropical land ecosystems contributed the most

to this variability (Bousquet et al., 2000; Rödenbeck et al., 2003; Peylin et al., 2005). However, there was significant disagreement in the relative contributions by the different ocean basins or the land sinks in North America and Asia (e.g., Fan et al., 1998; King et al., 2015). These differences were ascribed primarily to limitations in the observing network, the transport models adopted and other differences in the inversion methods.

To make progress the latter two areas, large multi-model intercomparison projects, such as the Atmospheric Carbon Cycle Inversion Intercomparison (TransCom 3; Gurney et al., 2002; 2003) and REgional Carbon Cycle Assessment and Processes (RECCAP) projects (Canadell et al., 2011; Peylin et al., 2013) were launched. Early results from these projects confirmed that model transport uncertainties were as large a source of error as the sampling uncertainties introduced by the sparse CO<sub>2</sub> measurement network (Gurney et al., 2002; 2003) and that transport errors had their largest impacts on northern latitudes (Baker et al., 2006b). More recent multi-model intercomparison experiments constrained by in situ observations, alone, show significant reductions in the spread of the model estimates when compared to independent observations (Gaubert et al., 2019; Ciais et al., 2020a). However, these inverse model experiments still do not have the spatial resolution needed to separately quantify natural and anthropogenic emissions on regional scales or to constrain the relative contributions of the global ocean and land sinks to better than  $\sim 1 \text{ Pg C yr}^{-1}$  (Jacobson et al., 2007; Chevallier et al., 2010; Sarmiento et al., 2010; Tohjima et al., 2019; Kondo et al., 2020; Friedlingstein et al., 2021).

With their improved spatial resolution and temporal coverage, atmospheric XCO<sub>2</sub> estimates derived from space-based observations are now providing new opportunities to study CO<sub>2</sub> emissions and uptake at policy-relevant spatial and temporal scales (e.g., Zhang et al., 2021; Chevallier, 2021). CO<sub>2</sub> estimates retrieved from GOSAT and OCO-2 measurements clearly show persistent positive anomalies associated with anthropogenic emissions over East Asia, Western Europe and eastern North America (Hakkarainen et al., 2016; 2019; Wang et al., 2018). They also show persistent positive anomalies over northern tropical Africa and northern tropical South America.

When these space-based XCO<sub>2</sub> estimates are analyzed with flux inversion models (e.g., Maksyutov et al., 2013; Chevallier et al., 2019; Crowell, et al., 2019; Peiro et al., 2022), they produce annual-averaged fluxes at sub-regional scales that reinforce and sometimes conflict with those derived from bottom-up methods or inverse modeling methods constrained by in situ CO<sub>2</sub> measurements, alone. For example, there is generally good agreement between the NBE estimates for northern hemisphere extratropical land derived using inverse methods constrained in situ and OCO-2 v9 XCO<sub>2</sub> estimates (Peiro et al., 2022; Zhang et al., 2021). However, both in situ and space-based inverse modeling results indicate a substantially larger summertime seasonal drawdown than the prior, which was constrained by bottom-up results from dynamic global vegetation models (DGVMs). Over tropical land, NBE estimates from ensembles of inverse models constrained by space-based measurements are both more positive and have a smaller spread across the ensemble than those constrained only by in situ measurements from the sparse tropical network or ensembles of DGVMs (Palmer et al., 2019; Crowell, et al., 2019; Peiro et al., 2022). These differences are explored in greater detail in Section 5.

Over the ocean, results from atmospheric inversions constrained by in situ and space-based observations are less conclusive. For example, Chevallier et al. (2019) find that inversions constrained by ACOS/GOSAT XCO<sub>2</sub> estimates reduce the ocean sink by  $\sim 0.5 \text{ Pg C yr}^{-1}$  in 2015, relative to a prior constrained by ocean pCO<sub>2</sub> estimates (Landschützer et al., 2017), a result that

is consistent with the onset of the strong 2015-2016 El Niño. However, when ACOS/OCO-2 version 9 (v9) XCO<sub>2</sub> ocean glint estimates are used to constrain inverse models, a known ~1 ppm negative bias in this product, produces an unrealistically large (3.75 Pg C yr<sup>-1</sup>) ocean sink during that period (Peiro et al., 2022), while methods constrained by ocean pCO<sub>2</sub> indicate an ocean sink between 2 and 3 Pg C yr<sup>-1</sup> during the 2010s' (Friedlingstein et al., 2019; 2020; 2021). Because of this, the OCO-2 v9 ocean glint observations have been excluded from most inverse model studies. This ocean glint bias was reduced by over 90% in the v10 ACOS/OCO-2 XCO<sub>2</sub> product (Müller et al., 2021), but there is still little evidence that space-based XCO<sub>2</sub> estimates can provide useful constraints on the ocean sink.

Atmospheric inverse models are also being used to constrain anthropogenic CO<sub>2</sub> emissions and removals (Chevallier, 2021; Deng et al., 2021; Hwang et al., 2021; Petrescu et al., 2021). On regional scales, estimates of CO<sub>2</sub> emissions and removals derived from atmospheric measurements of XCO<sub>2</sub> are not as source specific as the traditional bottom-up statistical methods used to compile national inventories, which infer CO<sub>2</sub> emissions from fuel use (e.g., Andrew 2020), land use change (e.g., Houghton and Nassikas, 2017) and other human activities. However, they complement those methods by providing an integral constraint on the total amount of CO<sub>2</sub> added to or removed from the atmosphere by all natural and anthropogenic processes. They can also be used to identify and track rapidly-evolving emission hotspots that are often missed in the bottom-up statistical inventories. As these tools are integrated into a more comprehensive carbon management system, they could also help carbon managers to assess the effectiveness of their carbon management strategies, and help to identify emerging emission reduction opportunities.

The current ground-based, airborne and space-based CO<sub>2</sub> measurement and modeling capabilities do not yet provide the resolution and coverage needed to estimate net emissions for all countries. In addition, ongoing concerns about the accuracy of the space-based estimates also compromise the reliability of these top-down products as an independent Monitoring and Verification System (MVS) for evaluating national inventory reports (Janssens-Maenhout et al., 2020). The current atmospheric CO<sub>2</sub> measurements and inverse modeling systems are not adequate to clearly distinguish the contributions of fossil fuel sources from land and ocean sources and sinks of CO<sub>2</sub> on regional scales (Ciais et al., 2020b; Chevallier, 2021).

However, atmospheric inverse systems are improving rapidly. Existing systems clearly illustrate many of the strengths and weaknesses of top-down methods for inventory development and assessment. To demonstrate these capabilities, pilot, national-scale flux inversion efforts focus on the largest countries. Most of these studies prescribe fossil fuel CO<sub>2</sub> emissions from a bottom-up emissions inventory and hold these as fixed, and then optimize the terrestrial and ocean carbon fluxes to match the spatial and temporal fluctuations in the observations within their uncertainties (e.g., Chevallier, 2021; Deng et al., 2021). Ongoing efforts to expand the ground-based and space-based atmospheric measurement and inverse modeling capabilities are expected to mitigate this limitation to some extent through the use of proxies, such as nitrogen dioxide (NO<sub>2</sub>), carbon monoxide (CO), and <sup>14</sup>C to distinguish fossil fuel emissions from biomass burning (e.g., Heymann et al., 2017; Reuter et al., 2019; Hakkarainen et al., 2021). Others are combining CO<sub>2</sub> observations with observations of carbonyl sulfide, OCS (Remaud et al., 2022) or SIF (Liu et al., 2017; Palmer et al. 2019; Yin et al., 2020) to discriminate the relative roles of photosynthesis and respiration.

### 3.2.2 *Constraining Atmospheric CO<sub>2</sub> emissions from Local Sources*

On smaller scales, space-based XCO<sub>2</sub> estimates are being combined with ground-based and airborne measurements to quantify CO<sub>2</sub> emissions from large urban areas (Hedelius et al., 2018; Wu et al., 2018; Wu et al., 2020) and individual power plants (e.g., Nassar et al., 2017; 2021; Reuter et al., 2019; Hakkarainen et al., 2021). Space-based sensors do not yet have the coverage needed to track all local sources, but they do provide opportunities to assess the precision that could be delivered by future space-based instruments. For example, Nassar et al. (2017; 2021) used OCO-2 XCO<sub>2</sub> estimates to quantify emissions from individual coal-fired power plants (Figure 4). They combine these estimates with wind speed and direction from ERA-5 (Hersbach et al., 2020) and MERRA-2 (Molod et al., 2015) in a simple Gaussian plume model to estimate the fluxes. They find emission rates of about 98 kilotons per day (kT day<sup>-1</sup>), which compare well with the reported value on that day of 103 kT day<sup>-1</sup>. OCO-2 XCO<sub>2</sub> observations are also being combined with NO<sub>2</sub> observations from the Copernicus Sentinel 5 Precursor TROPOMI instrument to track and quantify CO<sub>2</sub> emission plumes tens of km downwind of large powerplants (Reuter et al., 2019; Hakkarainen et al., 2021).

Other studies have focused on top-down estimates of emissions from large urban areas, which are responsible for ~70% of all anthropogenic CO<sub>2</sub> emissions. For example, Hedelius et al. (2018) estimate the net CO<sub>2</sub>, CH<sub>4</sub>, and CO flux from the Los Angeles South Coast Air Basin (So-CAB) using an inversion system that couples TCCON and OCO-2 observations with the Hybrid Single Particle Lagrangian Integrated Trajectory (HYSPLIT) model and the Open-source Data Inventory for Anthropogenic CO<sub>2</sub> (ODIAC). TCCON XCO<sub>2</sub> measurements indicate that the net CO<sub>2</sub> flux from the So-CAB is  $104 \pm 26$  megaton of CO<sub>2</sub> per year (MtCO<sub>2</sub> yr<sup>-1</sup>) for the study period of July 2013–August 2016. A slightly higher estimate of  $120 \pm 30$  MtCO<sub>2</sub> yr<sup>-1</sup> is obtained using OCO-2 data. These CO<sub>2</sub> emission estimates are slightly lower than those from previous work. In another study, Wu et al. (2020) analyzed OCO-2 XCO<sub>2</sub> data with an advanced version of the Stochastic Time-Inverted Lagrangian Transport model, XSTILT, to quantify per capita CO<sub>2</sub> emissions from 20 major urban areas. In general, they find that cities with greater population density have lower per capita emissions, which is consistent with earlier bottom-up estimates. However, they find that cities with heavy power industries or greater affluence stand out with higher per capita emissions. These studies suggest that space-based measurements could eventually play a significant role in emissions monitoring efforts.



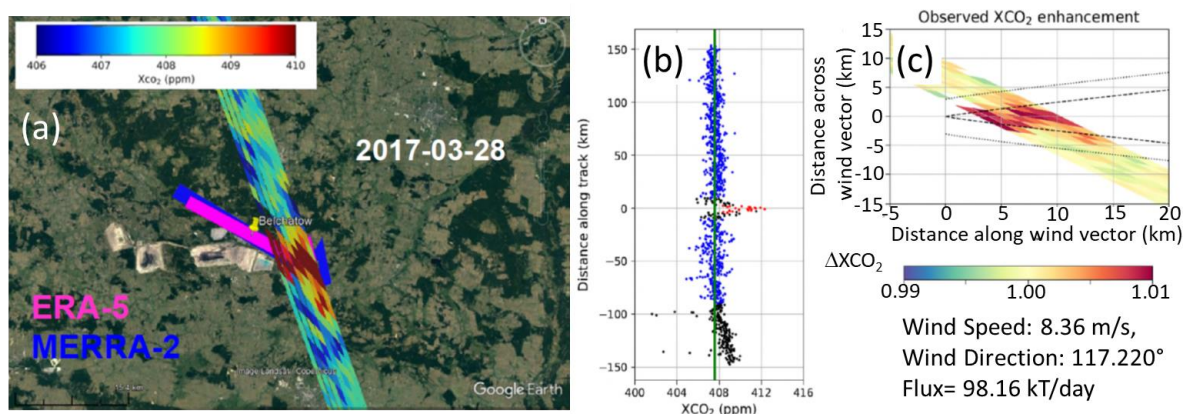


**Figure 4.** (a) OCO-2 flight track over the Bełchatów power station (Poland) on 28 March 2017, showing enhanced XCO<sub>2</sub> (red) downwind of the station. (b) XCO<sub>2</sub> values along ground track, showing a ~4 ppm enhancement downwind. (c) Gaussian plume model used to estimate the fluxes (adapted from Nassar et al., 2021).

The principal challenge of the space-based measurements is the need for unprecedented levels of precision and accuracy. While intense local sources, such as large coal-fired power plants or large urban areas can increase the near-surface CO<sub>2</sub> concentrations by more than 10%, these variations decay rapidly with altitude, such that they rarely yield XCO<sub>2</sub> variations larger than 1-2 ppm (0.25 to 0.5%) on the spatial scale of a satellite footprint (1 to 100 km<sup>2</sup>). Natural sinks of CO<sub>2</sub>, such as forests or ocean basins, are characterized by weak, spatially extensive, local fluxes and thus produce even smaller changes in XCO<sub>2</sub>, which place much greater demands on measurement precision and accuracy.

To ensure that these space-based XCO<sub>2</sub> estimates meet these demanding requirements, they are routinely validated through comparisons with co-incident, ground-based remote sensing estimates of XCO<sub>2</sub> derived from TCCON observations, which provide a transfer standard to the WMO in situ standard (Wunch et al., 2011; 2017). Using this approach, the current state of the art for space-based XCO<sub>2</sub> estimates is single-sounding random errors and biases between 0.5 and 1 ppm (Hedelius et al., 2017; O'Dell et al., 2018; Kiel et al., 2019; Müller et al., 2021). This is adequate to track regional scale changes in surface sources and sinks as small as those produced by the COVID-19 lockdowns (Weir et al., 2021), but not yet adequate to constrain relative roles of the ocean and land biospheric sinks to much better than 1 Pg C yr<sup>-1</sup>.

These new measurement capabilities are also driving the development of atmospheric inverse systems, spawning a new series of multi-model intercomparison experiments that use only ground-based and airborne in situ observations, space-based measurements, or both (Houweling et al., 2015; Chevallier et al., 2019; Crowell et al., 2019; Kondo et al., 2020; Ciais et al., 2020a; 2022; Peiro et al., 2022). These experiments are providing new insights into the relative roles of CO<sub>2</sub> measurement accuracy, atmospheric transport (Schuh et al., 2019; Gaubert et al., 2019; Torres et al., 2019) and other aspects of the model setup (Peiro et al., 2022). These efforts are expected to improve both the spatial resolution and accuracy of these methods and to help reconcile their results with bottom-up methods (Kondo et al., 2020; Ciais et al., 2022).

### 3.3 *Bottom-up Estimates of Anthropogenic Contributions to the Atmospheric Carbon Cycle*

CO<sub>2</sub> emissions from fossil fuel combustion in the energy sector constitute the largest direct anthropogenic contribution to the global carbon cycle (Andrew, 2020; Friedlingstein et al., 2021). Emissions of CO<sub>2</sub> and other GHGs from land use and land use change (LUC) on managed lands are the second largest contribution, accounting for almost one quarter of all anthropogenic GHG emissions (Houghton, 2003; Smith et al., 2014; Houghton and Nassikas, 2017). These emissions originate primarily from deforestation and forest degradation, but also include contributions from agricultural land, livestock, forest management, and secondary forest regrowth. This section summarizes the approaches used to track the emissions and removals of CO<sub>2</sub> by these and other human activities and quantifies their current values and uncertainties.

#### 3.3.1 *Anthropogenic CO<sub>2</sub> emissions inventories for regulation and commerce*

Atmospheric GHG emissions from fossil fuel use (Andrew, 2020) and cement production (Andrew, 2019) are currently being tracked by the regulatory, commercial and scientific communities. National regulatory organizations such as the U.S. Environmental Protection Agency (EPA), Japan's Ministry of the Environment (MOE) and the European Union's European Environment Agency (EEA) compile statistics for regulating and reporting national emissions to other government agencies or organizations such as the United Nations Framework Convention on Climate Change (UNFCCC). These inventories are compiled using best practices recommended in the Intergovernmental Panel on Climate Change (IPCC 2006; 2019) Guidelines for National Greenhouse Gas Inventories, which require reports of annual emissions by sources and removals by sinks in specific sectors and categories. For example, fossil fuel combustion is tracked in the energy sector while those from managed lands are tracked in the agriculture, forestry and other land use (AFOLU) sector. Net emissions and removals in each category of each sector are approximated either by multiplying the measured *activity data* (i.e., number of liters of oil burned) by an assumed *emission factor* (number of kilograms CO<sub>2</sub> emitted per liter of oil) or by sampling carbon stock changes directly, and summing the results to yield totals.

Additional information about GHG emissions associated with the extraction, transport and use of fossil fuels is compiled by several organizations. For example, the International Energy Agency (IEA) originally compiled fossil fuel statistics to avoid disruptions in the world's oil supplies, but now provides annual reports on a range of technologies to support sustainable energy development (IEA 2020). Commercial organizations, such as British Petroleum, produce inventories to track trends in energy markets (BP 2020). Those from national organizations, such as the U.S. Energy Information Administration (EIA), serve a similar purpose, tracking short-term and long-term trends in supply and demand globally to support the energy industry.

Similarly, to track emissions from LUC, international organizations such as the United Nations Food and Agriculture Organization (FAO) collect and disseminate global information on AFOLU. Several methods are used to track fluxes from LUC. For example, statistical data on land cover area collected by FAO are used in so-called bookkeeping models that prescribe carbon changes in biomass and soil pools over time and their resulting fluxes to the atmosphere (Hansis et al., 2015, Houghton and Nassikas, 2017). For tracking historical LUC, a map of historical land use is required such as LUH2-GCB2020 (Hurtt et al., 2020; see also Friedlingstein et al., 2020; Chini et al., 2021). Using this information, it is also possible to estimate fluxes from land-use change using the new generation of dynamic global vegetation models (DGVMs). Another approach uses satellite remote sensing data to determine the amount of land cover change (LCC) and to associate emission losses with LCC by applying emission factors or



detailed biogeochemical models, e.g., emissions from fires associated with deforestation and forest degradation (van der Werf et al., 2017). Finally, at the national level, LCC emissions are compiled and delivered to the UNFCCC by country level organizations such as the U.S. EPA, Japan's MOE and the European Union's EEA. These LCC estimates often differ from those derived by the carbon cycle community because they include different processes and quantities (Grassi et al., 2018; Ciais et al., 2022; Chevallier 2021).

### 3.3.2 Inventories of anthropogenic CO<sub>2</sub> supporting carbon cycle research

Scientific inventories, such as those compiled by the Carbon Dioxide Information Analysis Center (CDIAC; Boden et al., 2017) and the annual reports compiled by the Global Carbon Project (GCP), combine information from all of these sources to support scientific investigations and modeling of the energy and carbon cycles as well as other applications. The science community has also produced high resolution gridded inventories such as the Emissions Database for Global Atmospheric Research, EDGAR (Janssens-Maehout et al., 2019), Open-source Data Inventory for Anthropogenic CO<sub>2</sub>, ODIAC (Oda et al., 2018), and Hestia (Gurney et al., 2019). These inventories use other data (population, night lights, etc.) to disaggregate national-scale emissions from fossil fuel combustion, industry, LUC and other processes to support carbon cycle investigations on spatial scales spanning individual urban areas to countries. These gridded inventories also provide more actionable information on anthropogenic CO<sub>2</sub> emissions for policy makers working on urban to sub-national scales.

One limitation of these inventories is that there is typically a year or more lag in their availability. Motivated by reports of large reductions in fossil fuel use during the initial COVID-19 lockdowns in 2020, several groups began investigating the feasibility and utility of near-real-time (NRT) emission inventories based on proxy data. Le Quéré et al. (2020) derived daily, national estimates of emission changes based on a three-level Confinement Index that was based on historical relationships between confinement and activity data from six categories of the energy sector (power, industry, surface transport, public, and residential). They report that daily global CO<sub>2</sub> emissions decreased by 17% by early April 2020, compared to 2019 values. Liu et al. (2020b) created the near-real-time Carbon Monitor (<https://carbonmonitor.org/>) inventory by combining data from a variety sources including hourly datasets of electrical power use from 31 countries, daily vehicle traffic data from 416 cities, daily global passenger aircraft flights, and other sources. They found emission reductions similar to those reported Le Quéré et al., but with somewhat larger variability. These NRT inventories are not as complete or accurate as the more conventional scientific inventories, but are useful for tracking rapid changes in emissions associated with energy use.

The Global Carbon Project compiles the Global Carbon Budget (GCB) annually (LeQuéré et al., 2009; 2013; 2014; 2015a,b; 2016; 2018a,b; Friedlingstein et al., 2019; 2020; 2021) These papers document global imbalance budgets of anthropogenic carbon fluxes for five key components: atmosphere, fossil fuel emissions, LUC, uptake by the terrestrial biosphere ("land sink") and uptake by the ocean ("ocean sink"). The net land carbon balance represents the difference between the fluxes from land-use change (i.e., deforestation, degradation, secondary forest regrowth, forestry and crop management) and the natural land carbon sink. Decadal mean emissions from fossil fuel use and cement production increased from  $7.7 \pm 0.4$  Pg C yr<sup>-1</sup> in 2000-2010 to  $9.5$  Pg C yr<sup>-1</sup> for 2011-2020 with a peak of  $9.9 \pm 0.5$  Pg C yr<sup>-1</sup> in 2019. Over this same period, land use change emissions increased from  $1.4 \pm 0.7$  Pg C yr<sup>-1</sup> to  $1.6 \pm 0.7$  Pg C yr<sup>-1</sup>.

In 2020, fossil fuel emissions decreased to  $9.5 \pm 0.5 \text{ Pg C yr}^{-1}$  due to lockdowns and other measures adopted in response to the COVID-19 pandemic, but are projected to rebound to values around those from 2019 in 2021 (Friedlingstein et al., 2021). LUC emissions decreased slightly from  $1.2 \pm 0.7 \text{ Pg C yr}^{-1}$  in the decade, 2000-2010, to  $1.1 \pm 0.7 \text{ Pg C yr}^{-1}$  in the decade, 2011-2020. The ocean and land sinks increased during the same time from 2.2 to  $2.8 \pm 0.4 \text{ Pg C yr}^{-1}$  and 2.6 to  $3.1 \text{ Pg C yr}^{-1}$  respectively (Friedlingstein et al., 2021). The anthropogenic land and ocean sinks are defined as their responses to the direct effects of increasing atmospheric  $\text{CO}_2$  and indirect effects associated with climate change.

### 3.3.3 Tracking Uncertainties in Anthropogenic $\text{CO}_2$ Inventories

In addition to these flux estimates, the GCBs document uncertainties, expressed as one standard deviation around the mean. Figure 5 shows the relative error of these estimates (uncertainty/mean) as they progress through the years for the 2008–2019 budgets. The estimates refer to each individual year for which the budget was prepared. As such, they indicate the progression in understanding of the uncertainties in the budget at that time (as opposed to an *a posteriori* analysis of the uncertainties of all years in a similar manner).

The relatively low, stable uncertainties associated with both the fossil fuel emissions and atmospheric  $\text{CO}_2$  concentrations result from two factors (Ballantyne et al., 2012). The first is the precision of the atmospheric in situ  $\text{CO}_2$  measurements and efficient mixing of  $\text{CO}_2$  throughout the atmosphere, although analytical errors and sampling bias do play a role. Second, while fossil fuel combustion is the primary source of anthropogenic  $\text{CO}_2$  emissions, the relative error on this contribution is small ( $\sim 11\%$ , e.g., Quilcaille et al., 2018) because the fossil fuel industry provides reliable numbers on their sales, which are well correlated with the amount of fossil fuel burned. The largest relative errors are associated with LUC emissions. Compared to the early period, 2000-2010, the relative error for this component has not substantially decreased, nor has the mean value substantially changed.

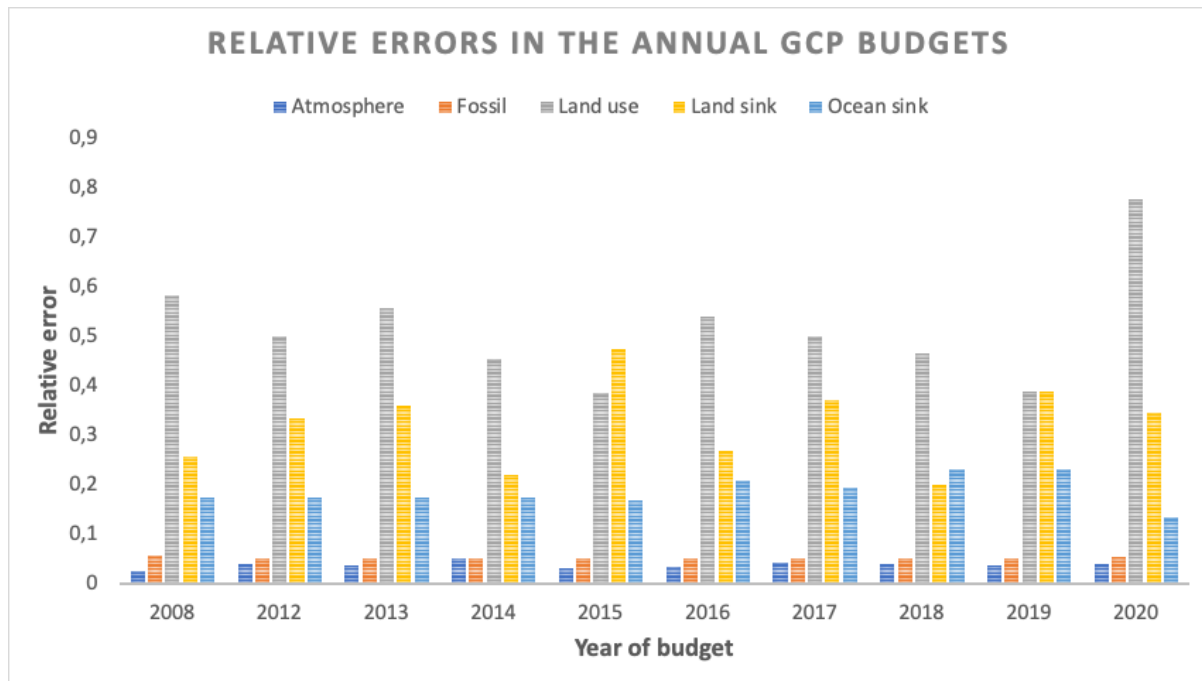


**Figure 5.** Relative error (1 standard deviation uncertainty / mean) for the Global Carbon Budget estimates since 2000. Numbers are taken for the individual year(s) reported each year from Canadell et al. (2007), LeQuéré et al. (2009) and LeQuéré et al. (2013-2018) and Friedlingstein et al. (2019-2021) and refer to the annual estimates.

In the 2015 GCB (LeQuéré et al., 2016) and before, the land sink was calculated as a residual, as described in Eq. 1:

$$\text{land sink} = \text{emissions (fossil fuel and LUC)} - \text{atmospheric growth rate} - \text{ocean sink} \quad (1)$$

Since 2017 (year 2016), the GCB has estimated LUC directly from bookkeeping models (Hansis et al., 2015; Gasser et al., 2020; Houghton and Nassikas, 2017). Uncertainties in these estimates are derived from the spread of these models and that of an ensemble of DGVMs (Friedlingstein et al., 2021).

At the same time, a normalization of the ocean sink estimate from models to a data-based estimate from the 1990s (Denman et al., 2007) was also discontinued. This normalization had previously been applied to ensure that the land sink estimate from the budget residual had a realistic mean value. This change in methodology led to a smaller mean 1990s ocean sink, and thus slightly increased the estimate of the relative uncertainty from 17% in 2015 to 19% in 2016. The ocean sink uncertainty had also varied between 17 and 19% for the years 2006 to 2015. In Friedlingstein et al., (2021), the ocean sink is derived from models and observation-based products and the uncertainty was re-assessed based on a combination of ensemble standard deviation and propagation of known uncertainties in the calculations.

With the advent of a direct estimate of the land sink from DGVMs, the GCP can now assess the degree to which the overall global carbon budget can be closed, i.e., the difference between the sum of the fluxes and the atmospheric accumulation. A budget imbalance represents a measure of our imperfect understanding of the carbon cycle and uncertainty in related measurements. Over decadal scales, the budget imbalance is close to zero, but with substantial interannual to semi-decadal variability, possibly relating to the response of natural sinks to climate variability. The budget imbalance was estimated at -0.3 Pg C for the decade 2011-2020, or approximately 10% of the magnitude of the land and ocean sinks (Friedlingstein et al., 2019, 2020; 2021). This budget imbalance and its associated uncertainties illustrates the limitations to our understanding of global annual mean fluxes at the interannual time scale.

#### 4 The Ocean Carbon Cycle

The ocean holds a large natural reservoir of carbon that exchanges with the atmosphere on time-scales of decades up to hundreds of thousands of years. Superimposed upon the cycling of this natural reservoir, the increasing atmospheric CO<sub>2</sub> partial pressure is causing the ocean to absorb a significant fraction of anthropogenic carbon emissions. Due to the natural carbon cycle of the ocean, 39,000 Pg C is stored in the ocean, which amounts to ~90% of the carbon contained in the combined land, ocean and atmosphere domains (Bolin et al., 1983; Sundquist 1993; Sabine and Tanhua, 2010). The natural carbon cycle is driven by ocean circulation, seasonal heating and cooling, and biological processes (Figure 6, left).

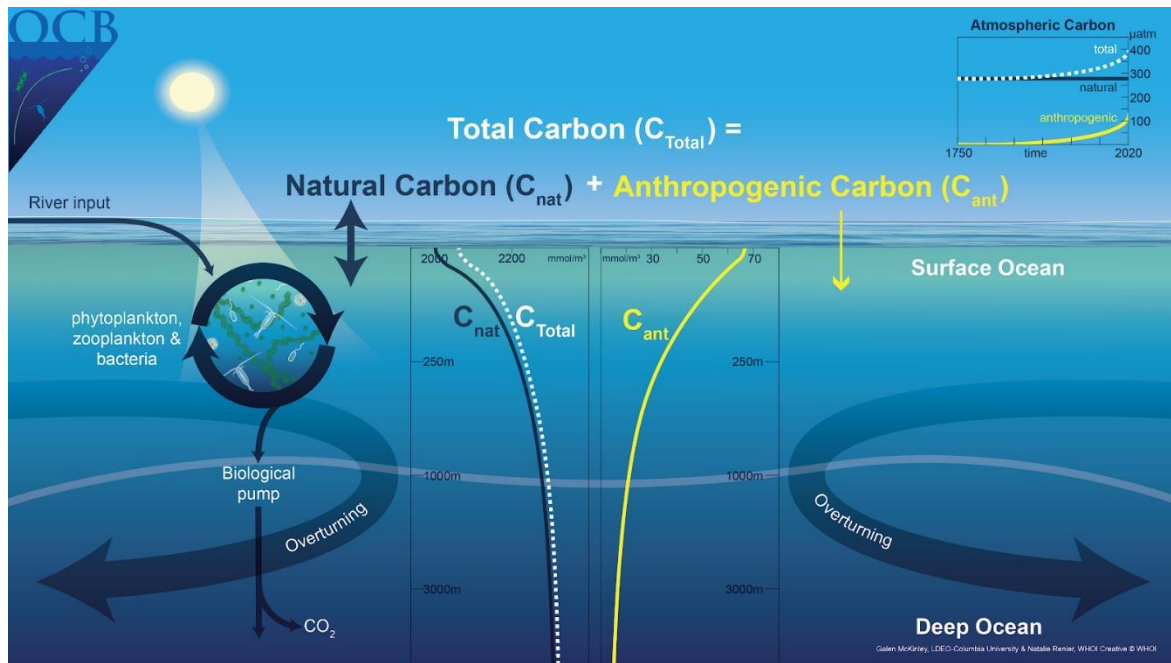


**Figure 6.** The total carbon cycle in the ocean ( $C_{Total}$ ) is the sum of the natural carbon cycle ( $C_{nat}$ ) and the anthropogenic carbon cycle ( $C_{ant}$ ). The natural carbon cycle is quantitatively dominant, as shown in the observed data (GLODAPv2, Olsen et al., 2016) plotted in the center, and includes contributions from biological activity and the large-scale circulation of the ocean. Overlain is the uptake of additional carbon due to anthropogenic emissions to the atmosphere that occurs in the present ocean as atmospheric pCO<sub>2</sub> continues to rise. The air-sea flux associated with  $C_{Total}$  is  $F_{net}$  (see text).

The ocean carbon budget can be quantified as the storage of inorganic and organic carbon in the ocean, the fluxes of carbon across the air-sea interface, river input, and a small term for sedimentation. The natural carbon inventory is very large compared to the anthropogenic component and is believed to have been near a long-term steady state in preindustrial times, such that there was zero net flux to the global ocean of natural carbon ( $F_{\text{nat}}$ ), i.e., there was a balance between riverine input, sedimentation rates and air-sea flux. The anthropogenic uptake flux ( $F_{\text{ant}}$ ) is the additional ocean uptake due to the direct effect of increasing atmospheric  $\text{CO}_2$  mixing ratio and occurs as a perturbation to the vigorous natural cycle (Figure 6, right), with the column inventory of anthropogenic carbon ( $C_{\text{ant}}$ ) from the latest data-based estimates mapped in Figure 7 (bottom).

The increase in natural carbon ( $C_{\text{nat}}$ ) from surface to depth (Figure 6) is largely due to the biological carbon pump (BCP) (Sarmiento and Gruber, 2006). If the BCP did not operate, the atmospheric  $\text{CO}_2$  mixing ratio would be around 200 ppm higher (Maier-Reimer et al., 1996). During the last glacial maximum, changes in the efficiency of the BCP may have played an important role in lowering atmospheric  $\text{CO}_2$  (Galbraith and Skinner, 2020; Sigman et al., 2010). Biological feedbacks may accompany anthropogenic climate change (Sabine & Tanhua, 2010, Hauck et al., 2015, Moore et al., 2018), but there is significant spread in model projections (Laufkötter et al., 2015, 2016; Frölicher et al., 2016). To date, observed time-series are too short to provide evidence for long-term biologically-driven trends in the ocean carbon cycle (Henson et al., 2016). Thus, the ocean carbon sink for anthropogenic carbon over the industrial era is currently understood as a physical and chemical process. In Figure 6, the contemporary (or ‘net’) air-sea  $\text{CO}_2$  flux ( $F_{\text{net}}$ ) is the sum of  $F_{\text{nat}}$  and  $F_{\text{ant}}$ .  $C_{\text{Total}}$  is the carbon concentration corresponding to  $F_{\text{net}}$ . Global maps of  $\text{pCO}_2$ , the  $\text{CO}_2$  flux and the interior ocean inventory of anthropogenic carbon ( $C_{\text{ant}}$ ) are shown in Figure 7.

The ocean surface layer carbon content equilibrates with the atmosphere on time-scales of months. The ocean continually removes  $C_{\text{ant}}$  from the atmosphere because the ocean circulation transports  $C_{\text{ant}}$ -laden waters away from the surface layer and into the ocean interior, while the water that returns to the surface tends to have low  $C_{\text{ant}}$  content. Thus, the ocean circulation is essential to continued  $\text{CO}_2$  uptake. At the global scale, the ocean mixes from surface to depth relatively slowly, on timescales of 1000 years. Thus, 75% of all anthropogenic carbon attributable to the industrial age remains in the upper 1000 m (Gruber et al., 2019a). Because carbon is highly soluble and exists as DIC in ocean water, the fundamental limit on the rate of anthropogenic carbon uptake by the ocean is the rate of exchange between surface and the deep ocean across the mixed layer depth and, ultimately, the large scale overturning circulation; these processes determine how fast intermediate and deep waters with  $C_{\text{ant}}$  uptake capacity are exposed to the surface.

Since the beginning of the industrial era, the ocean has been the primary cumulative  $C_{\text{ant}}$  sink (Friedlingstein et al., 2019; 2020), although there are large regional differences in the magnitude and sign of the flux (Figure 7, middle panel). Looking forward, the behavior of the ocean carbon sink is expected to play a critical role in determining how much anthropogenic carbon remains in the atmosphere (Randerson et al., 2015, Zickfeld et al., 2016, Schwinger and Tjiputra, 2018, Ridge and McKinley, 2021).



The following sections describe the approaches used to study the ocean carbon sink. A mechanistic understanding of this sink is essential for diagnosing its state and for making reliable future predictions. This requires quantification of air-sea fluxes at higher spatial and temporal resolution than is available from interior data alone. Air-sea fluxes on monthly to decadal timescales are quantified using surface ocean observations and ocean models of varying

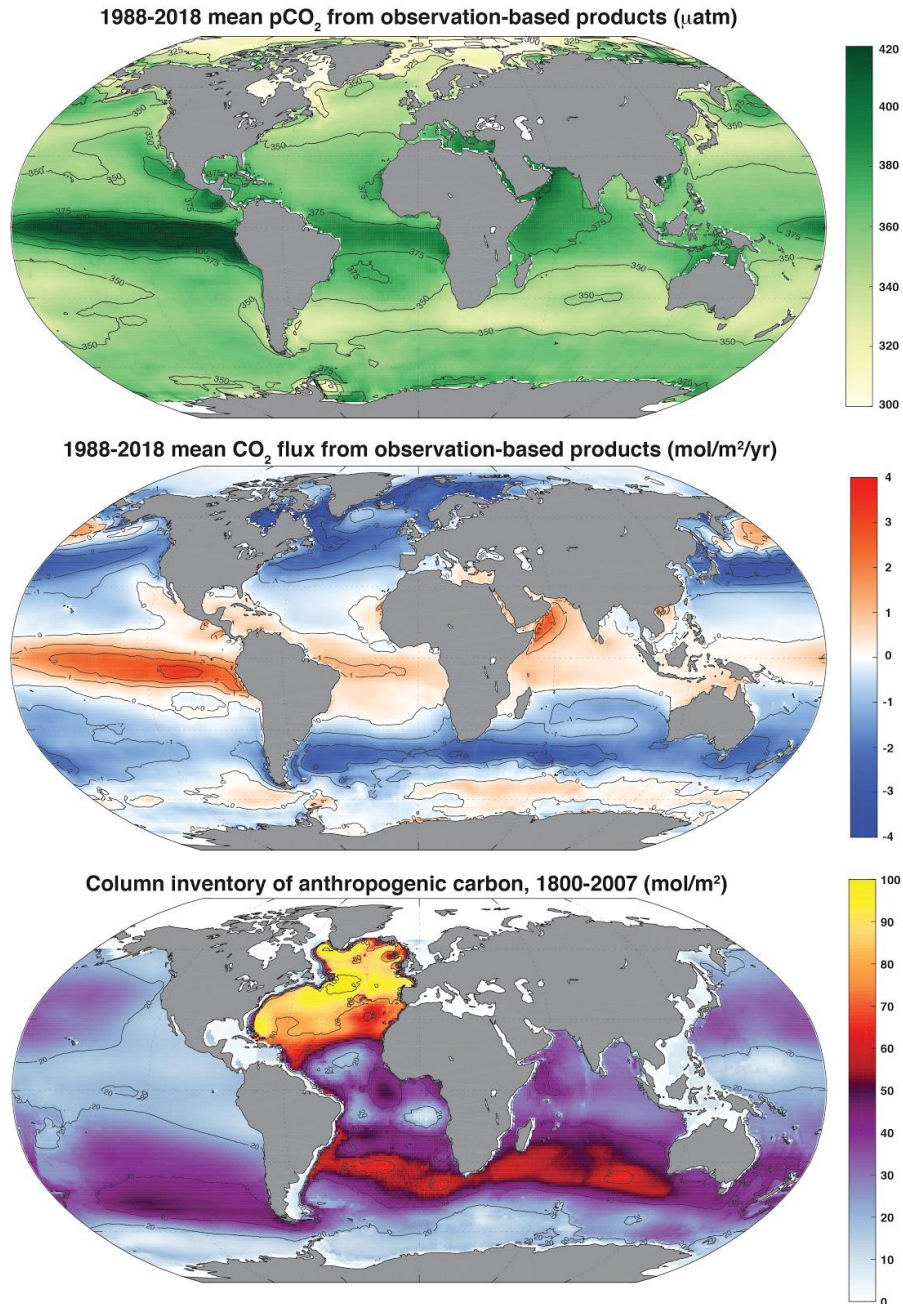


**Figure 7.** Surface ocean  $p\text{CO}_2$  (top); and air-sea  $\text{CO}_2$  flux ( $F_{\text{net}}$ ), positive flux to the atmosphere (middle), 1988-2018, mean of 6 observation-based products (Fay et al., 2021); column inventory of anthropogenic carbon ( $C_{\text{ant}}$ , bottom), 1800-2007 (Sabine et al., 2004, Gruber et al., 2019a).

complexity. Agreement between independent estimates for mean fluxes and temporal variability indicates growing confidence in global-scale mechanistic understanding. Yet, uncertainties remain and must be resolved to support better predictions for future ocean carbon sink and to allow for reduced diagnostic uncertainty for the global carbon cycle as it evolves. Substantial advances in observing systems, quantification of land-to-ocean fluxes of carbon, and models of ocean circulation and biogeochemistry are needed to reduce these uncertainties. In addition, as nations implement substantial reductions in carbon emissions, the near-term response of the ocean carbon sink to reduced atmospheric CO<sub>2</sub> growth rates must be accurately diagnosed and mechanistically explained.

#### **4.1 Bottom-up Estimates of Anthropogenic Carbon Accumulation in the Ocean from Interior Observations**

Based on a bottom-up accounting method using interior ocean data, Gruber et al. (2019a) find a total ocean C<sub>ant</sub> accumulation of  $152 \pm 20$  Pg C for the industrial era through 2007. By combining evidence from top-down and bottom-up approaches, Khatiwala et al. (2013) find an inventory of  $160 \pm 26$  Pg C in 2010. Consistent with previous inventories (Sabine et al., 2004), these studies find that the ocean has cumulatively absorbed excess carbon equivalent to 45% of industrial-era fossil fuel emissions until 2010, or 30% of the total anthropogenic emissions, including land use change. The column inventory of ocean C<sub>ant</sub> accumulation from Sabine et al. (2004) and Gruber et al. (2019a) is shown in Figure 7 (bottom).

The amount of C<sub>ant</sub> estimated for 2010 ( $160 \pm 26$  Pg C) represents only about ~0.4% of the ocean carbon stock, indicating the significant challenge of directly observing the temporal change in carbon stock over time. Direct measurements are only possible in areas with rapid change in dissolved inorganic carbon (DIC; e.g., Tanhua and Keeling, 2012). Instead, it is more practical to infer ocean storage of C<sub>ant</sub> against the large natural background, and then to calculate the change in storage over time.

A few different methods have been used to estimate the storage of C<sub>ant</sub>, either based on observations of biogeochemistry variables, or by transient tracers (see Sabine and Tanhua (2010) for a review). On a global scale, different methods converge within the uncertainties, but significant differences persist regionally (e.g., Waugh et al., 2006, Khatiwala et al., 2009). Multivariate techniques (e.g., Friis et al., 2005, Clement and Gruber, 2018) can be used to disentangle variability and calculate decadal-scale trends. A global estimate of the storage of anthropogenic carbon finds an increase of  $34 \pm 4$  Pg C between 1994 and 2007 (Gruber et al., 2019a), indicating a mean F<sub>ant</sub> uptake of  $-2.6 \pm 0.3$  Pg C (negative flux into the ocean) annually over this time frame. This relatively accurate (~12%) estimate provides an important benchmark for the ocean's role in sequestering anthropogenic carbon, and acts as a direct constraint on the net magnitude of the land flux, given low uncertainty on fossil fuel emissions and atmospheric carbon accumulation. The magnitude of the uptake implies that the ocean is continuing to take up anthropogenic carbon at a rate proportional to anthropogenic carbon emissions.

Critical elements to the success of global estimates of anthropogenic carbon stocks and changes in carbon storage are ship-based hydrographic sampling that collects carbon-relevant interior ocean data (Sloyan et al., 2019) and the GLODAP data product (Key et al., 2004; Olsen et al., 2020), which collates these interior data after extensive quality control (Tanhua et al., 2010). These data are required to quantify small changes over a large background. This data

product is now being released on an annual basis and the GLODAPv2.2021 version contains data from over 1.2 million water samples collected during 989 cruises (Lauvset et al., 2021).

#### 4.2 *Bottom-up Estimates of Ocean-Atmosphere CO<sub>2</sub> Fluxes from Observations of Surface Ocean pCO<sub>2</sub>*

In order to understand the ocean carbon sink on annual to interannual timescales relevant to climate change policy, more frequent estimates of the sink are required than those produced from decadal timescale interior ocean observations. These data come from observations of pCO<sub>2</sub>, and are used to estimate net air-sea CO<sub>2</sub> fluxes ( $F_{\text{net}}$ ). The reported variable is surface ocean fugacity of CO<sub>2</sub> (fCO<sub>2</sub>) which equals the partial pressure of CO<sub>2</sub> corrected for the non-ideal behavior of the gas (Pfeil et al., 2013). The fugacity of CO<sub>2</sub> is 0.3-0.4% smaller than the partial pressure of CO<sub>2</sub> (Zeebe and Wolf-Gladrow, 2001). However, the air-sea gradient,  $\Delta p\text{CO}_2$  or  $\Delta f\text{CO}_2$ , are essentially the same as the correction of the non-ideal gas behavior applies to both the ocean and atmospheric CO<sub>2</sub>. For simplicity, we use the terminology pCO<sub>2</sub> to refer to these data for the remainder of this paper. Over the past decade, the number of publicly available observations of pCO<sub>2</sub> has increased rapidly from 6 million in the first release of the Surface Ocean CO<sub>2</sub> Atlas (SOCAT) database (Pfeil et al., 2013, Bakker et al., 2014; 2016; 2020) in 2011 to 30 million in 2021 ([www.socat.info](http://www.socat.info)). These observations and their automated organization into a consistent database have enabled scientists to create a variety of new observationally-based estimates of the ocean carbon sink that use co-located data from satellite (sea surface temperature, height, and chlorophyll) or from climatologies of in situ data (sea surface salinity and mixed layer depth) to drive upper ocean extrapolation techniques and machine-learning algorithms so as to fill the observational gaps (Rödenbeck et al., 2014; 2015, Landschützer et al., 2013; 2014; 2020; Denvil-Sommer et al., 2019, Gregor et al., 2019; Gloege et al., 2021).

As the SOCAT database provides pCO<sub>2</sub> data for only ~2% of all months and 1° x 1° locations across the surface ocean from 1982 to present, a significant amount of extrapolation is needed to create full-coverage fields at monthly intervals. Nonetheless, comparisons of the extrapolated, observationally-based products to independent data indicate relatively low bias and convergence of the independent estimates (Gregor et al., 2019). Root mean square errors (RMSE) range from 10 to 35  $\mu\text{atm}$ . The fact that bias and RMSE comparisons are largely consistent across the variety of approaches suggests that it is data sparsity rather than extrapolation methodology that is now a fundamental limitation on further error reduction (Gregor et al., 2019). Additional tests of the machine-learning based extrapolation approaches using an Earth System Model testbed indicate that the techniques are able to reconstruct from sparse data with low bias and show skill for the amplitude and timing of seasonality across the global ocean. However, higher and lower frequency variations are more poorly represented because of inadequate sampling on these timescales (Gloege et al., 2021, Stamell et al., 2020). Several challenges remain in using these data, including the uneven distribution of data over time, methodological differences in the calculation of air-sea flux from pCO<sub>2</sub> (Fay et al., 2021, Woolf et al., 2019, Zavarsky and Marandino, 2019), and the potential need for adjustments to pCO<sub>2</sub> data to account for near-surface temperature and salinity gradients (Watson et al., 2020).

Despite the significant extrapolation and remaining uncertainties, it is a major advance for ocean carbon cycle science to have spatially-resolved, data-based estimates of air-sea CO<sub>2</sub> fluxes on monthly timescales. This allows for new investigation into the magnitudes and mechanisms of interannual and decadal variability in the ocean carbon sink, and a key point of



comparison to ocean models that were previously the only basis for this analysis. Models are discussed in the next section, and results are compared in the following.

### **4.3 Bottom-Up Estimates of Ocean-Atmosphere CO<sub>2</sub> Fluxes from Ocean Models**

Global ocean biogeochemical hindcast models estimate interior ocean carbon cycling and, from this, air-sea CO<sub>2</sub> fluxes. Models simulate the carbon distribution in the ocean due to the influences of currents, water mass formation and mixing, and biological processes. The bottleneck for ocean carbon uptake in the models, as in the real world, is the carbon transport across the mixed layer depth and its redistribution to greater depths via the overturning circulation. As a result, the models' carbon uptake is sensitive to simulated physics (Doney et al., 2004; Goris et al., 2018; Huber and Zanna, 2017). Models can also provide air-sea flux estimates prior to the 1990s when surface pCO<sub>2</sub> observations were rare.

Models are routinely evaluated against observations or observation-derived estimates that characterize the physical and biogeochemical state of the ocean for the last several decades (Doney et al., 2004; Schourup-Kristensen et al., 2014; Aumont et al., 2015; Schwinger et al., 2016; Stock et al., 2020; Séférian et al., 2020; Fay and McKinley, 2021). For the suite of models used in the GCP, comparison of pCO<sub>2</sub> at locations observed by SOCAT reveals the models' ability to capture variability and trends on annual (RMSE <10 µatm) and decadal timescales (RMSE <10 µatm). However, large model-data mismatches on the seasonal timescale also exist (RMSE of 20–80 µatm; Hauck et al., 2020).

Despite the overall concurrence with pCO<sub>2</sub> observations on annual and decadal timescales, model and data-based estimates of the ocean carbon sink started to diverge from each other since around 2002, particularly in the Southern Ocean (Hauck et al., 2020), reinforcing the need for evaluation of models in addition to that of data-products (section 4.2). As one way forward, Fay and McKinley (2021) evaluate the spatial distribution of modelled mean fluxes against an ensemble of these products adjusted by lateral fluxes from rivers,  $F_{\text{nat},\text{riv}}$ . They find that few models fall within 3 standard deviations of the product spread for each of five large regions that together cover the globe. The regional differences are to a large extent governed by the natural carbon fluxes and this metric therefore identifies models with the balance between physical and biological processes that is most consistent with observations.

Another approach evaluates models using the global anthropogenic carbon accumulation, thus assessing the global balance between atmospheric pCO<sub>2</sub> growth and global surface-to-deep ventilation instead of regional processes. Using simulations mimicking the anthropogenic carbon accumulation ( $F_{\text{ant},\text{ss}}$ ), Friedlingstein et al. (2021) compare the simulated ocean interior anthropogenic DIC inventory for 1994–2007 to the estimate of Gruber et al. (2019a). This reveals an underestimation of anthropogenic carbon uptake by the majority of the models on the order of 20% for the ensemble average. However, uncertainties on the interior estimates are also significant, and other interior estimates are lower for 1994–2007 by about 10% (DeVries, 2014). More models might fall within the constraint if both interior estimates were considered. Nonetheless, atmospheric inversions that take advantage of the constraint provided by the atmospheric CO<sub>2</sub> observation network also suggest that some models underestimate the sink (Friedlingstein et al., 2021). This conclusion is further supported by a recent estimate of the ocean sink from observed O<sub>2</sub>/N<sub>2</sub> (Tohjima et al., 2019) and the models' low 1990s estimate compared to the best estimate from different methodologies (Denman et al., 2007).

These are first efforts to exploit an array of observations to quantitatively assess regional and seasonal air-sea flux patterns in models, going beyond the typical discussion of spatial bias patterns (e.g., Séférian et al., 2020). A larger array of targeted metrics including seasonal cycles, trends and the interior ocean carbon inventory needs to be developed. Model development priorities include efforts to improve the regional and sub-regional distribution of mean fluxes and temporal variability from the seasonal cycle to the multi-decadal trend.

Global ocean biogeochemical models were the sole basis for quantifying the ocean sink in the GCB until 2020 (section 3). For example, for 2019, the GCB finds that the ocean sink accounted for 22% of 2019 anthropogenic CO<sub>2</sub> emissions (Friedlingstein et al., 2020). Models have also shed light on processes behind observed variability such as the weakening of the Southern Ocean carbon sink in response to increased westerlies (LeQuéré et al., 2007), and to explore the role of stationary Rossby waves in subduction of anthropogenic carbon (Langlais et al., 2017). As a component of Earth System Models, ocean models are the single tool for future projections. In the future, the rate of the ocean carbon sink will be largely determined by anthropogenic emissions, but ocean chemistry and physics will also play a significant role. On timescales from decadal to centennial, models project a decreased rate of uptake by the ocean carbon sink relative to the atmospheric pCO<sub>2</sub> concentration due to the fact that most of anthropogenic carbon already absorbed is in the near-surface ocean, and reduced buffer capacity (Schwinger et al., 2014, Randerson et al., 2015, Zickfeld et al., 2016, Schwinger and Tjiputra, 2018, Ridge and McKinley 2021).

#### **4.4 Reconciling Air-Sea Flux Estimates from Different Methods**

We must accurately quantify the ocean sink and understand its underlying mechanisms to diagnose its ongoing evolution and improve projections of future change. The best measure of our current understanding is the degree to which the above-mentioned independent estimates of the present-day sink's magnitude agree. We discuss the degree of agreement in this section, where a negative flux refers to a flux from atmosphere to ocean, and we discuss mechanistic understanding in the next section.

Surface ocean carbon observations indicate the net air-sea flux of carbon into the ocean (implicitly including riverine outgassing),  $F_{\text{net}}$ , is  $\sim -1.6 \text{ Pg C yr}^{-1}$ , while analysis of interior measurements yields estimates of the anthropogenic uptake and storage,  $F_{\text{ant}}$ , is  $\sim -2.6 \text{ Pg C yr}^{-1}$ , over the period, 1994 to 2007. Dynamic hindcast models used in the GCB, typically estimate the total of anthropogenic perturbations, that is the sum of anthropogenic uptake ( $F_{\text{ant}}$ ) and anthropogenic climate change induced natural carbon fluxes ( $F_{\text{nat, ns}}$ ). Closure terms of significant net magnitude ( $\sim 1 \text{ Pg C yr}^{-1}$ ) are required to bridge the gap between  $F_{\text{net}}$  and  $F_{\text{ant}}$ .

To reconcile flux estimates from pCO<sub>2</sub>-based data products with ocean models and estimates from interior data, an adjustment due to the riverine input of natural carbon that outgasses from the ocean ( $F_{\text{nat, riv}}$ ) must be applied (Sarmiento and Sundquist, 1992; Aumont et al., 2001; Lacroix et al., 2020). This adjustment is needed because these fluxes are not included in ocean models, but exist in the real world. Unfortunately, high quality direct estimates of  $F_{\text{nat, riv}}$  do not exist, so the closure between surface flux estimates of  $F_{\text{net}}$  and  $F_{\text{ant}}$  remains a significant uncertainty. Lacking better evidence, values typically used are between 0.45 and 0.78 Pg C yr<sup>-1</sup> (Jacobson et al., 2007, Resplandy et al., 2018), with large uncertainties. Recent work using stable carbon isotopes suggest an even larger efflux of 1.2 Pg C yr<sup>-1</sup> to the atmosphere from coastal margin inputs, also considering submarine groundwater discharge (Kwon et al., 2021).

Anthropogenic changes to the riverine input of carbon are an additional closure term not usually considered with no temporally-resolved estimates available and one estimate for 2000-2010 suggesting it to be small ( $0.1 \text{ Pg C yr}^{-1}$ , Regnier et al., 2013; Bauer et al., 2013). No estimates on anthropogenic changes to the outgassing of the riverine carbon in the ocean are yet available.

Climate change may already be having an effect on the natural carbon cycle fluxes ( $F_{\text{nat,ns}}$ ), although the magnitude of this non-steady state component is still uncertain. The first estimates of  $F_{\text{nat,ns}}$  came from one model for the period 1981-2007 (Le Quéré et al., 2010) and from a back-of-the-envelope calculation for the period 1994-2007 (Gruber et al., 2019a), suggesting a reduction of  $F_{\text{ant}}$  by 10 to 15%. Gruber et al. (2019a) estimate  $F_{\text{nat,ns}}$  by assuming that the accumulation of anthropogenic carbon in the ocean follows a linear scaling with the atmospheric load. However, this assumption is known to hold only when the atmospheric growth is strictly exponential, which has not been the case (Raupach et al., 2014; Ridge and McKinley, 2021), and thus the resulting estimate of  $+0.38 \text{ Pg C yr}^{-1}$  is likely an upper-bound. Another approach for estimating  $F_{\text{nat,ns}}$  is to use ocean models that represent the natural carbon cycle, and to make a reasonable assumption that the total carbon cycle response to climate variability is dominated by the natural component. With this assumption, models indicate for 1994-2007,  $F_{\text{nat,ns}} = +0.06$  to  $+0.31 \text{ Pg C yr}^{-1}$  (DeVries et al., 2019; McKinley et al., 2020) and for the recent decade, 2011-2020,  $F_{\text{nat,ns}} = +0.12 \pm 0.07 \text{ Pg C yr}^{-1}$ , equivalent to a 5% reduction of the ocean sink due to climate change (Friedlingstein et al., 2021). Better quantification of this term is clearly needed as well as a mechanistic understanding of the processes at play. Le Quéré et al. (2010) identified wind and temperature changes to be the dominant drivers behind this response, but the degree to which this is model dependent has not yet been investigated.

Estimates of the magnitude of the ocean sink relative to emissions vary between 23% and 48% in the literature (Friedlingstein et al., 2020; Khatiwala et al., 2013; Sabine et al., 2004). These seemingly contradicting numbers result from differences in the way the ocean sink is compared to different components of the emissions (Table 2). Quantitatively, the most important choice is the denominator used. For studies of the interior ocean cumulative ocean sink, the denominator typically used is the anthropogenic fossil emissions, resulting in an ocean sink of 44% for the industrial era through 2010 (Khatiwala et al., 2013), and 48% for the industrial era through 1994 (Sabine et al., 2004). GCB estimates, however, compare the ocean sink to total anthropogenic  $\text{CO}_2$  emissions, which also include emissions to the atmosphere from land-use change. Over the industrial era, GCB estimates that the ocean has absorbed  $171 \text{ Pg C}$ , while the cumulative fossil fuel emission is  $446 \text{ Pg C}$  and LUC is  $238 \text{ Pg C}$ . The ocean has thus absorbed 38% of the cumulative fossil fuel emissions, or 25% of the total anthropogenic emissions. For the period 2010-2019, GCB estimates a smaller percentage for the ocean sink, 23% of total anthropogenic emissions (Friedlingstein et al., 2020). A second difference between the estimates is that the GCB's approach also includes climate perturbation effects ( $F_{\text{nat,ns}} + F_{\text{ant,ns}}$ ), which reduces the magnitude of the ocean sink. Table 2 further illustrates the role of the chosen time-period in the various estimates with general agreement between GCB and interior ocean estimates when considering the spread in emission numbers used. For estimates stretching back to 1800 or before, the time-series extending to more recent years have a smaller proportion of the ocean sink relative to the fossil-fuel emissions, whereas the ratio relative to total emissions is more stable.

**Table 2.** Comparison of estimates of the relative magnitude of the ocean sink to emissions, ordered from shortest times-series to longest. GCB numbers are taken from Friedlingstein et al (2021). GCB fossil fuel emissions include the cement carbonation sink. GCB land-use change emissions are taken from annual time-series, plus 30 Pg C yr<sup>-1</sup> for the period 1750-1850 (Friedlingstein et al., 2021), and half of that number for the period 1800-1850. The same uncertainties are used for GCB estimates recomputed for 1750-2010 and 1800-1994 as for 1750-2020.

Source of Estimate	Time range	Cumulative fossil emissions (Pg C)	Cumulative land-use change emissions (Pg C)	Cumulative ocean sink (Pg C)	Ocean sink relative to fossil emissions	Ocean sink relative to total anthropogenic emissions
GCB (Friedlingstein et al., 2021)	2011-2020	95 ± 5	11 ± 7	28 ± 4	29%	26%
Sabine et al. (2004)	1800-1994	244 ± 20	100-180	118 ± 19	48%	28-34%
GCB	1800-1994	245 ± 25	185 ± 75	114 ± 35	47%	27%
Khatriwala et al. (2013)	1750-2010	~350	180 ± 50	155 ± 30	44%	29%
GCB	1750-2010	363 ± 25	220 ± 75	151 ± 35	42%	26%
GCB	1750-2020	458 ± 25	232 ± 75	179 ± 35	39%	26%

The choice to compare studies of interior ocean accumulation to fossil fuel emissions is motivated by the fact that these numbers are cumulative over the industrial era, and over this time, the land use source and land sink have been in approximate balance. Thus, this approach circumvents the large uncertainties associated with separate estimates of land-use change emissions and the land sink. The GCB's approach, on the other hand, acknowledges that fossil fuel and land-use change emissions add to the total atmospheric CO<sub>2</sub> mixing ratio, and that ocean and land carbon sinks respond to this increasing total. This is reinforced by the more stable ratio of the ocean carbon sink relative to total CO<sub>2</sub> emissions rather than the contribution from fossil fuel emissions, alone (Table 2).

#### 4.5 Recent Evidence for Decadal Variability of the Ocean Carbon Sink

In the mid-2000s, studies using ocean hindcast models suggested a slowing of the ocean carbon sink from the mid-1990s and attributed this change to processes in the Southern Ocean (Lovenduski et al., 2007; 2008; Le Quéré et al., 2007). In the following decade, the release of both the LDEO pCO<sub>2</sub> database (Takahashi et al., 2009) and the development of the international SOCAT database (Pfeil et al., 2013; Bakker et al., 2014; 2016; 2020) allowed for new analyses of trends in air-sea CO<sub>2</sub> fluxes directly from observations (Le Quéré et al., 2009; McKinley et al.,

2011; Fay and McKinley, 2013; Xue et al., 2018). Additionally, a variety of extrapolations of these data to global monthly coverage were developed (Rödenbeck et al., 2015), and a recovery of the ocean carbon sink following the low near the year 2000 was noted (Fay and McKinley, 2013; Landschützer et al., 2015; DeVries et al., 2017; Gruber et al., 2019b).

The Southern Ocean was generally identified as a significant regional driver of these mid-1990s to mid-2000s trends. A number of studies agreed that the stagnation of the Southern Ocean carbon sink in the 90s was related to a trend towards a more positive Southern Annular Mode (SAM) index associated with stronger westerly winds leading to more upwelling of natural carbon and hence dampened net air-to sea CO<sub>2</sub> flux (Le Quéré et al., 2007; Lovenduski et al., 2007; Lenton and Matear, 2007; Hauck et al., 2013).

Increasing nutrient concentrations in surface waters of all sectors of the Southern Ocean are consistent with a strengthened upwelling during the late 1990s (Iida et al., 2013; Ayers and Strutton, 2013; Hoppema et al., 2015; Pardo et al., 2017; Panassa et al., 2018). However, the same driving mechanisms cannot explain the reinvigoration of the sink in the 2000s, as the trends towards a more positive SAM and stronger winds in the 2000s continued. Asymmetric changes in atmospheric circulation (Landschützer et al., 2015), a weaker upper ocean overturning circulation (DeVries et al., 2017) and regional wind variability (Keppler and Landschützer, 2019) were proposed as possible explanations, but no consensus was reached on the driving mechanisms of the reinvigoration. Several studies concluded that ocean models were substantially underestimating the magnitude of decadal variability in the ocean carbon sink (De Vries et al., 2019; Gruber et al., 2019b).

In the last few years, more observation-based estimates have become available (Denvil-Sommer et al., 2019; Gregor et al., 2019), and now the size of the ensemble of observation-based estimates and of hindcast models is more comparable. With similar size ensembles for both observation-based and hindcast models, estimates of decadal variability are more similar in magnitude and phase, and not as large as the initial observation-based products had suggested (McKinley et al., 2020; Hauck et al., 2020). Both the ensemble of hindcast models and observation-based products indicate a larger ocean carbon sink in the early 1990s, then a slowing of the sink through about 2000, and then a strong and steady recovery through 2018 (Figure 8). In both the products and models, flux variability is largely homogenous across the globe outside the equatorial Pacific (McKinley et al., 2020).

By representing the surface ocean as a single abiotic box that exchanges water with the deep ocean at a constant rate, McKinley et al. (2020) are able to reproduce the variability of the ocean carbon sink with two external forcings (Figure 8). The two external forcings are the observed atmospheric pCO<sub>2</sub> and the forced change in upper ocean temperature due to the eruptions of large volcanoes (1982 El Chichon; 1991 Mt Pinatubo). This result emerges because the globally-averaged air to sea pCO<sub>2</sub> gradient - the fundamental driver of the flux - is only 6-10 µatm, and thus anomalies in the atmospheric growth rate of a few µatm over several years can rapidly modify the global air-sea gradient. Large volcanic eruptions, such as Mt Pinatubo in 1991, cause a rapid surface ocean cooling, which increases solubility and creates an uptake pulse (Church et al., 2005; Eddebbar et al., 2019). Then, as the ocean warms from this rapid cooling, solubility is lowered, and there is excess DIC in the upper ocean relative to what would have occurred without the eruption. These two effects contribute to a reduced growth rate of the sink for 5-7 years beyond the eruption (Figure 8).

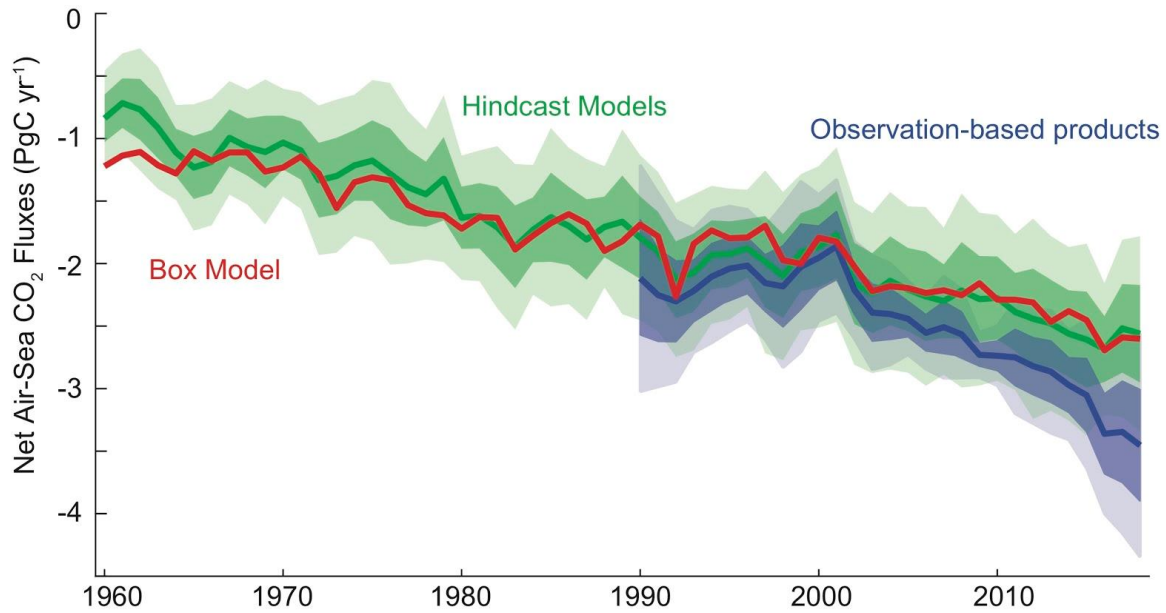


**Figure 8.** Air-sea CO<sub>2</sub> flux of carbon ( $F_{\text{ant}} + F_{\text{nat,ns}}$ ) from observationally-based products (blue), hindcast models (green) and upper ocean diagnostic box model (red); negative flux into the ocean. Global ensemble means (bold), with 1 sigma and 2 sigma of individual members (shading). Hindcast ocean models from Global Carbon Budget 2020 (Friedlingstein et al., 2020). Observationally-based product pCO<sub>2</sub> fields have missing ocean areas filled with a full-coverage climatology (Landschützer et al., 2020) and air-sea flux calculated as average of 3 wind reanalyses (CCMP, ERA5, JRA55) with a quadratic parameterization (Wanninkhof 2014, Fay et al., 2021); to this  $F_{\text{net}}$  estimate,  $F_{\text{nat,riv}} = 0.62 \text{ Pg C yr}^{-1}$  (Jacobson et al., 2007, Resplandy et al., 2018) is added. The upper ocean diagnostic box model (McKinley et al., 2020) is forced with observed atmospheric pCO<sub>2</sub> and surface ocean temperature changes forced by the eruptions of three large volcanoes of this period (1963 Agung, 1982 El Chichon, and 1991 Mt. Pinatubo; Eddebbbar et al., 2019).

This model of McKinley et al. (2020) is simple, considering a global surface ocean of 200 m depth that is uniformly impacted by atmospheric pCO<sub>2</sub> and upper ocean heat content anomalies forced by large volcanos. Yet, it can reproduce the ocean carbon uptake that occurs in the ensemble mean of much more complex models and observation-based products. What does this mean? It can be interpreted simply as Henry's Law operating at the global scale, wherein the partial pressure in the water is moving toward equilibration with the partial pressure in the air. Since the atmospheric pCO<sub>2</sub> continues to increase, the ocean continues to adjust toward equilibrium. McKinley et al. (2020) demonstrate that the ocean carbon sink temporal variability today is likely dominated by the external forcing from slight variations in the atmospheric pCO<sub>2</sub> growth rate. This perspective is consistent with recent analysis that shows heat uptake and interior redistribution in the ocean is far more sensitive to the details of the ocean circulation than is the pattern and magnitude of carbon uptake and storage (Bronseleer and Zanna, 2020). Ultimately, the mechanisms driving interannual to decadal timescale variability remains a topic of debate, and the focus of a significant research effort by the ocean carbon cycle community.

Observation-based products and hindcast models differ in the strength of sink increase since around 2002 (Figure 8). The growth rate of the ocean sink since 2010 is uncertain by a factor of three. Observation-based products indicate that the sink has increased by  $0.9 \text{ Pg C yr}^{-1}$  between 2010 and 2020 whereas models only simulate an increase of  $0.3 \text{ Pg C yr}^{-1}$  (Friedlingstein et al. 2021). This discrepancy is unresolved despite its importance for the near-term predictions of the remaining carbon budget and climate targets. Observation-based products may overestimate decadal variability of the ocean sink, consistent with too large a trend for these years (Gloege et al., 2021). Watson et al (2020) evidenced that the uncertainty of the sink estimate is generally a factor two higher at both ends of the time-series, independent of temporal and spatial data coverage, making the trend over the final one to two decades more uncertain.

Some models, however, underestimate the accumulation of anthropogenic carbon in the ocean interior for 1994-2007 (section 4.3; Friedlingstein et al., 2021), although the rate used as the basis for comparison (Gruber et al., 2019a) is on the high end of existing estimates (DeVries, 2014). If one assumes a steady state rate of anthropogenic carbon accumulation, an underestimated mean uptake rate for 1994-2007 would also imply an underestimated mean rate for 2002 to present. One possible explanation for this is that too little carbon is transported out of the mixed layer, which leads to a too strong increase in the buffer factor and hence to a reduction of ocean carbon uptake. Analysis of CMIP5 models in the Atlantic reveals that models that better represent current interior carbon storage have larger present-day and future carbon uptake (Goris et al., 2018). Biases in simulated ocean ventilation were identified as one process that affects ocean heat uptake (Bronse laer and Zanna, 2020) and to be the dominant cause of underestimated historical trends in modeled ocean oxygen decrease (Buchanan and Tagliabue, 2021). If ocean ventilation is too slow, models should underestimate the rate of the ocean carbon sink, and potentially also the sink's rate of change. It is also possible that variability in the ocean ventilation (DeVries et al., 2017) somewhat decouples the 1994-2007 rate of anthropogenic accumulation and ocean sink trends since 2002.

#### **4.6 Advancing Understanding of the Current and Future Ocean Carbon Sink**

To quantify the global carbon cycle, the constraint provided by the relatively low-uncertainty estimates for decadal anthropogenic carbon accumulation must be maintained. To better quantify fluxes on monthly to decadal timescales, increased observations of surface  $p\text{CO}_2$  and higher fidelity models are needed. In order to be prepared to support climate management efforts in the near-term, the likely behavior of the ocean sink under emissions mitigation must receive increased attention.

Observations of ocean interior carbon require measurements with high accuracy and precision due to the small perturbations on a large background signal. For example, in 2010, the  $C_{\text{ant}}$  content was  $\sim 160 \text{ Pg C}$  out of a total inorganic carbon content of  $\sim 39,000 \text{ Pg C}$ . For the surface ocean flux estimates, the high spatiotemporal variability in  $p\text{CO}_2$  and a low average deviation from air-sea equilibrium concentration needed to drive the observed net flux, i.e., a net flux of  $\sim 2.5 \text{ Pg C yr}^{-1}$  over a gross flux of  $\sim 90 \text{ Pg C yr}^{-1}$ , indicates that accuracy and data coverage are possibly the most important components of the observing system. There is a seasonal bias in the observing system, with fewer observations being made in winter at high latitudes. This is particularly important for observations of surface fluxes, which tend to be high in winter, but less so for the interior ocean observations where seasonality tends to be low below the winter mixed layer.

#### 1013 4.6.1 *Expanding Autonomous Observations*

1014 Although ship-based observations remain a central resource for the ocean carbon  
 1015 observing system, these are expensive and tend to be seasonally biased. Driven by these  
 1016 demands, there is a continuous development of sensors for inorganic carbon system  
 1017 measurements with at least some of these attributes: increased precision and accuracy, lower  
 1018 power consumption and lower instrument drift (Johnson et al., 2016; Sabine et al., 2020;  
 1019 Seelmann et al., 2019; Sutton et al., 2014). Similarly, there is a continuous development of  
 1020 autonomous platforms capable of carrying sensors for ocean carbon. These include moorings  
 1021 (Sutton et al., 2014), profiling floats (e.g., BGC Argo, Claustre et al., 2020), underwater gliders  
 1022 (Rudnick, 2016, Sutton et al., 2021), and autonomous surface vehicles powered by wind or  
 1023 waves (Sabine et al., 2020). These developments are rapidly changing the capability to monitor  
 1024 ocean carbon with higher spatial and temporal resolution. For instance, observations from  
 1025 Biogeochemical (BGC) Argos floats enable the calculation of surface  $p\text{CO}_2$  (from pH and  
 1026 alkalinity estimates) with reasonable accuracy and precision,  $\sim 11 \mu\text{atm}$  (Takeshita et al., 2018;  
 1027 Williams et al., 2017). Although not as good as the  $2 \mu\text{atm}$  target for the ship-based observations,  
 1028 this system has shown potential to fill spatiotemporal gaps in the observations, with important  
 1029 implications for the carbon flux estimates. For example, Bushinsky et al. (2019) report on  
 1030 significantly lower uptake of carbon in the Southern Ocean by including winter time  $p\text{CO}_2$  from  
 1031 BGC-Argo floats using a neural network interpolation. Uncrewed Surface Vehicles (USVs)  
 1032 directly measure  $p\text{CO}_2$  with an uncertainty of  $2 \mu\text{atm}$ , which is comparable to ship-based  
 1033 observations. The strong winter outgassing observed by floats in 2015-2016 was not detected by  
 1034 USVs in 2019, illustrating how these novel techniques can progress research on interannual  
 1035 variability (Sutton et al., 2021).

#### 1036 4.6.2 *Improving Constraints on Carbonate Chemistry*

1037 Although individual components of the ocean carbon observing system have high  
 1038 technical readiness levels, the new capabilities have not yet been integrated with existing, well-  
 1039 tested technologies to provide an observing system that can quantify ocean carbon uptake to  
 1040 within 10%. One critical need is an improved understanding of the ocean inorganic carbon  
 1041 system. There are four measurable inorganic carbon variables in the ocean - total alkalinity (TA),  
 1042 total dissolved inorganic carbon (DIC), pH and  $f\text{CO}_2$ . By measuring two out of those, the  
 1043 complete inorganic carbon system can, in theory, be calculated. Small errors in the dissociation  
 1044 constants, the boron-salinity ratio, and small contributions to the total alkalinity from unknown  
 1045 bases, can cause significant discrepancies in directly measured and calculated carbon variables  
 1046 (Fong and Dickson, 2019, Takeshita et al., 2020). A recent study by Álvarez et al. (2020) shows  
 1047 that inconsistencies between calculated and measured pH have decreased during the last decade,  
 1048 and they conclude that improved standard operating procedures for measurements and  
 1049 calculation of pH are urgently needed. An improved understanding of these issues is essential to  
 1050 fully utilize data from, for instance, BGC Argo floats equipped with pH sensors.

#### 1051 4.6.3 *Ensuring Quality Control and Timely Data Delivery*

1052 As noted above, the anthropogenic perturbation in the global ocean is more than an order  
 1053 of magnitude smaller than the background natural state. Thus, to track the changing  
 1054 anthropogenic carbon uptake by the ocean, very high standards for accuracy and precision of  
 1055 inorganic carbon system data must be maintained. New autonomous technologies offer great  
 1056 promise for expanding the observing system, but cannot be incorporated into the observing  
 1057 system if this substantially increases overall uncertainties. For the foreseeable future, ship-based



measurements will continue to be required to calibrate and validate autonomous observations. Cross-over evaluations should occur both with deployment and post-deployment (Fay et al., 2018). At the same time, ocean carbon data must be ingested into public databases or products (e.g., SOCAT, GLODAP) in a timely manner that supports annual diagnoses of the ocean carbon sink. It is essential that these data be carefully quality controlled. As the timescales at which the user community requires these diagnoses become shorter, these data will need to be available more quickly. One key component of this integration into scientific products is certified reference materials (CRMs). CRMs are critical because they allow for consistent observations across independent laboratories, which is essential for the development of high-quality global datasets. Currently, a single laboratory is the source for these materials and a plan for a long-term future source remains unclear (Catherman, 2021).

Similarly, better observational constraints on ocean carbon perturbations can be gained from stable carbon isotope observations. The ocean inorganic carbon pool is lightening due to the uptake of  $\text{CO}_2$  originating from the burning of  $^{13}\text{C}$ -depleted fossil fuel carbon, a phenomenon also known as the oceanic  $^{13}\text{C}$  Suess effect. By observing this temporal development, estimates of the anthropogenic carbon fraction of DIC are possible. Recent improvements in observations are making this approach attractive (e.g., Becker et al., 2012, Cheng et al., 2019, Cheng et al., 2021).

#### 4.6.4 *Quantifying Closure Terms to Link Estimates of Surface Flux and Interior $C_{\text{ant}}$ Accumulation*

In order to reduce uncertainties in the global and regional ocean carbon cycle, we need to understand how interior-based estimates of  $F_{\text{ant}}$  and surface flux estimates of  $F_{\text{net}}$  are quantitatively linked. An important barrier to this is the significant magnitude and high uncertainty in current estimates for natural fluxes of carbon in rivers ( $F_{\text{nat, riv}}$ ) and interannual variability in the natural carbon cycle ( $F_{\text{nat, ns}}$ ). More observations of these two quantities are needed to improve our understanding and reduce the uncertainties.

#### 4.6.5 *Constraining Mechanisms of Surface Flux Variability*

Recent work has identified the important role of external forcing from atmospheric  $\text{pCO}_2$  and volcanoes in driving ensemble-mean estimates of recent variability of the ocean carbon sink, but individual models and individual observation-based products deviate from the mean of the ensembles (Hauck et al., 2020, McKinley et al., 2020). These deviations are due to different methods for simulating the ocean circulation and biology in each individual ensemble member. We do not yet understand which of these individual estimates best represent the real ocean. To understand the actual total variability of the real ocean carbon sink (total = forced + internal), we need to select the observation-based products and models of highest fidelity. More stringent application of observational constraints (Fay and McKinley, 2021; Friedlingstein et al., 2021) would facilitate weighting of the models for global budgeting, focused analysis of the mechanisms driving variability in the highest-fidelity models and guidance for improving others.

Another approach for combining observations and models is through data-assimilation that constrains the model ocean state and fluxes using observations, and closes data gaps by model dynamics rather than extrapolation. While assimilation applications so far have not provided annually updated global ocean sink estimates with full spatial and temporal resolution (e.g., Mikaloff Fletcher et al., 2006; DeVries, 2014; Verdy and Mazloff, 2017;

DeVries et al., 2019), the first spatially and temporally resolved global data-assimilated models are starting to become available (Carroll et al., 2020).

#### 4.6.6 *Tracking the Magnitude of Trends in the Ocean Carbon Sink Since 2002*

The current divergence of ocean sink trends in observation-based products and models has implications for closure of the global carbon budget and remaining allowable emissions and the feasibility of internationally agreed climate targets. These trends may be methodological or may illustrate a fundamental knowledge gap in how the ocean sink responds to rising atmospheric CO<sub>2</sub> levels and the natural and anthropogenic physical changes occurring in the ocean. There are indications that observation-based products may overestimate decadal timescale trends (Gloege et al., 2021) and also that models may underestimate this trend (Goris et al., 2018) due to biases in ocean ventilation (Bronse laer and Zanna, 2020, Buchanan and Tagliabue, 2021). Understanding this deviation, and fixing potential methodological issues in both approaches is necessary to more accurately track the evolution of the ocean carbon sink.

#### 4.6.7 *Quantifying the Impact of Interactions Between the Natural Carbon Cycle and Climate*

Climate change induced modifications of the ocean, such as ocean acidification, warming and ecosystem composition could significantly influence the transport of particulate and dissolved organic carbon from the surface to the interior ocean, i.e., the “biological pump”. The efficiency of this transport is a key factor regulating the atmospheric CO<sub>2</sub> mixing ratio and is thought to play a role in regulating glacial / deglacial atmospheric CO<sub>2</sub> (e.g., Galbraith and Skinner, 2020). For instance, Marsay et al. (2015) suggest that a warmer ocean might lead to reduced sequestration of CO<sub>2</sub> by the biological pump. Complex interactions in the marine ecosystem will affect carbon export in a changing climate in ways that are difficult to predict and currently inadequately quantified (Laufkötter et al., 2015, 2016, Frölicher et al., 2016). In a recent work, Claustre et al. (2021) provide a research framework to improve the understanding of the oceans' biological carbon pump.

#### 4.6.8 *Tracking the Future Ocean Sink Under Scenarios of Emission Mitigation*

On centennial timescales under high emissions scenarios, slowing of the overturning circulation and reduced buffer capacity will significantly reduce the rate of ocean carbon uptake (Randerson et al., 2015, Ridge and McKinley, 2020; 2021). But how will the ocean sink evolve under the increasingly more likely scenario of substantial emissions mitigation (Hausfather and Peters, 2020)? Given that the long-term growth and interannual variability of the ocean sink observed to date is driven by the exponential growth of atmospheric pCO<sub>2</sub> (Joos et al., 1996, Raupach et al., 2014, McKinley et al., 2020, Ridge and McKinley, 2021), the ocean sink is expected to slow in response to reduced growth rates of atmospheric pCO<sub>2</sub>. In effect, the anthropogenic carbon trapped in the near-surface ocean will begin to equilibrate with the atmosphere and the sink will be significantly reduced in response to the mitigation of emissions. This will occur simply due a change in the growth of atmospheric pCO<sub>2</sub> - no change in the ocean circulation or buffer capacity is required (Ridge and McKinley, 2021). Slowing of the ocean sink will further offset the effect of reduced emissions. This will reduce the apparent effectiveness of mitigation actions in limiting climate warming (Jones et al., 2016). Despite a slowed rate of the sink, the largest share of cumulative emissions will be taken up by the ocean and land sink if a low emissions trajectory is followed (IPCC, 2021).

Though a series of idealized studies have established the general fact that the ocean sink will be reduced with mitigation (Joos et al., 1996, Raupach et al., 2014, Zickfeld et al., 2016,

Schwinger and Tjiputra, 2018, MacDougall et al., 2020, Ridge and McKinley, 2021), the spatially and temporally resolved response of the ocean sink to emission mitigation has received little attention. Thus, we do not know how rapidly the ocean sink will slow, nor where surface flux changes will be most substantial. We do not know what will be required from our monitoring systems to detect these changes.

Current uncertainties in ocean models suggest that, despite the fact that the current ensemble of models largely agrees as to the recent evolution of the sink (Figure 8), there may be substantial divergence in feedback strength and ocean sink response to emission mitigation. Since the majority of the anthropogenic carbon is held in the ocean's thermocline (Gruber et al., 2019a), the circulation here is critical to the ocean sink's near-term response to mitigation (Iudicone et al., 2016; Rodgers et al., 2020; Ridge and McKinley, 2020). There is substantial spread in the regional distribution of ocean carbon uptake in current models (McKinley et al., 2016, Hauck et al., 2020; Fay and McKinley 2021), and major differences in representations of seasonality (Mongwe et al., 2018), which illustrates knowledge gaps with respect to physical and biological processes and their representations in models. In addition, circulation in these critical upper-ocean regions is not consistently represented in state-of-the-art models (Bronse laer and Zanna, 2020). Uncertainties in the response of the ocean sink to emissions mitigation strategies need to be assessed, and then they need to be reduced by model development efforts and verified by observations, so that robust projections can be made. Especially in these first decades of climate management via emission mitigation, there will be great public interest in how emission cuts are changing atmospheric CO<sub>2</sub>. Scientists need to be prepared to explain ocean carbon sink changes as they occur.

## **5 The Terrestrial Carbon Cycle**

The terrestrial carbon cycle is characterized by large, spatially heterogeneous fluxes from anthropogenic activity and natural processes dominated by biospheric activity at daily, seasonal through interannual and multidecadal time-scales. Its primary stocks and fluxes are illustrated in Figure 9 and summarized in Table 3. The largest carbon stocks are held in aboveground biomass and soils in tropical and high latitude forests, respectively, with total stocks in vegetation and soils of 450-650 Pg C and 1500-2400 Pg C, respectively (Ciais et al., 2013; Scharlemann et al., 2014). As noted in Section 3, excluding fossil fuel combustion and other industrial activities (Section 3), the largest components of the net global land-atmosphere CO<sub>2</sub> fluxes are from land-use change and management and a sink in the terrestrial biosphere (Friedlingstein et al., 2021).

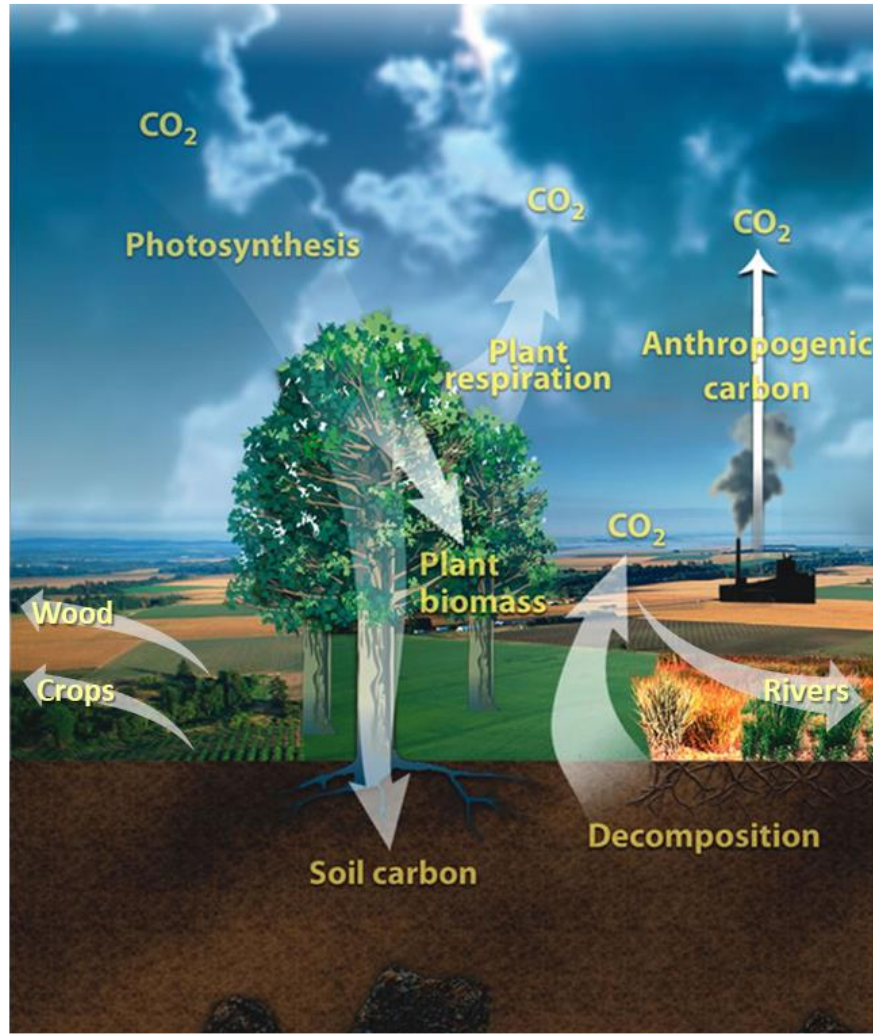


**Figure 9.** The land carbon cycle, showing the primary fluxes and reservoirs. The amplitudes of the primary land-atmosphere fluxes (white arrows), are listed in Table 3. “Lateral” land carbon fluxes such as land-to-ocean transfer of carbon by rivers and the import/export of harvested wood and agricultural products are also shown. (Adapted from U.S. Department of Energy Genomic Science program - <https://genomicscience.energy.gov>).

### 5.1 Processes Controlling Net Ecosystem Production

The net land carbon balance is determined primarily by the balance of CO<sub>2</sub> uptake through photosynthesis (GPP) and release by autotrophic respiration ( $R_a$ ), litter and soil organic matter decomposition (soil heterotrophic respiration,  $SHR$ ). It also includes smaller contributions such as source/sink dynamics from fires and other disturbances ( $F_{dist}$ ), emissions from crop product consumption and grazing ( $F_{crop}$ ,  $F_{grazing}$ ), wood product decay ( $F_{wood}$ ), outgassing from water bodies and lateral exports such as DIC/DOC ( $F_{nat,riv}$ ) and trade of crop and wood products ( $F_{trade}$ ). These quantities are related to Net Biome Productivity (NEP) in Eqs. 2-4.

$$NBP = GPP - R_a - SHR - F_{dist} - F_{crop} - F_{grazing} - F_{wood} - F_{nat,riv} - F_{trade} - F_{others} , \quad (2)$$

$$NPP = GPP - R_a, \quad (3)$$

$$TER = R_a + SHR. \quad (4)$$

Another commonly-used quantity, the Net Ecosystem Production (NEP), is similar to NBP on large ecosystem scales, but attempts to separate out carbon fluxes due to episodic disturbances (Schulze and Heimann 1998, Chapin et al., 2006). Additional fluxes of carbon in the form of carbon monoxide (CO), methane (CH<sub>4</sub>) or biogenic volatile compounds are included in  $F_{\text{others}}$ . Ciais et al. (2022) estimate these contributions as 0.3, 0.43, and 0.75 Pg C yr<sup>-1</sup>, respectively. These terms smaller than those included here and not considered further.

**Table 3.** Contemporary land carbon fluxes. (Note: numbers without uncertainties are assumed to have uncertainties comparable to their stated values.)

Quantity	Flux (P C yr <sup>-1</sup> )	Reference
Gross Primary Production (GPP)	115 to 190	Cai and Prentice (2020)
Net Primary Production (NPP)	~50 (44 to 57)	Ciais, Yao et al. (2020)
Autotrophic Respiration ( $R_a$ )	~64 ± 12	Ito (2020)
Soil Heterotrophic Respiration (SHR)	39 (33 to 46)	Ciais, Yao et al. (2020)
Outgassing by Rivers, Lakes and Estuaries	0.8 to 2.3	Ciais, Yao et al. (2020)
Fires	1.6	Ciais, Yao et al. (2020)
Consumption of Harvested Crops	1.5	Ciais, Yao et al. (2020)
Land Use Change (LUC)	1.1	Ciais, Yao et al. (2020)
Grazing	1.0	Ciais, Yao et al. (2020)
Biogenic Reduced Carbon	0.8	Ciais, Yao et al. (2020)
Decay and Burning of Wood Products	0.7	Ciais, Yao et al. (2020)

Land carbon stocks and fluxes, and thus the natural land sink, are affected by increases in atmospheric CO<sub>2</sub> as well as changes in nitrogen deposition, land use change (LUC) and the response of ecosystems to climate variability since the beginning of the industrial age. Elevated atmospheric CO<sub>2</sub> mixing ratios directly stimulate plant productivity through CO<sub>2</sub> fertilization and enhancements in plant water use efficiency in arid regions (Schimel et al., 2015; Gonsamo et al., 2021). These factors, combined with its contributions to warming at high latitudes, contribute to longer growing seasons. The magnitude of these effects is debated (Walker et al., 2021), underscoring remaining uncertainties in empirical understanding and modelling (Medlyn et al., 2015).

In the current paradigm for nutrient control on productivity, high-latitude ecosystems are potentially nitrogen limited. This reflects the young age of soils post glaciation, since nitrogen sourced through biological nitrogen fixation from the atmosphere and cold environments limit nutrient mineralization. In contrast, the tropics are more likely to be phosphorus limited as they typically have older and often highly weathered soils (phosphorus being sourced from bedrock;

see Vitousek et al., 2010). In terms of climate constraints on primary productivity, tropical systems are often characterized by distinct wet and dry seasons, and are water and/or radiation limited, the latter due to clouds (over moist tropical forests), whereas mid- and high-latitudes are typically temperature and light limited, except semi-arid and drylands, which are typically water limited (Nemani et al., 2003).

The net carbon balance can be determined by bottom-up methods, such as biomass and soil inventories and process-based models (e.g., DGVMs). Two biomass-based, bottom-up approaches are considered in this review: 1) stock change (difference between carbon stocks over a period of time) 2) gain/loss method (annual gains and losses in biomass carbon). The net carbon balance can also be inferred from top-down methods that infer net land-atmosphere CO<sub>2</sub> fluxes by analyzing spatially-and temporally-resolved measurements of CO<sub>2</sub> concentrations using atmospheric inverse models. Top-down atmospheric inversions provide spatially-explicit and temporally continuous estimates of the surface (land and ocean) fluxes that are consistent with CO<sub>2</sub> concentration measurements and ensure mass-balance, but require the choice of an atmospheric transport model, assumptions about uncertainties and depend on the priors used when the observational network is too sparse (Kaminski and Heimann, 2001). The extent to which the top-down and bottom-up estimates of the net carbon balance agree provides a measure of our understanding of the carbon cycle. Results from both approaches are summarized in the following sections. Here, we focus on contemporary fluxes, covering the past three decades (1990 – 2020), broadly aligning with the availability of global satellite remote-sensing data, although exact time periods will differ among individual studies reported.

## 5.2 *Bottom-up Inventories of Net Ecosystem Exchange*

CO<sub>2</sub> emissions or uptake by natural ecosystems, including those associated with deforestation, reforestation, disturbance, or land management are usually expressed in terms of the Net Ecosystem Exchange,  $NEE = -NEP$ . Bottom-up methods estimate NEE based on information about (i) the area affected by a given process, (ii) the corresponding carbon stock per unit area (and its trends) and (iii) the fraction of carbon exchanged with the atmosphere due to the observed change (e.g., Hubau et al., 2020). In practice, all three of these properties are challenging to quantify accurately (e.g., Saatchi et al., 2011; Ramankutty et al., 2007; Pearson et al., 2017, Xu et al., 2021), but all have benefited from new in situ and remote sensing measurement techniques and more advanced bottom-up modeling techniques.

The areal extent of land use and land cover change (LULCC) associated with human activities and natural processes are typically tracked using the bookkeeping methods and remote sensing observations summarized in Section 3.3. Recent advances in the remote sensing methods are summarized in Section 5.4. Estimates of the carbon stock per unit area are derived by combining above ground and below ground biomass and soil carbon. Until recently, estimates of all three quantities relied primarily on in situ measurements collected from a limited number of dedicated research plots at regular intervals (e.g., Pan et al., 2011). Soil carbon inventories still rely exclusively on in situ measurements, which are often characterized by limited spatial coverage and infrequent (decadal) repeat intervals (Scharlemann et al., 2014; Ciais et al., 2014). However, recent advances in microwave and lidar remote sensing technologies have provided dramatic improvements in above ground biomass measurements (see Section 5.4.2).

Alternately, NEE can also be estimated from direct measurement of CO<sub>2</sub> fluxes between the surface and the atmosphere using networks of eddy covariance flux towers, such as those



deployed by FLUXNET (Baldocchi et al., 2001). The global network of eddy covariance sites has grown substantially over the past 25 years, with some records spanning that full period. These data provide unique constraints on the CO<sub>2</sub> fluxes from a broad range of vegetation types, climate regions and disturbance types. Eddy flux data have been combined with other

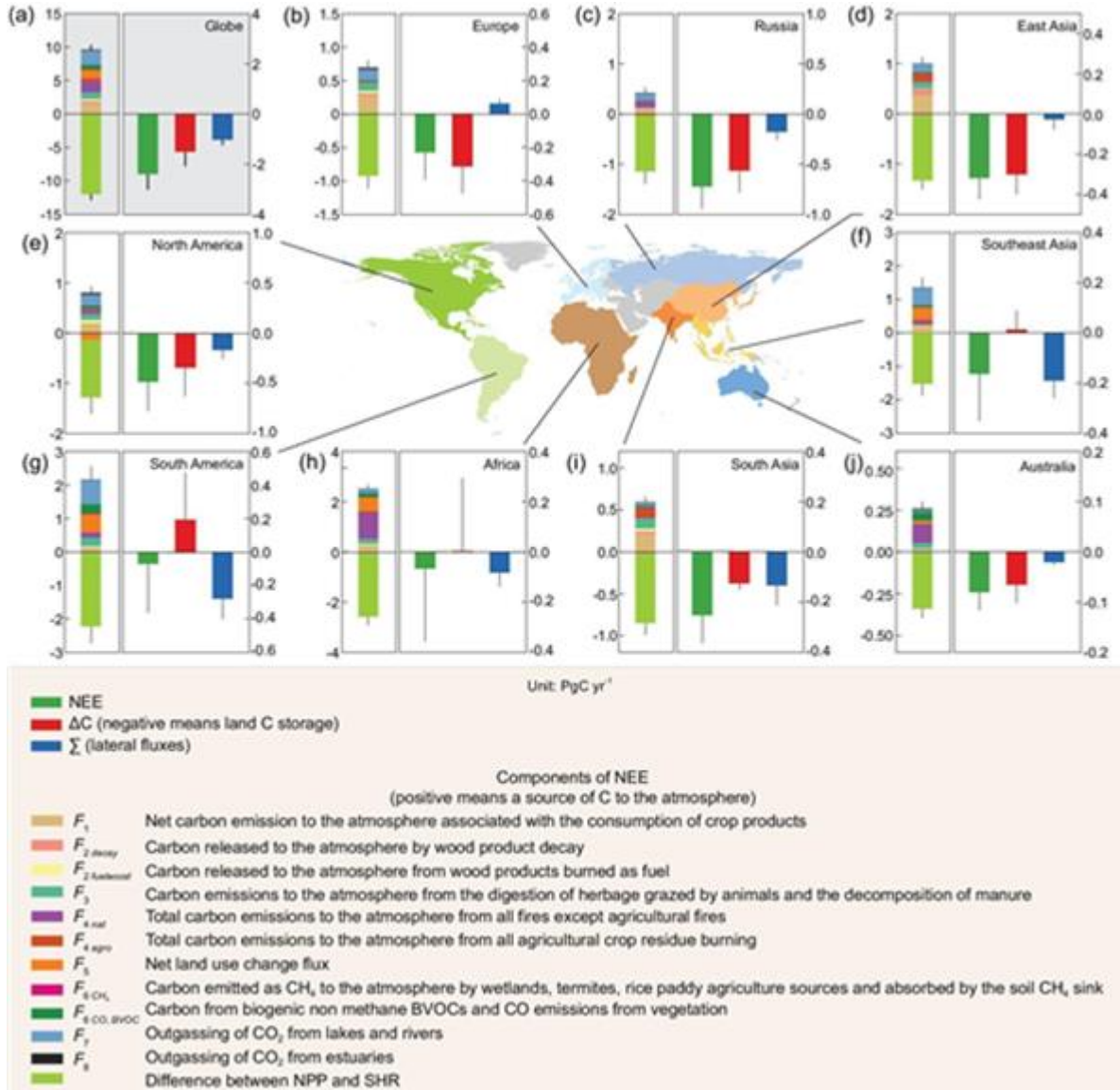


**Figure 10.** Contributions to net ecosystem exchange (NEE, as defined in Ciais, Yao et al., 2020, which corresponds to the definition of NBP in Eq. 2) at continental scales from bottom-up inventories, compiled by RECCAP2. All major flux components included in their definition of NEE are shown in the left sub-panel of each plot. The right sub-panels summarize NEE (green bars), the carbon-storage change, ΔC (red bars) and the combined lateral fluxes from trade and riverine-carbon export to the ocean,  $F_{trade} + F_{nat, riv}$  (blue bars) for different regions of the globe for the

climatological data to provide insights into the processes acting across these domains and their changes over time. Over the past two decades, the eddy flux network has expanded to span the globe, but still has large gaps, particularly in the tropics and at high latitudes, and each flux tower

characterizes the fluxes within a limited spatial footprint. Because of this, efforts to upscale results from local to regional or global scales are often associated with large uncertainties in the magnitude of the land  $\text{CO}_2$  sink and especially its interannual variability (Baldocchi, 2003; Jung et al., 2009; Beer et al., 2010; Xiao et al., 2012; Keenan and Williams, 2018; Jung et al., 2020).

Figure 10 shows the net carbon balance expressed as NEE across continents, drawn from a comparison of bottom-up methods employed in the REgional Carbon Cycle Assessment and Processes-2 (RECCAP2) project (Ciais et al., 2020a). Here, NEE is defined by subtracting lateral carbon fluxes ( $F_{\text{nat,riv}}$ ,  $F_{\text{trade}}$ ) from the total net land carbon stock change,  $\Delta C$ . In Europe, Russia and East Asia, the lateral fluxes tend to be small, and NEE almost equals the change in carbon stocks as observed from inventories. Overall, Ciais et al. (2020a) find a global sink of  $-2.2 \pm 0.6 \text{ Pg C yr}^{-1}$ , which is comparable to the independent estimate obtained by the DGVMs used in the GCB (Friedlingstein et al., 2021) of  $-2.7 \pm 0.6 \text{ Pg C yr}^{-1}$ . The results from bottom-up estimates in Ciais et al. (2020a) are also roughly consistent with results from an ensemble of atmospheric inversions (Peylin et al., 2013), which estimate a global net land sink of  $-1.32 \pm 0.39 \text{ Pg C yr}^{-1}$ , with a sink of  $-2.18 \pm 0.53 \text{ Pg C yr}^{-1}$  in the northern hemisphere but a highly uncertain source of  $0.91 \pm 0.93 \text{ Pg C yr}^{-1}$  in the tropics (estimated as a sink by Ciais et al., 2020a). These net sink estimates are not consistent with a sum of the mean values of GPP,  $R_a$ , SHR listed in Table 3, but are allowed within the range of uncertainties on these variables quoted there (see discussion in Ciais et al. 2020a).

### 5.3 Bottom-up Estimates of Gross $\text{CO}_2$ fluxes from land ecosystems – GPP, $R_a$ and SHR

To understand variability and trends in NEE, the component fluxes (Eq. 2) must be quantified. Gross primary productivity (GPP) reflects the total uptake of carbon through photosynthesis and is an essential variable to understand the carbon cycle. Up to 40% of the carbon in the atmosphere passes through leaf stomata annually, and approximately 16% ( $120 \text{ Pg C yr}^{-1}$ ) is assimilated in vegetation (GPP) (Ciais et al., 1997). Some of this carbon is used for plant functioning and growth, and the remainder is released back to the atmosphere through respiration. GPP minus autotrophic respiration ( $R_a$ ) equals Net Primary Production (NPP) and this is further reduced by soil heterotrophic respiration and disturbances.

An analysis of direct flux observation made by a network of eddy covariance towers yielded estimates of the global GPP near  $123 \text{ Pg C yr}^{-1}$  (Beer et al., 2010). Roughly one third of this ( $40.8 \text{ Pg C yr}^{-1}$ ) is produced in the tropical forests, and one quarter ( $31.3 \text{ Pg C yr}^{-1}$ ) in the tropical savannas, making the tropics by far the largest contributor to global GPP. Temperate and boreal forests are estimated to have a GPP of only  $9.9 \text{ Pg C yr}^{-1}$  and  $8.3 \text{ Pg C yr}^{-1}$ , respectively. When integrated over the globe, croplands contributes an estimated  $14.8 \text{ Pg C yr}^{-1}$  to GPP.

An alternate analysis using oxygen isotopes (Welp et al., 2011), suggests that this value of Global GPP may be too low and would be closer to  $150 - 175 \text{ Pg C yr}^{-1}$ . However, Anav et al. (2015) argue that Welp et al. used a limited number of observations and a simple model that included gross photosynthesis, but neglected photorespiration by land plants. They note that plants immediately respire away 20-40% of the carbon fixed by photosynthesis. When photorespiration is included, they note that these GPP values are more in line with those obtained from other methods. Table 4 presents a comparison of several GPP estimates. Noteworthy features include the large range, and the fact that the more recent estimates using SIF suggest a rather higher global total than the earlier estimates (see also Campbell et al., 2017).



**Table 4.** Comparisons of published contemporary (1990-2020) GPP Estimates.

Estimate (Pg C yr <sup>-1</sup> )	Method	Reference
140	MODIS, SIF, Fluxnet	Joiner et al. (2018)
150-175	isotopes	Welp et al. (2011)
123±8	Fluxnet +RS	Beer et al. (2010)
108-130	FLUXNET, RS, other	Jung et al., 2020
115-190	TRENDY models	Cai and Prentice (2020)
167 ±5	SIF, model assimilation	Norton et al. (2019)
166 ±10	SIF	MacBean et al. (2018)
120 ±30	Isotopes	Liang et al. (2017)
131–163	NIRv	Badgley et al. (2019)

More recent methods that combine flux tower data with remote sensing data in machine learning algorithms to produce upscaled fluxes (see Jung et al., 2020) yield global GPP estimates that agree well with those obtained from other methods, while providing insights into the processes controlling the carbon cycle of the land biosphere and their changes over time, particularly in the temperate Northern latitudes. Using radar derived estimates of biomass and soil carbon data from the harmonized world soil database and other sources combined with flux estimates of the global product of Beer et al. (2010), Carvalhais et al. (2014) calculated residence times of carbon. They found that the sensitivity of the residence time to soil moisture and temperature did not agree with the sensitivity of a set of DGVMs, while the overall pattern of increasing residence time at higher latitudes was reproduced. The following sections summarize recent results from bottom-up inventories that combine plot-based in situ measurements and remote sensing observations to constrain carbon uptake and emissions from the land biosphere.

Global autotrophic respiration,  $R_a$ , is estimated at  $64 \pm 12$  Pg C yr<sup>-1</sup> (Ito, 2020). This term is also called “maintenance respiration” and consists mainly of dark respiration. Precise determination of  $R_a$  is difficult as it also involves a substantial below ground component, and is expected to vary with biome and climate. Estimates of NPP ( $GPP - R_a$ ), are generally assumed to be of the order of 50% of GPP (i.e., Ito, 2020).

Estimates of soil (heterotrophic) respiration (SHR) associated with the decomposition of organic matter are even more challenging to constrain at regional to global scales. To estimate SHR, Ciais et al. (2020a) combined independent estimates of NPP, NEE and the last seven processes listed in Table 3 from a series of bottom-up inventories and observation-based datasets. They find a value of  $39$  Pg C yr<sup>-1</sup> with an interquartile range of  $33$ - $46$  Pg C yr<sup>-1</sup>. This estimate is lower than those conventionally assumed, but agrees with recent large-scale estimates based on site soil respiration measurements (Jian et al., 2021).

#### 5.4 *Advances in Remote Sensing of Primary Productivity and Biomass*

Since the launch of LandSat 1 in 1972, carbon cycle scientists have used a variety of optical and near infrared remote sensing observations to characterize plant productivity. One of the earliest indicators was the Normalized Difference Vegetation Index (NDVI), which is defined as the difference between the observed radiances within near-infrared (NIR) and red channels divided by their sum. NDVI and other vegetation indices such as Leaf Area Index (LAI; Zhu et al. 2013) or fraction of Absorbed Photosynthetically Active Radiation (fAPAR; Myneni et al., 2015) have been used as proxies for vegetation activity and photosynthesis. Such indices have also been used as proxies for fAPAR in semi-empirical light-use efficiency models, and combined with estimates of photosynthetically active radiation (PAR) (Zhao and Running, 2010; Smith et al., 2015) or more complex radiative transfer models (Jiang and Ryu, 2016) to estimate GPP. More recently, NDVI has been joined by other optical and near infrared indicators such as the Near Infrared Reflectance of Vegetation, NIRv, and SIF. Recent results derived from these indicators are summarized in this section.

##### 5.4.1 *Remote Sensing proxies for Photosynthesis and GPP*

SIF provides a closer proxy for photosynthesis than NDVI. As plants absorb sunlight to perform photosynthesis, a fraction of that light ( $< 2\%$ ) is re-emitted at longer NIR wavelengths (fluorescence), which can be detected in the cores of strong solar Fraunhofer lines or in the molecular oxygen ( $O_2$ ) A- and B-bands by high resolution space-based spectrometers (Meroni et al., 2009; Frankenberg et al., 2014; Guan et al., 2016; Sun et al., 2018).

SIF is a rapidly-responding indicator that shows strong linear relationships with GPP at site-scale and thus has been adopted as a functional proxy for photosynthesis and GPP. The availability of global SIF datasets from space-based sensors, such as GOME-2, GOSAT, OCO-2 and TROPOMI (Figure 11) have substantially expanded the use of this product in studies of the terrestrial carbon cycle. SIF-based estimates of global GPP are beginning to converge, but still differ, ranging from  $166 \pm 10 \text{ Pg C yr}^{-1}$  (Table 3). While SIF provides robust estimates of spatial distribution and seasonality of GPP, the strong relationship between SIF and GPP is largely explained by their common dependence on APAR (Mohammed et al., 2019), so that SIF might not be a good proxy for photosynthesis when down regulation occurs under stress conditions (Wohlfahrt et al., 2018; Marrs et al., 2020). SIF is now being combined with other vegetation indices and climate properties in diagnostic process models (e.g., Bacour et al. 2019; Bloom et al. 2020) to provide additional insight into NBE and GPP on regional-scales.

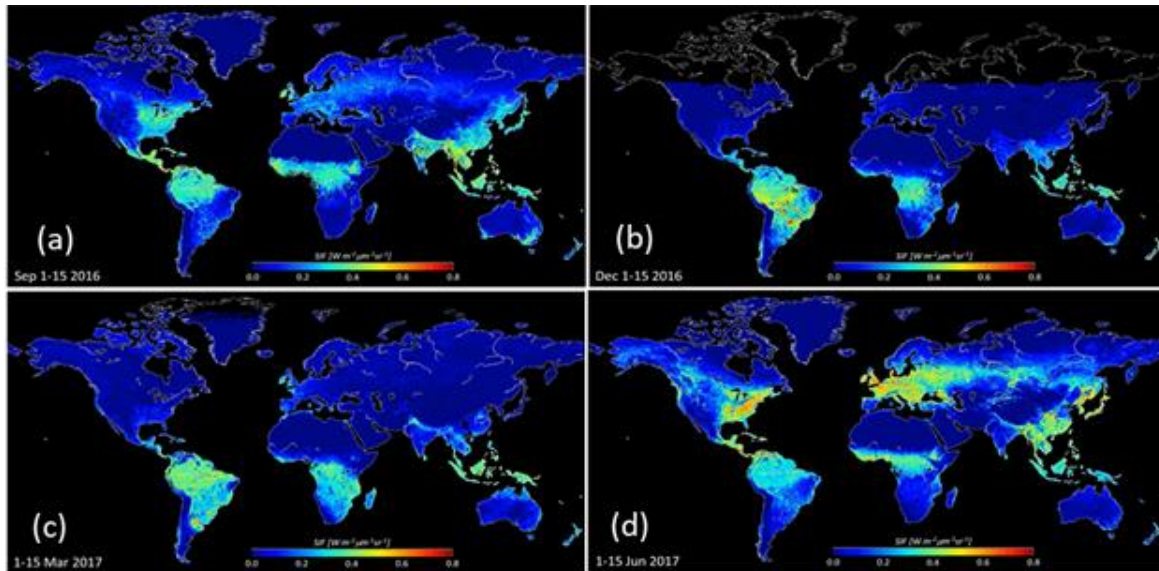


**Figure 11.** OCO-2 observations of SIF for (a) 1-15 September 2016; (b) 1-15 December 2016; (c) 1-15 March 2017, and (d) 1-15 June 2017. Blue indicates low SIF and therefore low photosynthetic activity. The warmer colors indicate higher SIF and higher photosynthetic activity (Ying Sun, Personal communication, 2018).

Recently, the NIRv (the product of NIR reflectance by NDVI) has been proposed as an alternative method to estimate GPP that overcomes some of the challenges of other indices and that shows high correlation with SIF. Using NIRv, Badgley et al. (2017) estimate global GPP to be 131-163 Pg C yr<sup>-1</sup>, in line with upper estimates of other studies and in line with isotope-based estimates by Welp et al. (2011) and Liang et al. (2017) (Table 4).

#### 5.4.2 Advances in Measurements of Above Ground Biomass

Vegetation optical depth (VOD) retrievals from satellite-based passive microwave instruments are sensitive to vegetation cover and water content (e.g., Liu et al., 2015). Passive microwave measurements have the advantage of not being affected by cloud cover, a common problem with other remote-sensing datasets. High frequency microwave measurements have been used to analyze seasonality and trends in vegetation (Barichivich et al., 2013) and to derive estimates above-ground biomass (AGB) based on empirical relationships between AGB and VOD (e.g., Liu et al., 2011; 2015).

Merging VOD data from multiple space-based microwave sensors, Liu et al. (2015) produced a global survey of AGB based on two decades of observations for both forests and non-forest biomes. They estimate a global average AGB of ~362 Pg C (310 – 422 Pg C) between 1998-2002, of which, 65% was in forests and 17% was in savannahs. Spawn et al. (2020) used satellite products of biomass with land cover with machine learning techniques to produce estimates of global AGB, and link this to below ground carbon density information. These estimates yield a total living terrestrial biomass of 409 Pg C, composed of an AGB of 287 Pg C and a below ground biomass carbon density of 122 Pg C (Figure 12).

Since 2010, the European Space Agency's Soil Moisture and Ocean Salinity (SMOS) measurements of lower frequency L-band microwave radiation at multiple angles have been used

to simultaneously obtain information about soil-moisture and vegetation structure, which are not fully attenuated at high biomass (Konings et al., 2017). Changes in peak VOD between years can be used to infer biomass changes, albeit at coarse ( $\sim 25$  km) spatial resolution (Brandt et al., 2018, Qin et al., 2021). VOD has also been used to derive GPP fluxes (Teubner et al., 2018).

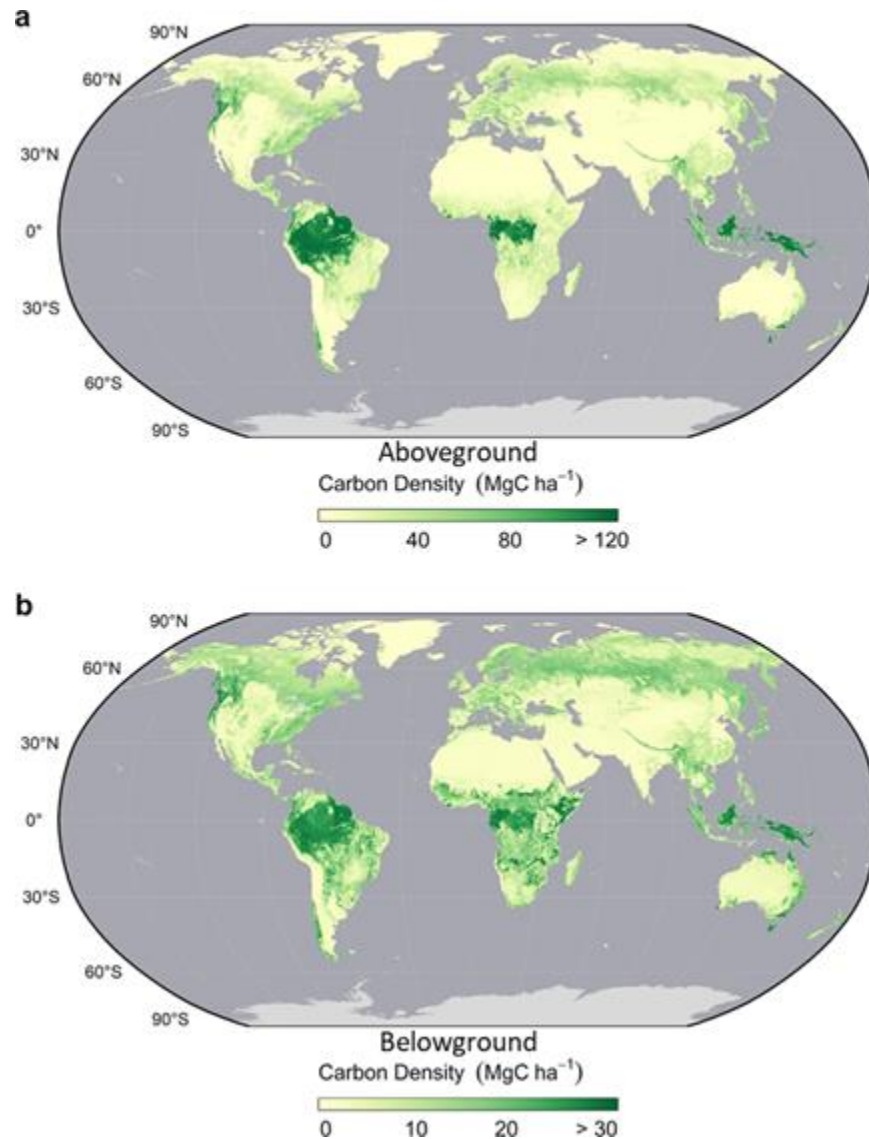


**Figure 12.** Maps of above and belowground living biomass carbon densities. (a) Aboveground biomass carbon density (AGBC) and (b) belowground biomass carbon density (BGBC). Maps have been aggregated at 5 km spatial resolution (Spawn et al., 2020).

The increasing availability of above-ground biomass estimates derived from light detection and ranging (Lidar) and radio detection and ranging (radar) sensors on airborne and space-based platforms are now providing improved spatial coverage and temporal sampling frequency (Xu et al., 2021). The availability of high-resolution space-based remote sensing observations from sensors such as LandSat Operational Land Imager (OLI), Moderate Resolution Spectroradiometer (MODIS) and Sentinel-2 Multi-Spectral Instrument (MSI) have

facilitated improved estimates of the land cover changes (Lamarche et al., 2017) and of burned areas (Chuvieco et al., 2016), and detection of changes in biomass to monitor forest carbon losses and gains (Hansen et al., 2013b). When combined with AGB estimates from VOD, these allow quantifying and attributing changes in biomass to human vs. natural sources (Harris et al., 2016; 2021), as discussed in Sections 5.7 and 5.8.

## 5.5 *Progress in Modelling Forest Land Use Change*

For several decades, estimates of emissions from land-use change by the research community were based primarily on a book-keeping model using a stock-change approach (Houghton and Nassikas 2017). This approach combines information on forest area and deforestation rates from the FAO Forest Resource Assessment (FRA) and other sources. Carbon fluxes are based on country-level surveys of vegetation and soil carbon density for different forest ecosystems and response curves for temporal carbon dynamics following disturbance and recovery, e.g., legacy fluxes and regrowth. More recently, satellite-based biomass data are being used in book-keeping approaches (e.g., Rosan et al., 2021) to more accurately reflect spatial variation in carbon stocks, and implicitly include the influence of environmental factors.

Process-based models offer an alternate, complementary approach to estimate land-use emissions. The first generation of DGVMs have been extensively used in land carbon-cycle research (Sitch et al., 2015). They typically build upon a detailed representation of leaf photosynthesis coupled to a water balance scheme and simulate gross fluxes, GPP,  $R_a$ , NPP, and carbon stocks in vegetation and soils. A new generation of DGVMs include more biological processes. These include nutrient cycling (N and now P), and more comprehensive representations of vegetation demography (Smith et al., 2001; Argles et al., 2020) with explicit representation of mortality, plant succession and temporal development of age/size classes, and explicit disturbance (e.g., fire-enabled DGVMs, Rabin et al., 2017). This enables comprehensive assessments of the impact of land management on the carbon cycle (e.g., forest growth and harvest), and separates effects of environmental and human drivers on the land carbon sink (Houghton et al., 2012). McGuire et al. (2001) pioneered the use of DGVMs in factorial experiment design to enable attribution of the land carbon sink to processes, CO<sub>2</sub>, Climate and Land Use and Land Cover Change (LULCC) over the 20<sup>th</sup> century.

A similar protocol is adopted for the DGVMs in the annual GCB assessment (Friedlingstein et al., 2021). The DGVM land-use flux is calculated as the difference between two simulations (1700 to present-day): the first (S2) with varying observed historical CO<sub>2</sub> and climate but fixed pre-industrial LU and a second (S3) with all three varying (CO<sub>2</sub>, climate and LUC). However, the natural vegetation in S2 is affected by temporal changes in environmental factors (e.g., CO<sub>2</sub> fertilization) - not included in static carbon density maps employed by book-keeping models. One would expect an additional carbon sink in forests relative to faster-turnover cultivated systems, which would be lost with deforestation; this foregone sink is referred to as the Loss of Additional Sink Capacity (Gitz and Ciais, 2003, Sitch et al., 2005; Gasser et al., 2020; Pongratz et al., 2014). Obermeier et al. (2021) has attempted to reconcile these methodological differences between the DGVM approach employed in GCB and book-keeping models.



More recent DGVMs updates capture more land-use change related processes, e.g., shifting cultivation (gross land-cover transitions), grazing/crop harvest and cropland management and wood harvest. Results including these newly incorporated processes suggest a substantial underestimation in land-use emissions in earlier DGVMs, with implications for the magnitude of the natural land sink, given that the net land sink is constrained (Arneth et al., 2017). Recent attempts to reconcile DGVMs estimates with country reporting of anthropogenic forest CO<sub>2</sub> sinks address conceptual differences in definitions of anthropogenic land fluxes between DGVMs (used in IPCC) and national GHG Inventories (Grassi et al., 2018).

### 5.6 Net Ecosystem Exchange from Atmospheric Measurements and Inverse Models

As noted in Section 3, top-down atmospheric inverse models have been used to study the land carbon cycle for more than 40 years. Early in this period, when there were only a few dozen ground-based stations, these flux inversions focused on continental to regional scales, with uncertainty increasing for smaller scales (Kaminski and Heimann, 2001; Chevallier et al., 2010). As the ground-based and airborne in situ network has expanded, its data have been used support flux estimates at regional scales for well-sampled regions, such as Europe (Monteil et al., 2020; Petrescu et al., 2021).

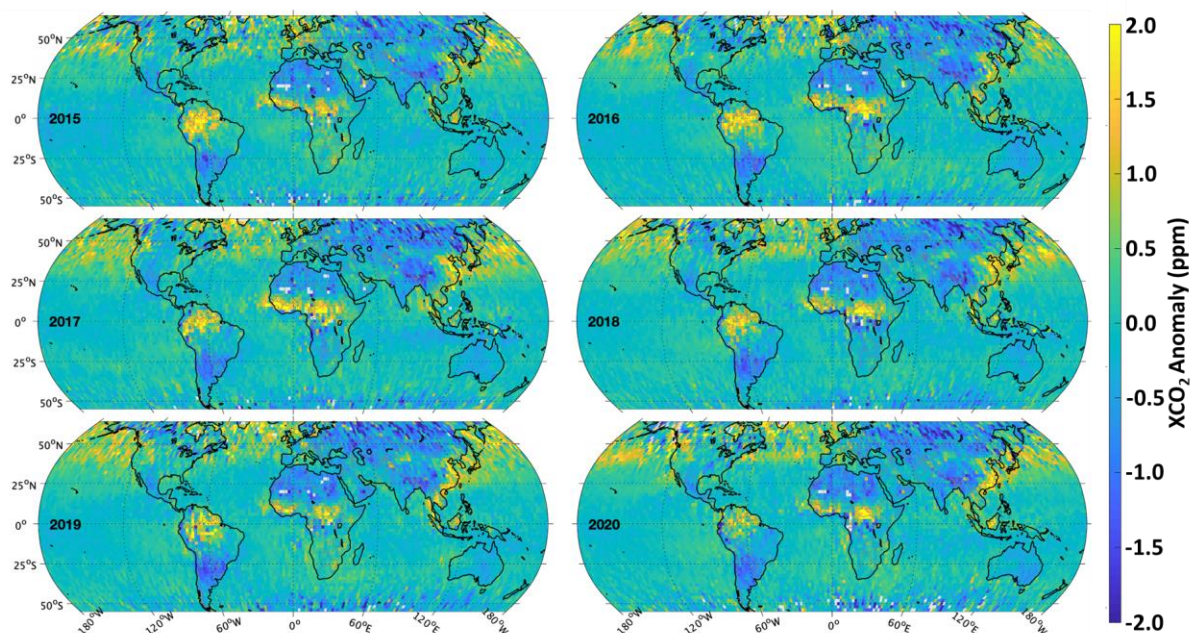


**Figure 13.** Maps of annually-averaged XCO<sub>2</sub> anomalies derived from OCO-2 XCO<sub>2</sub> estimates from 2015 - 2020. Positive anomalies (yellow) indicate regions that have XCO<sub>2</sub> values that are persistently higher than their surroundings while negative anomalies (blue) indicate regions where XCO<sub>2</sub> is lower than in the surrounding areas. (Updated from Hakkarainen et al., 2019 with the OCO-2 v10 product).

Space-based remote sensing estimates of XCO<sub>2</sub> have dramatically improved the spatial and temporal resolution and coverage of the atmospheric CO<sub>2</sub> field, enabling studies at much finer spatial and temporal scales. For example, Hakkarainen et al. (2016; 2019) processed OCO-2 XCO<sub>2</sub> observations to filter out the annual growth rate and seasonal cycle to yield maps of

temporally-persistent spatial anomalies (Figure 13). Here, positive XCO<sub>2</sub> anomalies are associated with persistent sources while negative XCO<sub>2</sub> anomalies are interpreted as persistent sinks. When averaged over the annual cycle, tropical land regions, including the Amazon, north equatorial Africa, and equatorial Asia have positive XCO<sub>2</sub> anomalies while, mid- and high-latitude land regions of Asia, North and South America have negative XCO<sub>2</sub> anomalies. The positive anomalies in east Asia and western Europe include contributions from intense fossil fuel combustion, biomass burning or other human activities. The positive anomalies over the north Pacific and Atlantic Oceans are just downwind of persistent CO<sub>2</sub> sources in east Asia and North America, respectively, indicating the effects of transport rather than local sources.

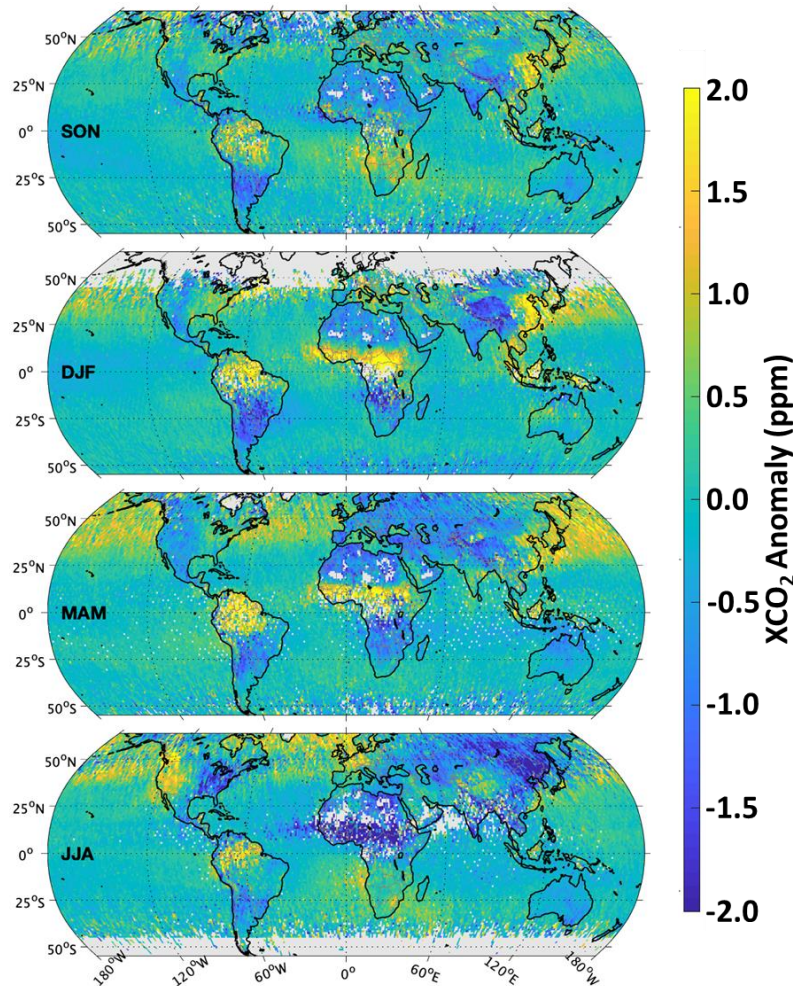


**Figure 14.** Maps of seasonally-averaged XCO<sub>2</sub> anomalies derived from OCO-2 XCO<sub>2</sub> estimates from 2015 – 2020, including September-October-November (SON), December-January-February (DJF), March-April-May (MAM) and June-July August (JJA). (Updated from Hakkarainen et al., 2019 with the OCO-2 v10 product).

Seasonally averaged maps (Figure 14) show that the XCO<sub>2</sub> anomalies over north equatorial Africa transition from negative values during June-August to positive values from December-May. In contrast, the Amazon appears to exhibit mostly positive XCO<sub>2</sub> anomalies throughout the year during this period. Strong negative XCO<sub>2</sub> anomalies over mid- and high



latitudes in the northern hemisphere in JJA are associated with strong uptake by the land biosphere. These negative anomalies even extend across heavily-industrialized east Asia during this season, as biospheric uptake temporarily balances anthropogenic emissions. The variations across North America are also noteworthy, with the western regions showing positive anomalies during JJA, while the mid-west and eastern United States shows strong negative anomalies. While none of these features are especially surprising, this is the first time that we have been able to quantify the atmospheric CO<sub>2</sub> distribution on sub-regional scales over the entire globe on seasonal to annual time scales.

These space-based XCO<sub>2</sub> estimates are being combined with ground-based and airborne in situ CO<sub>2</sub> measurements and analyzed with atmospheric inverse modeling systems to quantify sub-regional to continental changes in the land biosphere. Early efforts exploited the global coverage provided by GOSAT to constrain regional-scale CO<sub>2</sub> flux estimates. These investigations demonstrated the value of the improved coverage provided by the GOSAT data for reducing flux uncertainties, particularly in the tropics, where there are few in situ observations (e.g., Maksyutov et al., 2013; Deng et al., 2016; Byrne et al., 2020b). However, other inverse modeling showed large differences between top-down and bottom-up flux estimates in some regions, revealing limitations of this approach (e.g., Kondo et al., 2015; Reuter et al., 2014). For example, an unrealistically large sink in Europe (Reuter et al., 2014; Kaminski et al., 2017) has been ascribed to biases in the seasonal coverage (Houweling et al., 2015) and/or in the XCO<sub>2</sub> estimates themselves (Scholze et al., 2019).

As the accuracy, resolution and coverage of the atmospheric CO<sub>2</sub> measurements and inverse modeling systems have improved, the spread between the global land flux estimates from these top-down methods has decreased from  $> 3 \text{ Pg C yr}^{-1}$  to  $\sim 1 \text{ Pg C yr}^{-1}$  (i.e., Kondo et al., 2020). Significant improvements have been achieved on regional scales as well (Zhang et al., 2021). An ensemble of six inverse models constrained by in situ data used in the 2020 GCB (Friedlingstein et al., 2021) indicates that the Northern extratropics ( $>30^\circ\text{N}$ ) were indeed the main contributor to the global NEE land sink between 2010 and 2019, with a amplitude of  $-2.9 \pm 0.6 \text{ Pg C yr}^{-1}$ . This is slightly stronger than the northern extra-tropical land sink derived from DGVMs,  $-2.3 \pm 0.6 \text{ Pg C yr}^{-1}$ . On shorter time scales, an ensemble of nine inverse models constrained by OCO-2 v9 data (Peiro et al., 2022) indicates that the northern extratropical land sink increased from  $-2.5$  to  $-3 \pm 0.25 \text{ Pg C yr}^{-1}$  between 2015-2016 and then decreased to  $-2 \pm 0.25 \text{ Pg C yr}^{-1}$  in 2017 and to  $-1.75 \pm 0.25 \text{ Pg C yr}^{-1}$  in 2018. When this ensemble is constrained by in situ data, the results from 2015-2016 are the same, but the sink increases to  $-2.75 \text{ Pg C yr}^{-1}$  in 2017 and returns to  $-2.5 \pm 0.25$  in 2018. The source of the CO<sub>2</sub> data used to constrain the inverse models explains some of the remaining differences between the top-down and bottom-up results.

Meanwhile, recent inverse modeling intercomparisons indicate that tropical land is not a significant net sink for atmospheric CO<sub>2</sub> (Gaubert et al., 2019; Palmer et al., 2019; Crowell et al., 2019; Friedlingstein et al., 2021; Peiro et al., 2022). Gaubert et al. (2019) find near neutral tropical uptake for 2009-2011, but note that given reported emissions from deforestation, this result indicates substantial uptake by intact tropical forests. Friedlingstein et al. (2020) also use an inverse model ensemble constrained by in situ data and find that tropical land was roughly in total carbon balance between 2010 and 2019.

Inverse model ensembles constrained by space-based XCO<sub>2</sub> estimates indicate that the tropics are now a net source of CO<sub>2</sub> as the XCO<sub>2</sub> anomaly maps (Figures 13, 14) suggest. For example, Peiro et al. (2022) find that tropical land was strong source ( $1.0$  to  $2.0 \text{ Pg C yr}^{-1}$ ) during

the 2015-2016 El Niño, supporting earlier results by Crowell et al (2019) and Palmer et al. (2019), but then returned to near neutral conditions ( $-0.5$  to  $0.5 \text{ Pg C yr}^{-1}$ ) in 2017 and 2018. These results support other recent studies that attribute these net emissions to deforestation, forest degradation, drought and other factors (i.e., Aragão et al., 2018; Wigernon et al., 2020; Qin et al., 2021, Gatti et al., 2014; 2021). However, given the sparseness of the tropical in situ  $\text{CO}_2$  network and the shortness of the satellite X $\text{CO}_2$  data records, it is too soon to determine whether this represents a slow recovery from the intense 2015-2016 El Niño, or if tropical land has permanently transitioned from a net sink to a net source of  $\text{CO}_2$ .

A key set of quantities that explain some of the bias between the top-down and bottom-up estimates are the lateral fluxes of carbon, which are implicitly included in net land-atmosphere fluxes by inversions, but not in those estimated by DGVMs (Ciais, Yao et al., 2020; Ciais et al., 2022). When adjusted for lateral fluxes, the top-down and bottom-up estimates show good agreement on the long-term average land sink, but still show disagreements in the regional partitioning and inter-annual variability of the land sink (Bastos et al., 2020). Several processes contribute to the challenges in constraining the land-sink: large uncertainty in the regional partitioning of fluxes between individual inversions, the representation of land-use change and management in DGVMs, and the ability of DGVMs to simulate responses to disturbances and extreme events such as droughts or fires (Friedlingstein et al., 2020; Bastos et al., 2020).

However, flux inversions provide an integrated estimate of the net surface fluxes, including contributions from fossil fuel burning, land-use change and management, disturbances,  $\text{CO}_2$  outgassing, etc. This makes attribution of inverse model-based fluxes to specific sectors (e.g., separating between natural and anthropogenic fluxes or fossil fuel and LUC contributions) challenging, especially given the high uncertainty associated with some of these terms. One approach for addressing this limitation combines geostatistical inverse models with MERRA-2 estimates of air and soil temperature, precipitation, soil moisture, humidity, PAR and other variables to identify the processes driving interannual variability (IAV) in the observed  $\text{CO}_2$  fluxes (Chen et al., 2021a, b). Their results from OCO-2 observations indicate that the tropical grassland biome, including grasslands, savanna, and agricultural lands, contribute as much to IAV as the tropical forests and that temperature and precipitation produce comparable contributions to IAV. This supports the conclusion of Ahlström et al. (2015), but Chen et al. (2021b) note that these results contradict those from most the DGVMs included in the TRENDY project (Sitch et al., 2015; Friedlingstein, et al., 2019; 2020; Piao et al., 2020b).

## **5.7 Long-term Trends in the Land Sink**

Multiple lines of evidence support an increasing sink in the terrestrial biosphere. In innovative studies using atmospheric  $\text{CO}_2$  and  $\delta^{13}\text{C}$  measurements, Keeling et al. (1989) pointed out an increase in the retention of  $\text{CO}_2$  emitted from fossil fuel combustion, which they attributed to an increasing sink in the terrestrial biosphere. These results have been supported by subsequent updates (Keeling et al., 2001) and additional studies using different approaches (McGuire et al., 2001; Khatiwala et al., 2009; Ballantyne et al., 2012; Le Quéré et al., 2009; 2013; 2018a,b; Friedlingstein et al., 2019; 2020; 2021). While the existence of an increasing global land sink is undisputed (Friedlingstein et al., 2020, Fernández-Martínez et al., 2019), the location and drivers of the inferred increase in the past decades remain a matter of debate (Casperson et al., 2000; McGuire et al., 2001, Pacala et al., 2001; Nabuurs et al., 2013; Piao et al., 2009). These include the fertilization effects of elevated  $\text{CO}_2$  (McGuire et al., 2001),

increased nitrogen deposition in northern latitudes (Fernández-Martínez et al., 2019), agricultural intensification (Zeng et al., 2014), lengthening of the growing seasons in the northern hemisphere and/or vegetation expansion (Forkel et al., 2019) and forest expansion (Casperson et al., 2000) and management (Nabuurs et al., 2013; Erb et al., 2018). Disentangling the compound effects of CO<sub>2</sub> fertilization, i.e., the increased rate of photosynthesis resulting from increased levels of CO<sub>2</sub> in the atmosphere, and increased temperature and drought, is, however, challenging. Here, we discuss the observational evidence for some of these effects.

The global AGB dataset compiled from microwave VOD measurements by Liu et al. (2015) indicate no statistically significant global trend in AGB ( $-0.07 \text{ Pg C yr}^{-1}$ ) from 1993-2012. However, they do show large losses over tropical forests ( $-0.26 \text{ Pg C yr}^{-1}$ ) that were offset by net gains ( $0.13 \text{ Pg C yr}^{-1}$ ) over temperate and boreal forests. More recently, Xu et al. (2021) used forest inventory plots, airborne laser scanning (ALS) data and satellite lidar inventories of forest height to estimate global AGB and adopted allometric relationships to derive below ground carbon stocks. They conclude that globally, woody carbon stocks are increasing at  $0.23 \pm 0.09 \text{ Pg C yr}^{-1}$ . Regions with carbon gains are located in western conifer and boreal forests of North America, tropical forests in Africa, subtropical forests in eastern China, and the boreal forests of eastern Siberia. Tropical forest and subtropical dry forest and savannah lands gained carbon at a rate of  $0.09 \pm 0.04 \text{ Pg C yr}^{-1}$ . Temperate and boreal forests had accumulation at rates of  $0.10 \pm 0.03$  and  $0.04 \pm 0.02 \text{ Pg C yr}^{-1}$ .

Satellite observations collected since the 1980s indicate a significant global increase in the area covered by green vegetation, or “greening” (IPCC, 2014; Zhu et al., 2016; Piao et al., 2020b; Cortés et al., 2021). Zhu et al., (2016) used long-term satellite observations of LAI to study this greening trend from 1982-2009. They report a persistent, widespread greening over 25-50% of the global vegetated area. In a more recent study, Piao et al. (2020b) use a combination of vegetation indices (NDVI, LAI, EVI, and NIRv) to quantify global greening between the early 1980s and 2018. They conclude that globally, ~34% of vegetated land shows signs of greening over this period (Figure 15). They also note significant greening over China and India, which they attribute primarily to afforestation and agricultural intensification.

Both studies also note that a small fraction (3 – 4%) of vegetated land experienced browning (less greening) between 1982 and 2014. Piao et al. (2020b) note that there is considerable debate about the relative roles of greenness and brownness over the Amazon due to saturation effects in dense vegetation and contamination by clouds and aerosols. However, they conclude that about 5% of the area has experienced browning, which they attribute to drought, heat stress and human activities, but concede that the relative roles of these processes are not well resolved by these data. In the Arctic, browning is seen over ~3% of the land area, with North American boreal forests exhibiting browning areas nearly 20 times larger than the Eurasian boreal forests (Piao et al., 2020b).

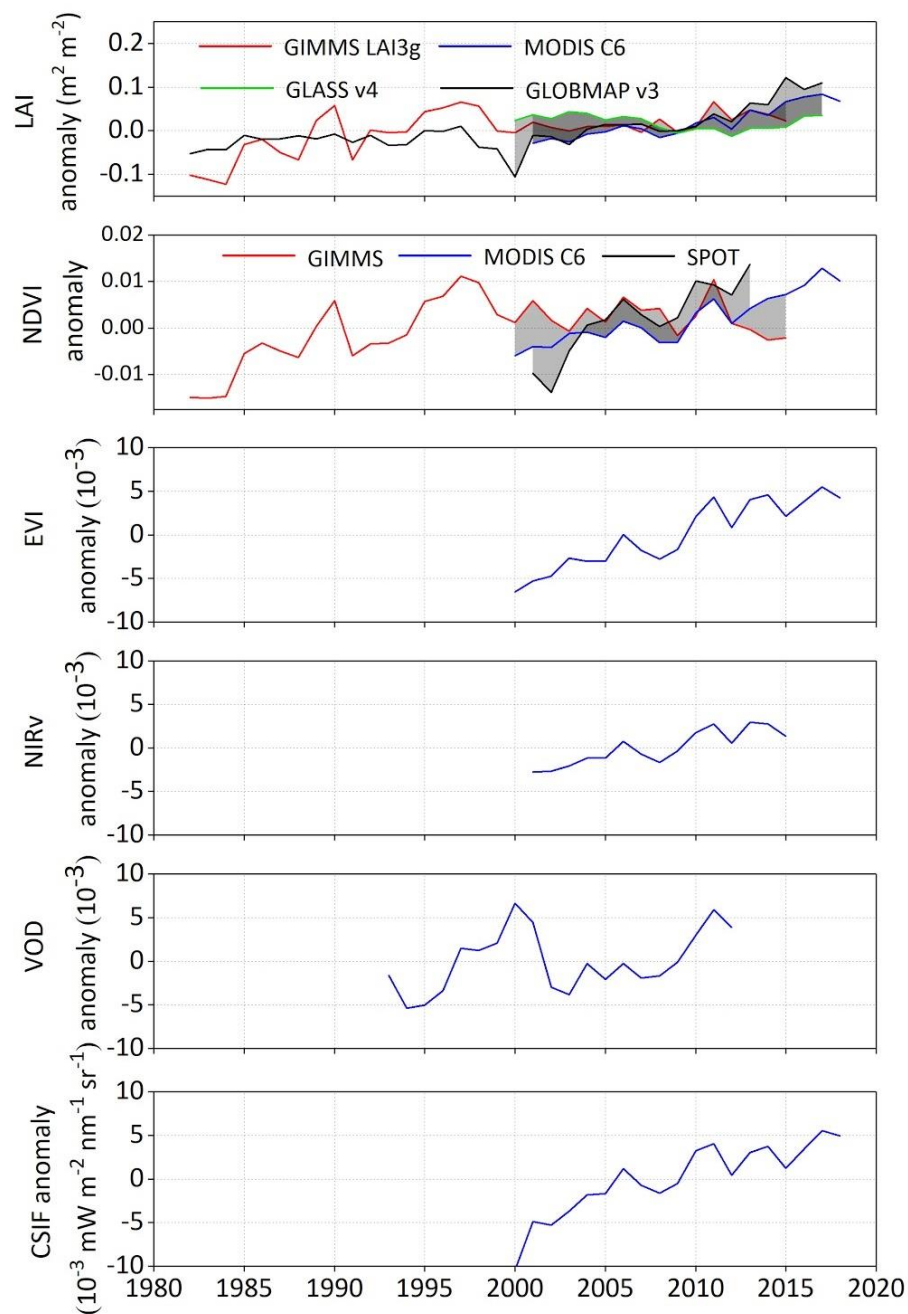


**Figure 15.** Changes in satellite- derived global vegetation indices, including anomalies in the normalized difference vegetation index (NDVI), Enhanced Vegetation Index (EVI), near-infrared reflectance of vegetation (NIRv), vegetation optical depth (VOD) and contiguous solar- induced fluorescence (CSIF) (Data: Piao et al., 2020b.)

At mid- and high-latitudes, bottom-up and top-down models constrained by space-based remote sensing measurements largely reinforce the in situ results, showing a long term increase in the CO<sub>2</sub> seasonal cycle amplitude (SCA) and indicate that mid-latitude and boreal forests are strong net sinks of CO<sub>2</sub> (Keeling et al., 1996; Graven et al., 2013; Jeong et al., 2018; Byrne et al., 2018; 2020a; Piao et al., 2020b; Liu et al., 2020a). It is important to note that estimates derived

using the stock change approach still differ by as much as a factor of two or three in the rates quoted above (Xu et al., 2021, see their Table 2). With increasing data availability, new satellites (e.g., BIOMASS expected to launch in 2023, and the GEDI instrument on board of the ISS) are expected to reduce uncertainties and increase consistency in the global estimates.

Based on the results presented above, two things can be stated with relative certainty: (1) in the tropics, LUC approximately balances the land sink (Grace et al., 2014, Gatti et al., 2021) and (2) in the northern extratropics, a sink exists that is still growing. The mechanisms driving these long term trends are explored in the following two sub-sections.

#### 5.7.1 *Mechanisms Driving Long-Term Trends in the Tropical Land Sink*

Long-term changes in the land sink are typically attributed to CO<sub>2</sub> fertilization, secular trends in nutrient and water availability, temperature changes, disturbance or other factors, but the relative roles of these processes are often challenging to diagnose because they often work in concert (e.g., Bastos et al., 2019; Piao et al., 2020a; Hubau et al., 2020; Liu et al., 2020a; Gampe et al., 2021). All of these factors have been considered in studies of long term trends in the tropical forest sink. For example, Hubau et al. (2020) assess the carbon sink in intact African and Amazon forests (Figure 16) and conclude that while the African sink strength showed no trend (0.66 Mg C ha<sup>-1</sup> yr<sup>-1</sup>), the Amazon forest sink slowed down -0.034 Mg C ha<sup>-1</sup> yr<sup>-2</sup> between 1983 and 2010, citing Brien et al. (2015). The results presented in Figure 16 show that this trend has persisted. Hubau et al. (2020) attribute the downward trend in sink strength by intact forests primarily to higher temperature and droughts, leading to increased tree mortality. DGVMs simulate strong CO<sub>2</sub>-induced sinks in moist tropical forests, counterbalanced by a negative effect of climate change and variability. An improved representation of mortality processes is needed in DGVMs, particularly those relating to drought response.

Other studies have focused on the differing impacts of increasing temperature on photosynthesis and heterotrophic respiration in the tropics. For example, Doughty and Goulden (2008) show that on short time scales, the efficiency of photosynthesis decreases beyond a critical temperature, while that of heterotrophic respiration continues to increase. Mau et al. (2018) suggest that many species of tropical trees may be especially sensitive to these effects. Possible evidence for this behavior was recently obtained by Duffy et al. (2021) using FLUXNET data, albeit with the caveat that CO<sub>2</sub> effects on GPP were not considered in their temporal extrapolation. Meanwhile, process-based models provide conflicting insights into the role of plant physiological processes including plant thermal responses and acclimation (McGuire et al., 2001; Friedlingstein et al., 2006; Booth et al., 2012, Mercado et al., 2018). There is also little consensus on how these changes will progress on longer time scales, when heterotrophic carbon limitation on microbial decomposition may also start playing a role (Soong et al., 2019).

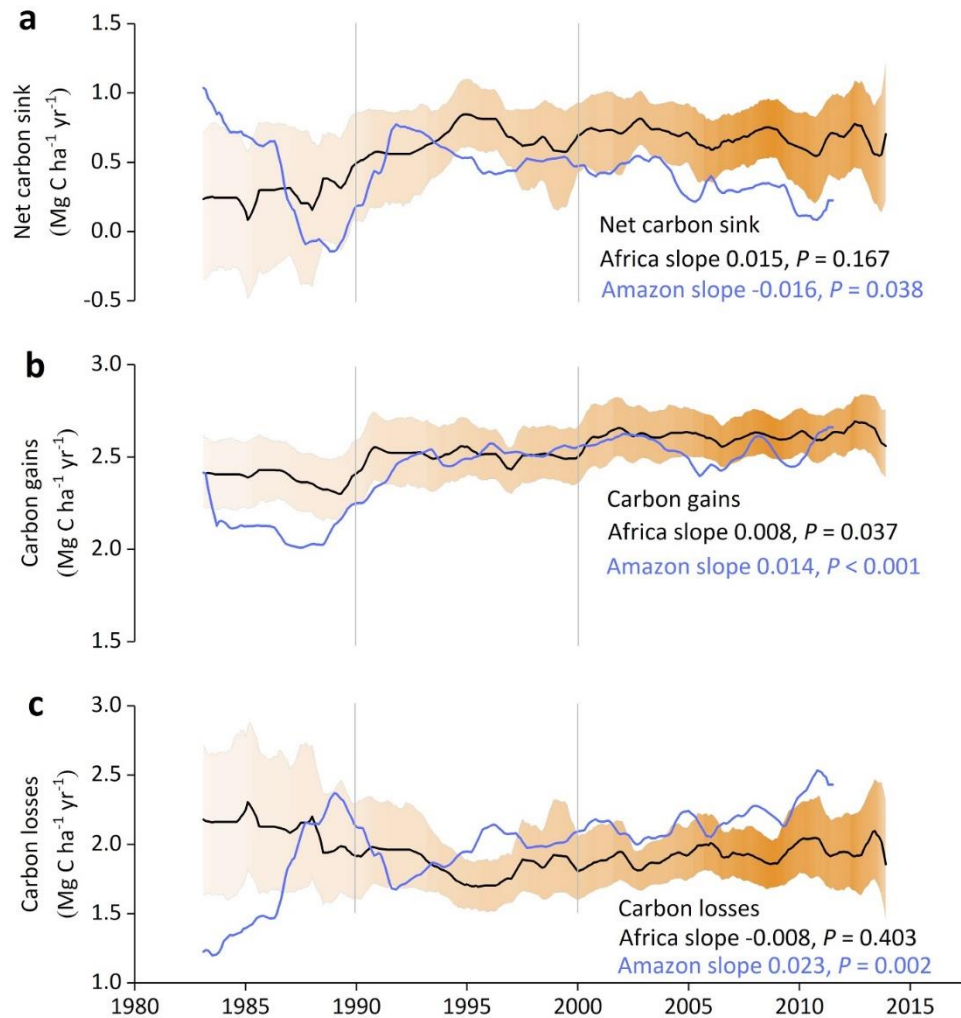


**Figure 16.** Time series of carbon dynamics from structurally-intact old-growth tropical forests in Africa and Amazonia from 1985 through 2015 (Data: Hubau et al., 2020). Note, the net carbon sink in Panel, a, refers to the net of two processes, carbon gains (productivity) and carbon losses (mortality), over intact tropical forests only. To obtain a net carbon sink estimate for the whole-region to compare with atmospheric measurements and inversions (e.g., Gatti et al., 2021), in addition to the intact forest sink, fluxes associated with disturbance (deforestation, degradation through fire and selective logging), secondary forest regrowth and land-use fluxes (fluxes over crop and pasture), must be considered.

### 5.7.2 Mechanisms Driving Long-term Trends in the Extratropical Land Sink

In the extratropics, studies have focused on identifying the mechanisms responsible for the changes in greening, seasonal cycle amplitude (SCA) and net  $\text{CO}_2$  uptake across the high-latitude northern forests since at least the 1960s. Unlike the tropics, where heat-related increases in respiration and water stress are key growth limiters, here, the forests have adequate water, but their growth is thought to be limited primarily by low light levels, low summer temperatures and short growing seasons (Song et al., 2018). Therefore, vegetation cover and phenology changes in response to warming trends and the effects elevated  $\text{CO}_2$  have been identified as the likely

drivers of increase in SCA (Graven et al., 2013; Forkel et al., 2019; Piao et al., 2017). At mid-latitudes, Zhu et al. (2016) and Piao et al. (2020b) analyzed their greenness time series with ensembles of DGVMs to identify the primary drivers of the observed increases. Both studies conclude that CO<sub>2</sub> fertilization is the primary driver of global greening since the 1980s. However, they concede that other processes dominate on regional scales. For example, Piao et al. (2020b) attribute the enhanced greening over China and India primarily to afforestation and agricultural intensification.

To explain the mechanisms behind the enhanced SCA at higher northern latitudes, Keenan and Riley (2018) used observations of fAPAR collected between 1982 and 2012 to characterize the relationship between maximum annual foliage cover and summer warmth index. They attribute these changes to the recent warming (reduced spatial extent of temperature limitation) rather than CO<sub>2</sub> fertilization. In another observation-based study, Liu et al. (2020a) analyzed data from a variety of sources to determine the extent to which temperature changes alone could account for the long-term trends in SCA and CO<sub>2</sub> uptake of high latitude northern forests. They analyze space-based observations of SIF and XCO<sub>2</sub> from OCO-2 to estimate monthly mean GPP and NEE, respectively, at 4°×5° resolution for 2015-2017 and derive total ecosystem respiration, TER, as the difference between NEE and GPP. They fit simple exponential functions to the observed temperature dependence of GPP/PAR and TER and then hindcast spatially-resolved, monthly mean estimates of these variables to produce a time series spanning 1960 to 2014. They find that growing season mean temperature (GSMT) is the dominant driver of fPAR and GPP, explaining 70% of the observed spatial and temporal variability at latitudes between 50N and 75N over this time period, accounting for a 60% to 70% of the observed ~20% growth in SCA.

While these results support the conclusions of Keenan and Riley (2018), they appear to contradict the studies by Zhu et al. (2016) and Piao et al. (2020b), which analyzed greenness time series with ensembles of DGVMs to identify the primary drivers of the observed greening trends. Both studies conclude that CO<sub>2</sub> fertilization is the primary driver of global greening since the 1980s. Other studies based on atmospheric data and biogeochemical models have also pointed out a key role of CO<sub>2</sub> fertilization in SCA trends (Forkel et al., 2019; Thomas et al., 2016; Bastos et al., 2019; Piao et al., 2017).

A noteworthy difference between the observation-based studies and the model-based studies is the relationship between SCA and temperature adopted at high northern latitudes. While Keenan and Riley (2018) and Liu et al. (2020a) found that fPAR, NEE, and SCA are positively correlated with temperature at 50N-75N, model-based studies (e.g., Bastos et al., 2019) find a negative relationship between SCA and temperature during the growing season at latitudes > 40N, which they attribute to moisture deficits and fires. This would be consistent with browning trends at high latitudes, attributed to disturbances such as fires, harvesting and insect defoliation (Beck and Goetz, 2011; Cortés et al., 2021). Regional differences across the arctic and boreal regions might also play a role. For example, North American boreal forests exhibit browning areas nearly 20 times larger than the Eurasian boreal forests (Harris et al., 2016; Piao et al., 2020b). Large-scale fire disturbances and insect infestation such as those from the bark beetle (Hlásny et al., 2021) have also been seen in browning areas in temperate regions in the past decade. Peñuelas et al. (2017) identified recent signs of a slow-down of SCA increase at Barrow, pointing to a limitation of the positive effect of temperature in stimulating northern hemisphere CO<sub>2</sub> uptake, possibly due to increasingly negative impacts of weather extremes and



disturbances. This lack of consensus on the relative roles of temperature, CO<sub>2</sub> fertilization and disturbance at high latitudes must be resolved, given their implications for the future evolution of this rapidly changing part of the land carbon cycle.

## 5.8 *Patterns and Drivers of Interannual Variability in the Land Sink*

In spite of the steady increase in fossil fuel CO<sub>2</sub> emissions over recent decades, the annual growth rate in atmospheric CO<sub>2</sub> varies markedly from year to year (Ballantyne et al., 2012; Piao et al., 2020a). The global growth rate of atmospheric CO<sub>2</sub> positively correlates with temperature. This relationship has been used to diagnose and constrain the future climate-carbon cycle feedback (Cox et al., 2013). The strong positive correlation between atmospheric growth rate and tropical temperature has been a conundrum, since the dynamics in tropical ecosystems are thought to be primarily driven by variations in moisture, i.e., dry season length and severity. Indeed, Jung et al. (2017) argue that at the local scale, the tropical carbon cycle is driven by moisture but at larger spatially scales the moisture signal is lost due to compensatory water effects (essentially there is greater spatial variability in moisture and thus regional signals counterbalance) leaving the temperature signal, which is more spatially coherent at the larger spatial scales.

Humphrey et al. (2018) challenged this conclusion showing a strong relationship between atmospheric CO<sub>2</sub> growth rate and observed changes in terrestrial water storage. Disentangling the land response to variation in temperature and water is complicated, for a variety of reasons. For example, soil-moisture-atmosphere feedbacks modify temperature and humidity, which impact vapor pressure deficit (VPD), which drive plant stomata opening and closure. Yuan et al. (2019) found that an increase in VPD reduces global vegetation growth, while Liu et al. (2020a) suggest that soil moisture dominates dryness-related stress on global productivity, using SIF as a proxy. Finally, Humphrey et al. (2021) clarified the picture, showing how global NEE variability is driven by temperature and VPD effects controlled by soil moisture.

### 5.8.1 *The Role of Climate Variability in the Interannual Variations of the Land Sink*

Large interannual variations in global NBE are attributed to modes of climate variability, e.g., the impacts of the El Niño Southern Oscillation (ENSO) in tropical and southern regions (Figure 17). Two other modes of coupled ocean-atmosphere variability in addition to ENSO influence land-atmosphere CO<sub>2</sub> fluxes over the globe. The Pacific Decadal Oscillation (PDO) impacts tropical regions and extratropical North and South American regions. The Atlantic Multidecadal Oscillation (AMO) influences CO<sub>2</sub> fluxes in Eurasia, northern North-America, and is an important influence in the Sahel and sub-tropical South American regions (Bastos et al., 2017; Zhu et al., 2017). These three modes of climate variability are thought to explain inter-annual variability (IAV) in CO<sub>2</sub> fluxes over more than 50% of the land surface (Zhu et al., 2017). Other processes, such as global cooling following large volcanic eruptions also contribute to IAV (e.g., Lucht et al., 2002; Angert et al., 2004).

In the Northern extratropics, regional modes of atmospheric variability also play a role in IAV in CO<sub>2</sub> fluxes. Dannenberg et al. (2018) showed that two leading modes of north Pacific variability controlled the onset of growing seasons over large regions in North America: the West-Pacific and the Pacific-North American patterns. In the Southern Hemisphere, in addition to ENSO, two other modes influence land carbon uptake: the Indian Ocean Dipole (IOD: Marchant et al., 2006) and the Southern Annular Mode (SAM; Marshall, 2003). Positive phases of IOD have been associated with reduced GPP and increased bushfires in Australia, and

1742 increased productivity in South Africa (Cai et al., 2009, Wang et al., 2021). Cleverly et al. (2016)  
 1743 have shown that periods when synchrony between ENSO, the IOD and the SAM occur, they  
 1744 were associated with carbon cycle extremes in Australia.

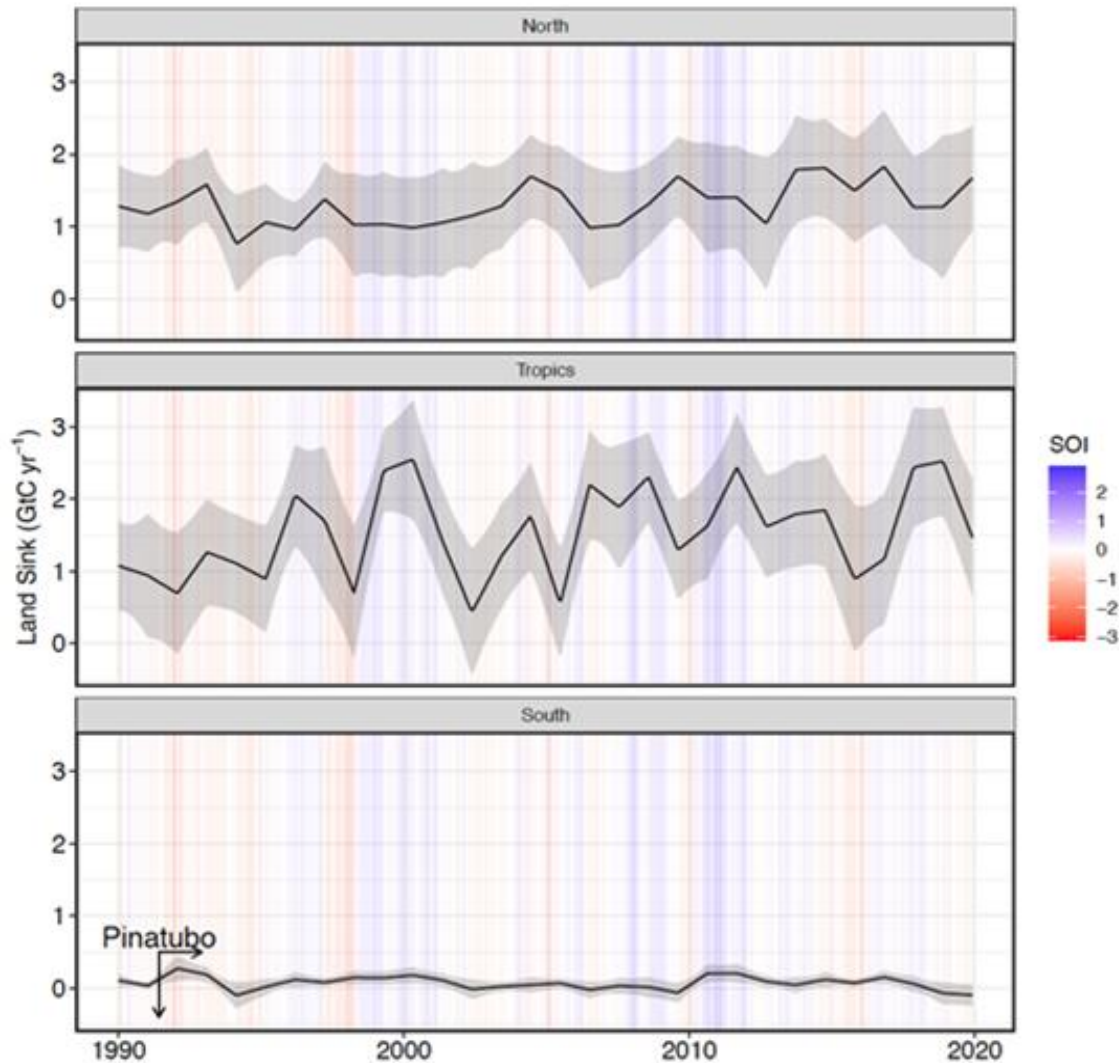


**Figure 17.** The multi-model mean land sink as derived from 14 TRENDY DGVMs for three regions and Southern Oscillation Index (SOI) between 1990 and 2020. The grey band represents 1 standard deviation. The Mount Pinatubo eruption in June 1991 in the Philippines is indicated with a vertical arrow with a horizontal arrow showing the duration of its effect on regional and global climate.

1745

1746 Extreme weather and climate conditions and associated disturbances are important  
 1747 contributors to the regional land carbon cycle (Reichstein et al., 2013; Zscheischler et al., 2014).  
 1748 While a few extremes have been found to explain 78% of IAV in GPP, they only accounted for  
 1749 8-22% of IAV in NEE (Zscheischler et al., 2014). In their study, Zscheischler et al. (2014)  
 1750 indicate that drought is the most common driver of negative extremes in GPP (>50% of the

events), followed by fires (20-30% of events). There is also evidence for an increasing impact of warm droughts on northern ecosystem productivity in recent decades (Gampe et al., 2021).

Drought is a primary driver of reductions in photosynthesis and enhanced tree mortality through hydraulic failure (Rowland et al., 2015). Major droughts in recent years have been associated to strong reductions in regional GPP and net carbon uptake (Ma et al., 2016; Wolf et al., 2016; Peters et al., 2020), in some cases even turning ecosystems from sinks to sources of CO<sub>2</sub> (Ciais et al., 2005; van der Laan-Luijkx et al., 2015). In addition to direct impacts, droughts further contribute to subsequent disturbances, e.g., by increasing fire risk or insect outbreaks, and can lead to lagged tree mortality and consequent carbon losses (Anderegg et al., 2015).

Globally, fires constitute a major flux of carbon to the atmosphere (1.3-3.0 Pg C yr<sup>-1</sup>, van der Werf et al., 2017), which is followed by regrowth sinks in the subsequent years. Even though fires can have both natural and human (e.g., deforestation, degradation and management) drivers, hot and dry conditions increase fire risk through increased fuel flammability. Therefore, all else being equal (i.e., human drivers), hot and dry periods, such as El Niño years, are associated with higher burnt area and CO<sub>2</sub> emissions, e.g., the massive burning associated in part with the 1997 El Niño over equatorial Asia. An increase in “mega- or extreme-“ wildfires and associated large carbon emissions are anticipated with continued warming (Bowman et al., 2017; 2021; van der Velde et al., 2021).

#### 5.8.2 ENSO as a Dominant Driver to Interannual Variability

El Niño is a climate mode associated with coupled atmosphere-ocean dynamics, originating in the tropical Pacific basin, with a frequency of between 2 and 7 years (McPhaden et al., 2006, p.200). At the onset of El Niño (ENSO “warm-phase”), the trade-winds weaken, reducing the upwelling along the western coast of South America, allowing the pool of warm surface water and associated convection and rainfall to move eastwards towards the central Pacific. South East Asia and eastern Australia experience a large reduction in precipitation and increased warming, and teleconnections lead to reductions in precipitation over Amazonia and east Africa (Diaz et al., 2001). Because ENSO usually peaks during the wet seasons over tropical continents, this reduced rainfall leads to longer and more severe dry seasons, decreasing photosynthesis and reducing plant carbon uptake by tropical forests.

In contrast, La Niña (ENSO “cold phase”) is associated with stronger than usual trade winds and wetter, cooler conditions that promote enhanced land carbon uptake over Equatorial Asia and Amazonia. The TRENDS in land carbon cycle (TRENDY; Sitch et al., 2015) results for the tropical latitude band (30°N-30°S) in Figure 10 illustrate the impact of El Niño and La Niña on the land carbon uptake. Because tropical forests usually account for ~50% of the global NPP by terrestrial ecosystems, these impacts are reflected in the global growth rate of atmospheric CO<sub>2</sub>. However, there is some evidence for an asymmetry in land response to ENSO (Cadule et al., 2010), whereby rainforests are less responsive to increased precipitation during La Niña than water deficit during El Niño. In addition to the asymmetry between El Niño and La Niña events, two types of ENSO can be distinguished: the “East Pacific”, described above, and the “central Pacific” type, where the warm SST pool is shifted to the central Pacific region (Kao and Yu, 2009). Central Pacific El Niño events have been associated with even stronger responses by the land carbon cycle (Dannenbergh et al., 2021).

ENSO is also the dominant mode of interannual variability in air-sea CO<sub>2</sub> fluxes (Feely et al., 1999; McKinley et al., 2004; 2017; Chatterjee et al., 2017). With the El Niño phase,

upwelling of high-DIC waters in the eastern equatorial Pacific is reduced, lowering surface ocean  $p\text{CO}_2$ . At the same time, reduced wind speeds slow gas exchange. The net effect is to substantially reduce eastern equatorial Pacific  $\text{CO}_2$  outgassing. In the La Niña phase, upwelling is enhanced and outgassing is increased. The magnitude of these variations is up to  $\pm 0.5 \text{ Pg C yr}^{-1}$ , and the type of ENSO event is a significant modulator of the flux (Liao et al., 2020). The effect on atmospheric  $\text{CO}_2$  concentration from the ocean from ENSO is thus the opposite from that from land, with a greater ocean sink during El Niño and a lesser ocean sink during La Niña.

In addition to the tropical regions, ENSO is known to influence IAV in land  $\text{CO}_2$  fluxes in some extratropical regions, especially semi-arid regions in the Southern Hemisphere such as Australia, South Africa and parts of Southern South America (Poulter et al., 2014; Bastos et al., 2013). Indeed, tropical drylands are now thought to contribute about equally or more to IAV in the global carbon cycle as humid tropical biomes (Ahlström et al., 2015; Piao et al., 2020a). These ecosystems are characterized by lower biomass and productivity than forests. Nevertheless, their vast spatial area allows them to be important to the global carbon cycle. Extra-tropical ecosystems are estimated to contribute up to 30% to global land sink IAV (Piao et al., 2020a).

While it is difficult to show the impact of climate extremes such as a strong El Niño using in situ inventory data alone, bottom-up inventories of AGB stocks compiled from microwave remote sensing observations provide a temporally denser record of such impacts. For example, contrary to the conclusions of Hubau et al. (2020), who found negligible change in the African forest, Wigneron et al. (2020) show that there was a strong “legacy effect” after the 2015-2016 El Niño event in both African and Amazonian forests, extending the duration of the response in both regions (0.9 and 0.5  $\text{Pg C}$  loss in 2014-2017 respectively). For the overall tropics, Fan et al. (2019) use VOD data from microwave sensors to show how changes in the AGB of the forests of tropical Africa and tropical Asia contributed strongly to the IAV in  $\text{CO}_2$  growth rates, but concluded that AGB in semi-arid biomes dominated the IAV in these growth rates.

### 5.8.3 The Best Observed ENSO Ever - the 2015-2016 El Niño

The record-setting 2015-2016 El Niño was the first large ENSO event for which atmospheric  $\text{CO}_2$  and SIF estimates were available at high spatial and temporal resolution from space based platforms. This data-rich perspective provided a more comprehensive description of the impacts of climate perturbations on the exchange of carbon between land and ocean reservoirs and the atmosphere on regional scales. Chatterjee et al. (2017) compared  $\text{XCO}_2$  estimates derived from Orbiting Carbon Observatory-2 (OCO-2) observations over the central and eastern tropical Pacific basin to an  $\text{XCO}_2$  climatology of this region based on observations from the Greenhouse gases Observing SATellite (GOSAT). Between March and July 2015, these comparisons reveal a 0.5 ppm decrease in  $\text{XCO}_2$  that is attributed to reductions in outgassing in the tropical Pacific Ocean (Chatterjee et al., 2017). By September of 2015, these reduced  $\text{XCO}_2$  values were replaced by 0.5 to 2 ppm increases in  $\text{XCO}_2$  that were attributed to reduced uptake and increased emissions of  $\text{CO}_2$  by tropical forests in South America, Africa and tropical Asia (Liu et al., 2017; Heymann et al., 2017; Palmer et al., 2019; Crowell et al., 2019; Figure 18).

Observations of SIF provided similar insights. Koren et al. (2018) find that SIF was strongly suppressed in late 2015 over tropical areas with anomalously high temperatures and reduced soil moisture. Their observations show that SIF fell below its climatological range starting from the end of the 2015 dry season (October), but returned to normal levels by February

2016 when atmospheric conditions returned to normal. Importantly, the impacts of the El Niño were not uniform across the Amazon basin.

Additional insight into the tropical land carbon cycle's response to the 2015-2016 El Niño was gained by comparing coincident observations of XCO<sub>2</sub> anomalies and SIF (Liu et al., 2017). Specifically, the largest positive CO<sub>2</sub> anomalies derived from the space-based XCO<sub>2</sub> estimates are seen in regions where SIF observations indicate the highest photosynthetic activity (Figure 11). This suggests that in spite of significant growth, tropical forests are now emitting more CO<sub>2</sub> than they absorb, when integrated over the annual cycle. This may be due to human activities, such as deforestation and forest degradation or climate related factors such as temperature-dependent respiration increases, drought stress, fires, and other processes.

Liu et al. (2017) find that the pan-tropical biosphere released an additional  $2.5 \pm 0.34$  Pg C into the atmosphere, or about 78% of the global total emissions of CO<sub>2</sub> from the land biosphere during the 2015-2016 El Niño compared with the 2011 La Niña year. These values are substantially larger than those inferred from ensembles of bottom-up land surface models or inverse models constrained the sparse in situ network alone (Bastos et al., 2018; Crowell et al., 2019). Liu et al. find that emissions originated throughout the tropics with  $0.91 \pm 0.24$ ,  $0.85 \pm 0.21$ , and  $0.60 \pm 0.31$  Pg C from tropical South America, tropical Africa, and tropical Asia, respectively. Although the enhanced emissions from these three regions were comparable, *different* processes appeared to dominate in each region. Fire emissions dominated over tropical Asia. Both increased respiration and fires associated with historically high temperatures dominated over tropical Africa. Increased atmospheric CO<sub>2</sub> mixing ratios over the Amazon in 2015-2016 were attributed to GPP reductions associated with drought. These results support the hypothesis that El Niño related increases in CO<sub>2</sub> growth rates are primarily due to tropical land carbon fluxes, but they show that specific mechanisms can differ from continent to continent.

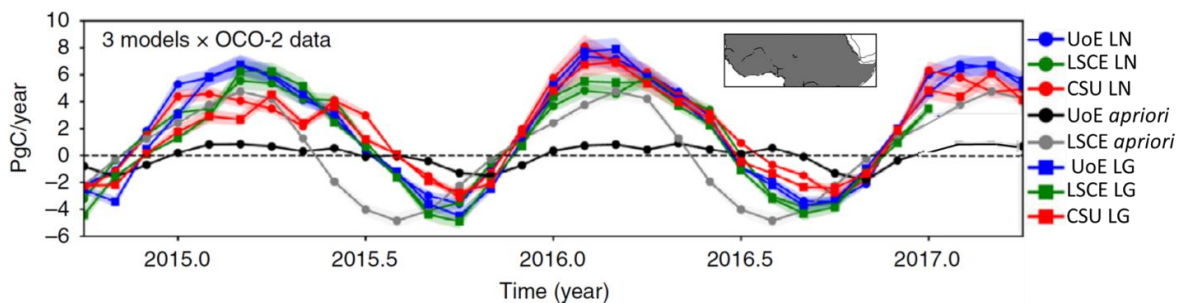


**Figure 18.** CO<sub>2</sub> fluxes from tropical northern Africa inferred from the University of Edinburgh (UoE), LSCE and Colorado State University (CSU) models constrained by in situ CO<sub>2</sub> measurements as well as XCO<sub>2</sub> data from GOSAT and OCO-2. Positive fluxes indicate CO<sub>2</sub> emissions from the land surface to the atmosphere. LN and LG denote OCO-2 XCO<sub>2</sub> measurements taken using nadir and glint observing modes, respectively. The geographical region is shown in the inset. Fluxes inferred from OCO-2 data have larger amplitudes and a larger seasonal cycle than those from in situ data (Adapted from Palmer et al., 2019).

Palmer et al. (2019) and Crowell et al. (2019) use ensembles of models to analyze in situ CO<sub>2</sub> measurements along with XCO<sub>2</sub> and SIF observations from GOSAT and OCO-2 (Figure 18). Like Liu et al., in 2015–2016, they find that the largest CO<sub>2</sub> emissions were over western

Ethiopia and western tropical Africa, where there are large soil organic carbon stores and substantial LUC. While the amplitude of the XCO<sub>2</sub> anomalies that produced these sources may have been overestimated in the early OCO-2 XCO<sub>2</sub> products used in this investigation (version 7), they clearly reveal an important source of emissions from the tropical carbon budget that is largely missing from in carbon flux inverse models constrained by *in situ* measurements alone.

It is interesting to compare the terrestrial carbon cycle's response to the two largest recent El Niño events in 1997 and 2015/16. Large fire emissions in equatorial Asia were responsible for ~1 Pg C yr<sup>-1</sup> emissions in 1997 (i.e., Page et al., 2002), yet far smaller fire emissions were estimated in 2015/16. This is largely due to the timing of the El Niño in relation to the dry season (i.e., in 2015/16 the El Niño was about 1 month later). El Niño events are associated with reductions in GPP in Amazonia and a lagged increase in respiration (Braswell et al., 1997). This is likely related to the lagged mortality associated with forest degradation, and thus respiration from the larger necromass pool. More generally, forest degradation is becoming a larger carbon source than deforestation, with highest ground-level forest fires associated with drought years.

As the 2015-2016 El Niño transitioned to a weak La Niña in 2017 and then to more neutral conditions in 2018, OCO-2 XCO<sub>2</sub> estimates indicate that tropical forests, once thought to be significant net sinks of CO<sub>2</sub> (Pan et al., 2011; Sellers et al., 2018) may now be net sources (Palmer et al., 2019; Crowell et al., 2019; Peiro et al., 2022). The atmospheric inversions support the inferences from XCO<sub>2</sub> anomaly maps (Hakkarainen et al., 2016; 2019; Figures 13, 14) which show positive XCO<sub>2</sub> anomalies over tropical forests with amplitudes of 1-2 ppm above the background since 2015. For the Amazon, both the spatial extent of the positive anomaly and the amplitude of the inferred source were greater during the 2015–2016 El Niño (~0.5 Pg C yr<sup>-1</sup>) than in later years (0.1-0.2 Pg C yr<sup>-1</sup>), but both indicate that this region has been a net source from season to season and from year to year since 2015. These conclusions are consistent with results inferred from *in situ* CO<sub>2</sub> profiles described by Gatti et al. (2021), which indicate that the Amazon has been a source of CO<sub>2</sub>, rather than a sink since 2010.

Positive XCO<sub>2</sub> anomalies over tropical Africa and Southeast Asia are seen on annual time scales (Figures 13). However, tropical African fluxes are negative during June-July-August (Figure 18), indicating that this region becomes a weak sink during that season (Palmer et al., 2019). These conclusions are supported by some satellite-based aboveground biomass studies (Baccini et al., 2017; Wigneron et al., 2020), but are inconsistent with plot-based studies (Pan et al., 2011; Hubau et al., 2020), which conclude that tropical forests are absorbing less CO<sub>2</sub>, but are still a net sink of carbon.

## **5.9 Observations Needed to Advance Understanding of Trends in the Land Carbon Sink**

The overall picture that emerges from recent observations of AGB stocks is that the classical sinks in the tropical humid forests are slowly losing strength, with these changes amplified by deforestation. In extra-tropical areas, greening has taken place due to afforestation, increased agriculture and longer growing seasons. In some parts of the Arctic and boreal regions, browning, i.e., a loss of vegetation activity, is increasing. These trends provide the fragile background for a still slowly increasing land uptake. The underlying causes for these increases are complex and consist of interacting processes of CO<sub>2</sub> fertilization, nutrient and water availability compounded by variability and secular changes in climate. On top of this, the impact of human activities including deforestation, afforestation and intensifying agriculture are additional complications.

This myriad of interacting processes complicates predictions of the future trajectory of the terrestrial sink in a warming climate. Until now, the sink has grown in harmony with increased fossil fuel emissions with the result that the airborne fraction has remained remarkably constant over the past 60 years or so. Theoretical and empirical evidence, such as that summarized in this paper, suggests that the sink may stop growing at some point in the future as water and nutrient shortages will start to impede increased growth.

#### 5.9.1 *Linking Stocks and Fluxes with Bottom-up Measurements and DGVMs*

One factor that has impeded progress in the analysis of trends inferred from AGB stocks is they are not well represented in the current generation of DGVMs. For example, Sitch et al. (2015) use an ensemble of nine DGVMs to study global and regional processes and trends in the land sink for a period extending from 1990 - 2009. They conclude that for this period, the global land sink is increasing, led by CO<sub>2</sub> fertilization of plant production, with the largest increases seen in the natural ecosystems of the tropics. They find no significant trend in northern land regions. More recent studies with updated versions of DGVMs now estimate increasing trends in the Northern Hemisphere land sink, although with large spread across models (Ciais et al., 2019; Fernández-Martínez et al., 2019) and regional mismatches with observation-based estimated (Bastos et al., 2020).

Fortunately, advances in bottom-up observation capabilities and modeling tools are coming on line to facilitate more comprehensive and responsive monitoring and analysis of the land carbon cycle. Ground-based estimates of stocks and fluxes will continue to provide the most accurate and site-specific information. However, remote sensing observations from airborne and space-based active and passive sensors and modeling tools will play an increasingly important role for upscaling these results to yield useful constraints on regional to global scales. While new space-based datasets provide an increasingly diverse set of measurements to monitor the land-surface with high spatial and temporal resolution, long-term in situ datasets still provide crucial information to properly constrain patterns and drivers of long-term trends and inter-annual to decadal variability.

#### 5.9.2 *Space-based Estimates of Fluxes and Stocks*

Xiao et al. (2019) review the evolution of remote sensing observations of terrestrial carbon stocks over the past 50 years, spanning the electromagnetic spectrum from the visible, infrared, and microwave. They then review the methods being used to analyze the observations to yield quantitative estimates of carbon stocks and fluxes, including vegetation indices, SIF, light use efficiency models, DGVMs, as well as data driven (including machine learning) techniques. Xiao et al. discuss the use of these data and analysis techniques to quantify the impacts of disturbances and to quantify uncertainties in carbon stock estimates, noting advances achieved by integrating in situ and remote sensing observations into progressively more advanced, process-based carbon cycle models. Looking forward, they predict substantial improvements in our ability to track AGB stocks through the use of merged datasets, such as the NASA Harmonized LandSat and Sentinel 2 (HLS) products, ultra-high resolution imaging products from QuickBird, IKONOS, and UAVs, lidar measurements from GEDI, future active microwave products from NASA's NISAR (Rosen et al., 2016), TanDEM-L and BIOMASS missions (Quegan et al., 2019).

While in situ and space-based measurements of AGB play a critical role in efforts to monitor trends in managed and natural forests, they do not have the sensitivity needed for



monitoring the rapid turnover of carbon stocks in croplands and grasslands, where the biomass changes are spatially extensive, but below the detection limits of these measurements. Until recently, high resolution imaging observations and moderate resolution estimates of vegetation indices provided the primary tools for scaling up plot-based observations to national and continental scales. Recently, these capabilities have been augmented by space-based observations of SIF. SIF relates the emission of excess radiative energy from the photosynthesis process of leaves at two wavelengths (685 nm and 740 nm) to photosynthesis or GPP. Estimates of SIF from GOME, GOME2, GOSAT, OCO-2 and TROPOMI are increasingly being used to monitor crop and grassland productivity and for crop yield prediction (Guan et al., 2017; He et al., 2020; Peng et al., 2020; Parazoo et al., 2020; Qiu et al., 2020; Yin et al., 2020). Future SIF observations from the ESA FLuorescence EXplorer (FLEX), Japan's GOSAT-GW, NASA's GeoCarb, and the Copernicus CO2M missions promise substantial improvements in resolution.

Space-based observations of XCO<sub>2</sub> and SIF are being combined with observations of vegetation indices (LAI, NDVI, NIRv), VOD and other environmental properties to provide new insights into the high latitude terrestrial carbon cycle. Unlike for the tropics, top-down estimates of CO<sub>2</sub> fluxes derived from space-based observations of XCO<sub>2</sub> anomalies over northern temperate and boreal forests tend to reinforce the conclusions from other observations and modeling studies. During the northern hemisphere summer, negative XCO<sub>2</sub> anomalies (JJA in Figure 14) and large positive SIF emissions (Figure 11d) prevail across most of this region. NBE estimates from flux inversion experiments constrained by space-based XCO<sub>2</sub> data (Figure 19) show negative NBE in regions where models constrained by satellite-derived reflectance and SIF data (e.g., Figure 11 and Joiner et al., 2018) show moderately strong GPP (Liu et al., 2020a). These satellite-derived NBE estimates therefore indicate that northern forests have continued to act as significant net CO<sub>2</sub> sinks as the CO<sub>2</sub> seasonal cycle amplitude has grown in response to warming.

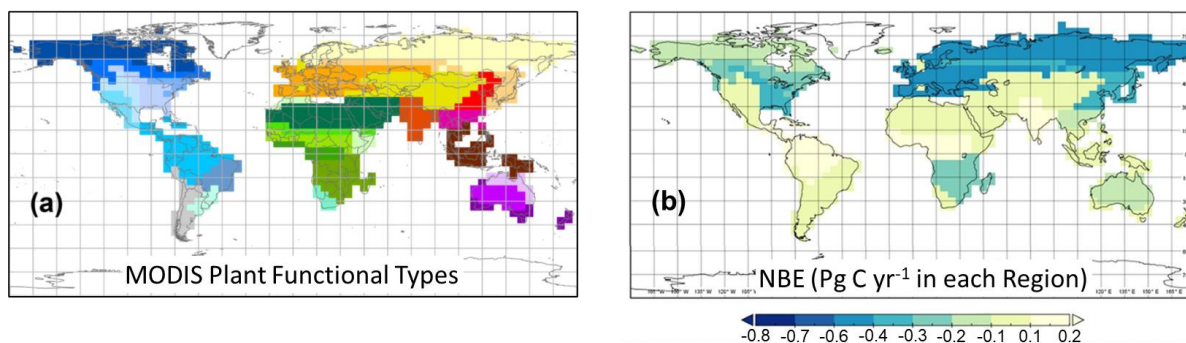


**Figure 19.** (a) Regional mask based on MODIS International Geosphere-Biosphere Programme (IGBP) plant functional types (see Liu et al., 2020a for a more complete description) (B) Net Biospheric Exchange (NBE) from XCO<sub>2</sub> and SIF, expressed in Pg C yr<sup>-1</sup> from each region shown in panel (a) for 2010-2018. Negative NBE indicates sinks while positive values indicate sources. (adapted from Liu et al., 2020a).

Observations of XCO<sub>2</sub> and SIF also provide unique opportunities to study the relationships between the land and atmospheric carbon cycles and the hydrological cycle. Yin et al. (2020) combine SIF with atmospheric CO<sub>2</sub> observations to quantify the effects of large-scale flooding on cropland carbon sequestration. Widespread flooding during spring and early summer

of 2019 delayed crop planting across the U.S. Midwest. As a result, satellite observations of SIF from OCO-2 and the TROPospheric Monitoring Instrument (TROPOMI) reveal a delay of 16 days in the seasonal increase of photosynthetic activity relative to 2018, along with a 15% lower peak photosynthesis. Yin et al. find that the 2019 anomaly produced an estimated GPP reduction of  $-0.21 \text{ Pg C}$  in June and July that was partially compensated in August and September with a  $+0.14 \text{ Pg C}$  increase. The growing season integral corresponds to a 4% reduction in cropland GPP for the Midwest, but a 3% increase for areas where cropland occupies less than 10% of the land. Using an atmospheric transport model, they show that a decline of  $\sim 0.1 \text{ Pg C}$  in the net carbon uptake in June and July is consistent with observed  $\sim 10 \text{ ppm CO}_2$  enhancements in the midday boundary layer from the Atmospheric Carbon and Transport - America (ACT-America) aircraft and the  $\sim 1 \text{ ppm}$  increases in  $\text{XCO}_2$  seen by OCO-2.

In another study, Gonsamo et al. (2019) combined OCO-2 SIF observations with soil moisture (SM) observations from NASA's Soil Moisture Active Passive (SMAP) mission to study the impact of environmental limiting factors on terrestrial ecosystem productivity of drylands and croplands. For drylands (dry sub-humid, semi-arid, and arid zones) and the majority of croplands, soil water content is typically low and topsoil moisture is critical for plant growth. As expected, SMAP SM retrievals show positive daily relationships with OCO-2 SIF for drylands and croplands of the tropics and Australia, where SM is limiting plant growth and concurrent data records are sufficient to make statistical inferences. Negative relationships between SIF and SM were observed in forested areas of mid-latitude dry sub humid zones with high average annual SM. In these regions, SIF showed a positive relationship with air temperature. They find strong evidence that the OCO-2 SIF is accurately capturing monthly SMAP SM dynamics, particularly for regions with distinct seasonality of rainfall such as Sub-Saharan North Africa, Indian subcontinent, and southern Africa.

Other advances in remote-sensing capabilities are expected to accelerate progress in monitoring, verification and understanding of temporal changes in biomass and productivity. Until very recently, the remote-sensing community has pioneered static biomass maps, based on a composite of products and field-truthing, or inferred biomass change from products like VOD. Now, with new missions and sensors, e.g., GEDI and BIOMASS, the community is at the cusp of direct monitoring biomass change at scale for the first time. This information in combination with monitoring of productivity directly and land cover change, will revolutionize research on the land carbon cycle.

To fully exploit these new measurements to describe long term trends in the terrestrial carbon cycle, the in situ and remote sensing measurements must be reconciled so that their climate data records can be combined to increase their spatial and temporal resolution and coverage. The protocol for cross-validating aboveground biomass products described by Duncanson et al. (2019) and the effort by the Forest Observation Initiative to develop a global in situ forest biomass databases for validating remote sensing observations (Schepaschenko et al., 2018) are positive steps in this direction.

While the current generation of DGVMs and other terrestrial biosphere models are evolving rapidly and providing important insights into the processes driving the land carbon cycle, these modeling tools are still yielding widely diverging results the uptake of  $\text{CO}_2$  by the land biosphere and its trends (e.g., Fisher et al., 2014; Sitch et al., 2015; Keenan and Williams, 2018; Parazoo et al., 2020). These limitations have raised concerns about their use in  $\text{CO}_2$  emission inventory development activities (Grassi et al., 2018; Petrescu et al., 2020). Pioneering

model intercomparison efforts such as the Carbon-Land Model Intercomparison Project (CLAMP; Randerson et al., 2009) are being followed up by the International Land Model Benchmarking (ILAMB) project (see <https://www.ilamb.org/>) to address these concerns and accelerate the development of these critical tools.

## 6 Discussion

When integrated over the industrial age, the land sink associated with intact forests and other natural parts of the terrestrial biosphere has roughly balanced sources associated with LUC while the ocean has been a cumulative net sink of anthropogenic carbon emissions (Friedlingstein et al., 2021). Since 1958, when continuous atmospheric CO<sub>2</sub> measurements have been available, CO<sub>2</sub> emissions from fossil fuel combustion have increased by about a factor of four, from less than 2.5 Pg C yr<sup>-1</sup> to almost 10 Pg C yr<sup>-1</sup> in 2019. During this period, the land sink grew as well, absorbing a near constant fraction of the anthropogenic emissions (~30%). Together, sinks in ocean and on land have absorbed enough anthropogenic CO<sub>2</sub> to limit the fraction that has remained in the atmosphere to a remarkably constant value around 45% (Raupach et al., 2014). This implies that, to first order, the uptake by the ocean and land sinks has increased proportionally with the emissions (Friedlingstein et al., 2021).

There has been debate as to whether increases in the airborne fraction since 1958, i.e., declines in sink efficiency, are already observable (Canadell et al., 2007; Knorr 2009; Gloor et al., 2010; Raupach et al., 2014). Even if an increasing airborne fraction is not yet detectable, process-level understanding and regional trends indicate that the airborne fraction should increase as climate change progresses (Raupach et al., 2014; Canadell et al., 2021). While the exact timing and magnitude of changes in the land and ocean sinks remains unclear, the likelihood is high that substantial climate-carbon feedbacks will occur during this century. Any upward change in the airborne fraction, or reduction in sink capacity, will decrease the allowable fossil carbon that can still be burned without violating the temperature targets specified in the Paris Agreement.

For the ocean, despite remaining uncertainties and missing closure terms, distinct methodologies for quantifying the ocean uptake of anthropogenic CO<sub>2</sub> agree that the sink has increased over the industrial era, including in recent decades. Since the uptake of atmospheric CO<sub>2</sub> on annual to decadal time scales is primarily controlled by the pCO<sub>2</sub> gradient at its surface, the carbon sink is expected to grow as long as near-exponential growth of atmospheric pCO<sub>2</sub> continues. However, if anthropogenic emissions are reduced, atmospheric pCO<sub>2</sub> will grow more slowly, and thus there will be a reduced ocean carbon sink even if the ocean circulation and chemical buffer capacity do not change (Ridge and McKinley, 2021). To understand these likely changes, it is essential that ocean carbon studies start to focus more attention on the near-term response to emission mitigation scenarios (Hausfather and Peters, 2020). If emissions are not mitigated, current climate models suggest that by the middle to late 21st century, a slowing ocean overturning rate and reduced chemical capacity in the ocean will reduce the rate of growth in the global ocean sink (Randerson et al., 2015).

To develop an integrated ocean carbon observing system that can track the evolution of the ocean sink on the annual to interannual timescales most relevant to climate change policy, we need to sustain existing and continue to develop improved observation systems for the surface and interior ocean. Ocean carbon instruments deployed on autonomous platforms are revolutionizing the spatial and temporal resolution and coverage of ocean carbon measurements,

but reduced uncertainties in the carbonate constants are needed to fully exploit these data. High-quality shipboard observations will continue to be required. We also need improved ocean hindcast models and better understanding of uncertainties in observation-based data products derived through statistical extrapolation of sparse surface ocean  $p\text{CO}_2$  data in order to track the real-time evolution of the ocean carbon sink and its decadal trend reliably.

For the land carbon cycle, the current state, trends and near-future evolution is less clear. Classical sinks in the tropical humid forest sinks are slowly losing their strength and these changes are amplified by the losses associated with deforestation, forest degradation and extreme climate events. In the extratropics, multiple data sources support the existence of an increasing terrestrial sink, driven by  $\text{CO}_2$  fertilization, afforestation, agricultural intensification and other factors. Across the Arctic and boreal regions, which are experiencing roughly twice the average rate of global warming, most regions have seen significant increases in GPP, NBE and SCA since the 1960s due to higher growing season temperatures and other factors. However, a small fraction of this region is seeing reduced NBE that is attributed to increases in fire disturbances, drought stress, and insect infestation. Both improved observations and models are needed to track these changes as the carbon cycle continues to respond to human activities and climate change.

Space-based remote sensing observations are helping to revolutionize our ability to monitor the response of the global carbon cycle to anthropogenic forcing and a changing climate. In the ocean, sea surface temperature and chlorophyll are critical to process-based and machine learning extrapolations of sparse  $p\text{CO}_2$  data to global coverage. From a bottom-up perspective, microwave and lidar measurements are providing higher spatial and temporal resolution estimates of AGB stocks. SIF measurements are providing a more responsive estimate of light use efficiency and  $\text{CO}_2$  uptake by plants. From a top-down perspective, space-based remote sensing estimates of  $\text{XCO}_2$  are complementing ground-based and aircraft in situ measurements with much greater spatial and temporal resolution and coverage.

These space-based measurements can reinforce or contradict conclusions about the land carbon cycle inferred from ground-based in situ measurements, painting a somewhat controversial picture of the evolution of the land carbon cycle. For example, in the tropics, both space-based microwave estimates of AGB (Wigneron et al., 2020) and top-down atmospheric inverse models constrained by space-based estimates of  $\text{XCO}_2$  (Liu et al., 2017; 2020; Palmer et al., 2019; Crowell et al., 2019; Gatti et al., 2021) indicate that the humid tropical forests did not fully recover from the 2015-2016 El Niño, and have transitioned from net sinks to net sources of  $\text{CO}_2$ . More generally, the space-based measurements are also providing more information about rapid changes in the land carbon cycle associated with severe weather, such as droughts (Gonsamo et al., 2019; Castro et al., 2020) and floods (Yin et al., 2020). They are also beginning to provide estimates of  $\text{CO}_2$  emissions from fossil fuel combustion and other human activities (Hakkarainen et al., 2016; 2019; Wang et al., 2018; Hedelius et al., 2018; Wu et al., 2018; 2020; Reuter et al., 2019).

In spite of these advances, the reliability of the space-based remote sensing results are still a subject of substantial debate within the land carbon cycle community. This is especially true for the tropics, where  $\text{CO}_2$  fluxes derived from the space-based  $\text{XCO}_2$  estimates differ in both sign and magnitude from the results of earlier flux inversion experiments constrained by bottom-up stock or flux estimates or ground-based in situ measurements of atmospheric  $\text{CO}_2$ . This apparent inconsistency suggests one of three possibilities. First, the space-based  $\text{XCO}_2$

estimates might still include biases that compromise the accuracy of the top-down flux estimates. Recent efforts to validate the space-based XCO<sub>2</sub> estimates using measurements from TCCON and other standards (Wunch et al., 2017) indicate biases with amplitudes less than one third as large as the observed tropical XCO<sub>2</sub> anomalies. However, there are few TCCON stations or other validation capabilities in the tropics. Second, fluxes constrained by surface in situ measurements, alone, may tell an incomplete story of the land carbon cycle in sparsely sampled regions. The spatial resolution and coverage provided by surface in situ measurements of carbon stocks, fluxes, or atmospheric CO<sub>2</sub> are still very limited, especially in the tropics and boreal regions, where the largest flux differences are seen. Both top-down and bottom-up methods may yield unreliable results where there are few measurements. Third, flux estimates based on the much denser space-based XCO<sub>2</sub> measurements may be tracking changes in the natural carbon cycle on time and space scales too short to be resolved by the in situ measurements of stocks or CO<sub>2</sub> concentrations. A tropical land carbon monitoring system with even greater spatial and temporal coverage is needed to track these changes as these areas continue to respond to human activity and climate change.

While these space-based observations and top-down inverse models are providing new insights into this system, they have also revealed measurement gaps and modeling limitations that must be addressed to develop a true global carbon monitoring system that can track changes in both natural and anthropogenic sources and sinks of CO<sub>2</sub> on policy relevant time and space scales. For example, space-based remote sensing observations of atmospheric CO<sub>2</sub> and land and ocean surface properties can expand the coverage and resolution of surface-based in situ measurements. However, passive remote sensing observations are largely precluded in persistently cloudy regions such as tropical rain forests, or mid- and high-latitude forests during the fall, winter and spring. These regions are often centers of action in the carbon cycle, but are also among the most challenging to observe systematically with surface-based in situ measurement systems. Similarly, remote sensing observations provide little insight into the carbon budget of the interior ocean, but here networks of autonomous in situ sensors have great potential to greatly expand opportunities for gathering critical ocean carbon data. Like remote sensing observations, their data typically has larger uncertainties and biases than conventional shipboard in situ measurements. Thus, a robust ocean carbon observing system will require continued shipboard observations for calibration and validation.

These perspectives reinforce the continuing need to maintain and expand the ground-based, ship-based and airborne CO<sub>2</sub> measurement networks. These networks fill three critical needs. First, as noted above, in situ measurements are needed to complement the coverage provided by remote sensing observations in persistently cloudy regions. In addition, because the air-sea flux of CO<sub>2</sub> is determined mainly by the pCO<sub>2</sub> gradient between the ocean surface layer and the atmospheric surface boundary layer, in situ vertical profiles of near-surface atmospheric CO<sub>2</sub> concentrations are critical for validating flux estimates over the ocean. Second, because surface and airborne in situ and surface remote sensing observations are more accurate than space-based remote sensing measurements, these data are critical for validating the space-based remote sensing measurements. Finally, while atmospheric CO<sub>2</sub> and CH<sub>4</sub> can now be measured from space with the accuracies needed to quantify surface fluxes, other critical greenhouse gases (N<sub>2</sub>O, CFCs, HCFCs, SF<sub>6</sub> etc.) can only be measured to adequate accuracy with ground-based and airborne sensors. Other species that are useful for distinguishing fossil fuel from biospheric CO<sub>2</sub> emissions, such as carbon-14 (<sup>14</sup>C) can also only be measured in situ (Miller et al., 2012; 2020).

To address these needs, national agencies such as the U.S. National Oceanic and Atmospheric Administration (NOAA), Japan's National Institute for Environmental Studies (NIES) and European organizations, including the European Space Agency (ESA), Copernicus, Integrated Carbon Observation System (ICOS) and IAGOS, are working with WMO Global Atmospheric Watch (GAW) and the Global Climate Observing System and the Global Ocean Observing System (GCOS, GOOS) to coordinate and expand the deployment of ground-based, ocean and airborne in situ sensors. While the number of ground-based and airborne CO<sub>2</sub> monitoring stations has grown slowly over the past decade, new measurement capabilities are coming on line that promise substantial increases in coverage. The up-looking remote sensing measurements being collected by the TCCON spectrometers are being complemented by measurements from smaller, less costly, and more portable Bruker EM27/SUN systems. These spectrometers are now being deployed as networks in urban settings (Hedelius et al., 2018) and in remote locations (Frey et al., 2019). In situ vertical profiles of CO<sub>2</sub>, CH<sub>4</sub> and other gases are now being collected at altitudes as high as 25 km by AirCore instruments deployed on low-cost weather balloons (Karion et al., 2010; Baier et al., 2020). Additional in situ profiles and upper tropospheric measurements are now being made by commercial aircraft in Japan's Comprehensive Observation Network for Trace gases by Airliner (CONTRAIL) and Europe's In-service Aircraft for a Global Observing System (IAGOS).

The world's space agencies are actively working to coordinate ambitious plans for an expanded space-based remote sensing capability that supports atmospheric CO<sub>2</sub> measurements, high resolution maps of land surface type and biomass and ocean biological productivity. These efforts are being led by the Committee on Earth Observation Satellites (CEOS) and Coordination Group on Meteorological Satellites (CGMS) through their Joint Working Group on Climate (WGClimate) Greenhouse Gas Task team. The modeling systems needed to ingest and analyze the data collected by these expanding measurement systems are also advancing. However, efforts to coordinate carbon cycle modeling efforts are receiving less attention from the carbon cycle science community and their stakeholders.

## 7 Conclusions

Fossil fuel use, LUC and other human activities are now adding more than 10 petagrams of carbon to the atmosphere each year. These emissions have increased the atmospheric CO<sub>2</sub> mixing ratio by almost 50% since the beginning of the industrial age and would have produced much larger changes if natural sinks in the land biosphere and ocean had not removed over half of this anthropogenic CO<sub>2</sub>. As the world embarks on efforts to monitor and control CO<sub>2</sub> emissions, there is growing evidence that the natural carbon cycle is evolving in response to human activities, severe weather, disturbances and climate change.

Our understanding of the carbon cycle and its response to natural and anthropogenic forcing has grown steadily over the past two decades as more advanced carbon cycle measurement systems have been deployed and their results have been analyzed with more sophisticated top-down atmospheric CO<sub>2</sub> flux inversions as well as bottom-up diagnostic and prognostic carbon cycle models. These measurements and models reveal a strongly coupled, dynamic system that responds on daily, to seasonal, to interannual time scales across spatial scales spanning individual fields, forest plots or coal-fired power plants on land or individual eddies in the ocean to entire continents or ocean basins.

On decadal or longer time scales, measurements of changes in carbon stocks in the ocean and on land provide a reliable integral constraint on fluxes of CO<sub>2</sub> to the atmosphere. These measurements show that while the ocean and terrestrial biosphere now absorb comparable amounts of anthropogenic CO<sub>2</sub>, LUC emissions have roughly balanced the terrestrial sink over the industrial era and the ocean has provided the primary cumulative net sink of anthropogenic carbon. Over this period, the CO<sub>2</sub> uptake by the ocean has increased as the atmospheric CO<sub>2</sub> partial pressure (pCO<sub>2</sub>) has increased nearly exponentially and the ocean overturning has continually circulated from depth to surface, thus exposing pristine deep waters to the anthropogenically-perturbed atmosphere. However, additional study is needed to reconcile diverging estimates of the decadal trend of the ocean sink. For the land carbon cycle, the emerging picture is regionally dependent. Over the past three decades, the uptake of CO<sub>2</sub> by intact tropical humid forests appears to be declining. These reductions in the tropical land sink are offset by net increases across mid- and high-latitudes associated with CO<sub>2</sub> fertilization, afforestation, the agricultural green revolution, and longer growing seasons associated with climate change.

Direct measurements and model-derived estimates of CO<sub>2</sub> fluxes at the Earth's surface provide additional insight into variability on seasonal to decadal timescales. Surface ocean pCO<sub>2</sub> measurements and ocean models indicate that the global ocean carbon sink did not grow significantly over the 1990s, but then grew steadily since 2000, a pattern that can be explained, to first order, by the changing growth rate of atmospheric pCO<sub>2</sub>. This implies that a rapid decline of the ocean sink can be expected when atmospheric levels are reduced through emission reductions. The evolution of the land sink is more difficult to predict given its ongoing declines in strength in tropical regions and enhancements in strength across the extratropics, both strongly driven by human activities and climate change.

While these observations and models are providing new insights into the carbon cycle, they are also revealing measurement gaps and modeling limitations that will have to be addressed to diagnose its current state and predict its evolution. In particular, they reinforce the urgent need for more comprehensive measurements of stocks, fluxes and atmospheric CO<sub>2</sub> concentrations in humid tropical forests and at high latitudes, which appear to be experiencing rapid changes. This requires expanded ground-based and airborne measurement capabilities, because these regions are intrinsically difficult to monitor with emerging remote sensing techniques due to persistent cloud cover and limited sunlight at high latitudes during the winter. Similarly, existing uncertainties in the measurements and the physical and biological processes controlling air-sea CO<sub>2</sub> fluxes on seasonal to decadal time scales support the need for continued ship-based observations combined with expanded deployments of autonomous platforms with next-generation sensors to quantify ocean-atmosphere fluxes with increased accuracy and greater spatial and temporal resolution. These updates, combined with ongoing advances in space-based remote sensing and modeling capabilities are essential elements of the global carbon monitoring system that is critically needed to diagnose ongoing trends in the emissions and uptake of CO<sub>2</sub> by the land biosphere and oceans and to predict their evolution as the climate evolves.

## 8 Open Research

This is a review of other published work. No new data has been created or archived specifically for this manuscript. Original data are available through the citations listed here. Figures have been redrawn to avoid copyright conflicts.



## 9 Acknowledgments

Some of the work presented here was performed at the Jet Propulsion Laboratory, California Institute of Technology under contract to the National Aeronautics and Space Administration (NASA). Government sponsorship acknowledged. Figure 6 was designed by GAM and Natalie Renier, WHOI Creative, with funding from Ocean Carbon & Biogeochemistry (OCB) Project Office that has support from the US National Science Foundation (NSF) and NSF, NASA. We thank Amanda Fay for assistance with Figures 7 and 8. GAM acknowledges support from NSF OCE-1948624 and US National Oceanic and Atmospheric Administration (NA20OAR4310340). HD was supported by the European Commission, Horizon 2020 Framework Programme (VERIFY, grant no. 776810, COCO2 grant no. 958927) and the Netherlands Earth System Science Centre (NESSC), financially supported by the Ministry of Education, Culture and Science (OCW) (grant 024.002.001). JH acknowledges funding from the Initiative and Networking Fund of the Helmholtz Association (Helmholtz Young Investigator Group Marine Carbon and Ecosystem Feedbacks in the Earth System, MarESys), Grant Number: VH- NG-1301. TT acknowledges support from the EU H2020 framework program (EuroSea, grant no. 862626). AB acknowledges funding by the European Space Agency Climate Change Initiative ESA-CCI RECCAP2 project (ESRIN/ 4000123002/18/I-NB). The writing of this paper was initiated at the GCOS joint panel meeting in Marrakech, 18-22 March, 2019. We thank Mike O’Sullivan for the provision of Figure 17 and the TRENDY consortium modelers for use of the multi-model mean ensemble. We also wish to acknowledge the tremendous value of the products produced annually the Global Carbon Project.

## 10 References

- Ahlström, A., Raupach, M. R., Schurgers, G., Smith, B., Arneth, A., Jung, M., Reichstein, M., Canadell, J. G., Friedlingstein, P., Jain, A. K., and Kato, E. (2015). The dominant role of semi-arid ecosystems in the trend and variability of the land CO<sub>2</sub> sink, *Science*, **348**, 895–899. doi: 10.1126/science.aal1668
- Álvarez, M., Fajar, N. M., Carter, B. R., Gualart, E. F., Pérez, F. F., Woosley, R. J. and Murata, A. (2020). Global Ocean Spectrophotometric pH Assessment: Consistent Inconsistencies. *Environmental Science and Technology*, **54**, 10977-10988. doi:10.1021/acs.est.9b06932
- Anav, A., Friedlingstein, P., Beer, C., Ciais, P., Harper, A., Jones, C., Murray-Tortarolo, G., Papale, D., Parazoo, N. C., Peylin, P., Piao, S., Sitch, S., Viovy, N., Wiltshire, A. and Zhao, M. (2015). Spatiotemporal patterns of terrestrial gross primary production: A review. *Rev. Geophys.*, **53**, 785–818. doi:10.1002/2015RG000483
- Anderegg, W. R. L., Hicke, J. A., Fisher, R. A., Allen, C. D., Aukema, J., Bentz, B., Hood, S., Lichstein, J. W., Macalady, A. K., McDowell, N., Pan, Y., Raffa, K., Sala, A., Shaw, J. D., Stephenson, N. L., Tague, C. and Zeppel, M. (2015). Tree mortality from drought, insects, and their interactions in a changing climate. *New Phytologist*, **208**: 674-683. doi:10.1111/nph.13477
- Andrew, R. M. (2019). Global CO<sub>2</sub> emissions from cement production, 1928–2018. *Earth System Science Data*, **11**, 1675–1710. doi: 10.5194/essd-11-1675-2019
- Andrew, R. M. (2020). A comparison of estimates of global carbon dioxide emissions from fossil carbon sources. *Earth System Science Data*, **12**, 1437–1465. doi:10.5194/essd-12-1437-2020

- 2296 Angert, A., Biraud, S., Bonfils, C., Buermann, W. & Fung, I. (2004). CO<sub>2</sub> seasonality indicates  
2297 origins of post-Pinatubo sink. *Geophys Res Letters*, **31**, L11103. doi:  
2298 10.1029/2004GL019760
- 2299 Aragão, L. E. O. C., Anderson, L. O., Fonseca, M. G., Rosan, T. M., Vedovato, L. B., Wagner, F.  
2300 H., Silva, C. V. J., Silva Junior, C. H. L., Arai, E., Aguiar, A. P. Barlow, J., Berenguer, E.,  
2301 Deeter, M. N., Domingues, L. G., Gatti, L., Gloor, M., Malhi, Y., Marengo, J. A., Miller, J.  
2302 B., Phillips, O., L., and Saatchi, S. (2018). 21st Century drought-related fires counteract the  
2303 decline of Amazon deforestation carbon emissions. *Nature Communications*, **9**, 536. doi:  
2304 10.1038/s41467-017-02771-y
- 2305 Argles, A. P. K., Moore, J. R., Huntingford, C., Wiltshire, A. J., Harper, A. B., Jones, C. D., and  
2306 Cox, P. M. (2020). Robust Ecosystem Demography (RED version 1.0): a parsimonious  
2307 approach to modelling vegetation dynamics in Earth system models, *Geoscientific Model*  
2308 *Development*, **13**, 4067–4089. doi:10.5194/gmd-13-4067-2020
- 2309 Arneth, A., Sitch, S., Pongratz, J., Stocker, B. D., Ciais, P., Poulter, B., Bayer, A. D., Bondeau,  
2310 A., Calle, L., Chini, L. P., Grassler, T., Fader, M., Friedlingstein, P., Kato, E., Li, W.,  
2311 Lindeskog, M., Nabel, J. E. M. S., Pugh, T. A. M., Robertson, E., Viovy, N., Yue, C. and  
2312 Zaehle, S. (2017). Historical carbon dioxide emissions caused by land-use changes are  
2313 possibly larger than assumed, *Nature Geoscience*, **10**, 79-84. doi: 10.1038/NGEO2882.
- 2314 Aumont, O., Orr, J. C., Monfray, P., Ludwig, W., Amiotte-Suchet, P. and Probst, J. -L. (2001).  
2315 Riverine-driven interhemispheric transport of carbon. *Global Biogeochemical Cycles*. **15**,  
2316 393–405. doi:10.1029/1999GB001238
- 2317 Aumont, O., Ethé, C., Tagliabue, A., Bopp, L. and Gehlen, M. (2015). PISCES-v2: An ocean  
2318 biogeochemical model for carbon and ecosystem studies. *Geoscientific Model Development*,  
2319 **8**, 2465–2513. doi:10.5194/gmd-8-2465-2015
- 2320 Ayers, J.M. and Strutton, P.G. (2013). Nutrient variability in Subantarctic Mode Waters forced by  
2321 the Southern Annular Mode and ENSO: Subantarctic mode water nutrients. *Geophysical*  
2322 *Research Letters*, **40**, 3419–3423. doi:10.1002/grl.50638
- 2323 Bacastow, R. B., Keeling, C. D., and Whorf, T. P. (1985). Seasonal amplitude increase in  
2324 atmospheric CO<sub>2</sub> concentration at Mauna Loa, Hawaii, 1959–1982. *Journal of Geophysical*  
2325 *Research: Atmospheres*, **90**, 10529– 10540.
- 2326 Baccini, A., Walker, W., Carvalho, L., Farini, M., Sulla-Menashe, D. and Houghton, R. A.  
2327 (2017). Tropical forests are a net carbon source based on aboveground measurements of  
2328 gain and loss. *Science*. **358**, 230–234. doi:10.1126/science.aam5962
- 2329 Bacour, C., Maignan, F., MacBean, N., Porcar-Castell, A., Flexas, J., Frankenberg, C., Peylin, P.,  
2330 Chevallier, F., Vuichard, N., and Bastrikov, V. (2019). Improving estimates of Gross  
2331 Primary Productivity by assimilating solar-induced fluorescence satellite retrievals in a  
2332 terrestrial biosphere model using a process-based SIF model, *Journal of Geophysical.*  
2333 *Research-Biogeosciences*, **124**, 3281–3306
- 2334 Badgley G., Field C. B., Berry J. A. (2017). Canopy near-infrared reflectance and terrestrial  
2335 photosynthesis. *Science Advances*, **3**, e1602244. doi: 10.1126/sciadv.1602244. PMID:  
2336 28345046; PMCID: PMC5362170
- 2337 Badgley, G. Anderegg, L. D. L., Berry, J. A., and Field, C. B. (2019). Terrestrial gross primary  
2338 production: Using NIRV to scale from site to globe. *Global Change Biology*, **25**, 3731-  
2339 3740. doi: 10.1111/gcb.14729

- 2340 Baier, B., Sweeney, C., Wolter, S., Newberger, T. and Higgs, J. (2020). 2017-2018 Full-Column  
2341 Greenhouse Gas Sampling Field Campaign Report. DOE/SC-ARM-19-014
- 2342 Baker, D. F., Doney, S. C., and Schimel, D. S. (2006a). Variational data assimilation for  
2343 atmospheric CO<sub>2</sub>, *Tellus, B*, 359–365. doi: 10.1111/j.1600-0889.2006.00218.x
- 2344 Baker, D. F., Law, R. M., Gurney, K. R., Rayner, P., Peylin, P., Denning, A. S., Bousquet, P.,  
2345 Bruhwiler, L., Chen, Y. H., Ciais, P., Fung, I. Y., Heimann, M., John, J., Maki, T.,  
2346 Maksyutov, S., Masarie, K., Prather, M., Pak, B., Taguchi, S., and Zhu, Z. (2006b).  
2347 TransCom 3 inversion intercomparison: Impact of transport model errors on the interannual  
2348 variability of regional CO<sub>2</sub> fluxes, 1988-2003. *Global Biogeochem. Cycles*, **20**, 01  
2349 [GB1002]. doi:10.1029/2004GB002439
- 2350 Bakker, D. C. E., Pfeil, B., Smith, K., Hankin, S., Olsen, A., Alin, S. R., Cosca, C., Harasawa, S.,  
2351 Kozyr, A., Nojiri, Y., O'Brien, K. M., Schuster, U., Telszewski, M., Tilbrook, B., Wada, C.,  
2352 Akl, J., Barbero, L., Bates, N. R., Boutin, J., Bozec, Y., Cai, W.-J., Castle, R. D., Chavez, F.  
2353 P., Chen, L., Chierici, M., Currie, K., de Baar, H. J. W., Evans, W., Feely, R. A., Fransson,  
2354 A., Gao, Z., Hales, B., Hardman-Mountford, N. J., Hoppema, M., Huang, W.-J., Hunt, C.  
2355 W., Huss, B., Ichikawa, T., Johannessen, T., Jones, E. M., Jones, S. D., Jutterström, S.,  
2356 Kitidis, V., Körtzinger, A., Landschützer, P., Lauvset, S. K., Lefèvre, N., Manke, A. B.,  
2357 Mathis, J. T., Merlivat, L., Metzl, N., Murata, A., Newberger, T., Omar, A. M., Ono, T.,  
2358 Park, G.-H., Paterson, K., Pierrot, D., Ríos, A. F., Sabine, C. L., Saito, S., Salisbury, J.,  
2359 Sarma, V. V. S. S., Schlitzer, R., Sieger, R., Skjelvan, I., Steinhoff, T., Sullivan, K. F., Sun,  
2360 H., Sutton, A. J., Suzuki, T., Sweeney, C., Takahashi, T., Tjiputra, J., Tsurushima, N., van  
2361 Heuven, S. M. A. C., Vandemark, D., Vlahos, P., Wallace, D. W. R., Wanninkhof, R. and  
2362 Watson, A. J. (2014). An update to the Surface Ocean CO<sub>2</sub> Atlas (SOCAT version 2). *Earth*  
2363 *System Science Data*, **6**, 69-90. doi:10.5194/essd-6-69-2014
- 2364 Bakker, D. C. E., Pfeil, B., Landa, C. S., Metzl, N., O'Brien, K. M., Olsen, A., Smith, K., Cosca,  
2365 C., Harasawa, S., Jones, S. D., Nakaoka, S. I., Nojiri, Y., Schuster, U., Steinhoff, T.,  
2366 Sweeney, C., Takahashi, T., Tilbrook, B., Wada, C., Wanninkhof, R., Alin, S. R., Balestrini,  
2367 C. F., Barbero, L., Bates, N. R., Bianchi, A. A., Bonou, F., Boutin, J., Bozec, Y., Burger, E.  
2368 F., Cai, W. J., Castle, R. D., Chen, L., Chierici, M., Currie, K., Evans, W., Featherstone, C.,  
2369 Feely, R. A., Fransson, A., Goyet, C., Greenwood, N., Gregor, L., Hankin, S., Hardman-  
2370 Mountford, N. J., Harlay, J., Hauck, J., Hoppema, M., Humphreys, M. P., Hunt, C. W., Huss,  
2371 B., Ibanhez, J. S. P., Johannessen, T., Keeling, R., Kitidis, V., Kortzinger, A., Kozyr, A.,  
2372 Krasakopoulou, E., Kuwata, A., Landschützer, P., Lauvset, S. K., Lefevre, N., Lo Monaco,  
2373 C., Manke, A., Mathis, J. T., Merlivat, L., Millero, F. J., Monteiro, P. M. S., Munro, D. R.,  
2374 Murata, A., Newberger, T., Omar, A. M., Ono, T., Paterson, K., Pearce, D., Pierrot, D.,  
2375 Robbins, L. L., Saito, S., Salisbury, J., Schlitzer, R., Schneider, B., Schweitzer, R., Sieger,  
2376 R., Skjelvan, I., Sullivan, K. F., Sutherland, S. C., Sutton, A. J., Tadokoro, K., Telszewski,  
2377 M., Tuma, M., van Heuven, S. M. A. C., Vandemark, D., Ward, B., Watson, A. J. and Xu, S.  
2378 (2016). A multi-decade record of high-quality fCO<sub>2</sub> data in version 3 of the Surface Ocean  
2379 CO<sub>2</sub> Atlas (SOCAT). *Earth System Science Data*, **8**, 383-413. doi:10.5194/essd-8-383-2016
- 2380 Bakker, D. C. E., Alin, S. R., Bates, N., Becker, M., Castaño-Primo, R., Cosca, C. E., Cronin, M.,  
2381 Kadono, K., Kozyr, A., Lauvset, S. K., Metzl, N., Munro, D. R., Nakaoka, S., O'Brien, K.  
2382 M., Ólafsson, J., Olsen, A., Pfeil, B., Pierrot, D., Smith, K., Sutton, A. J., Takahashi, T.,  
2383 Tilbrook, B., Wanninkhof, R., Andersson, A., Atamanchuk, D., Benoit-Cattin, A., Bott, R.,  
2384 Burger, E. F., Cai, W.-J., Cantoni, C., Collins, A., Corredor, J. E., Cronin, M. F., Cross, J. N.,  
2385 Currie, K. I., De Carlo, E. H., DeGrandpre, M. D., Dietrich, C., Emerson, S., Enright, M. P.,

- 2386 Evans, W., Feely, R. A., García-Ibáñez, M. I., Gkritzalis, T., Glockzin, M., Hales, B.,  
 2387 Hartman, S. E., Hashida, G., Herndon, J., Howden, S. D., Humphreys, M. P., Hunt, C. W.,  
 2388 Jones, S. D., Kim, S., Kitidis, V., Landa, C. S., Landschützer, P., Lebon, G. T., Lefèvre, N.,  
 2389 Lo Monaco, C., Luchetta, A., Maenner Jones, S., Manke, A. B., Manzello, D., Mears, P.,  
 2390 Mickett, J., Monacci, N. M., Morell, J. M., Musielewicz, S., Newberger, T., Newton, J.,  
 2391 Noakes, S., Noh, J.-H., Nojiri, Y., Ohman, M., Ólafsdóttir, S., Omar, A. M., Ono, T.,  
 2392 Osborne, J., Plueddemann, A. J., Rehder, G., Sabine, C. L., Salisbury, J. E., Schlitzer, R.,  
 2393 Send, U., Skjelvan, I., Sparnocchia, S., Steinhoff, T., Sullivan, K. F., Sutherland, S. C.,  
 2394 Sweeney, C., Tadokoro, K., Tanhua, T., Telszewski, M., Tomlinson, M., Tribollet, A., Trull,  
 2395 T., Vandemark, D., Wada, C., Wallace, D. W. R., Weller, R. A., and Woosley, R. J. (2020).  
 2396 Surface Ocean CO<sub>2</sub> Atlas Database Version 2020 (SOCATv2020) (NCEI Accession  
 2397 0210711), NOAA National Centers for Environmental Information. doi:10.25921/4xkx-ss49
- 2398 Baldocchi, D., Falge, E., Gu, L., Olson, R., Hollinger, D., Running, S. W., Anthoni, P.,  
 2399 Bernhofer, C., Davis, K. J., Evans, R., Fuentes, J., Goldstein, A., Katul, G., Law, B., Lee,  
 2400 X., Malhi, Y., Meyers, T., Munger, W., Oechel, W., Paw, U. K. T., Pilegaard, K., Schmid, H.  
 2401 P., Valentini, R., Verma, S., Vesala, T., Wilson, K. and Wofsy, S. (2001). FLUXNET: A new  
 2402 tool to study the temporal and spatial variability of ecosystem-scale carbon dioxide, water  
 2403 vapor, and energy flux densities. *Bull. Amer. Meteor. Soc.*, **82**, 2415–2434.  
 2404 doi:10.1175/1520-0477
- 2405 Baldocchi D. D. (2003). Assessing the eddy covariance technique for evaluating carbon dioxide  
 2406 exchange rates of ecosystems: past, present and future. *Global Change Biology*, **9**, 479–492.  
 2407 doi:10.1046/j.1365-2486.2003.00629.x
- 2408 Ballantyne, A. P., Alden, C. B., Miller, J. B., Tans, P. P. and White, J. W. C. (2012). Increase in  
 2409 observed net carbon dioxide uptake by land and oceans during the past 50 years. *Nature*,  
 2410 **488**, 70–72. doi:10.1038/nature11299
- 2411 Ballantyne, A. P., Andres, R., Houghton, R., Stocker, B. D., Wanninkhof, R., Anderegg, W.,  
 2412 Cooper, L. A., DeGrandpre, M., Tans, P. P., Miller, J. B., Alden, C., and White, J. W. C.  
 2413 (2015). Audit of the global carbon budget: estimate errors and their impact on uptake  
 2414 uncertainty, *Biogeosciences*, **12**, 2565–2584. doi: 10.5194/bg-12-2565-2015.
- 2415 Barichivich, J., Briffa, K.R., Myneni, R.B., Osborn T.J., Melvin, T.M., Ciais, P., Piao, S.,  
 2416 Tucker, C. (2013). Large-scale variations in the vegetation growing season and annual cycle  
 2417 of atmospheric CO<sub>2</sub> at high northern latitudes from 1950 to 2011. *Global Change. Biology*,  
 2418 **19**, 3167–3183. doi:10.1111/gcb.12283
- 2419 Bastos, A., Running, S. W., Gouveia, C., and Trigo, R. M. (2013). The global NPP dependence  
 2420 on ENSO: La Niña and the extraordinary year of 2011. *Journal of Geophysical Research:*  
 2421 *Biogeosciences*, **118**, 1247–1255. doi: 10.1002/jgrg.20100
- 2422 Bastos, A., Ciais, P., Park, T., Zscheischler, J., Yue, C., Barichivich, J., Myneni, R. B., Peng, S.,  
 2423 Piao, S., and Zhu, Z. (2017). Was the extreme Northern Hemisphere greening in 2015  
 2424 predictable? *Environmental Research Letters*, **12**, 044016. doi: 10.1088/1748-9326/aa67b5
- 2425 Bastos, A., Friedlingstein, P., Sitch, S., Chen, C., Mialon, A., Wigneron, J.-P., Arora, V. K.,  
 2426 Briggs, P. R., Canadell, J. G., and Ciais, P. (2018). Impact of the 2015/2016 El Niño on the  
 2427 terrestrial carbon cycle constrained by bottom-up and top-down approaches, *Philosophical*  
 2428 *Transactions of the Royal Society London B*, **373**, 1760. doi: 10.1098/rstb.2017.0304
- 2429 Bastos, A., Ciais, P., Chevallier, F., Rödenbeck, C., Ballantyne, A. P., Maignan, F., Yin, Y.,  
 2430 Fernández-Martínez, M., Friedlingstein, P., Peñuelas, J., Piao, S. L., Sitch, S., Smith, W. K.,

- 2431 Wang, X., Zhu, Z., Haverd, V., Kato, E., Jain, A. K., Lienert, S., Lombardozzi, D., Nabel, J.  
2432 E. M. S., Peylin, P., Poulter, B., and Zhu, D. (2019). Contrasting effects of CO<sub>2</sub> fertilization,  
2433 land-use change and warming on seasonal amplitude of Northern Hemisphere CO<sub>2</sub>  
2434 exchange, *Atmospheric Chemistry and Physics*, **19**, 12361–12375,  
2435 <https://doi.org/10.5194/acp-19-12361-2019>.
- 2436 Bastos, A., O'Sullivan, M., Ciais, P., Makowski, D., Sitch, S., Friedlingstein, P., Chevallier, F.,  
2437 Rödenbeck, C., Pongratz, J., Luijkx, I. T., Patra, P. K., Peylin, P., Canadell, J. G.,  
2438 Lauerwald, R., Li, W., Smith, N. E., Peters, W., Goll, D. S., Jain, A.K., Kato, E., Lienert, S.,  
2439 Lombardozzi, D. L., Haverd V., Nabel, J. E. M. S., Poulter, B., Tian, H., Walker, A. P. and  
2440 Zaehle, S. (2020). Sources of uncertainty in regional and global terrestrial CO<sub>2</sub> exchange  
2441 estimates. *Global Biogeochemical Cycles*, **34**, e2019GB006393. doi:  
2442 10.1029/2019GB006393
- 2443 Bauer, J. E., Cai, W. -J., Raymond, P. A., Bianchi, T. S., Hopkinson, C. S., and Regnier, P. A. G.  
2444 (2013). The changing carbon cycle of the coastal ocean. *Nature* **504**, 61-70. doi:  
2445 10.1038/nature12857
- 2446 Beck, S. A. and Goetz, S. J. (2011). Satellite observations of high northern latitude vegetation  
2447 productivity changes between 1982 and 2008: ecological variability and regional  
2448 differences. *Environmental Research Letters*, **6**, 045501. doi:10.1088/1748-  
2449 9326/6/4/045501
- 2450 Becker, M., Andersen, N., Fiedler, B., Fietzek, P., Körtzinger, A., Steinhoff, T., and Friedrichs, G.  
2451 (2012). Using cavity ringdown spectroscopy for continuous monitoring of  $\delta^{13}\text{C}(\text{CO}_2)$  and  
2452  $f\text{CO}_2$  in the surface ocean. *Limnology and Oceanography: Methods*, **10**, 752-766.  
2453 doi:10.4319/lom.2012.10.752
- 2454 Beer, C., Reichstein, M., Tomelleri, E., Ciais, P., Jung, M., Carvalhais, N., Rödenbeck, C.,  
2455 Arain, M. A., Baldocchi, D., Bonan, G., B., Bondeau, A., Cescatti, A., Lasslop, G., Lindroth,  
2456 A., Lomas, M., Luyssaert, S., Margolis, H., Oleson, K. W., Rouspard, O., Veenendaal, E.,  
2457 Viovy, N., Williams, C., Woodward, F. I. and Papale, D. (2010). Terrestrial gross carbon  
2458 dioxide uptake: global distribution and covariation with climate. *Science*, **329**, 834–838.  
2459 doi:10.1126/science.1184984
- 2460 Bennedsen, M., Hildebrand, E. and Koopman, S. (2019). Trend analysis of the airborne fraction  
2461 and sink rate of anthropogenically released CO<sub>2</sub>. *Biogeosciences*, **16**, 3651–3663.  
2462 doi:10.5194/bg-16-3651-2019
- 2463 Bloom, A. A., Bowman, K. W., Liu, J., Konings, A. G., Worden, J. R., Parazoo, N. C., Meyer, V.,  
2464 Reager, J. T., Worden, H. M., Jiang, Z., Quetin, G. R., Smallman, T. L., Exbrayat, J.-F., Yin,  
2465 Y., Saatchi, S. S., Williams, M., and Schimel, D. S. (2020). Lagged effects regulate the  
2466 inter-annual variability of the tropical carbon balance, *Biogeosciences*, **17**, 6393–6422,  
2467 2020. doi: 10.5194/bg-17-6393-2020
- 2468 Boden T. A., Marland G. and Andres R. J. (2017). Global, Regional, and National Fossil-Fuel  
2469 CO<sub>2</sub> Emissions. Carbon Dioxide Information Analysis Center, Oak Ridge National  
2470 Laboratory, U.S. Department of Energy, Oak Ridge, Tenn., U.S.A.  
2471 doi:10.3334/CDIAC/00001\_V2017
- 2472 Bolin, B., Björkström, A., Holmén, K. and Moore, B. (1983). The simultaneous use of tracers for  
2473 ocean circulation studies. *Tellus B*, **35B**, 206–236. doi:10.1111/j.1600-0889.1983.tb00025.x
- 2474 Bronselaer, B., and Zanna, L. (2020). Heat and carbon coupling reveals ocean warming due to  
2475 circulation changes. *Nature*, **584**, 227-233. doi: 10.1038/s41586-020-2573-5

- Booth, B. B. B., C. D. Jones, M. Collins, I. J. Totterdell, P. M. Cox, S. Sitch, C. Huntingford, R. Betts, G. R. Harris, and J. Lloyd. (2012). High sensitivity of future global warming to land carbon cycle processes, *Environmental Research Letters*, **7**, 024002. doi: 10.1088/1748-9326/7/2/024002
- Bousquet, P., Peylin, P., Ciais, P., Le Quéré, C., Friedlingstein, P., and Tans, P. (2000). Regional Changes in Carbon Dioxide Fluxes of Land and Oceans Since 1980. *Science*, **290**,1342-1346. doi: 10.1126/science.290.5495.1342
- Bowman, D. M. J. S., Williamson, G. J., Abatzoglou, J. T., Kolden, C. A., Cochrane, M. A. and Smith, A. M. S. (2017). Human exposure and sensitivity to globally extreme wildfire events. *Nature Ecology and Evolution*, **1**, 0058. doi: 10.1038/s41559-016-0058
- Bowman, D. M. J. S., Williamson, G. J., Price, O. F., Ndalila, M. N., and Bradstock, R. A. (2021). Australian forests, megafires and the risk of dwindling carbon stocks. *Plant Cell & Environment*, **44**, 347–355. doi: 10.1111/pce.13916
- BP Statistical Review of World Energy 2020. available at <https://www.bp.com/en/global/corporate/energy-economics/statistical-review-of-world-energy/co2-emissions.html>, last access 30 November 2021.
- Brandt, M., Wigneron, J.-P., Chave, J., Tagesson, T., Peñuelas, J., Ciais, P., Rasmussen, K., Tian, F., Mbow, C., Al-Yaari, A., Rodriguez-Fernandez, N., Schurgers, G., Zhang, W., Chang, J., Kerr, Y., Verger, A., Tucker, C., Mialon, A., Rasmussen, L., Fan, L., and Fensholt, R. (2018). Satellite passive microwaves reveal recent climate-induced carbon losses in African drylands. *Nature Ecology and Evolution*, **2**, 827–835. doi: 10.1038/s41559-018-0530-6
- Braswell, B. H., Schimel, D. S., Linder, E., and Moore, B. (1997). The Response of Global Terrestrial Ecosystems to Interannual Temperature Variability, *Science*, **278**, 870-873. doi: 10.1126/science.278.5339.870
- Brienen, R. J.W., Phillips, O. L., Feldpausch, T. R., Gloor, E., Baker, T. R., Lloyd, J., Lopez-Gonzalez, G., Monteagudo-Mendoza, A., Malhi, Y., Lewis, S. L., Vásquez Martinez, R., Alexiades, M., Álvarez Dávila, E., Alvarez-Loayza, P., Andrade, A., Aragão, L. E. O. C., Araujo-Murakami, A., Arets, E. J. M. M., Arroyo, L., Aymard, C. A. G., Bánki, O.S., Baraloto, C., Barroso, J., Bonal, D., Boot, R. G. A., Camargo, J. L. C., Castilho, C. V., Chama, V., Chao, K. J., Chave, J., Comiskey, J. A., Cornejo Valverde, F., da Costa, L., de Oliveira, E. A., Di Fiore, A., Erwin, T. L., Fauset, S., Forsthofer, M., Galbraith, D. R., Grahame, E. S., Groot, N., Hérault, B., Higuchi, N., Honorio Coronado, E. N., Keeling, H., Killeen, T. J., Laurance, W. F., Laurance, S., Licona, J., Magnussen, W. E., Marimon, B. S., Marimon-Junior, B. H., Mendoza, C., Neill, D. A., Nogueira, E. M., Núñez, P., Pallqui Camacho, N. C., Parada, A., Pardo-Molina, G., Peacock, J., Peña-Claros, M., Pickavance, G. C., Pitman, N. C. A., Poorter, L., Prieto, A., Quesada C. A., Ramírez, F., Ramírez-Angulo, H., Restrepo, Z., Roopsind, A., Rudas, A., Salomão, R. P., Schwarz, M., Silva, N., Silva-Espejo, J. E., Silveira, M., Stropp, J., Talbot, J., ter Steege, H., Teran-Aguilar, J., Terborgh, J., Thomas-Caesar, R., Toledo, M., Torello-Raventos, M., Umetsu, R. K., van der Heijden, G. M. F., van der Hout, P., Guimarães, Vieira I. C., Vieira, S. A., Vilanova, E., Vos, V. A. and Zagt, R. J. (2015). Long-term decline of the Amazon carbon sink. *Nature*, **519**, 344-348. doi: 10.1038/nature14283
- Bronselaer,B., and Zanna, L. (2020), Heat and carbon coupling reveals ocean warming due to circulation changes. *Nature*, **584**, 227–233. doi:10.1038/s41586-020-2573-5

- 2520 Buchanan, P. J., and Tagliabue, A. (2021). The Regional Importance of Oxygen Demand and  
2521 Supply for Historical Ocean Oxygen Trends. *Geophysical Research Letters*, **48**,  
2522 e2021GL094797. doi: 10.1029/2021GL094797
- 2523 Bushinsky, S. M., Landschützer, P., Rödenbeck, C., Gray, A. R., Baker, D., Mazloff, M. R.,  
2524 Resplandy, L., Johnson, K. S., and Sarmiento, J. L. (2019). Reassessing Southern Ocean air-  
2525 sea CO<sub>2</sub> flux estimates with the addition of biogeochemical float observations. *Global*  
2526 *Biogeochemical Cycles*, **33**, 1370-1388, doi:10.1029/2019GB006176
- 2527 Byrne, B., Wunch, D., Jones, D. B. A., Strong, K., Deng, F., Baker, I., Köhler, P., Frankenberg,  
2528 C., Joiner, J., Arora, V. K., Badawy, B., Harper, A. B., Warneke, T., Petri, C., Kivi, R. and  
2529 Roehl, C. M. (2018). Evaluating GPP and respiration estimates over northern midlatitude  
2530 ecosystems using solar-induced fluorescence and atmospheric CO<sub>2</sub> measurements. *Journal*  
2531 *of Geophysical Research: Biogeosciences*, **123**, 2976–2997. doi:10.1029/2018JG004472
- 2532 Byrne, B., Liu, J., Lee, M., Baker, I., Bowman, K. W., Deutscher, N. M., Feist, D. G., Griffith D.  
2533 W. T., Iraci, L. T., Kiel, M., Kimball, J. S., Miller, C. E., Morino, I., Parazoo, N. C., Petri,  
2534 C., Roehl, C. M., Sha, M. K., Strong, K., Velazco, V. A., Wennberg, P. O. and Wunch, D.  
2535 (2020a). Improved constraints on northern extratropical CO<sub>2</sub> fluxes obtained by combining  
2536 surface-based and space-based atmospheric CO<sub>2</sub> measurements. *Journal of Geophysical*  
2537 *Research: Atmospheres*, **125**, e2019JD032029. doi:10.1029/2019JD032029
- 2538 Byrne, B., Liu, J., Lee, M., Baker, I., Bowman, K. W., Deutscher, N. M., Feist, D. G., Griffith D.  
2539 W. T., Iraci, L. T., Kiel, M., Kimball, J. S., Miller, C. E., Morino, I., Parazoo, N. C., Petri, C.,  
2540 Roehl, C. M., Sha, M. K., Strong, K., Velazco, V. A., Wennberg, P. O., and Wunch, D.  
2541 (2020b). Improved constraints on northern extratropical CO<sub>2</sub> fluxes obtained by combining  
2542 surface-based and space-based atmospheric CO<sub>2</sub> measurements. *Journal of Geophysical*  
2543 *Research: Atmospheres*, **125**, e2019JD032029. doi: 10.1029/2019JD032029
- 2544 Cadule P., Friedlingstein P., Bopp L., Sitch, S., Jones, C. D., Ciais, P., Piao, S. L., and Peylin, P.  
2545 (2010). Benchmarking coupled climate-carbon models against long-term atmospheric CO<sub>2</sub>  
2546 measurements. *Global Biogeochemical Cycles*, **24**, GB2016. doi: 10.1029/2009gb003556
- 2547 Cai, W., Cowan, T., and Raupach, M. (2009), Positive Indian Ocean Dipole events precondition  
2548 southeast Australia bushfires, *Geophysical Research Letters*, **36**, L19710, doi:  
2549 10.1029/2009GL039902
- 2550 Cai, W., and Prentice, I. C. (2020). Recent trends in gross primary production and their drivers:  
2551 analysis and modelling at flux-site and global scales. *Environmental Research Letters*, **15**,  
2552 124050. doi: 10.1088/1748-9326/abc64e
- 2553 Campbell, J. E., Berry, J. A., Seibt, U., Smith, S. J., Montzka, S. A., Launois, T., Belviso, S.,  
2554 Bopp, L., and Laine, M. (2017). Large historical growth in global terrestrial gross primary  
2555 production, *Nature*, **544**, 84–87. doi: 10.1038/nature22030
- 2556 Canadell, J. G., Le Quéré, C., Raupach, M. R., Field, C. B., Buitenhuis, E., Ciais, P., Conway, T.  
2557 J., Gilett, N. P., Houghton, J. T. and Marland, G. (2007). Contributions to accelerating  
2558 atmospheric CO<sub>2</sub> growth from economic activity, carbon intensity, and efficiency of natural  
2559 sinks. *Proceedings of the National Academy of Sciences, USA*, **104**, 18,866 – 18,870.  
2560 doi:10.1073/pnas.0702737104
- 2561 Canadell, J. G., Ciais, P., Gurney, K., Le Quéré, C., Piao, S., Raupach, M. R., and Sabine, C. L.  
2562 (2011). An International Effort to Quantify Regional Carbon Fluxes, *Eos Transactions*  
2563 *AGU*, **92**, 81–82. doi: 10.1029/2011EO100001



- Canadell, J. G., Monteiro, P. M. S., Costa, M. H., Cotrim da Cunha, L., Cox, P. M., Eliseev, A.V., Henson, S., Ishii, M., Jaccard, S., Koven, C., Lohila, A., Patra, P. K., Piao, S., Rogelj, J., Syampungani, S., Zaehle, S., and Zickfeld, K.: Global Carbon and other Biogeochemical Cycles and Feedbacks. In: *Climate Change 2021: The Physical Science Basis. Contribution of Working Group I to the Sixth Assessment Report of the Intergovernmental Panel on Climate Change* [Masson-Delmotte, V., P. Zhai, A. Pirani, S. L. Connors, C. Péan, S. Berger, N. Caud, Y. Chen, L. Goldfarb, M. I. Gomis, M. Huang, K. Leitzell, E. Lonnoy, J.B.R. Matthews, T. K. Maycock, T. Waterfield, O. Yelekçi, R. Yu and B. Zhou (eds.)]. Cambridge University Press. In Press., 2021.
- Carroll, D., Menemenlis, D., Adkins, J. F., Bowman, K. W., Brix, H., Dutkiewicz, S., Fenty, I., Gierach, M. M., Hill, C., Jahn, O., Landschützer, P., Lauderdale, J. M., Liu, J., Manizza, M., Naviaux, J. D., Rödenbeck, C., Schimel, D. S., Van der Stocken, T. and Zhang, H. (2020). The ECCO-Darwin data-assimilative global ocean biogeochemistry model: Estimates of seasonal to multi-decadal surface ocean pCO<sub>2</sub> and air-sea CO<sub>2</sub> flux. *Journal of Advances in Modeling Earth Systems*, **12**, e2019MS001888. doi:10.1029/2019MS001888
- Carvalho, N., Forkel, M., Khomik, M., Bellarby, J., Jung, M., Migliavacca, M. Mu, M., Saatchi, S., Santoro, M., Thurner, M., Weber, U., Ahrens, B., Beer, C., Cescatti, A., Randerson, J. T. and Reichstein, M. (2014). Global covariation of carbon turnover times with climate in terrestrial ecosystems. *Nature*, **514**, 213-217. doi:10.1038/nature13731
- Casperson, J. P., S. W. Pacala, J. C. Jenkins, G. C. Hurtt, P. R. Moorcroft, and R. A. Birdsey (2000). Contributions of land use history to carbon accumulation in U.S. Forests. *Science*, **290**, 1148-1151. doi: 10.1126/science.290.5494.1148
- Castro, A. O., Chen, J., Zang, C. S., Shekhar, A., Jimenez, J. C., Bhattacharjee, S., Kindu, M., Morales, V. H. and Ramming, A. (2020). OCO-2 Solar-Induced Chlorophyll Fluorescence Variability across Ecoregions of the Amazon Basin and the Extreme Drought Effects of El Nino (2015-2016), *Remote Sensing*, **12**, 1202. doi:10.3390/rs12071202
- Catherman, C. (2021). Ocean scientists confront a critical bottleneck, *Science*, **374** (6563), doi: 10.1126/science.acx9218
- Chapin, F. S., Woodwell, G. M., Randerson, J. T., Rastetter, E. B., Lovett, G. M., Baldocchi, D. D., Clark, D. A., Harmon, M. E., Schimel, D. S., Valentini, R., Wirth, C., Aber, J. D., Cole, J. J., Goulden, M. L., Harden, J. W., Heimann, M., Howarth, R. W., Matson, P. A., McGuire, A. D., Melillo, J. M., Mooney, H. A., Neff, J. C., Houghton, R. A., Pace, M. L., Ryan, M. G., Running, S. W., Sala, O. E., Schlesinger, W. H. and Schulze, E. D. (2006). Reconciling carbon-cycle concepts, terminology, and methods. *Ecosystems*, **9**, 1041-1050. doi: 10.1007/s10021-005-0105-7
- Chatterjee, A., Gierach, M. M., Sutton, A. J., Feely, R. A., Crisp, D., Eldering, A., Gunson, M. R., O'Dell, C. W., Stephens, B. B. and Schimel, D. S. (2017). Influence of El Niño on atmospheric CO<sub>2</sub> over the tropical Pacific Ocean: Findings from NASA's OCO-2 mission. *Science*, **358**, eaam5776. doi:10.1126/science.aam5776
- Chen, Z., Huntzinger, D. N., Liu, J. Piao, S., Wang, X. Sitch, S., Friedlingstein, P., Anthoni, P., Arneeth, A., Bastrikov, V., Goll, D. S., Haverd, V., Jain, A. K., Joetzjer, E., Kato, E., Lienert, S., Lombardozzi, D. L., McGuire, P. C., Melton, J. R., Nabel, J. E. M. S., Pongratz, J., Poulter, B., Tian, H., Wiltshire, A., J., and Miller, S. (2021a). Five years of variability in the global carbon cycle: comparing an estimate from the Orbiting Carbon Observatory-2 and

- 2608 process-based models. *Environmental Research Letters*, **16**, 054041. doi: 10.1088/1748-  
2609 9326/abfac1
- 2610 Chen, Z., Liu, J., Henze, D. K., Huntzinger, D. N., Wells, K. C., Sitch, S., Friedlingstein, P.,  
2611 Joetzjer, E., Bastrikov, V., Goll, D. S., Haverd, V., Jain, A. K., Kato, E., Lienert, S.,  
2612 Lombardozzi, D. L., McGuire, P. C., Melton, J. R., Nabel, J. E. M. S., Poulter, B., Tian, H.,  
2613 Wiltshire, A. J., Zaehle, S., and Miller, S. M. (2021b). Linking global terrestrial CO<sub>2</sub> fluxes  
2614 and environmental drivers: inferences from the Orbiting Carbon Observatory 2 satellite and  
2615 terrestrial biospheric models. *Atmospheric Chemistry and Physics*, **21**, 6663–6680.  
2616 doi:10.5194/acp-21-6663-2021
- 2617 Cheng, L., Normandeau, C., Bowden, R., Doucett, R., Gallagher, B., Gillikin, D.P., Kumamoto,  
2618 Y., Mckay, J.L., Middlestead, P., Ninnemann, U., Nothaft, D., Dubinina, E.O., Quay, P.,  
2619 Reverdin, G., Shirai, K., Mørkved, P.T., Theiling, B.P., Van Geldern, R., and Wallace,  
2620 D.W.R. (2019). An international intercomparison of stable carbon isotope composition  
2621 measurements of dissolved inorganic carbon in seawater. *Limnology and Oceanography*:  
2622 *Methods*, **17**, 200-209. doi: 10.1002/lom3.10300
- 2623 Cheng, L., Normandeau, C., Cai, W.-J., Wallace D.W.R. (2021). Shipboard measurement of DIC  
2624 and  $\delta^{13}\text{C}$ -DIC on discrete seawater samples using Cavity Ring-Down Spectroscopy: system  
2625 testing and performance during three research cruises in the North Atlantic. *Isotopes in*  
2626 *Environmental and Health Studies*, In revision, [preprint]
- 2627 Chevallier, F., Ciais, P., Conway, T. J., Aalto, T., Anderson, B. E., Bousquet, P., Brunke, E. G.,  
2628 Ciattaglia, L., Esaki, Y., Frohlich, M., Gomez, A. J., Gomez-Pelaez, A. J., Haszpra, L.,  
2629 Krummel, P., Langenfelds, R., Leuenberger, M., Machida, T., Maignan, F., Matsueda, H.,  
2630 Morgui, J. A., Mukai, H., Nakazawa, T., Peylin, P., Ramonet, M., Rivier, L., Sawa, Y.,  
2631 Schmidt, M., Steele, P., Vay, S. A., Vermeulen, A. T., Wofsy, S. and Worthy, D. (2010). CO<sub>2</sub>  
2632 surface fluxes at grid point scale estimated from a global 21-year reanalysis of atmospheric  
2633 measurements. *Journal of Geophysical Research: Atmospheres*, **115**, D21307.  
2634 doi:10.1029/2010JD013887
- 2635 Chevallier, F., Remaud, M. O'Dell, C. W., Baker, D., Peylin, P. and Cozic, A. (2019). Objective  
2636 evaluation of surface and satellite driven CO<sub>2</sub> atmospheric inversion. *Atmospheric*  
2637 *Chemistry and Physics*, **19**, 14233–14251. doi:10.5194/acp-19-14233-2019
- 2638 Chevallier, F. (2021). Fluxes of carbon dioxide from managed ecosystems estimated by national  
2639 inventories compared to atmospheric inverse modeling. *Geophysical Research Letters*, **48**,  
2640 e2021GL093565. doi: 10.1029/2021GL093565
- 2641 Chini, L., Hurtt, G., Sahajpal, R., Frohling, S., Goldewijk, K. K., Sitch, S., Ganzenmüller, R.,  
2642 Ma, L., Ott, L., Pongratz, J., and Poulter, B. (2021). Land-use harmonization datasets for  
2643 annual global carbon budgets, *Earth System Science Data*, **13**, 4175–4189. doi:  
2644 10.5194/essd-13-4175-2021
- 2645 Church, J. A., White, N. J., Arblaster, J. M. (2005). Significant decadal-scale impact of volcanic  
2646 eruptions on sea level and ocean heat content. *Nature*, **438**, 74–77. doi:10.1038/nature04237
- 2647 Chuvieco, E., Yue, C., Heil, A., Mouillot, F., Alonso-Canas, I., Padilla, M., Pereira, J.M.C., Oom,  
2648 D., Tansey, K. (2016) A new global burned area product for climate assessment of fire  
2649 impacts. *Global Ecology and Biogeography*, **25**, 619-629. doi:10.1111/geb.12440
- 2650 Ciais, P., Tans, P. P., Trolier, M., White, J. W. C., and Francey, R. J. (1995). A Large Northern  
2651 Hemisphere Terrestrial CO<sub>2</sub> Sink Indicated by the <sup>13</sup>C/<sup>12</sup>C Ratio of Atmospheric CO<sub>2</sub>.  
2652 *Science*, **269**, 1098-1102. doi: 10.1126/science.269.5227.1098

- 2653 Ciais, P., Tans, P. P., Denning, A. S., Francey, R. J., Trolier, M., Meijer, A. J., White, J. W. C.,  
2654 Berry, J. A., Randall, D. A., Collatz, G. J., Sellers, P. J., Monfray, P., and Heimann, M.  
2655 (1997). A three-dimensional synthesis study of  $\delta^{18}\text{O}$  in atmospheric  $\text{CO}_2$  2. Simulations with  
2656 the TM2 transport model. *Journal of Geophysical Research*, **102**, 5873-5883. doi:  
2657 10.1029/96JD02361
- 2658 Ciais, P., Reichstein, M., Viovy, N., Granier, A., Ogee, J., Allard, V., Aubinet, M., Buchmann, N.,  
2659 Bernhofer, C., Carrara, A., Chevallier, F., De Noblet, N., Friend, A. D., Friedlingstein, P.,  
2660 Grunwald, T., Heinesch, B., Keronen, P., Knohl, A., Drinner, G., Loustau, D., Manca, G.,  
2661 Matteucci, G., Miglietta, F., Ourcival, J. M., Papale, D., Pilegaard, K., Rambal, S., Seufert,  
2662 G., Soussana, J. F., Sanz, M. J., Schulze, E. D., Vesala, T. and Valentini, R. (2005). Europe-  
2663 wide reduction in primary productivity caused by the heat and drought in 2003. *Nature*, **437**,  
2664 529–533. doi: 10.1038/nature03972
- 2665 Ciais, P., Sabine, C., Bala, G., Bopp, L., Brovkin, V., Canadell, J., Chhabra, A., DeFries, R.,  
2666 Galloway, J., Heimann, M., Jones, C., Le Quere, C., Myneni, R.B., Piao, S. and Thornton, P.  
2667 (2013). Carbon and Other Biogeochemical Cycles. In: Climate Change 2013: The Physical  
2668 Science Basis. Contribution of Working Group I to the Fifth Assessment Report of the  
2669 Intergovernmental Panel on Climate Change [Stocker, T.F., D. Qin, G.-K. Plattner, M.  
2670 Tignor, S.K. Allen, J. Boschung, A. Nauels, Y. Xia, V. Bex and P.M. Midgley (eds.)].  
2671 Cambridge University Press, Cambridge, United Kingdom and New York, NY, USA.
- 2672 Ciais, P., Dolman, A. J., Bombelli, A., Duren, R., Peregon, A., Rayner, P. J., Miller, C., Gobron,  
2673 N., Kinderman, G., Marland, G., Gruber, N., Chevallier, F., Andres, R. J., Balsamo, G.,  
2674 Bopp, L., Bréon, F.-M., Broquet, G., Dargaville, R., Battin, T. J., Borges, A., Bovensmann,  
2675 H., Buchwitz, M., Butler, J., Canadell, J. G., Cook, R. B., DeFries, R., Engelen, R., Gurney,  
2676 K. R., Heinze, C., Heimann, M., Held, A., Henry, M., Law, B., Luyssaert, S., Miller, J.,  
2677 Moriyama, T., Moulin, C., Myneni, R. B., Nussli, C., Obersteiner, M., Ojima, D., Pan, Y.,  
2678 Paris, J.-D., Piao, S. L., Poulter, B., Plummer, S., Quegan, S., Raymond, P., Reichstein, M.,  
2679 Rivier, L., Sabine, C., Schimel, D., Tarasova, O., Valentini, R., Wang, R., van der Werf, G.,  
2680 Wickland, D., Williams, M. and Zehner, C. (2014). Current systematic carbon-cycle  
2681 observations and the need for implementing a policy-relevant carbon observing system,  
2682 *Biogeosciences*, **11**, 3547–3602. doi:10.5194/bg-11-3547-2014
- 2683 Ciais, P., Tan, J., Wang, X., Roedenbeck, C., Chevallier, F., Piao, S.-L., Broquet, G., Le Quéré,  
2684 C., Canadell, J. G., Peng, S., Poulter, B., Liu, Z., and Tans, P. (2019). Five decades of  
2685 northern land carbon uptake revealed by the interhemispheric  $\text{CO}_2$  gradient. *Nature*, **568**,  
2686 221-225. doi: 10.1038/s41586-019-1078-6
- 2687 Ciais, P., Yao, Y., Gasser, T., Baccini, A., Wang, Y., Lauerwald, R., Peng, S., Bastos, A., Li, W.,  
2688 Raymnd, P. A., Canadell, J. G., Peters, G. P., Andres, R. J., Chang, J., Yue, C., Dolman, A.  
2689 J., Haverd, V., Hartman, J., Laruelle, G., Konings, A. G., King, A. W., Liu, Y., Luyssaert, S.,  
2690 Maignan, F., Patra, P. K., Peregon, A., Regnier, P., Pongratz, J., Poulter, B., Shvidenko, A.,  
2691 Valentini, R., Wang, R., Broquet, G., Yin, Y., Zscheischler, J., Guenet, B., Goll, D., S.,  
2692 Ballantyne, A.-P., Yang, H., Qiu, C. and Zhu, D. (2020a). Empirical estimates of regional  
2693 carbon budgets imply reduced global soil heterotrophic respiration. *National Science*  
2694 *Review*, **0**, nwaa145,1-14. doi:10.1093/nsr/nwaa145
- 2695 Ciais, P. Wang, Y., Andrew, R. M., Bréon, F. M., Chevallier, F., Broquet, G., Nabuurs, G. J.,  
2696 Peters, G. P., McGrath, M. J., Meng, W., Zheng, B. and Tao, S. (2020b). Biofuel burning  
2697 and human respiration bias on satellite estimates of fossil fuel  $\text{CO}_2$  emissions.  
2698 *Environmental Research Letters*, **15**, 074036. doi:10.1088/1748-9326/ab7835

- Ciais, P., Bastos, A., Chevallier, F., Lauerwald, R., Poulter, B., Canadell, P., Hugelius, G., Jackson, R. B., Jain, A., Jones, M., Kondo, M., Luijkx, I. T., Patra, P. K., Peters, W., Pongratz, J., Petrescu, A. M., R., Piao, S., Qiu, C., Von Randow, C., Regnier, P., Saunois, M., Scholes, R., Shvidenko, A., Tian, H., Yang, H., Wang, X., and Zheng, B (2022). Definitions and methods to estimate regional land carbon fluxes for the second phase of the REgional Carbon Cycle Assessment and Processes Project (RECCAP-2). *Geoscientific Model Development*, **15**, 1289–1316. doi: 10.5194/gmd-15-1289-2022
- Clark, H., Bennouna, Y., Tsvilidou, M., Wolff, P., Sauvage, B., Barret, B., Le Flochmoën, E., Blot, R., Boulanger, D., Cousin, J.-M., Nédélec, P., Petzold, A., and Thouret, V. (2021). The effects of the COVID-19 lockdowns on the composition of the troposphere as seen by In-service Aircraft for a Global Observing System (IAGOS) at Frankfurt, *Atmospheric Chemistry and Physics*, **21**, 16237–16256. doi: 10.5194/acp-21-16237-2021
- Claustre, H., Johnson, K. S., and Takeshita, Y. (2020). Observing the global ocean with Biogeochemical-Argo, *Annual Review of Marine Science*, **12**, 23–48. doi:10.1146/annurev-marine-010419-010956
- Claustre, H., Legendre, L., Boyde, P.W., and Levy, M. (2021). The Oceans' Biological Carbon Pumps: Framework for a Research Observational Community Approach. *Frontiers in Marine Science, Ocean Observation*, **8**, 780052. doi: 10.3389/fmars.2021.780052
- Clement, D., and Gruber, N. (2018). The eMLR(C\*) Method to determine decadal changes in the global ocean storage of anthropogenic CO<sub>2</sub>. *Global Biogeochemical Cycles*, **32**, 654–679. doi:10.1002/2017gb005819
- Cleverly, J., Eamus, D., Luo, Q., Coupe, N. R., Kljun, N., Ma, X., Ewenz, C., Li, L., Yu, Q. and Huete, A. (2016). The importance of interacting climate modes on Australia's contribution to global carbon cycle extremes. *Scientific Reports*, **6**, 23113. doi: 10.1038/srep23113
- Cortés, J., Mahecha, M. D., Reichstein, M., Myneni, R. B., Chen, C., and Brenning, A. (2021). Where are global vegetation greening and browning trends significant? *Geophysical Research Letters*, **48**, e2020GL091496. doi:10.1029/2020GL091496
- Cox, P. M., Pearson, D., Booth, B. B., Friedlingstein, P., Huntingford, C., Jones, C. D., and Luke, C. M. (2013). Sensitivity of tropical carbon to climate change constrained by carbon dioxide variability, *Nature*, **494**, 341–344. doi: 10.1038/nature11882
- Crisp, D., Atlas, R. M., Bréon, F.-B., Brown, L. R., Burrows, J. P., Ciais, P., Connor, B.J., Doney, S. C., Fung, I. Y., Jacob, D. J., Miller, C. E., O'Brien, D., Pawson, S., Randerson, J. T., Rayner, P., Salawitch, R. J., Sander, S. P., Sen, B., Stephens, G. L., Tans, P. P., Toon, G. C., Wennberg, P. O., Wofsy, S. C., Yung, Y. L., Kuang, Z., Chudasama, B., Sprague, G., Weiss, B., Pollock, R., Kenyon, D., Schroll, S. (2004). The Orbiting Carbon Observatory (OCO) mission. *Advances in Space Research*, **34**, 700–709, doi: 10.1016/j.asr.2003.08.062
- Crisp, D., Miller, C. E., and DeCola, P. L. (2008). NASA Orbiting Carbon Observatory: measuring the column averaged carbon dioxide mole fraction from space. *Journal of Applied Remote Sensing*, **2**, 023508; doi: 10.1117/1.2898457
- Crowell, S., Baker, D., Schuh, A., Basu, S., Jacobson, A., Chevallier, F., Liu, J., Deng, F., Feng, L., McKain, K., Chatterjee, A., Miller, J., Stephens, B., Eldering, A., Crisp, D., Schimel, D., Nassar, R., O'Dell, C., Oda, T., Sweeney, C., Palmer, P., and Jones, D. (2019). The 2015–2016 carbon cycle as seen from OCO-2 and the global in situ network. *Atmospheric Chemistry and Physics*, **19**, 7347–7376. doi:10.5194/acp-19-7347-2019

- 2743 Dannenberg, M. P., Wise, E. K., Janko, M., Hwang, T., and Smith, W. K. (2018). Atmospheric  
2744 teleconnection influence on North American land surface phenology. *Environmental*  
2745 *Research Letters*, **13**, 034029. doi: 10.1088/1748-9326/aaa85a/meta
- 2746 Dannenberg, M. P., Smith, W. K., Zhang, Y., Song, C., Huntzinger, D. N., and Moore, D. J. P.  
2747 (2021). Large-Scale Reductions in Terrestrial Carbon Uptake Following Central Pacific El  
2748 Niño, *Geophysical Research Letters*, **48**, e2020GL092367. doi: 10.1029/2020GL092367
- 2749 Deng, F., D. B. A. Jones, C. W. O'Dell, R. Nassar, and N. C. Parazoo (2016). Combining GOSAT  
2750 XCO<sub>2</sub> observations over land and ocean to improve regional CO<sub>2</sub> flux estimates, *Journal of*  
2751 *Geophysical Research Atmospheres*, **121**, 1896–1913. doi:10.1002/2015JD024157.
- 2752 Deng, Z., Ciais, P., Tzompa-Sosa, Z. A., Saunois, M., Qiu, C., Tan, C., Sun, T., Ke, P., Cui, Y.,  
2753 Tanaka, K., Lin, X., Thompson, R. L., Tian, H., Yao, Y., Huang, Y., Lauerwald, R., Jain, A.  
2754 K., Xu, X., Bastos, A., Sitch, S., Palmer, P. I., Lauvaux, T., d'Aspremont, A., Giron, C.,  
2755 Benoit, A., Poulter, B., Chang, J., Petrescu, A. M. R., Davis, S. J., Liu, Z., Grassi, G.,  
2756 Albergel, C., and Chevallier, F. (2021). Comparing national greenhouse gas budgets  
2757 reported in UNFCCC inventories against atmospheric inversions, *Earth System Science*  
2758 *Data Discuss.* [preprint]. doi:10.5194/essd-2021-235
- 2759 Denman, K. L., Brasseur, G., Chidthaisong, A., Ciais, P., Cox, P. M., Dickinson, R. E.,  
2760 Hauglustaine, D., Heinze, C., Holland, E., Jacob, D., Lohmann, U., Ramachandran, S., Leite  
2761 da Silva Dias, P., Wofsy, S. C., and Zhang, X. (2007). Couplings Between Changes in the  
2762 Climate System and Biogeochemistry, in: *Climate Change 2007: The Physical Science*  
2763 *Basis*. Contribution of Working Group I to the Fourth Assessment Report of the  
2764 Intergovernmental Panel on Climate Change, edited by: Solomon, S., Qin, D., Manning, M.,  
2765 Marquis, M., Averyt, K., Tignor, M. M. B., Miller, H. L., and Chen, Z. L., Cambridge  
2766 University Press, Cambridge, UK and New York, USA, 499–587.
- 2767 Denvil-Sommer, A., M. Gehlen, M. Vrac, and C. Mejia (2019). LSCE-FFNN-v1: A two-step  
2768 neural network model for the reconstruction of surface ocean pCO<sub>2</sub> over the global ocean.  
2769 *Geoscientific Model Development*, **12**, 2091–2105. doi:10.5194/gmd-12-2091-2019
- 2770 DeVries, T. (2014). The oceanic anthropogenic CO<sub>2</sub> sink: Storage, air-sea fluxes, and transports  
2771 over the industrial era, *Global Biogeochemical Cycles*, **28**, 631–647.  
2772 doi:10.1002/2013GB004739
- 2773 DeVries, T., Holzer, M. and Primeau, F. (2017). Recent increase in oceanic carbon uptake driven  
2774 by weaker upper-ocean overturning. *Nature*, **542**, 215–218. doi:10.1038/nature21068
- 2775 DeVries, T., Le Quéré, C., Andrews, O., Berthet, S., Hauck, J., Ilyina, T., Landschützer, P.,  
2776 Lenton, A., Lima, I. D., Nowicki, M., Schwinger, J., Séférian, R. (2019). Decadal trends in  
2777 the ocean carbon sink. *Proceedings of the National Academy of Sciences*, **116**, 11646–11651.  
2778 doi:10.1073/pnas.1900371116
- 2779 Diaz, H. F., Hoerling, M. P. and Eischeid, J. K. (2001). ENSO variability, teleconnections and  
2780 climate change, *Int. J. Climatol.*, **21**, 1845–1862. doi: 10.1002/joc.631
- 2781 Dlugokencky, E. J., Hall, B.D., Montzka, S.A., Dutton, G., Muhle, J. and Elkins, J.W. (2018).  
2782 Long-lived greenhouse gases [in "State of the Climate in 2017"]. *Bulletin of the American*  
2783 *Meteorological Society*, **99**, S46–S48. doi:10.1175/2018BAMSStateoftheClimate.1
- 2784 Doney S.C., Lindsay, K., Caldeira, K., Campin, J.-M., Drange, H., Dutay, J. C., Follows, M.,  
2785 Gao, Y., Gnanadesikan, A., Gruber, N., Ishida, A., Joos, F., Madec, G., Maier-Reimer, E.,  
2786 Marshall, J. C., Matear, R. J., Monfray, P., Mouchet, A., Najjar, R., Orr, J. C., Plattner, G.-  
2787 K., Sarmiento, J., Schlitzer, R., Slater, R., Totterdell, I. J., Weirig, M. F., Yamanaka, Y.

- and Yool, A. (2004). Evaluating global ocean carbon models: The importance of realistic physics. *Global Biogeochemical Cycles*, **18** (3), GB3017. doi:10.1029/2003GB002150
- Doughty, C. E. and Goulden, M. L. (2008). Are tropical forests near a high temperature threshold? *Journal of Geophysical Research: Biogeosciences*, **113**, G00B07. doi:10.1029/2007JG000632
- Duffy, K., A., Schwalm, C. R., Arcus, V. L., Koch, G. W., Liang, L. L. and Schipper, L. A. (2021). How close are we to the temperature tipping point of the terrestrial biosphere? *Science Advances*, **7**, eaay1052. doi: 10.1126/sciadv.aay1052
- Duncanson, L., Armston, J., Disney, M., Avitabile, V., Barbier, N., Calders, K., Carter, S., Chave, J., Herold, M., Crowther, T. W., Falkowski, M., Kellner, J. R., Labrière, N., Lucas, R., MacBean, N., McRoberts, R. E., Meyer, V., Naesset, E., Nickeson, J. E., Paul, K. I., Phillips, O. L., Réjou-Méchain, M., Román, M., Roxburgh, S., Saatchi, S., Schepaschenko, D., Scipal, K., Siqueira, P. R., Whitehurst, A. and Williams, M. (2019). The importance of consistent global forest aboveground biomass product Validation. *Surveys in Geophysics*, **40**, 979–999. doi: 10.1007/s10712-019-09538-8
- Eddebbbar, Y. A., Rodgers, K. B., Long, M. C., Subramanian, A. C., Xie S.-P. and Keeling, R. F. (2019). El Niño-like physical and biogeochemical ocean response to tropical eruptions. *Journal of Climate*, **32**, JCLI-D–18–0458.1, doi:10.1175/JCLI-D-18-0458.1
- Eldering, A., Wennberg, P. O., Crisp, D., Schimel, D., Gunson, M. R., Chatterjee, A., Liu J., Schwandner, Y. Sun, C.W. O'Dell, C. Frankenberg, T. Taylor, B. Fisher, G.B. Osterman, D. Wunch, F., Hakkarainen, J. and Tamminen, J. (2017). The Orbiting Carbon Observatory-2 early science investigations of regional carbon dioxide fluxes. *Science*, **358**, eaam5745. doi:10.1126/science.aam5745
- Enting, I.G., Trudinger, C.M. and Francey, R.J. (1995). A synthesis inversion of the concentration and  $\delta^{13}\text{C}$  atmospheric  $\text{CO}_2$ . *Tellus*, **47B**, 35-52. doi:10.1034/j.1600-0889.47.issue1.5.x
- Enting, I. G. (2002). *Inverse Problems in Atmospheric Constituent Transport*, Cambridge University Press, Cambridge, doi: 10.1017/CBO9780511535741
- Erb, K. H., Kastner, T., Plutzar, C., Bais, A. L. S., Carvalhais, N., Fetzel, T., Gingrich, S., Haberl, H., Lauk, C., Niedertscheider, M., Pongratz, J., Thurner, M. and Luyssaert, S. (2018). Unexpectedly large impact of forest management and grazing on global vegetation biomass. *Nature*, **553**, 73–76. doi: 10.1038/nature25138
- Etheridge, D. M., Steele, L. P., Langenfelds, R. L. and Francey (1996). Natural and anthropogenic changes in atmospheric  $\text{CO}_2$  over the last 1000 years from air in Antarctic ice and firn. *Journal of Geophysical Research*, **101**, 4115-4128. doi: 10.1029/95JD03410
- Fan, S., Gloor, M., Mahlman, J., Pacala, S., Sarmiento, J., Takahashi, T., and Tans, P. (1998). A Large Terrestrial Carbon Sink in North America Implied by Atmospheric and Oceanic Carbon Dioxide Data and Models. *Science*, **282**, 442-446. doi: 10.1126/science.282.5388.442
- Fan, L., Wigneron, J.-P., Ciais, P., Chave, J., Brandt, M., Fensholt, R., Saatchi, S. S. Bastos, A., Al-Yaari, A., Hufkens, K., Qin, Y., Xiao, X., Chen, C., Myneni, R. B., Rernandez-Moran, R., Mialon, A., Rodriguez-Fernandez, N. J., Kerr, Y., Tian, F. and Peñuelas, J. (2019). Satellite-observed pantropical carbon dynamics. *Nature Plants*, **5**, 944–951. doi:10.1038/s41477-019-0478-9



- Fay, A. R. and McKinley, G. A. (2013). Global trends in surface ocean pCO<sub>2</sub> from in situ data. *Global Biogeochemical Cycles*, **27**, 541–557. doi:10.1002/gbc.20051
- Fay, A. R., Lovenduski, N. S., McKinley, G. A., Munro, D. R., Sweeney, C., Gray, A. R., Landschützer, P., Stephens, B. B., Takahashi, T. and Williams, N. (2018). Utilizing the Drake Passage Time-series to understand variability and change in subpolar Southern Ocean pCO<sub>2</sub>. *Biogeosciences*, **15**, 3841–3855. doi:10.5194/bg-15-3841-2018
- Fay, A.R., Gregor, L., Landschützer, P. McKinley, G.A., Gruber, N., Gehlen, M., Iida, Y., Laruelle, G. G., Rödenbeck, C. and Zeng J. (2021). Harmonization of global surface ocean pCO<sub>2</sub> mapped products and their flux calculations; an improved estimate of the ocean carbon sink. *Earth System Science Data*, doi: 10.5194/essd-2021-16 [preprint]
- Fay, A. R., and McKinley, G. A. (2021). Observed regional fluxes to constrain modeled estimates of the ocean carbon sink. *Geophysical Research Letters*, **48**, e2021GL095325. doi: 10.1029/2021GL095325
- Feely, R. A., Wanninkhof, R., Takahashi, T., and, Tans P. (1999). Influence of El Niño on the equatorial Pacific contribution of atmospheric CO<sub>2</sub> accumulation, *Nature*, **398**, 597–601. doi: 10.1038/19273
- Fernández-Martínez, M., Sardans, J., Chevallier, F., Ciais, P., Obersteiner, M., Vicca, S., Canadell, J. G., Bastos, A., Friedlingstein, P., Sitch, S., Piao, S. L., Janssens, I. A. and Peñuelas, J. (2019). Global trends in carbon sinks and their relationships with CO<sub>2</sub> and temperature. *Nature Climate Change*, **9**, 73–79. doi: 10.1038/s41558-018-0367-7
- Fisher, J. B., Huntzinger, D. N., Schwalm, C. R. and Sitch, S. (2014). Modeling the terrestrial biosphere. *Annual Review of Environment and Resources*, **39**, 91–123. doi:10.1146/annurev-environ-012913-093456
- Fong, M. B. and Dickson, A. G. (2019). Insights from GO-SHIP hydrography data into the thermodynamic consistency of CO<sub>2</sub> system measurements in seawater. *Marine Chemistry*, **211**, 52–63. doi:10.1016/j.marchem.2019.03.006
- Forkel, M., Drüke, M., Thurner, M., Dorigo, W., Schaphoff, S., Thonicke, K., von Bloh, W., and Carvalhais, N. (2019) Constraining modelled global vegetation dynamics and carbon turnover using multiple satellite observations. *Scientific Reports*, **9**, 18757. doi:10.1038/s41598-019-55187-7
- Francey, R., Tans, P., Allison, C. E., Enting, I. G., White, J. W., C. and Troler, M. (1995). Changes in oceanic and terrestrial carbon uptake since 1982. *Nature* **373**, 326–330. doi: 10.1038/373326a0
- Frankenberg, C., O'Dell, C., Berry, J., Guanter, L., Joiner, J., Köhler, P., Pollock, R. and Taylor, T. E. (2014). Prospects for chlorophyll fluorescence remote sensing from the orbiting carbon observatory-2. *Remote Sensing of Environment*, **147**, 1–12. doi: 10.1016/j.rse.2014.02.007. ISSN 0034-4257
- Frey, M., Sha, M. K., Hase, F., Kiel, M., Blumenstock, T., Harig, R., Surawicz, G., Deutscher, N. M., Shiomi, K., Franklin, J. E., Bösch, H., Chen, J., Grutter, M., Ohyama, H., Sun, Y., Butz, A., Mengistu Tsidu, G., Ene, D., Wunch, D., Cao, Z., Garcia, O., Ramonet, M., Vogel, F. and Orphal, J. (2019). Building the Collaborative Carbon Column Observing Network (COCCON): long-term stability and ensemble performance of the EM27/SUN Fourier transform spectrometer. *Atmospheric Measurement Technologies*, **12**, 1513–1530. doi: 10.5194/amt-12-1513-2019



- 2876 Friedlingstein, P., Cox, P., Betts, R., Bopp, L., von Bloh, W., Brovkin, V., Cadule, P., Doney, S.,  
 2877 Eby, M., Fung, I., Bala, G., John, J., Jones, C., Joos, F., Kato, T., Kawamiya, M., Koor, W.,  
 2878 Lindsay, D., Matthews, H. D., Raddatz, T., Rayner, P., Reick, C., Roekner, E., Schnitzler,  
 2879 D.-G., Schnur, R., Strassmann, K., Weaver, A., J., Yoshikawa, C., and Zeng, N. (2006).  
 2880 Climate–Carbon Cycle Feedback Analysis: Results from the C<sup>4</sup>MIP Model Intercomparison.  
 2881 *Journal of Climate*, **19**, 3337–3353. doi: 10.1175/JCLI3800.1
- 2882 Friedlingstein, P., Jones, M. W., O'Sullivan, M., Andrew, R. M., Hauck, J., Peters, G. P., Peters,  
 2883 W., Pongratz, J., Sitch, S., Le Quéré, C., Bakker, D. C. E., Canadell, J. G., Ciais, P., Jackson,  
 2884 R. B., Anthoni, P., Barbero, L., Bastos, A., Bastrikov, V., Becker, M., Bopp, L., Buitenhuis,  
 2885 E., Chandra, N., Chevallier, F., Chini, L. P., Currie, K. I., Feely, R. A., Gehlen, M., Gilfillan,  
 2886 D., Gkritzalis, T., Goll, D. S., Gruber, N., Gutekunst, S., Harris, I., Haverd, V., Houghton, R.  
 2887 A., Hurtt, G., Ilyina, T., Jain, A. K., Joetzjer, E., Kaplan, J. O., Kato, E., Klein Goldewijk,  
 2888 K., Korsbakken, J. I., Landschützer, P., Lauvset, S. K., Lefèvre, N., Lenton, A., Lienert, S.,  
 2889 Lombardozzi, D., Marland, G., McGuire, P. C., Melton, J. R., Metzl, N., Munro, D. R.,  
 2890 Nabel, J. E. M. S., Nakaoka, S.-I., Neill, C., Omar, A. M., Ono, T., Peregon, A., Pierrot, D.,  
 2891 Poulter, B., Rehder, G., Resplandy, L., Robertson, E., Rödenbeck, C., Séférian, R.,  
 2892 Schwinger, J., Smith, N., Tans, P. P., Tian, H., Tilbrook, B., Tubiello, F. N., van der Werf, G.  
 2893 R., Wiltshire, A. J. and Zaehle, S. (2019). Global Carbon Budget 2019. *Earth System*  
 2894 *Science Data*, **11**, 1783–1838. doi:10.5194/essd-11-1783-2019
- 2895 Friedlingstein, P., O'Sullivan, M., Jones, M. W., Andrew, R. M., Hauck, J., Olsen, A., Peters, G.  
 2896 P., Peters, W., Pongratz, J., Sitch, S., Le Quéré, C., Canadell, J. G., Ciais, P., Jackson, R. B.,  
 2897 Alin, S., Aragão, L. E. O. C., Arneeth, A., Arora, V., Bates, N. R., Becker, M., Benoit-Cattin,  
 2898 A., Bittig, H. C., Bopp, L., Bultan, S., Chandra, N., Chevallier, F., Chini, L. P., Evans, W.,  
 2899 Florentie, L., Forster, P. M., Gasser, T., Gehlen, M., Gilfillan, D., Gkritzalis, T., Gregor, L.,  
 2900 Gruber, N., Harris, I., Hartung, K., Haverd, V., Houghton, R. A., Ilyina, T., Jain, A. K.,  
 2901 Joetzjer, E., Kadono, K., Kato, E., Kitidis, V., Korsbakken, J. I., Landschützer, P., Lefèvre,  
 2902 N., Lenton, A., Lienert, S., Liu, Z., Lombardozzi, D., Marland, G., Metzl, N., Munro, D. R.,  
 2903 Nabel, J. E. M. S., Nakaoka, S.-I., Niwa, Y., O'Brien, K., Ono, T., Palmer, P. I., Pierrot, D.,  
 2904 Poulter, B., Resplandy, L., Robertson, E., Rödenbeck, C., Schwinger, J., Séférian, R.,  
 2905 Skjelvan, I., Smith, A. J. P., Sutton, A. J., Tanhua, T., Tans, P. P., Tian, H., Tilbrook, B., van  
 2906 der Werf, G., Vuichard, N., Walker, A. P., Wanninkhof, R., Watson, A. J., Willis, D.,  
 2907 Wiltshire, A. J., Yuan, W., Yue, X. and Zaehle, S. (2020). Global Carbon Budget 2020.  
 2908 *Earth System Science Data*, **12**, 3269–3340. doi:10.5194/essd-12-3269-2020
- 2909 Friedlingstein, P., Jones, M. W., O'Sullivan, M., Andrew, R. M., Bakker, D. C. E., Hauck, J., Le  
 2910 Quéré, C., Peters, G. P., Peters, W., Pongratz, J., Sitch, S., Canadell, J. G., Ciais, P., Jackson,  
 2911 R. B., Alin, S. R., Anthoni, P., Bates, N. R., Becker, M., Bellouin, N., Bopp, L., Chau, T. T.  
 2912 T., Chevallier, F., Chini, L. P., Cronin, M., Currie, K. I., Decharme, B., Djeutchouang, L.,  
 2913 Dou, X., Evans, W., Feely, R. A., Feng, L., Gasser, T., Gilfillan, D., Gkritzalis, T., Grassi,  
 2914 G., Gregor, L., Gruber, N., Gürses, Ö., Harris, I., Houghton, R. A., Hurtt, G. C., Iida, Y.,  
 2915 Ilyina, T., Luijkx, I. T., Jain, A. K., Jones, S. D., Kato, E., Kennedy, D., Klein Goldewijk,  
 2916 K., Knauer, J., Korsbakken, J. I., Körtzinger, A., Landschützer, P., Lauvset, S. K., Lefèvre,  
 2917 N., Lienert, S., Liu, J., Marland, G., McGuire, P. C., Melton, J. R., Munro, D. R., Nabel, J.  
 2918 E. M. S., Nakaoka, S.-I., Niwa, Y., Ono, T., Pierrot, D., Poulter, B., Rehder, G., Resplandy,  
 2919 L., Robertson, E., Rödenbeck, C., Rosan, T. M., Schwinger, J., Schwingshackl, C., Séférian,  
 2920 R., Sutton, A. J., Sweeney, C., Tanhua, T., Tans, P. P., Tian, H., Tilbrook, B., Tubiello, F.,  
 2921 van der Werf, G., Vuichard, N., Wada, C., Wanninkhof, R., Watson, A., Willis, D., Wiltshire,

- 2922 A. J., Yuan, W., Yue, C., Yue, X., Zaehle, S., and Zeng, J. (2021). Global Carbon Budget  
2923 2021, Earth System Science Data Discuss. [preprint], doi: 10.5194/essd-2021-386, in  
2924 review, 2021.
- 2925 Friis, K., Körtzinger, A., Pätsch, J. and Wallace, D. W. R. (2005). On the temporal increase of  
2926 anthropogenic CO<sub>2</sub> in the subpolar North Atlantic. *Deep-Sea Research.* **52**, 681-698.  
2927 doi:10.1016/j.dsr.2004.11.017
- 2928 Frölicher, T. L., Joos, F. and Raible, C. C. (2011). Sensitivity of atmospheric CO<sub>2</sub> and climate to  
2929 explosive volcanic eruptions. *Biogeosciences*, **8**, 2317–2339. doi: 10.5194/bg-8-2317-2011
- 2930 Frölicher, T. L., Joos, F., Raible, C. C. and Sarmiento, J. L. (2013). Atmospheric CO<sub>2</sub> response to  
2931 volcanic eruptions: The role of ENSO, season, and variability. *Global Biogeochemical*  
2932 *Cycles*, **27**, 239-251. doi:10.1002/gbc.20028
- 2933 Frölicher, T.L., Rodgers, K. B., Stock, C. A., Cheung, W. W. L. (2016). Sources of uncertainties  
2934 in 21st century projections of potential ocean ecosystem stressors: Uncertainties in stressor  
2935 projections. *Global Biogeochemical Cycles*, **30**, 1224–1243. doi:10.1002/2015GB005338
- 2936 Galbraith, E. D. and Skinner, L. C. (2020). The biological pump during the last glacial  
2937 maximum. *Annual Reviews of Marine Science* **12**, 559–586. doi:10.1146/annurev-marine-  
2938 010419-010906
- 2939 Gampe, D., Zscheischler, J., Reichstein, M., O’Sullivan, M., Smith, W. K., Sitch, S. and  
2940 Buermann, W. (2021). Increasing impact of warm droughts on northern ecosystem  
2941 productivity over recent decades. *Nature Climate Change*, **11**, 772–779. doi:  
2942 10.1038/s41558-021-01112-8
- 2943 Gasser, T., Crepin, L., Quilcaille, Y., Houghton, R. A., Ciais, P., and Obersteiner, M. (2020).  
2944 Historical CO<sub>2</sub> emissions from land use and land cover change and their uncertainty,  
2945 *Biogeosciences*, **17**, 4075–4101. doi: 10.5194/bg-17-4075-202
- 2946 Gatti, L.V., Gloor, M., Miller, J. B., Doughty, C. E., Malhi, Y., Domingues, L. G., Basso, L. S.,  
2947 Martinewski, A., Correia, C. S., Borges, V. F., Freitas, S., Braz, R., Anderson, L. O., Rocha,  
2948 H., Grace, J., Phillips, O. L. and Lloyd, J. (2014). Drought sensitivity of Amazonian carbon  
2949 balance revealed by atmospheric measurements. *Nature*, **506**, 76-80.  
2950 doi:10.1038/nature12957
- 2951 Gatti, L. V., Basso, L., S., Miller, J., B., Gloor, M., Domingues, L. G., Cassol, H. L. G., Tejada,  
2952 G., Arango, L. E. O. C. Nobre, C., Peters, W., Marani, L., Arai, E., Sanches, A. H., Correa,  
2953 S. M., Anderson, L., von Randow, C., Correia, C. S. C., Crispim, S., P., and Neves, R. A. L.  
2954 (2021). Amazonia as a carbon source linked to deforestation and climate change. *Nature*,  
2955 **595**, 388-393. doi: 10.1038/s41586-021-03629-6
- 2956 Gaubert, B., Stephens, B. B., Basu, S., Chevallier, F., Deng, F., Kort, E. A., Patra, P. K., Peters,  
2957 W., Rödenbeck, C., Saeki, T., Schimel, D., Van der Laan-Luijx, I., Wofsy, S., Yin, Y. (2019).  
2958 Global atmospheric CO<sub>2</sub> inverse models converging on neutral tropical land exchange, but  
2959 disagreeing on fossil fuel and atmospheric growth rate. *Biogeosciences*, **16**, 117–134. doi:  
2960 10.5194/bg-16-117-2019
- 2961 Gitz, V. and Ciais, P. (2003) Amplifying effects of land-use change on future atmospheric CO<sub>2</sub>  
2962 levels. *Global Biogeochemical Cycles*, **17**, 1024. doi: 10.1029/2002GB001963
- 2963 Gloor, L., McKinley, G. A., Landschützer, P., Fay, A., Frölicher, T., Fyfe, J. C., Illyina, T.,  
2964 Jones, S.D., Lovenduski, N. S., Rödenbeck, C., Rodgers K. B., Schlunegger, S. and Takano,  
2965 Y. (2021). Quantifying errors in observationally-based estimates of ocean carbon sink

- 2966 variability. *Global Biogeochemical Cycles*, **35**, e2020GB006788. doi:  
2967 10.1029/2020GB006788
- 2968 Gloor, L., Yan, M., Zheng, T., & McKinley, G. A. (2022). Improved quantification of ocean  
2969 carbon uptake by using machine learning to merge global models and pCO<sub>2</sub> data. *Journal*  
2970 *of Advances in Modeling Earth Systems*, **14**, e2021MS002620. doi:  
2971 10.1029/2021MS002620
- 2972 Gloor, M., Sarmiento, J. L. and Gruber, N. (2010). What can be learned about carbon cycle  
2973 climate feedbacks from the CO<sub>2</sub> airborne fraction? *Atmospheric Chemistry and Physics*, **10**,  
2974 7739–7751. doi: 10.5194/acp-10-7739-2010
- 2975 Gonsamo, A., Chen, J. M., He, L., Sun, Y., Rogers, C. and Liu, J. (2019). Exploring SMAP and  
2976 OCO-2 observations to monitor soil moisture control on photosynthetic activity of global  
2977 drylands and croplands, *Remote Sensing of Environment*, **232**, 111314.  
2978 doi:10.1016/j.rse.2019.111314
- 2979 Gonsamo, A., Ciais, P., Miralles, D. G., Sitch, S., Dorigo, W., Lombardozzi, D., Friedlingstein,  
2980 P., Nabel, J. E. M. S., Goll, D. S., O'Sullivan, M., Arneth, A., Anthoni, P., Jain, A. K.,  
2981 Wiltshire, A., Peylin, P. and Cescatti, A. (2021). Greening drylands despite warming  
2982 consistent with carbon dioxide fertilization effect. *Glob Change Biol*, **27**, 3336-3349. doi:  
2983 10.1111/gcb.15658
- 2984 Goris, N., Tjiputra, J. F., Olsen, A., Schwinger, J., Lauvset S. K. and Jeansson E. (2018).  
2985 Constraining projection-based estimates of the future North Atlantic carbon uptake. *Journal*  
2986 *of Climate*, **31**, 3959–3978, doi:10.1175/JCLI-D-17-0564.1
- 2987 Grace, J., Mitchard, E., and Gloor, E. (2014). Perturbations in the carbon budget of the tropics.  
2988 *Global Change Biology*, **20**, 3238–3255. doi: 10.1111/gcb.12600
- 2989 Grassi, G., House, J., Kurz, W. A., Cescatti, A., Houghton, R. A., Peters, G. P., Sanz, M. J.,  
2990 Viñas, R. A., Alkama, R., Arneth, A., Bondeau, A., Dentener, F., Fader, M., Federici, S.,  
2991 Friedlingstein, P., Jain, A. K., Kato, E., Koven, C. D., Lee, D., Nabel, J. E. M. S., Nassikas,  
2992 A. A., Perugini, L., Rossi, S., Sitch, S., Viovy, N., Wiltshire, A. and Zaehle, S. (2018).  
2993 Reconciling global-model estimates and country reporting of anthropogenic forest CO<sub>2</sub>  
2994 sinks. *Nature Climate Change*, **8**, 914–920. doi: 10.1038/s41558-018-0283-x
- 2995 Graven, H. D., Keeling, R. F., Piper, S. C., Patra, P. K., Stephens, B. B., Wofsy, S. C., Welp, L.  
2996 R., Sweeney, C. and Tans, P. P. (2013). Enhanced seasonal exchange of CO<sub>2</sub> by northern  
2997 ecosystems since 1960, *Science*, **341**, 1085–1089. doi:10.1126/science.1239207
- 2998 Gregor, L., Lebehot, A. D. Kok, S. and Scheel Monteiro, P. M. (2019). A comparative assessment  
2999 of the uncertainties of global surface-ocean CO<sub>2</sub> estimates using a machine learning  
3000 ensemble (CSIR-ML6 version 2019a); have we hit the wall? *Geoscientific Model*  
3001 *Development*, **12**, 5113–5136. doi:10.5194/gmd-12-5113-2019
- 3002 Gruber, N., Clement, D., Carter, B.R., Feely, R.A., Van Heuven, S., Hoppema, M., Ishii, M., Key,  
3003 R.M., Kozyr, A., Lauvset, S.K., Lo Monaco, C., Mathis, J.T., Murata, A., Olsen, A., Perez,  
3004 F.F., Sabine, C.L., Tanhua, T., and Wanninkhof, R. (2019a). The oceanic sink for  
3005 anthropogenic CO<sub>2</sub> from 1994 to 2007. *Science*, **363**, 1193-1199.  
3006 doi:10.1126/science.aau5153
- 3007 Gruber, N., Landschützer, P., and Lovendus, N. S. (2019b). The variable Southern Ocean  
3008 carbon sink. *Annual Reviews of Marine Science*, **11**, 159–186. doi:10.1146/annurev-marine-  
3009 121916-063407

- Guan, K., Berry, J. A., Zhang, Y., Joiner, J., Guanter, L., Badgley, G. and Lobell, D. B. (2016). Improving the monitoring of crop productivity using spaceborne solar-induced fluorescence. *Global Change Biology*, **22**, 716–726. doi:10.1111/gcb.13136
- Guan, K., Wu, J., Kimball, J. S., Anderson, M. C., Frolking, S., Li, B., Hain, C. R. and Lobell, D. B. (2017). The shared and unique values of optical, fluorescence, thermal and microwave satellite data for estimating large-scale crop yields. *Remote Sensing of Environment*, **199**, 333–349. doi:10.1016/j.rse.2017.06.043
- Gurney, K. R., Law, R. M., Denning, A. S., Rayner, P. J., Baker, D., Bousquet, P., Bruhwiler, L., Chen, Y.-H., Ciais, P., Fan, S., Fung, I. Y., Gloor, M., Heimann, M., Higuchi, K., John, J., Maki, T., Maksyutov, S., Masarie, K., Peylin, P., Prather, M., Pak, B. C., Randerson, J., Sarmiento, J., Taguchi, S., Takahashi, T., and Yuen, C.-W. (2002). Towards robust regional estimates of CO<sub>2</sub> sources and sinks using atmospheric transport models, *Nature*, **415**, 626–630. doi: 10.1038/415626a
- Gurney, K. R., Law, R. M., Denning, A. S., Rayner, P. J., Baker, D., Bousquet, P., Bruhwiler, L., Chen, Y.-H., Ciais, P., Fan, S., Fung, I. Y., Gloor, M., Heimann, M., Higuchi, K., John, J., Kowalczyk, E., Maki, T., Maksyutov, S., Peylin, P., Prather, M., Pak, B. C., Sarmiento, J., Taguchi, S., Takahashi, T., and Yuen, C.-W. (2003). TransCom 3 CO<sub>2</sub> inversion intercomparison: 1. Annual mean control results and sensitivity to transport and prior flux information, *Tellus B*, **55**, 555–579. doi: 10.3402/tellusb.v55i2.16728
- Gurney, K. R., Liang, J., O'Keeffe, D., Patarasuk, R., Hutchins, M., Huang, J., Rao, P. and Song, Y. (2019). Comparison of global downscaled versus bottom-up fossil fuel CO<sub>2</sub> emissions at the urban scale in four U.S. urban areas. *Journal of Geophysical Research: Atmospheres*, **124**, 2823–2840. doi:10.1029/2018JD028859
- Hakkarainen, J., Ialongo, I. and Tamminen, J. (2016). Direct space-based observations of anthropogenic CO<sub>2</sub> emission areas from OCO-2. *Geophysical Research Letters*, **43**, 11,400–11,406. doi:10.1002/2016GL070885
- Hakkarainen, J., Ialongo, I., Maksyutov, S., and Crisp, D. (2019). Analysis of Four Years of Global XCO<sub>2</sub> Anomalies as Seen by Orbiting Carbon Observatory-2, *Remote Sensing*, **11**, 850. doi:10.3390/rs11070850
- Hakkarainen, J., Szelag, M. E., Ialongo, I., Retscher, C., Oda, T. and Crisp, D. (2021). Analyzing nitrogen oxides to carbon dioxide emission ratios from space: A case study of Matimba Power Station in South Africa. *Atmospheric Environment*, **10**, 100110. doi: 10.1016/j.aeaoa.2021.100110
- Hansen, J., Sato, M., Russell, G. and Kharecha, P., (2013). Climate sensitivity, sea level and atmospheric carbon dioxide, *Philosophical Transactions of the Royal Society. A.*, **371**, 20120294. doi: 10.1098/rsta.2012.0294
- Hansen, M. C., Potapov, P. V., Moore, R., Hancher, M., Turubanova, S. A., Tyukavina, A., Thau, D., Stehman, S. V., Goetz, S. J., Loveland, T. R., Kommareddy, A., Egorov, A., Chini, L., Justice, C. O., and Townshend, J. R. G. (2013b). High-Resolution Global Maps of 21st-Century Forest Cover Change. *Science*, **342**, 850–53. doi: 10.1126/science.1244693.
- Hansis, E., Davis, S. J. and Pongratz, J. (2015). Relevance of methodological choices for accounting of land use change carbon fluxes. *Global Biogeochemical Cycles*, **29**, 1230–1246. doi:10.1002/2014GB004997
- Harris, N. L., Hagen, S. C., Saatchi, S. S., Pearson, T. R. H., Woodall, C. W., Domke, G. M., Braswell, B. H., Walters, B. F., Brown, S., Salas, W., Fore, A., and Yu, Y. (2016). Attribution

- of net carbon change by disturbance type across forest lands of the conterminous United States. *Carbon Balance and Management*, **11**, 24. doi: 10.1186/s13021-016-0066-5
- Harris, N. L., Gibbs, D. A., Baccini, A., Birdsey, R. A., de Bruin, S., Farina, M., Fatoyinbo, L., Hansen, M. C., Herold, M., Houghton, R. A., Potapov, P. V., Suarez, D. R., Roman-Cuesta, R. M., Saatchi, S., S., Slay, C. M., Turubanova, S., A., and Tyukavina, A. (2021). Global maps of twenty-first century forest carbon fluxes. *Nature Climate Change*, **11**, 234–240. doi:10.1038/s41558-020-00976-6
- Hauck, J., Völker, C., Wang, T., Hoppema, M., Losch, M. and Wolf-Gladrow, D.A. (2013). Seasonally different carbon flux changes in the Southern Ocean in response to the southern annular mode. *Global Biogeochemical Cycles*, **27**, 1236–1245. doi:10.1002/2013GB004600
- Hauck, J., Völker, C., Wolf-Gladrow, D. A., Laufkötter, C., Vogt, M., Aumont, O., Bopp, L., Buitenhuis, E. T., Doney, S. C., Dunne, J., Gruber, N., Hashioka, T., John, J., Le Quéré, C., Lima, I. D., Nakano, H., Séférian, R. and Totterdell, I. (2015). On the Southern Ocean CO<sub>2</sub> uptake and the role of the biological carbon pump in the 21st century. *Global Biogeochemical Cycles*, **29**, 1451–1470. doi:10.1002/2015GB005140
- Hauck, J., Zeising, M., Le Quéré, C., Gruber, N., Bakker, D. C. E., Bopp, L., Chau, T. T. T., Gürses, Ö., Ilyina, T., Landschützer, P., Lenton, A., Resplandy, L., Rödenbeck, C., Schwinger, J. and Séférian, R. (2020). Consistency and challenges in the ocean carbon sink estimate for the Global Carbon Budget. *Frontiers in Marine Science*, **7**, 571720. doi:10.3389/fmars.2020.571720
- Hausfather, Z. and Peters, G. P. (2020). Emissions - the “business as usual” story is misleading. *Nature*, **577**, 618–620, doi:10.1038/d41586-020-00177-3
- He, L., Magney, T., Dutta, D., Yin, Y., Köhler, P., Grossmann, K., Stutz, J., Dold, C., Hatfield, J., Guan, K., Peng, B. and Frankenberg, C. (2020). From the ground to space: Using solar-induced chlorophyll fluorescence to estimate crop productivity. *Geophysical Research Letters*, **47**, e2020GL087474. doi:10.1029/2020GL087474
- Hedelius, J. K., Feng, S., Roehl, C. M., Wunch, D., Hillyard, P. W., Podolske, J. R., Iraci, L. T., Patarasuk, R., Roa, P., O’Keeffe, D., Gurney, K. R., Lauvaux, T., and Wennberg, P. O. (2017). Emissions and topographic effects on column CO<sub>2</sub> (XCO<sub>2</sub>) variations, with a focus on the Southern California Megacity. *Journal of Geophysical Research, Atmospheres*, **122**, 7200–7215, doi:10.1002/2017JD026455
- Hedelius, J. K., Liu, J., Oda, T., Maksyutov, S., Roehl, C. M., Iraci, L., Podolske, J., Hillyard, P., Liang, J., Gurney, K., Wunch, D. and Wennberg P. (2018). Southern California megacity CO<sub>2</sub>, CH<sub>4</sub>, and CO flux estimates using ground- and space-based remote sensing and a Lagrangian model, *Atmospheric Chemistry and Physics*, **18**, 16271–16291. doi:10.5194/acp-18-16271-2018
- Heimann, M., Esser, G., Haxeltine, A., Kaduk, J., Kicklighter, D. W., Knorr, W., Kohlmaier, G. H., McGuire, A. D., Melillo, J., Moore III, B., Otto, R. D., Prentice, I. C., Sauf, W., A. Schloss, Sitch, S., Wittenberg, U., Wurth, G. (1998). Evaluation of terrestrial carbon cycle models through simulations of the seasonal cycle of atmospheric CO<sub>2</sub>: First results of a model intercomparison study. *Global Biogeochemical Cycles*, **12**, 1, p 1–24. doi: 10.1029/97GB01936
- Henson, S. A., Beaulieu, C. and Lampitt, R. (2016). Observing climate change trends in ocean biogeochemistry: when and where. *Global Change Biology*, **22**, 1561–1571. doi:10.1111/gcb.13152

- 3100 Hersbach, H., Bell, B., Berrisford, P., Hirahara, S., Horányi, A., Muñoz-Sabater, J., Nicolas, J.,  
 3101 Peubey, C., Radu, R., Schepers, D., Simmons, A., Soci, C., Abdalla, S., Abellan, X.,  
 3102 Balsamo, G., Bechtold, P., Biavati, G., Bidlot, J., Bonavita, M., De Chiara, G., Dahlgren, P.,  
 3103 Dee, D., Diamantakis, M., Dragani, R., Flemming, J., Forbes, R., Fuentes, M., Geer, A.,  
 3104 Haimberger, L., Healy, S., Hogan, R. J., Hólm, E., Janisková, M., Keeley, S., Laloyaux, P.,  
 3105 Lopez, P., Radnoti, G., de Rosnay, P., Rozum, I., Vamborg, F., Villaume, S. and Thépaut, J.-  
 3106 N. (2020). The ERA5 Global Reanalysis. *Quarterly Journal of the Royal Meteorological*  
 3107 *Society*, **146**, 1999–2049. doi: <https://doi.org/10.1002/qj.3803>
- 3108 Heymann, J., Reuter, M., Buchwitz, M., Schneising, O., Bovensmann, H., Burrows, J. P.,  
 3109 Massart, S., Kaiser, J. W., and Crisp, D. (2017). CO<sub>2</sub> emission of Indonesian fires in 2015  
 3110 estimated from satellite-derived atmospheric CO<sub>2</sub> concentrations. *Geophysical Research*  
 3111 *Letters*, **44**, 1537–1544. doi: [10.1002/2016GL072042](https://doi.org/10.1002/2016GL072042)
- 3112 Hlásny, T., Zimová, S., Merganičová, K., Štěpánek, P., Modlinger, R., and Turčáni, M. (2021).  
 3113 Devastating outbreak of bark beetles in the Czech Republic: Drivers, impacts, and  
 3114 management implications, *Forest Ecology and Management*, **490**, 119075, doi:  
 3115 [10.1016/j.foreco.2021.119075](https://doi.org/10.1016/j.foreco.2021.119075)
- 3116 Hong, C., Burney, J. A., Pongratz, J., Nabel, J. E. M. S., Mueller, N. D., Jackson, R. B., and  
 3117 Davis, S. J. (2021). Global and regional drivers of land-use emissions in 1961–2017.  
 3118 *Nature*, **589**, 554–561. doi: [10.1038/s41586-020-03138-y](https://doi.org/10.1038/s41586-020-03138-y)
- 3119 Hoppema, M., Bakker, K., van Heuven, S. M. A. C., van Ooijen, J. C. and de Baar, H. J. W.  
 3120 (2015). Distributions, trends and inter-annual variability of nutrients along a repeat section  
 3121 through the Weddell Sea (1996–2011). *Marine Chemistry*, **177**, 545–553.  
 3122 doi:[10.1016/j.marchem.2015.08.007](https://doi.org/10.1016/j.marchem.2015.08.007)
- 3123 Houghton, R. A. (2003). Revised estimates of the annual net flux of carbon to the atmosphere  
 3124 from changes in land use and land management 1850–2000. *Tellus*, **55B**, 378–390.  
 3125 doi:[10.1034/j.1600-0889.2003.01450.x](https://doi.org/10.1034/j.1600-0889.2003.01450.x)
- 3126 Houghton, R. A., House, J. I., Pongratz, J., van der Werf, G. R., DeFries, R. S., Hansen, M. C.,  
 3127 Le Quéré, C., and Ramankutty, N. (2012). Carbon emissions from land use and land-cover  
 3128 change, *Biogeosciences*, **9**, 5125–5142, doi: [10.5194/bg-9-5125-2012](https://doi.org/10.5194/bg-9-5125-2012)
- 3129 Houghton, R. A. and Nassikas, A. A. (2017). Global and regional fluxes of carbon from land use  
 3130 and land cover change 1850–2015. *Global Biogeochemical Cycles*, **31**, 456–472.  
 3131 doi:[10.1002/2016GB005546](https://doi.org/10.1002/2016GB005546)
- 3132 Houweling, S., Baker, D., Basu, S., Boesch, H., Butz, A., Chevallier, F., Deng, F., Dlugokencky,  
 3133 E. J., Feng, L., Ganshin, A., Hasekamp, O., Jones, D., Maksyutov, S., Marshall, J., Oda, T.,  
 3134 O'Dell, C. W., Oshchepkov, S., Palmer, P. I., Peylin, P., Poussi, Z., Reum, F., Takagi, H.,  
 3135 Yoshida, Y., and Zhuravlev, R. (2015). An intercomparison of inverse models for estimating  
 3136 sources and sinks of CO<sub>2</sub> using GOSAT measurements, *Journal of Geophysical Research*  
 3137 *Atmospheres*, **120**, 5253–5266. doi: [10.1002/2014JD022962](https://doi.org/10.1002/2014JD022962)
- 3138 Hubau, W., Lewis, S. L., Phillips, O. L., Affum-Baffoe, B., Bockheim, K. H., Cuni-Sanchez, A.,  
 3139 Ewango, C. E. N., Fauset, S., Sheil, D., Sonké, B., Sullivan, M. J. P., Sunderland, T.,  
 3140 Thomas, S. C., Abernethy, K. A., Adu-Bredu, S., Amani, C. A., Baker, T. R., Banin, L. F.,  
 3141 Baya, F., Begne, S. K., Bennett, A. C., Benedet, F., Bitariho, R., Bocko, Y. E., Boeckx, P.,  
 3142 Boundja, P., Brienen, R. J. W., Brncic, T., Chezeaux, E., Chuyong, G. B., Clark, C. J.,  
 3143 Collins, M., Comiskey, J. A., Coomes, D. A., Dargie, G. C., de Haulleville, T., Kamdem, M.  
 3144 N. D., Doucet, J. L., Esquivel-Muelbert, A., Feldpausch, T. R., Fofanah, A., Folli, E. G.,

- Gilpin, M., Gloor, E., Gonmadje, C., Gourlet-Fleury, S., Hall, J. S., Hamilton, A. C., Harris, D. J., Hart, T. B., Hockemba, M. B. N., Hladik, A., Ifo, S. F., Jeffery, K. J., Jucker, T., Yakusu, E. K., Kearsley, E., Kenfack, D., Koch, A., Leal, M. E., Levesley, A., Lindsell, J. A., Lisingo, J., Lopez-Gonzalez, G., Lovett, J. C., Makana, J. R., Malhi, Y., Marshall, A. R., Martin, J., Martin, E. H., Mbayu, F. M., Medjibe, V. P., Mitchard, E. T. A., Moore, S., Munishi, P. K. T., Bengone, N. N., Ojo, L., Ondo, F. E., Peh, K. S., Pickavance, G. C., Poulsen, A. D., Poulsen, J. R., Qie, L., Reitsma, J., Rovero, F., Swaine, M. D., Talbot, J., Taplin J., Taylor, D. D., Thomas, D. W., Toirambe, B., Mukendi, J. T., Tuagben, D., Umunay, P. M., van der Heijden, G. M. F., Verbeeck, H., Vleminckx, J., Willcock, S., Wöll, H., Woods, J. T. and Zemagho, L. (2020). Asynchronous carbon sink saturation in African and Amazonian tropical forests. *Nature*, **579**, 80–87. doi:10.1038/s41586-020-2035-0
- Huber, M. B. and Zanna, L. (2017). Drivers of uncertainty in simulated ocean circulation and heat uptake. *Geophysical Research Letters*, **44**, 1402–1413. doi:10.1002/2016GL071587
- Humphrey, V., Zscheischler, J., Ciais, P., Gudmundsson, L., Sitch, S., & Seneviratne, S. I. (2018). Sensitivity of atmospheric CO<sub>2</sub> growth rate to observed changes in terrestrial water storage. *Nature*, **560**, 628. doi: 10.1038/s41586-018-0424-4
- Humphrey, V., Berg, A., Ciais, P., Gentine, P., Jung, M., Relchstein, M., Seneviratne, S. I., and Frankenberg, C. (2021). Soil moisture–atmosphere feedback dominates land carbon uptake variability. *Nature*, **592**, 65–69. doi: 10.1038/s41586-021-03325-5
- Hurtt, G. C., Chini, L., Sahajpal, R., Frolking, S., Bodirsky, B. L., Calvin, K., Doelman, J. C., Fisk, J., Fujimori, S., Klein Goldewijk, K., Hasegawa, T., Havlik, P., Heinimann, A., Humpenöder, F., Jungclaus, J., Kaplan, J. O., Kennedy, J., Krisztin, T., Lawrence, D., Lawrence, P., Ma, L., Mertz, O., Pongratz, J., Popp, A., Poulter, B., Riahi, K., Shevliakova, E., Stehfest, E., Thornton, P., Tubiello, F. N., van Vuuren, D. P. and Zhang, X. (2020). Harmonization of global land use change and management for the period 850–2100 (LUH2) for CMIP6. *Geoscientific Model Development*, **13**, 5425–5464. doi: 10.5194/gmd-13-5425-2020
- Hwang, Y. Schlüter, S. Choudhury, T.; Um, J.-S. (2021). Comparative Evaluation of Top-Down GOSAT XCO<sub>2</sub> vs. Bottom-Up National Reports in the European Countries. *Sustainability*, **13**, 6700. doi: 10.3390/su1312670
- Iida, T., Odate, T., Fukuchi, M. (2013). Long-Term Trends of Nutrients and Apparent Oxygen Utilization South of the Polar Front in Southern Ocean Intermediate Water from 1965 to 2008. *PLoS ONE*, **8**, e71766. doi:10.1371/journal.pone.0071766
- IEA World Energy Balances, 2020 Edition. Available from <https://www.iea.org/subscribe-to-data-services/world-energy-balances-and-statistics>, last viewed on 30 November 2021.
- IPCC 2006, 2006 IPCC Guidelines for National Greenhouse Gas Inventories, Prepared by the National Greenhouse Gas Inventories Programme, Eggleston H.S., Buendia L., Miwa K., Ngara T. and Tanabe K. (eds). Published: IGES, Japan.
- IPCC 2014, Intergovernmental Panel on Climate Change. (2014). Climate change 2013: The physical science basis: Working Group I contribution to the Fifth Assessment Report of the Intergovernmental Panel on Climate Change. In T. F. Stocker, D. Qin, G.-K. Plattner, M. Tignor, S. K. Allen, J. Boschung, et al. (Eds.), Cambridge University Press. doi: 10.1017/CBO9781107415324
- IPCC 2019, 2019 Refinement to the 2006 IPCC Guidelines for National Greenhouse Gas Inventories, Calvo Buendia, E., Tanabe, K., Kranjc, A., Baasansuren, J., Fukuda, M.,



- 3190 Ngarize S., Osako, A., Pyrozhenko, Y., Shermanau, P. and Federici, S. (eds). Published:  
3191 IPCC, Switzerland.
- 3192 IPCC, 2021: Summary for Policymakers. In: Climate Change 2021: The Physical Science Basis.  
3193 Contribution of Working Group I to the Sixth Assessment Report of the Intergovernmental  
3194 Panel on Climate Change [Masson-Delmotte, V., P. Zhai, A. Pirani, S.L. Connors, C. Péan,  
3195 S. Berger, N. Caud, Y. Chen, L. Goldfarb, M.I. Gomis, M. Huang, K. Leitzell, E. Lonnoy,  
3196 J.B.R. Matthews, T.K. Maycock, T. Waterfield, O. Yelekçi, R. Yu, and B. Zhou (eds.)].  
3197 Cambridge University Press. In Press.
- 3198 Ito, A. (2020). Constraining size-dependence of vegetation respiration rates, *Scientific Reports*,  
3199 **10**, 4304. doi:10.1038/s41598-020-61239-0
- 3200 Iudicone, D., Rodgers, K. B., Plancherel, Y., Aumont, O., Ito, T., Key, R. M., Madec, G. and  
3201 Ishii, M. (2016). The formation of the ocean's anthropogenic carbon reservoir. *Scientific*  
3202 *Reports*, **6**, 35473. doi:10.1038/srep35473
- 3203 Jacobson, A. R., Mikaloff Fletcher, S. E., Gruber, N., Sarmiento, J. L. and Gloor, M. (2007). A  
3204 joint atmosphere-ocean inversion for surface fluxes of carbon dioxide: 1. Methods and  
3205 global-scale fluxes. *Global Biogeochemical Cycles*, **21**, 273. doi:10.1029/1999GL900363
- 3206 Janssens-Maenhout, G., Crippa, M., Guizzardi, D., Muntean, M., Schaaf, E., Dentener, F.,  
3207 Bergamaschi, P., Pagliari, V., Olivier, J. G. J., Peters, J. A. H. W., van Aardenne, J. A.,  
3208 Monni, S., Doering, U., Petrescu, A. M. R., Solazzo, E. and Oreggioni, G. D. (2019).  
3209 EDGAR v4.3.2 Global Atlas of the three major greenhouse gas emissions for the period  
3210 1970–2012. *Earth System Science Data*, **11**, 959-1002. doi:10.5194/essd-11-959-2019
- 3211 Janssens-Maenhout, G., Pinty, B., Dowell, M., Zunker, H., Andersson, E., Balsamo, G., Bézy, J.  
3212 L., Brunhes, T., Bösch, H., Bojkov, B., Brunner, D., Buchwitz, M., Crisp, D., Ciais, P.,  
3213 Counet, P., Dee, D., Denier van der Gon, H., Dolman, H., Drinkwater, M., Dubovnik O.,  
3214 Engelen, R., Fehr, T., Fernandez, V., Heimann, M., Holmlund, K., Houweling, S., Husband,  
3215 R., Juvyns, O., Kentarchos, A., Landgraf, J., Lang, R., Löschner, A., Marshall, J., Meijer, Y.,  
3216 Nakajima, M., Palmer, P. I., Peylin, P., Rayner, P., Scholze, M., Sierk, B., Tamminen, J.,  
3217 Veefkind, P. (2020). Toward an operational anthropogenic CO<sub>2</sub> emissions monitoring and  
3218 verification support capacity. *Bulletin of the American Meteorological Society*, **101**, E1439-  
3219 E1451. doi:10.1175/BAMS-D-19-0017.1
- 3220 Jeong, S.-J., Bloom, A. A., Schimel, D., Sweeney, C., Parazoo, N. C., Medvigy, D., Schaepman-  
3221 Strub, G., Zheng, C., Schwalm, C. R., Huntzinger, D. N., Michalak, A. M., and Miller, C. E.  
3222 (2018). Accelerating rates of Arctic carbon cycling revealed by long-term atmospheric CO<sub>2</sub>  
3223 measurements. *Science Advances*, **4**, Eaao1167. doi: 10.1126/sciadv.aao1167
- 3224 Jian, J., Vargas, R., Anderson-Teixeira, K., Stell, E., Herrmann, V., Horn, M., Kholod, N.,  
3225 Manzon, J., Marchesi, R., Paredes, D. and Bond-Lamberty, B. (2021). A restructured and  
3226 updated global soil respiration database (SRDB-V5). *Earth System Science Data*, **13**, 255-  
3227 267, doi: 10.5194/essd-13-255-2021
- 3228 Jiang, C., and Ryu, Y. (2016). Multi-scale evaluation of global gross primary productivity and  
3229 evapotranspiration products derived from Breathing Earth System Simulator (BESS).  
3230 *Remote Sensing of Environment*, **186**, 528-547. doi: 10.1016/j.rse.2016.08.030
- 3231 Johnson, K. S., Jannasch, H. W., Coletti, L. J., Elrod, V. A., Martz, T. R., Takeshita, Y., Carlson,  
3232 R. J. and Connery, J. G. (2016). Deep-Sea DuraFET: A pressure tolerant pH sensor designed  
3233 for global sensor networks. *Analytical Chemistry*, **88**, 3249-3256.  
3234 doi:10.1021/acs.analchem.5b04653

- 3235 Joiner, J., Yoshida, Y., Zhang, Y., Duveiller, G., Jung, M., Lyapustin, A., Wang, Y., and Tucker C.  
3236 J. (2018). Estimation of Terrestrial Global Gross Primary Production (GPP) with Satellite  
3237 Data-Driven Models and Eddy Covariance Flux Data. *Remote Sensing*, 10, 1346, doi:  
3238 10.3390/rs10091346
- 3239 Jones, C. D. Ciais, P., Davis, S. J., Friedlingstein, P., Gasser, T., Peters, G. P., Rogelj, J., van  
3240 Vuuren, D. P., Canadell, J. G., Cowie, A., Jackson, R. B., Jonas, M., Kriegler, E., Littleton,  
3241 E., Lowe, J. A., Milne, J., Shrestha, G., Smith, P., Torvanger, A., and Wiltshire, A. (2016).  
3242 Simulating the Earth system response to negative emissions. *Environmental Research*  
3243 *Letters*, 11, 095012. doi: 10.1088/1748-9326/11/9/095012
- 3244 Joos, F., Bruno, M., Fink, R., Siegenthaler, U., Stocker, T. F., Le Quéré, C. and Sarmiento, J. L.  
3245 (1996). An efficient and accurate representation of complex oceanic and biospheric models  
3246 of anthropogenic carbon uptake. *Tellus B*, 48, 397. doi:10.1034/j.1600-0889.1996.t01-2-  
3247 00006.x
- 3248 Joos, F. and Spahni, R. (2008). Rates of change in natural and anthropogenic radiative forcing  
3249 over the past 20,000 years, *Proceedings of the National Academy of Sciences, USA*, 105,  
3250 1425–1430. doi: 10.1073/pnas.0707386105
- 3251 Jung, M., Reichstein, M. and Bondeau, A. (2009). Towards global empirical upscaling of  
3252 FLUXNET eddy covariance observations: validation of a model tree ensemble approach  
3253 using a biosphere model. *Biogeosciences*, 6, 2001–2013. doi:10.5194/bg-6-2001-2009
- 3254 Jung, M., Reichstein, M., Schwalm, C. R., Huntingford, C., Sitch, S., Ahlström, A., Arneeth, A.,  
3255 Camps-Valls, G., Ciais, P., Friedlingstein, P., Gans, F., Ichii, K., Jain, A. K., Kato, E.,  
3256 Papale, D., Poulter, B., Raduly, B., Rödenbeck, C., Tramontana, G., Viovy, N., Wang, Y.-P.,  
3257 Weber, U., Zaehle, S., and Zeng, N. (2017). Compensatory water effects link yearly global  
3258 land CO<sub>2</sub> sink changes to temperature, *Nature*, 541, 516–520. doi: 10.1038/nature20780
- 3259 Jung, M., Schwalm, C. Migliavacca, M., Walther, S., Camps-Valls, G., Koirala, S., Anthoni, P.,  
3260 Besnard, S., Bodesheim, P., Carvalhais, N., Chevallier, F., Gans, F., Goll, D. S., Haverd, V.,  
3261 Koehler, P., Ichii, K., Jain, A. K., Liu, J., Lombardozzi, D., Nabel, J. E. M. S., Nelson, J. A.,  
3262 O’Sullivan, M., Pallandt, M., Papale, D., Peters, W., Pongratz, J., Roedenbeck, C., Sitch, S.,  
3263 Tramontana, G., Walker, A., Weber, U. and Reichstein, M. (2020). Scaling carbon fluxes  
3264 from eddy covariance sites to globe: synthesis and evaluation of the FLUXCOM approach.  
3265 *Biogeosciences*, 17, 1343–1365. doi: 10.5194/bg-17-1343-2020
- 3266 Kao, H.-Y. and Yu, J.-Y. (2009). Contrasting Eastern-Pacific and Central-Pacific Types of ENSO,  
3267 *J. Clim.*, 22, 615–632. doi: 10.1175/2008JCLI2309.1
- 3268 Kaminski, T., and Heimann, M. (2001). Inverse Modeling of Atmospheric Carbon Dioxide  
3269 Fluxes. *Science*, 294, 259a. doi: 10.1126/science.294.5541.259a
- 3270 Kaminski, T., Scholze, M., Vossbeck, M., Knorr, W., Buchwitz, M., & Reuter, M. (2017).  
3271 Constraining a terrestrial biosphere model with remotely sensed atmospheric carbon  
3272 dioxide. *Remote Sensing of Environment*, 203, 109–124. doi: 10.1016/j.rse.2017.08.017
- 3273 Karion, A., Sweeney, C., Tans, P. P. and Newberger, T. (2010). AirCore: An innovative  
3274 atmospheric sampling system. *Journal of Atmospheric and Oceanic Technology*, 27, 1839–  
3275 1853. doi:10.1175/2010JTECHA1448.1
- 3276 Keeling, C. D. (1960). The concentration and isotopic abundances of carbon dioxide in the  
3277 atmosphere. *Tellus*, 12, 200-203. doi: 10.1111/j.2153-3490.1960.tb01300.x

- 3278 Keeling, C. D. (1973) *The Carbon Dioxide Cycle: Reservoir Models to Depict the Exchange of*  
 3279 *Atmospheric Carbon Dioxide with the Oceans and Land Plants*. In Chemistry of the Lower  
 3280 Atmosphere. Springer. doi: 10.1007/978-1-4684-1986-3\_6
- 3281 Keeling, C. D., Bacastow, R. B., Carter, A. F., Piper, S. C., Whorf, T. P., Heimann, M., Mook, W.  
 3282 G., and Roeloffzen, H. (1989). A Three-Dimensional Model of Atmospheric CO<sub>2</sub> Transport  
 3283 Based on Observed Winds: 1. Analysis of Observational Data. *Geophysical Monograph*,  
 3284 **55**, 165-236. doi: 10.1029/GM055p0165
- 3285 Keeling, C., Whorf, T., Wahlen, M., and van der Plichtt, J. (1995). Interannual extremes in the  
 3286 rate of rise of atmospheric carbon dioxide since 1980. *Nature*, **375**, 666–670 (1995). doi:  
 3287 10.1038/375666a0
- 3288 Keeling, C. D., Chin, J. F. S., and Whorf, T. P. (1996). Increased activity of northern vegetation  
 3289 inferred from atmospheric CO<sub>2</sub> measurements. *Nature*, **382**, 146-149. doi:  
 3290 10.1038/382146a0
- 3291 Keeling, C. D., Piper, S. C., Bacastow, R. B., Wahlen, M., Whorf, T. P., Heimann, M., and  
 3292 Meijer, H. A. (2001). Exchanges of Atmospheric CO<sub>2</sub> and <sup>13</sup>CO<sub>2</sub> with the Terrestrial  
 3293 Biosphere and Oceans from 1978 to 2000.I. Global Aspects, UC San Diego: Library –  
 3294 Scripps Digital Collection. Retrieved from <https://escholarship.org/uc/item/09v319r9>
- 3295 Keeling, C. D., Piper, S. C., Bacastow, R. B., Wahlen, M., Wahlen, M., Whorf, T. P., Heinmann,  
 3296 M. and Meijer, H. A. (2005) ‘Atmospheric CO<sub>2</sub> and <sup>13</sup>CO<sub>2</sub> exchange with the terrestrial  
 3297 biosphere and oceans from 1978 to 2000: Observations and carbon cycle implications’, in *A*  
 3298 *history of atmospheric CO<sub>2</sub> and its effects on plants, animals, and ecosystems*. Springer, pp.  
 3299 83–113.
- 3300 Keenan, T. F., and Riley, W. J. (2018). Greening of the land surface in the world’s cold regions  
 3301 consistent with recent warming. *Nature Climate Change*, **8**, 825-828. doi: 10.1038/s41558-  
 3302 018-0258-y
- 3303 Keenan, T. F., and Williams, C. A. (2018). The terrestrial carbon sink. *Annual Review of*  
 3304 *Environment and Resources*. **43**, 219-243. doi:10.1146/annurev-environ- 102017-030204
- 3305 Keppler, L., Landschützer, P. (2019). Regional wind variability modulates the Southern Ocean  
 3306 carbon sink. *Scientific Reports*, **9**, 7384. doi:10.1038/s41598-019-43826-y
- 3307 Key, R. M., Kozyr, A., Sabine, C. L., Lee, K., Wanninkhof, R., Bullister, J. L., Feely, R. A.,  
 3308 Millero, F. J., Mordy, C. and Peng, T. H. (2004). A global ocean carbon climatology: Results  
 3309 from Global Data Analysis Project (GLODAP). *Global Biogeochemical Cycles*, **18**(4),  
 3310 GB4031. doi:10.1029/2004GB002247
- 3311 Khatiwala, S., Primeau, F. and Hall, T. (2009). Reconstruction of the history of anthropogenic  
 3312 CO<sub>2</sub> concentrations in the ocean. *Nature*, **462**, 346–349. doi:10.1038/nature08526
- 3313 Khatiwala, S., Tanhua, T., Mikaloff Fletcher, S., Gerber, M., Doney, C. S., Graven, H. D.,  
 3314 Gruber, N., Mckinley, G. A., Murata, A. and Sabine, C. (2013). Global storage of  
 3315 anthropogenic carbon. *Biogeosciences*, **10**, 2169-2191, 2013. doi: 10.519/bg-10-2169-2013
- 3316 Kiel, M., O’Dell, C. W., Fisher, B., Eldering, A., Nassar, R., MacDonald, C. G. and Wennberg, P.  
 3317 O. (2019). How bias correction goes wrong: measurement of XCO<sub>2</sub> affected by erroneous  
 3318 surface pressure estimates. *Atmospheric Measurement Techniques*, **12**, 2241-2259. doi:  
 3319 10.5194/amt-12-2241-2019
- 3320 King, A. W., Andres, R. J., Davis, K. J., Hafer, M., Hayes, D. J., Huntzinger, D. N., de Jong, B.,  
 3321 Kurz, W. A., McGuire, A. D., Vargas, R., Wei, Y., West, T. O., and Woodall, C. W. (2015).

- 3322 North America's net terrestrial CO<sub>2</sub> exchange with the atmosphere 1990–2009.
- 3323 *Biogeosciences*, **12**, 399–414. doi: 10.5194/bg-12-399-2015
- 3324 Knorr, W. (2009). Is the airborne fraction of anthropogenic CO<sub>2</sub> emissions increasing?
- 3325 *Geophysical Research Letters*, **36**, L21710. doi:10.1029/2009GL040613
- 3326 Kondo, M., Ichii, K., Takagi, H., & Sasakawa, M. (2015). Comparison of the data-driven top-
- 3327 down and bottom-up global terrestrial CO<sub>2</sub> exchanges: GOSAT CO<sub>2</sub> inversion and empirical
- 3328 eddy flux upscaling. *Journal of Geophysical Research: Biogeosciences*, **120**(7), 1226–1245.
- 3329 doi: 10.1002/2014JG002866
- 3330 Kondo, M., Patra, P. K., Sitch, S., Friedlingstein, P., Poulter, B., Chevallier, F., Ciais, P.,
- 3331 Canadell, J. G., Bastos, A., Lauerwald, R., Calle, L., Ichii, K., Anthoni, P., Arneeth, A.,
- 3332 Haverd, V., Jain, A. K., Kato, E., Kautz, M., Law, R. M., Lienert, S., Lombardozzi, D.,
- 3333 Maki, T., Nakamura, T., Peylin, P., Rödenbeck, C., Zhuravlev, R., Saeki, T., Tian, H., Zhu, D
- 3334 and Ziehn, T. (2020). State of the science in reconciling top-down and bottom-up
- 3335 approaches for terrestrial CO<sub>2</sub> budget. *Global Change Biology*, **26**, 1068–1084. doi:
- 3336 10.1111/gcb.14917
- 3337 Konings, A. G., Piles, M., Das, N., and Entekhabi, D.(2017). L-band vegetation optical depth
- 3338 and effective scattering albedo estimation from SMAP, *Remote Sensing of Environment*,
- 3339 **198**, 460-470. doi:10.1016/j.rse
- 3340 Koren, G., van Schaik, E., Araujo, A. C., Boersma, K. F., Gartner, A., Killaars, L., Kooreman, M.
- 3341 L., Kruijt, B., van der Laan-Luijkx, I. T., von Randow, C., Smith, N. E., and Peters, W.
- 3342 (2018). Widespread reduction in sun-induced fluorescence from the Amazon during the
- 3343 2015/2016 El Nino. *Philosophical Transactions of the Royal Society of London. Series B:*
- 3344 *Biological Sciences*, **373**, 20170408. doi:10.1098/rstb.2017.0408
- 3345 Kuze, A., Suto, H., Nakajima, M., and Hamazaki, T. (2009). Thermal and near infrared sensor for
- 3346 carbon observation Fourier-transform spectrometer on the Greenhouse Gases Observing
- 3347 Satellite for greenhouse gases monitoring, *Applied Optics*, **48**, 6716–6733,
- 3348 doi:10.1364/AO.48.006716
- 3349 Kuze, A., Suto, H., Shiomi, K., Kawakami, S., Tanaka, M., Ueda, Y., Deguchi, A., Yoshida, J.,
- 3350 Yamamoto, Y., Kataoka, F., Taylor, T. E., and Buijs, H. L. (2016). Update on GOSAT
- 3351 TANSOFTS performance, operations, and data products after more than 6 years in space,
- 3352 *Atmospheric Measurement Technology*, **9**, 2445–2461. doi: 10.5194/amt-9-2445-2016
- 3353 Kwon, E.Y., Devries, T., Galbraith, E.D., Hwang, J., Kim, G., and Timmermann, A. (2021).
- 3354 Stable carbon isotopes suggest large terrestrial carbon inputs to the global ocean. *Global*
- 3355 *Biogeochemical Cycles*, **35**, e2020GB006684. doi: 10.1029/2020GB006684
- 3356 Lacroix, F., T. Ilyina, and J. Hartmann (2020). Oceanic CO<sub>2</sub> outgassing and biological production
- 3357 hotspots induced by pre-industrial river loads of nutrients and carbon in a global modeling
- 3358 approach. *Biogeosciences*, **17**(1), 55–88. doi:10.5194/bg-17-55-2020
- 3359 Lamarche, C., Santoro, M., Bontemps, S., d'Andrimont, R., Radoux, J., Giustarini, L.,
- 3360 Brockmann, C., Wevers, J., Defourny, P. and Arino, O. (2017). Compilation and validation
- 3361 of SAR and optical data products for a complete and global map of inland/ocean water
- 3362 tailored to the climate modeling community. *Remote Sensing*, **9**, 36. doi:10.3390/rs9010036
- 3363 Landschützer, P., Gruber, N., Bakker, D. C. E., Schuster, U., Nakaoka, S., Payne, M. R., Sasse, T.
- 3364 P. and Zeng, J. (2013). A neural network-based estimate of the seasonal to inter-annual
- 3365 variability of the Atlantic Ocean carbon sink. *Biogeosciences*, **10**, 7793–7815.
- 3366 doi:10.5194/bg-10-7793-2013

- 3367 Landschützer, P., Gruber, N., Bakker, D. C. E. and Schuster, U. (2014). Recent variability of the  
3368 global ocean carbon sink. *Global Biogeochemical Cycles*, **28**, 927–949.  
3369 doi:10.1002/2014GB004853
- 3370 Landschützer, P., Gruber, N., Haumann, F. A., Rödenbeck, C., Bakker, D. C. E., van Heuven, S.,  
3371 Hoppema, M., Metzl, N., Sweeney, C., Takahashi, T., Tilbrook, B. and Wanninkhof, R.  
3372 (2015). The reinvigoration of the Southern Ocean carbon sink. *Science*, **349**, 1221–1224.  
3373 doi:10.1126/science.aab2620
- 3374 Landschützer, P., Gruber, N., and Bakker, D. C. E. (2017). An updated observation-based global  
3375 monthly gridded sea surface pCO<sub>2</sub> and air-sea CO<sub>2</sub> flux product from 1982 through 2015  
3376 and its monthly climatology (NCEI Accession 0160558), Version 2.2, NOAA National  
3377 Centers for Environmental Information, Dataset [2017-07-11].
- 3378 Landschützer, P., Laruelle, G. G., Roobaert, A. and Regnier, P. (2020). A uniform pCO<sub>2</sub>  
3379 climatology combining open and coastal oceans. *Earth System Science Data*, **12**, 2537–  
3380 2553. doi:10.5194/essd-2020-90
- 3381 Langlais, C. E., Lenton, A., Matear, R., Monselesan, D., Legresy, B., Cougnon, E. and Rintoul,  
3382 S. (2017). Stationary Rossby waves dominate subduction of anthropogenic carbon in the  
3383 Southern Ocean. *Scientific Reports*, **7**, 17076. doi:10.1038/s41598-017-17292-3
- 3384 Laufkötter, C., Vogt, M., Gruber, N., Aita-Noguchi, M., Aumont, O., Bopp, L., Buitenhuis, E.,  
3385 Doney, S. C., Dunne, J., Hashioka, T., Hauck, J., Hirata, T., John, J., Le Quéré, C., Lima,  
3386 I.D., Nakano, H., Seferian, R., Totterdell, I., Vichi, M. and Völker, C. (2015). Drivers and  
3387 uncertainties of future global marine primary production in marine ecosystem models.  
3388 *Biogeosciences*, **12**, 6955–6984. doi:10.5194/bg-12-6955-2015
- 3389 Laufkötter, C., Vogt, M., Gruber, N., Aumont, O., Bopp, L., Doney, S.C., Dunne, J.P., Hauck, J.,  
3390 John, J.G., Lima, I.D., Seferian, R. and Völker, C. (2016). Projected decreases in future  
3391 marine export production: the role of the carbon flux through the upper ocean ecosystem.  
3392 *Biogeosciences*, **13**, 4023–4047. doi:10.5194/bg-13-4023-2016
- 3393 Lauvset, S. K., Lange, N., Tanhua, T., Bittig, H. C., Olsen, A., Kozyr, A., Álvarez, M., Becker,  
3394 S., Brown, P. J., Carter, B. R., Cotrim Da Cunha, L., Feely, R. A., van Heuven, S.,  
3395 Hoppema, M., Ishii, M., Jeansson, E., Jutterström, S., Jones, S. D., Karlsen, M. K., Lo  
3396 Monaco, C., Michaelis, P., Murata, A., Pérez, F. F., Pfeil, B., Schirnack, C., Steinfeldt, R.,  
3397 Suzuki, T., Tilbrook, B., Velo, A., Wanninkhof, R., Woosley, R. J., and Key, R. M. (2021).  
3398 An updated version of the global interior ocean biogeochemical data product,  
3399 GLODAPv2.2021. *Earth System Science Data*. **13**, 5565–5589. doi: 10.5194/essd-13-5565-  
3400 2021
- 3401 Lei, R., Feng, S., Danjou, A., Broquet, G., Wu, D., Lin, J. C., O'Dell, C. W., and Lauvaux, T.  
3402 (2021). Fossil fuel CO<sub>2</sub> emissions over metropolitan areas from space: A multi-model  
3403 analysis of OCO-2 data over Lahore, Pakistan. *Remote Sensing of Environment*, **264**,  
3404 112625. doi: 10.1016/j.rse.2021.112625
- 3405 Lenton, A. and Matear, R. J. (2007). Role of the Southern Annular Mode (SAM) in Southern  
3406 Ocean CO<sub>2</sub> uptake. *Global Biogeochemical Cycles*, **21**, GB2016.  
3407 doi:10.1029/2006GB002714
- 3408 Le Quéré, C., Rödenbeck, C., Buitenhuis, E. T., Conway, T. J., Langenfelds, R., Gomez, A.,  
3409 Labuschagne, C., Ramonet, M., Nakazawa, T., Metzl, N., Gillett, N. and Heimann, M.  
3410 (2007). Saturation of the Southern Ocean CO<sub>2</sub> Sink Due to Recent Climate Change.  
3411 *Science*, **316**, 1735–1738. doi:10.1126/science.1136188

- 3412 Le Quéré, C., Raupach, M. R., Canadell, J. G., Marland, G., Bopp, L., Ciais, P., Conway, T. J.,  
 3413 Doney, S. C., Feely, R. A., Foster, P., Friedlingstein, P., Gurney, K., Houghton, R. A., House,  
 3414 J. I., Huntingford, C., Levy, P. E., Lomas, M. R., Majkut, J., Metzl, N., Ometto, J. P., Peters,  
 3415 G. P., Prentice, I. C., Randerson, J. T., Running, S. W., Sarmiento, J. L., Schuster, U., Sitch,  
 3416 S., Takahashi, T., Viovy, N., van der Werf, G. R. and Woodward, F. I. (2009). Trends in the  
 3417 sources and sinks of carbon dioxide. *Nature Geosciences*, **2**, 831–836. doi:10.1038/ngeo689
- 3418 Le Quéré, C., Takahashi, T., Buitenhuis, E. T., Rödenbeck, C. and Sutherland, S. C. (2010).  
 3419 Impact of climate change and variability on the global oceanic sink of CO<sub>2</sub>. *Global*  
 3420 *Biogeochemical Cycles*, **24**, GB4007. doi:10.1029/2009GB003599
- 3421 Le Quéré, C., Andres, R. J., Boden, T., Conway, T., Houghton, R. A., House, J. I., Marland, G.,  
 3422 Peters, G. P., van der Werf, G. R., Ahlström, A., Andrew, R. M., Bopp, L., Canadell, J. G.,  
 3423 Ciais, P., Doney, S. C., Enright, C., Friedlingstein, P., Huntingford, C., Jain, A. K., Jourdain,  
 3424 C., Kato, E., Keeling, R. F., Klein Goldewijk, K., Levis, S., Levy, P., Lomas, M., Poulter,  
 3425 B., Raupach, M. R., Schwinger, J., Sitch, S., Stocker, B. D., Viovy, N., Zaehle and S. and  
 3426 Zeng, N. (2013). The global carbon budget 1959–2011. *Earth System Science Data*, **5**, 165–  
 3427 185. doi:10.5194/essd-5-165-2013
- 3428 Le Quéré, C., Peters, G. P., Andres, R. J., Andrew, R. M., Boden, T. A., Ciais, P., Friedlingstein,  
 3429 P., Houghton, R. A., Marland, G., Moriarty, R., Sitch, S., Tans, P., Arneth, A., Arvanitis, A.,  
 3430 Bakker, D. C. E., Bopp, L., Canadell, J. G., Chini, L. P., Doney, S. C., Harper, A., Harris, I.,  
 3431 House, J. I., Jain, A. K., Jones, S. D., Kato, E., Keeling, R. F., Klein Goldewijk, K.,  
 3432 Körtzinger, A., Koven, C., Lefèvre, N., Maignan, F., Omar, A., Ono, T., Park, G.-H., Pfeil,  
 3433 B., Poulter, B., Raupach, M.R., Regnier, P., Rödenbeck, C., Saito, S., Schwinger, J.,  
 3434 Segschneider, J., Stocker, B.D., Takahashi, T., Tilbrook, B., van Heuven, S., Viovy, N.,  
 3435 Wanninkhof, R., Wiltshire, A. and Zaehle, S. (2014). Global carbon budget 2013. *Earth*  
 3436 *System Science Data*, **6**, 235–263. doi:10.5194/essd-6-235-2014
- 3437 Le Quéré, C., Moriarty, R., Andrew, R. M., Peters, G. P., Ciais, P., Friedlingstein, P., Jones, S. D.,  
 3438 Sitch, S., Tans, P., Arneth, A., Boden, T. A., Bopp, L., Bozec, Y., Canadell, J. G., Chini, L.  
 3439 P., Chevallier, F., Cosca, C. E., Harris, I., Hoppema, M., Houghton, R. A., House, J. I., Jain,  
 3440 A. K., Johannessen, T., Kato, E., Keeling, R. F., Kitidis, V., Klein Goldewijk, K., Koven, C.,  
 3441 Landa, C. S., Landschützer, P., Lenton, A., Lima, I. D., Marland, G., Mathis, J. T., Metzl,  
 3442 N., Nojiri, Y., Olsen, A., Ono, T., Peng, S., Peters, W., Pfeil, B., Poulter, B., Raupach, M. R.,  
 3443 Regnier, P., Rödenbeck, C., Saito, S., Salisbury, J. E., Schuster, U., Schwinger, J., Séférian,  
 3444 R., Segschneider, J., Steinhoff, T., Stocker, B. D., Sutton, A. J., Takahashi, T., Tilbrook, B.,  
 3445 van der Werf, G. R., Viovy, N., Wang, Y.-P., Wanninkhof, R., Wiltshire, A. and Zeng, N.  
 3446 (2015a). Global carbon budget 2014. *Earth System Science Data*, **7**, 47–85.  
 3447 doi:10.5194/essd-7-47-2015
- 3448 Le Quéré, C., Moriarty, R., Andrew, R. M., Canadell, J. G., Sitch, S., Korsbakken, J. I.,  
 3449 Friedlingstein, P., Peters, G. P., Andres, R.J., Boden, T. A., Houghton, R. A., House, J. I.,  
 3450 Keeling, R. F., Tans, P., Arneth, A., Bakker, D. C. E., Barbero, L., Bopp, L., Chang, J.,  
 3451 Chevallier, F., Chini, L. P., Ciais, P., Fader, M., Feely, R. A., Gkritzalis, T., Harris, I., Hauck,  
 3452 J., Ilyina, T., Jain, A. K., Kato, E., Kitidis, V., Klein Goldewijk, K., Koven, C.,  
 3453 Landschützer, P., Lauvset, S. K., Lefèvre, N., Lenton, A., Lima, I. D., Metzl, N., Millero, F.,  
 3454 Munro, D. R., Murata, A., Nabel, J. E. M. S., Nakaoka, S., Nojiri, Y., O'Brien, K., Olsen,  
 3455 A., Ono, T., Pérez, F. F., Pfeil, B., Pierrot, D., Poulter, B., Rehder, G., Rödenbeck, C., Saito,  
 3456 S., Schuster, U., Schwinger, J., Séférian, R., Steinhoff, T., Stocker, B. D., Sutton, A. J.,  
 3457 Takahashi, T., Tilbrook, B., van der Laan-Luijkx, I. T., van der Werf, G. R., van Heuven, S.,

- Vandemark, D., Viovy, N., Wiltshire, A., Zaehle, S. and Zeng, N. (2015b). Global Carbon Budget 2015. *Earth System Science Data*, **7**, 349–396. doi:10.5194/essd-7-349-2015
- Le Quéré, C., Andrew, R. M., Canadell, J. G., Sitch, S., Korsbakken, J. I., Peters, G. P., Manning, A. C., Boden, T. A., Tans, P. P., Houghton, R. A., Keeling, R. F., Alin, S., Andrews, O. D., Anthoni, P., Barbero, L., Bopp, L., Chevallier, F., Chini, L. P., Ciais, P., Currie, K., Delire, C., Doney, S. C., Friedlingstein, P., Gkritzalis, T., Harris, I., Hauck, J., Haverd, V., Hoppema, M., Klein Goldewijk, K., Jain, A. K., Kato, E., Körtzinger, A., Landschützer, P., Lefèvre, N., Lenton, A., Lienert, S., Lombardozzi, D., Melton, J. R., Metzl, N., Millero, F., Monteiro, P. M. S., Munro, D. R., Nabel, J. E. M. S., Nakaoka, S., O'Brien, K., Olsen, A., Omar, A. M., Ono, T., Pierrot, D., Poulter, B., Rödenbeck, C., Salisbury, J., Schuster, U., Schwinger, J., Séférian, R., Skjelvan, I., Stocker, B. D., Sutton, A. J., Takahashi, T., Tian, H., Tilbrook, B., van der Laan-Luijkx, I. T., van der Werf, G. R., Viovy, N., Walker, A. P., Wiltshire, A. J. and Zaehle, S. (2016). Global Carbon Budget 2016. *Earth System Science Data*, **8**, 605–649. doi:10.5194/essd-8-605-2016
- Le Quéré, C., Andrew, R. M., Friedlingstein, P., Sitch, S., Pongratz, J., Manning, A. C., Korsbakken, J. I., Peters, G. P., Canadell, J. G., Jackson, R. B., Boden, T. A., Tans, P. P., Andrews, O. D., Arora, V. K., Bakker, D. C. E., Barbero, L., Becker, M., Betts, R. A., Bopp, L., Chevallier, F., Chini, L. P., Ciais, P., Cosca, C. E., Cross, J., Currie, K., Gasser, T., Harris, I., Hauck, J., Haverd, V., Houghton, R. A., Hunt, C. W., Hurtt, G., Ilyina, T., Jain, A. K., Kato, E., Kautz, M., Keeling, R. F., Klein Goldewijk, K., Körtzinger, A., Landschützer, P., Lefèvre, N., Lenton, A., Lienert, S., Lima, I., Lombardozzi, D., Metzl, N., Millero, F., Monteiro, P. M. S., Munro, D. R., Nabel, J. E. M. S., Nakaoka, S., Nojiri, Y., Padin, X. A., Peregon, A., Pfeil, B., Pierrot, D., Poulter, B., Rehder, G., Reimer, J., Rödenbeck, C., Schwinger, J., Séférian, R., Skjelvan, I., Stocker, B. D., Tian, H., Tilbrook, B., Tubiello, F. N., van der Laan-Luijkx, I. T., van der Werf, G. R., van Heuven, S., Viovy, N., Vuichard, N., Walker, A. P., Watson, A. J., Wiltshire, A. J., Zaehle, S. and Zhu, D. (2018a). Global Carbon Budget 2017. *Earth System Science Data*, **10**, 405–448. doi:10.5194/essd-10-405-2018
- Le Quéré, C., Andrew, R. M., Friedlingstein, P., Sitch, S., Hauck, J., Pongratz, J., Pickers, P. A., Korsbakken, J. I., Peters, G. P., Canadell, J. G., Arneeth, A., Arora, V. K., Barbero, L., Bastos, A., Bopp, L., Chevallier, F., Chini, L. P., Ciais, P., Doney, S. C., Gkritzalis, T., Goll, D. S., Harris, I., Haverd, V., Hoffman, F. M., Hoppema, M., Houghton, R. A., Hurtt, G., Ilyina, T., Jain, A. K., Johannessen, T., Jones, C. D., Kato, E., Keeling, R. F., Goldewijk, K., Landschützer, P., Lefèvre, N., Lienert, S., Liu, Z., Lombardozzi, D., Metzl, N., Munro, D. R., Nabel, J. E. M. S., Nakaoka, S., Neill, C., Olsen, A., Ono, T., Patra, P., Peregon, A., Peters, W., Peylin, P., Pfeil, B., Pierrot, D., Poulter, B., Rehder, G., Resplandy, L., Robertson, E., Rocher, M., Rödenbeck, C., Schuster, U., Schwinger, J., Séférian, R., Skjelvan, I., Steinhoff, T., Sutton, A., Tans, P. P., Tian, H., Tilbrook, B., Tubiello, F. N., van der Laan-Luijkx, I. T., van der Werf, G. R., Viovy, N., Walker, A. P., Wiltshire, A. J., Wright, R., Zaehle, S. and Zheng, B. (2018b). Global Carbon Budget 2018. *Earth System Science Data*, **10**, 2141–2194. doi:10.5194/essd-10-2141-2018
- Le Quéré, C., Jackson, R. B., Jones, M. W., Smith, A. J. P., Abernethy, S., Andrew, R. M., De-Gol, A. J., Willis, D. R., Shan, Y., Canadell, J. G., Friedlingstein, P., Creutzig, F. and Peters, G. P. (2020). Temporary reduction in daily global CO<sub>2</sub> emissions during the COVID-19 forced confinement. *Nature Climate Change* **10**, 647–653. doi: 10.1038/s41558-020-0797-x
- Liang, M. C., Mahata, S., Laskar, A. H., Thieme, M. H., and Newman, S. (2017). Oxygen isotope anomaly in tropospheric CO<sub>2</sub> and implications for CO<sub>2</sub> residence time in the



- atmosphere and gross primary productivity. *Scientific Reports*, **7**, 13180. doi: 10.1038/s41598-017-12774-w
- Liao, E., Resplandy, L., Liu, J. and Bowman, K. W. (2020). Amplification of the Ocean Carbon Sink During El Niños: Role of Poleward Ekman Transport and Influence on Atmospheric CO<sub>2</sub>. *Global Biogeochemical Cycles* **34**, e2020GB006574. doi: 10.1029/2020GB006574
- Liu, J., Bowman, K., Schimel, D., Parazoo, N., Jiang, Z., Lee, M., Bloom, A., Wunch, D., Gurney, K., Menemenlis, D., Girerach, M., Crisp, D. and Eldering A. (2017). Contrasting carbon cycle responses of the tropical continents to the 2015–2016 El Niño. *Science*, **358**, eaam5690. doi: 10.1126/science.aam5690
- Liu, J., Wennberg, P. O., Parazoo, N. C., Yin, Y. and Frankenberg, C. (2020a). Observational constraints on the response of high-latitude northern forests to warming. *AGU Advances*, **2**, e2020AV000228. doi:10.1029/2020AV000228
- Liu, Y. Y., de Jeu, R. A. M., McCabe, M. F., Evans, J. P., and van Dijk, A. I. J. M. (2011), Global long-term passive microwave satellite-based retrievals of vegetation optical depth, *Geophysical Research Letters*, **38**, L18402, doi:10.1029/2011GL048684.
- Liu, Y. Y., Van Dijk, A. I., De Jeu, R. A., Canadell, J. G., McCabe, M. F., Evans, J. P., and Wang, G. (2015). Recent reversal in loss of global terrestrial biomass, *Nature Climate Change*, **5**, 470–474. doi: 10.1038/nclimate2581
- Liu, Z., Ciais, P., Deng, Z., Lei, R., Davis, S. J., Feng, S., Zheng, B., Cui, D., Dou, X., Zhu, B., Guo, R., Ke, P., Sun, T., Lu, C., He, P., Wang, Y., Yue, X., Wang, Y., Lei, Y., Zhou, H., Cai, Z., Wu, Y., Guo, R., Han, T., Xue, J., Boucher, O., Boucher, E., Chevallier, F., Tanaka, K., Wei, Y., Zhong, H., Kang, C., Zhang, N., Chen, B., Xi, F., Liu, M., Bréon, F. M., Lu, Y., Zhang, Q., Guan, D., Gong, P., Kammen, D. M., He, K., and Schellnhuber, H. J. (2020b). Near-real-time monitoring of global CO<sub>2</sub> emissions reveals the effects of the COVID-19 pandemic, *Nature Communications*, **11**, 1–12. doi: 10.1038/s41467-020-18922-7
- Long, M. C., Lindsay, K., Peacock, S., Moore, J. K., and Doney, S. C. (2013). Twentieth-century oceanic carbon uptake and storage in CESM1(BGC). *Journal of Climate*, **26**, 6775–6800. doi:10.1175/JCLI-D-12-00184.1
- Lovenduski, N. S., Gruber, N., Doney, S. C. and Lima, I. D. (2007). Enhanced CO<sub>2</sub> outgassing in the Southern Ocean from a positive phase of the Southern Annular Mode. *Global Biogeochemical Cycles*, **21**, GB2026. doi:10.1029/2006GB002900
- Lovenduski, N. S., Gruber, N. and Doney, S.C. (2008). Toward a mechanistic understanding of the decadal trends in the Southern Ocean carbon sink: Southern Ocean CO<sub>2</sub> flux trends. *Global Biogeochemical Cycles*, **22**(3), GB3016. doi:10.1029/2007GB003139
- Lucht, W., Prentice, C., Myneni, R. B., Sitch, S., Friedlingstein, P., Cramer, W., Bousquet, P., Buermann, W. and Smith, B. (2002). Climatic control of the high-latitude vegetation greening trend and Pinatubo effect. *Science*, **296**, 1687–1689. doi:10.1126/science.1071828
- Ma, X., Huete, A., Cleverly, J., Eamus, D., Chevallier, F., Joiner, J., Poulter, B., Zhang, Y., Guanter, L., Meyer, W., Xie, Z. and Ponce-Campos, G. (2016). Drought rapidly diminishes the large net CO<sub>2</sub> uptake in 2011 over semi-arid Australia. *Scientific Reports*, **6**, 37747 (2016). doi: 10.1038/srep37747
- Macbean, N., Maignan, F., Bacour, C., Lewis, P., Peylin, P., Guanter, L., Köhler, P., Gomez-Dans, J., and Disney, M. (2018). Strong constraint on modelled global carbon uptake using solar-induced chlorophyll fluorescence data. *Scientific Reports*, **8**, 1973. doi: 10.1038/s41598-018-20024-w

- MacDougall, A. H., Frölicher, T. L., Jones, C. D., Rogelj, J., Matthews, H. D., Zickfeld, K., Arora, V. K., Barrett, N. J., Brovkin, V., Burger, F. A., Eby, M., Eliseev, A. V., Hajima, T., Holden, P. B., Jeltsch-Thömmes, A., Koven, C., Mengis, N., Menviel, L., Michou, M., Mokhov, I. I., Oka, A., Schwinger, J., Séférian, R., Shaffer, G., Sokolov, A., Tachiiri, K., Tjiputra, J., Wiltshire, A. and Ziehn, T. (2020). Is there warming in the pipeline? A multi-model analysis of the zero emissions commitment from CO<sub>2</sub>. *Biogeosciences*, **17**, 2987–3016. doi:10.5194/bg-17-2987-2020
- Maier-Reimer, E., Mikolajewicz, U. and Winguth, A. (1996). Future ocean uptake of CO<sub>2</sub>: interaction between ocean circulation and biology. *Climate Dynamics*, **12**, 711–721. doi: 10.1007/s003820050138
- Maksyutov, S., Takagi, H., Valsala, V. K., Saito, M., Oda, T., Saeki, T., Belikov, D. A., Saito, R., Ito, A., Yoshida, Y., Morino, I., Uchino, O., Andres, R. J. and Yokota, T. (2013). Regional CO<sub>2</sub> flux estimates for 2009–2010 based on GOSAT and ground-based CO<sub>2</sub> observations. *Atmospheric Chemistry and Physics*, **13**, 2351–9373. doi: 10.5194/acp-13-9351-2013
- Marsay, C.M., Sanders, R. J., Henson, S. A., Pabortsava, K., Achterberg, E. P. and Lampitt, R. S. (2015). Attenuation of sinking particulate organic carbon flux through the mesopelagic ocean. *Proceedings of the National Academy of Sciences*, **112**, 1089. doi:10.1073/pnas.1415311112
- Marchant, R., Mumbi, C., Behera, S., and Yamagata, T. (2006). The Indian Ocean dipole – the unsung driver of climatic variability in East Africa. *African Journal of Ecology*, **45**, 4–16. doi: 10.1111/j.1365-2028.2006.00707.x
- Marrs, J. K., Reblin, J. S., Logan, B. A., Allen, D. W., Reinmann, A. B., Bombard, D. M., Tabachnik, D. and Hutyrá, L. R. (2020). Solar-induced fluorescence does not track photosynthetic carbon assimilation following induced stomatal closure. *Geophysical Research Letters*, **47**, e2020GL087956. doi: 10.1029/2020GL087956
- Marshall, G. J., Trends in the Southern Annular Mode from Observations and Reanalyses. *Journal of Climate*, **16**, 4134–4143. doi: 10.1175/1520-0442(2003)016<4134:TITSAM>2.0.CO;2
- Mau, A. C., Reed, S. C., Wood, T. E. and Cavaleri, M. A. (2018). Temperate and tropical forest canopies are already functioning beyond their thermal thresholds for photosynthesis. *Forests*, **9**, 47. doi:10.3390/f9010047
- McGuire, A. D., Sitch, J. S., Clein, R., Dargaville, G., Esser, J., Foley, M., Heimann, F., Joos, J., Kaplan, D. W., Kicklighter, R. A., Meier, J. M., Melillo, B., Moore, I. C., Prentice, N., Ramankutty, T., Reichenau, A., Schloss, H., Tian, L. J., Williams, and U. Wittenberg. (2001). Carbon balance of the terrestrial biosphere in the twentieth century: analyses of CO<sub>2</sub>, climate and land use effects with four process-based ecosystem models. *Global Biogeochemical Cycles* **15**, 183–206. doi: 10.1029/2000GB001298
- McKinley, G., Follows, M. & Marshall, J. (2004). Mechanisms of air-sea CO<sub>2</sub> flux variability in the equatorial Pacific and the North Atlantic. *Global Biogeochemical Cycles*, **18**, GB2011. doi:10.1029/2003GB002179
- McKinley, G., Follows, M., and Marshall, J. (2004). Mechanisms of air-sea CO<sub>2</sub> flux variability in the equatorial Pacific and the North Atlantic. *Global Biogeochemical Cycles*, **18**, GB2011. doi:10.1029/2003GB002179

- McKinley, G. A., Fay, A. R., Takahashi, T. and Metzl, N. (2011). Convergence of atmospheric and North Atlantic carbon dioxide trends on multidecadal timescales. *Nature Geosci*, **4**, 606–610. doi:10.1038/ngeo1193
- McKinley, G. A., Pilcher, D. J., Fay, A. R., Lindsay, K., Long, M. C. and Lovenduski, N. S. (2016). Timescales for detection of trends in the ocean carbon sink. *Nature*, **530**, 469–472. doi:10.1038/nature16958
- McKinley, G. A., Fay, A. R., Lovenduski, N. S. and Pilcher, D. J. (2017). Natural variability and anthropogenic trends in the ocean carbon sink. *Annual Review of Marine Science*, **9**, 125–150, doi:10.1146/annurev-marine-010816-060529
- McKinley, G. A., Fay, A. R., Eddebbar, Y. A., Gloege L. and Lovenduski, N. S. (2020). External forcing explains recent decadal variability of the ocean carbon sink. *AGU Advances*, **1**, 1, e2019AV000149. doi:10.1029/2019AV000149
- McPhaden, M. J., Zebiak, S. E., and Glantz, M. H. (2006). ENSO as an Integrating Concept in Earth Science, *Science*, **314**, 1740–1745. doi: 10.1126/science.1132588
- Medlyn, B., Zaehle, S., De Kauwe, M., Walker, A. P., Dietze, M. C., Hanson, P. J., Hickler, T., Jain, A. K., Luo, Y., Parton, W., Prentice, I., C., Thornton, P. E., Wang, S., Wang, Y.-P., Weng, E., Iversen, C. M., McCarthy, H. R., Warren, J. M., Oren, R., and Norby, R. J. (2015). Using ecosystem experiments to improve vegetation models. *Nature Climate Change*, **5**, 528–534. doi: 10.1038/nclimate2621
- Mercado, L.M., Medlyn, B. E., Huntingford, C., Oliver, R. J., Clark, D. B., Sitch, S., Zelazowski, P., Kattge, J., Harper, A. B. and Cox, P. M. (2018). Large sensitivity in land carbon storage due to geographical and temporal variation in the thermal response of photosynthetic capacity, *New Phytologist*, **218**, 1462–1477, doi: 10.1111/nph.15100.
- Meroni, M., Rossini, M., Guanter, L., Alonso L., Rascher, U., Colombo, R., and Moreno, J. (2009). Remote sensing of solar-induced chlorophyll fluorescence: Review of methods and applications, *Remote Sensing of Environment*, **113**, 2037–2051, ISSN 0034-4257, doi: 10.1016/j.rse.2009.05.003
- Mikaloff Fletcher, S. E., Gruber, N., Jacobson, A. R., Doney, S., C., Sutkiewicz, S., Gerber, M., Follows, M., Joos, F., Lindsay, K., Menemenlis, D., Mouchet, A., Müller, S., A. and Sarmiento, J. L. (2006). Inverse estimates of anthropogenic CO<sub>2</sub> uptake, transport, and storage by the ocean, *Global Biogeochemical Cycles*, **20**, GB2002. doi:10.1029/2005GB002530
- Miller, J. B., Lehman, S. J., Montzka, S. A., Sweeney, C., Miller, B. R., Karion, A., Wolak, C., Dlugokencky, E. J., Southon, J., Turnbull, J. C. and Tans, P. P. (2012). Linking emissions of fossil fuel CO<sub>2</sub> and other anthropogenic trace gases using atmospheric <sup>14</sup>CO<sub>2</sub>. *Journal of Geophysical Research: Atmospheres*, **117**, D08302. doi:10.1029/2011JD017048
- Miller, J. B., Lehman, S. J., Verhulst, K. R., Miler, C., E., Duren, R. M., Yadav, V., Newman, S. and Sloop, C. D. (2020). Large and seasonally varying biospheric CO<sub>2</sub> fluxes in the Los Angeles megacity revealed by atmospheric radiocarbon. *Proceedings of the National Academy of Sciences*, **117**, 26681–26687. doi:10.1073/pnas.2005253117
- Mohammed, G. H., Colombo, R., Middleton, E. M., Rascher, U., van der Tol, C., Nedbal, L., Goulasf, Y., Pérez-Priego, O., Damm, A., Meroni, M., Joiner, J., Cogliati, S., Verhoef, W., Malenovsky, Z., Gastellu-Etcheberry, J.-P., Miller, J. R., Guanter, L., Moreno, J., Moya, I., Berry, J. A., Frankenberg, C., Zarco-Tejada, P. J. (2019). Remote sensing of solar-

- induced chlorophyll fluorescence (SIF) in vegetation: 50 years of progress, *Remote Sensing of Environment*, **31** 111177. doi:10.1016/j.rse.2019.04.030
- Molod, A., Takacs, L., Suarez, M., & Bacmeister, J. (2015). Development of the GEOS-5 atmospheric general circulation model: Evolution from MERRA to MERRA2. *Geoscientific Model Development*, **8**, 1339–1356. doi: 10.5194/gmd-8-1339-015.
- Mongwe, N. P., Vichi, M. and Monteiro, P. M. S. (2018). The seasonal cycle of pCO<sub>2</sub> and CO<sub>2</sub> fluxes in the Southern Ocean: diagnosing anomalies in CMIP5 Earth system models. *Biogeosciences*, **15**, 2851–2872. doi:10.5194/bg-15-2851-2018
- Monteil, G., Broquet, G., Scholze, M., Lang, M., Karstens, U., Gerbig, C., Koch, F.-T., Smith, N. E., Thompson, R. L., Luijkx, I. T., White, E., Meesters, A., Ciais, P., Ganesan, A. L., Manning, A., Mischurow, M., Peters, W., Peylin, P., Tarniewicz, J., Rigby, M., Rödenbeck, C., Vermeulen, A., and Walton, E. M. (2020). The regional European atmospheric transport inversion comparison, EUROCOM: first results on European-wide terrestrial carbon fluxes for the period 2006–2015, *Atmospheric Chemistry and Physics*, **20**, 12063–12091. doi: 10.5194/acp-20-12063-2020
- Moore, J. K., Fu, W., Primeau, F., Britten, G. L., Lindsay, K., Long, M., Doney, S. C., Mahowald, N., Hoffman, F. and Randerson, J. T. (2018). Sustained climate warming drives declining marine biological productivity. *Science*, **359**, 1139–1143. doi:10.1126/science.aao6379
- Müller, A., Tanimoto, H., Sugita, T., Machida, T., Nakaoka, S., Patra, P. K., Laughner, J., and Crisp, D. (2021). New approach to evaluate satellite-derived XCO<sub>2</sub> over oceans by integrating ship and aircraft observations, *Atmospheric Chemistry and Physics*, **21**, 8255–8271. doi: 10.5194/acp-21-8255-2021.
- Myneni, R., Knyazikhin, Y., Park, T. (2015). MOD15A2H MODIS Leaf Area Index/FPAR 8-Day L4 Global 500m SIN Grid V006. NASA EOSDIS Land Processes DAAC. <http://doi.org/10.5067/MODIS/MOD15A2H.006> (Last referenced 5 Dec 2021)
- Nabuurs, G. J., Lindner, M., Verkerk, P., Gunia, K., Deda, Paola, Michalak, R. and Grassi, G. (2013). First signs of carbon sink saturation in European forest biomass. *Nature Climate Change*, **3**, 792–796. doi: 10.1038/nclimate1853
- Nassar, R., Hill, T. G., McLinden, C. A., Wunch, D., Jones, D. B.A. and Crisp D. (2017). Quantifying CO<sub>2</sub> emissions from individual power plants from space. *Geophysical Research Letters*, **44**, 10045–10053. doi:10.1002/2017GL074702
- Nassar, R., Mastrogiacomo, J.-P., Bateman-Hemphill, W., McCracken, C., MacDonald, C. G., Hill, T., O'Dell, C. W., Kiel, M., Crisp, D. (2021): Advances in quantifying power plant CO<sub>2</sub> emissions with OCO-2. *Remote Sensing of Environment*, **264**, 112579. doi: 10.1016/j.rse.2021.112579
- Nemani, R. R., Keeling, C. D., Hashimoto, H., Jolly, W. M., Piper, S. C., Tucker, C. J., Myneni, R. B., and Running, S. W. (2003). Climate-Driven Increases in Global Terrestrial Net Primary Production from 1982 to 1999. *Science*, **300**, 1560–1563. doi: 10.1126/science.1082750
- Norton, A. J., Rayner, P. J., Koffi, E. N., Scholze, M., Silver, J. D., and Wang, Y.-P. (2019). Estimating global gross primary productivity using chlorophyll fluorescence and a data assimilation system with the BETHY-SCOPE model. *Biogeosciences*, **16**, 3069–3093. doi: 10.5194/bg-16-3069-2019

- Obermeier, W. A., Nabel, J. E. M. S., Loughran, T., Hartung, K., Bastos, A., Havermann, F., Anthoni, P., Arneth, A., Goll, D. S., Lienert, S., Lombardozzi, D., Luyssaert, S., McGuire, P. C., Melton, J. R., Poulter, B., Sitch, S., Sullivan, M. O., Tian, H., Walker, A. P., Wiltshire, A. J., Zaehle, S., and Pongratz, J. (2021). Modelled land use and land cover change emissions – a spatio-temporal comparison of different approaches, *Earth System Dynamics*, **12**, 635–670, doi: 10.5194/esd-12-635-2021
- Oda, T., Maksyutov, S. and Andres, S. J. (2018). The Open-source Data Inventory for Anthropogenic Carbon dioxide (CO<sub>2</sub>), version 2016 (ODIAC2016): A global, monthly fossil-fuel CO<sub>2</sub> gridded emission data product for tracer transport simulations and surface flux inversions. *Earth System Science Data*, **10**, 87-107. doi:10.5194/essd-10-87-2018
- O'Dell, C. W., Eldering, A., Wennberg, P. O., Crisp, D., Gunson, M. R., Fisher, B., Frankenberg, C., Kiel, M., Lindqvist, H., Mandrake, L., Merrelli, A., Natraj, V., Nelson, R. R., Osterman, G. B., Payne, V. H., Taylor, T. E., Wunch, D., Drouin, B. J., Oyafuso, F., Chang, A., McDuffie, J., Smyth, M., Baker, D. F., Basu, S., Chevallier, F., Crowell, S. M. R., Feng, L., Palmer, P. I., Dubey, M., García, O. E., Griffith, D. W. T., Hase, F., Iraci, L. T., Kivi, R., Morino, I., Notholt, J., Ohyama, H., Petri, C., Roehl, C. M., Sha, M. K., Strong, K., Sussmann, R., Te, Y., Uchino, O. and Velasco, V. A. (2018). Improved retrievals of carbon dioxide from Orbiting Carbon Observatory-2 with the version 8 ACOS algorithm, *Atmospheric Measurement Techniques*, **11**: 6539–6576. doi:10.5194/amt-11-6539-2018
- Olsen, A., Key, R. M., van Heuven, S., Lauvset, S. K., Velo, A., Lin, X. H., Schirnick, C., Kozyr, A., Tanhua, T., Hoppema, M., Jutterstrom, S., Steinfeldt, R., Jeansson, E., Ishii, M., Perez, F. F., and Suzuki, T. (2016). The Global Ocean Data Analysis Project version 2 (GLODAPv2) - an internally consistent data product for the world ocean, *Earth System Science Data*, **8**, 297-323. doi: 10.5194/essd-8-297-2016
- Olsen, A., Lange, N., Key, R. M., Tanhua, T., Bittig, H. C., Kozyr, A., Álvarez, M., Azetsu-Scott, K., Becker, S., Brown, P. J., Carter, B. R., Cotrim da Cunha, L., Feely, R. A., van Heuven, S., Hoppema, M., Ishii, M., Jeansson, E., Jutterström, S., Landa, C. S., Lauvset, S. K., Michaelis, P., Murata, A., Pérez, F. F., Pfeil, B., Schirnick, C., Steinfeldt, R., Suzuki, T., Tilbrook, B., Velo, A., Wanninkhof, R. and Woosley, R. J. (2020): An updated version of the global interior ocean biogeochemical data product, GLODAPv2.2020, *Earth System Science Data*, **12**, 3653-3678. doi: 10.5194/essd-12-3653-2020
- Pacala, S. W., Hurtt, G. C., Baker, D., Peylin, P., Houghton, R. A., Birdsey, R. A., Heath, L., Sundquist, E. T., Stallard, R. F., Ciais, P., Moorcroft, P., Caspersen, J. P., Shevliakova, E., Moore, B., Kohlmaier, G., Holland, E., Gloor, M., Harmon, M. E., Fan, S.-M., Sarmiento, J. L., Goodale, C. L., Schimel, D. and Field, C. B. (2001), Consistent land- and atmosphere-based U.S. carbon sink estimates, *Science*, **292**, 2316– 2320, doi: 10.1126/science.1057320
- Page, S. E., Siegert, F., Rieley, L. O., Boehm, H.-D. V., Jaya, A., and Limin, S. (2002). The amount of carbon released from peat and forest fires in Indonesia during 1997. *Nature*, **420**, 61–65. doi: 10.1038/nature01131
- Palmer, P. I., Feng, L., Baker, D., Chevallier, F., Bösch, H. and Somkuti, P. (2019). Net carbon emissions from African biosphere dominate pan-tropical atmospheric CO<sub>2</sub> signal, *Nature Communications*, **10**, 3344. doi:10.1038/s41467-019-11097-w
- Pan, Y., Birdsey, R. A., Fang, J., Houghton, R., Kauppi, P. E., Kurz, W. A., Phillips, O. L., Shvidenko, A., Lewis, S. L., Canadell, J. G., Ciais, P., Jackson, R. B., Pacala, S. W., McGuire, A. S., Piao, S., Rautiainen, A., Sitch, S. and Hayes, D. (2011). A large and

- 3725 persistent carbon sink in the world's forests. *Science*, **333**, 988-993.  
 3726 doi:10.1126/science.1201609
- 3727 Panassa, E., Santana-Casiano, J. M., González-Dávila, M., Hoppema, M., van Heuven, S. M. A.  
 3728 C., Völker, C., Wolf-Gladrow, D. and Hauck, J. (2018). Variability of nutrients and carbon  
 3729 dioxide in the Antarctic Intermediate Water between 1990 and 2014. *Ocean Dynamics*, **68**,  
 3730 295–308. doi:10.1007/s10236-018-1131-2
- 3731 Parazoo, N. C., Magney, T., Norton, A., Raczka, B., Bacour, C., Maignan, F., Baker, I., Zhang,  
 3732 Y., Qiu, B., Shi, M., MacBean, N., Bowling, D. R., Burns, S., Blanken, P. D., Stutz, J.,  
 3733 Grossmann, K. and Frankenberg, C. (2020). Wide discrepancies in the magnitude and  
 3734 direction of modeled solar-induced chlorophyll fluorescence in response to light conditions.  
 3735 *Biogeosciences*, **17**, 3733–3755. doi:10.5194/bg-17-3733-2020
- 3736 Pardo, P. C., Tilbrook, B., Langlais, C., Trull, T.W. and Rintoul, S. R. (2017). Carbon uptake and  
 3737 biogeochemical change in the Southern Ocean, south of Tasmania. *Biogeosciences*, **14**,  
 3738 5217–5237. doi:10.5194/bg-14-5217-2017
- 3739 Pearson, T. R. H., Brown, S., Murray, L. and Sidman, G. (2017). Greenhouse gas emissions from  
 3740 tropical forest degradation: an underestimated source. *Carbon Balance and Management*,  
 3741 **12**, 3. doi:10.1186/s13021-017-0072-2
- 3742 Peiro, H., Crowell, S., Schuh, A., Baker, D. F., O'Dell, C., Jacobson, A. R., Chevallier, F., Liu, J.,  
 3743 Eldering, A., Crisp, D., Deng, F., Weir, B., Basu, S., Johnson, M. S., Philip, S., and Baker, I.  
 3744 (2022). Four years of global carbon cycle observed from the Orbiting Carbon Observatory 2  
 3745 (OCO-2) version 9 and in situ data and comparison to OCO-2 version 7, *Atmos. Chem.*  
 3746 *Phys.*, **22**, 1097–1130, doi: 10.5194/acp-22-1097-2022
- 3747 Peng, B., Guan, K. Y., Zhou, W., Jiang, C. Y., Frankenberg, C., Sun, Y., He, L. Y. and Kohler, P.  
 3748 (2020). Assessing the benefit of satellite-based Solar-Induced Chlorophyll Fluorescence in  
 3749 crop yield prediction. *International Journal of Applied Earth Observation and*  
 3750 *Geoinformation*, **90**, 102126. doi:10.1016/j.jag.2020.102126
- 3751 Peñuelas, J., Ciais, P., Canadell, J. G., Janssens, I. A., Fernández-Martínez, M., Carnicer, J.,  
 3752 Obersteiner, M., Piao, S., Vautard, R., Sardans, J. (2017). Shifting from a fertilization-  
 3753 dominated to a warming-dominated period. *Nat Ecol Evol.* **1**, 1438-1445. doi:  
 3754 10.1038/s41559-017-0274-8.
- 3755 Peters, W., Miller, J. B., Whitaker, J., Denning, A. S., Hirsch, A., Krol, M. C., Zupanski, D.,  
 3756 Bruhwiler, L., and Tan, P. P. (2005). An ensemble data assimilation system to estimate  
 3757 CO<sub>2</sub> surface fluxes from atmospheric trace gas observations, *Journal of Geophysical*  
 3758 *Research*, **110**, D24304, doi:10.1029/2005JD006157
- 3759 Peters, W., Bastos, A., Ciais, P., and Vermeulen, A. (2020). A historical, geographical and  
 3760 ecological perspective on the 2018 European summer drought. *Philosophical Transactions*  
 3761 *of the Royal Society B: Biological Sciences*, **375**, 20190505, doi: 10.1098/rstb.2019.0505
- 3762 Petrescu, A. M. R., Peters, G. P., Janssens-Maenhout, G., Ciais, P., Tubiello, F. N., Grassi, G.,  
 3763 Nabuurs, G.-J., Leip, A., Carmona-Garcia, G., Winiwarer, W., Höglund-Isaksson, L.,  
 3764 Günther, D., Solazzo, E., Kiesow, A., Bastos, A., Pongratz, J., Nabel, J. E. M. S.,  
 3765 Conchedda, G., Pilli, R., Andrew, R. M., Schelhaas, M.-J. and Dolman, A. J. (2020).  
 3766 European anthropogenic AFOLU greenhouse gas emissions: a review and benchmark data.  
 3767 *Earth System Science Data*, **12**, 961–1001, doi:10.5194/essd-12-961-2020
- 3768 Petrescu, A. M. R., McGrath, M. J., Andrew, R. M., Peylin, P., Peters, G. P., Ciais, P., Broquet,  
 3769 G., Tubiello, F. N., Gerbig, C., Pongratz, J., Janssens-Maenhout, G., Grassi, G., Nabuurs,

- G.-J., Regnier, P., Lauerwald, R., Kuhnert, M., Balkovič, J., Schelhaas, M.-J., Denier van der Gon, H. A. C., Solazzo, E., Qiu, C., Pilli, R., Konovalov, I. B., Houghton, R. A., Günther, D., Perugini, L., Crippa, M., Ganzenmüller, R., Luijkx, I. T., Smith, P., Munassar, S., Thompson, R. L., Conchedda, G., Monteil, G., Scholze, M., Karstens, U., Brockmann, P., and Dolman, A. J. (2021). The consolidated European synthesis of CO<sub>2</sub> emissions and removals for the European Union and United Kingdom: 1990–2018, *Earth System Science Data*, **13**, 2363–2406, <https://doi.org/10.5194/essd-13-2363-2021>
- Peylin, P., Bousquet, P., Le Quéré, C., Sitch, S., Friedlingstein, P., McKinley, G., Gruber, N., Rayner, P., and Ciais, P. (2005). Multiple constraints on regional CO<sub>2</sub> flux variations over land and oceans, *Global Biogeochemical Cycles*, **19**, GB1011. doi: 10.1029/2003GB002214
- Peylin, P., Law, R. M., Gurney, K. R., Chevallier, F., Jacobson, A. R., Maki, T., Niwa, Y., Patra, P. K., Peters, W., Rayner, P. J., Rödenbeck, C., van der Laan-Luijkx, I. T., and Zhang, X. (2013). Global atmospheric carbon budget: results from an ensemble of atmospheric CO<sub>2</sub> inversions. *Biogeosciences*, **10**, 6699–6720. doi: 10.5194/bg-10-6699-2013
- Pfeil, B., Olsen, A., Bakker, D. C. E., Hankin, S., Koyuk, H., Kozyr, A., Malczyk, J., Manke, A., Metzl, N., Sabine, C. L., Akl, J., Alin, S. R., Bates, N., Bellerby, R. G. J., Borges, A., Boutin, J., Brown, P. J., Cai, W.-J., Chavez, F. P., Chen, A., Cosca, C., Fassbender, A. J., Feely, R. A., González-Dávila, M., Goyet, C., Hales, B., Hardman-Mountford, N., Heinze, C., Hood, M., Hoppema, M., Hunt, C. W., Hydes, D., Ishii, M., Johannessen, T., Jones, S. D., Key, R. M., Körtzinger, A., Landschützer, P., Lauvset, S. K., Lefèvre, N., Lenton, A., Lourantou, A., Merlivat, L., Midorikawa, T., Mintrop, L., Miyazaki, C., Murata, A., Nakadate, A., Nakano, Y., Nakaoka, S., Nojiri, Y., Omar, A. M., Padin, X. A., Park, G.-H., Paterson, K., Perez, F. F., Pierrot, D., Poisson, A., Ríos, A. F., Santana-Casiano, J. M., Salisbury, J., Sarma, V. V. S. S., Schlitzer, R., Schneider, B., Schuster, U., Sieger, R., Skjelvan, I., Steinhoff, T., Suzuki, T., Takahashi, T., Tedesco, K., Telszewski, M., Thomas, H., Tilbrook, B., Tjiputra, J., Vandemark, D., Veness, T., Wanninkhof, R., Watson, A. J., Weiss, R., Wong, C. S. and Yoshikawa-Inoue, H. (2013). A uniform, quality controlled Surface Ocean CO<sub>2</sub> Atlas (SOCAT). *Earth System Science Data*, **5**, 125–143. doi:10.5194/essd-5-125-2013
- Piao, S., Fang, J., Ciais, P., Peylin, P., Huang, Y., Sitch, S. and Wang T. (2009). The carbon balance of terrestrial ecosystems in China. *Nature*, **458**, 1009–1013. doi: 10.1038/nature07944
- Piao, S., Liu, Z., Wang, Y., Ciais, P., Yao, Y., Peng, S., Chevallier, F., Friedlingstein, P., Janssens, I. A., Peñuelas, J., and Sitch, S. (2017). On the causes of trends in the seasonal amplitude of atmospheric CO<sub>2</sub>. *Global Change Biology*, **24**, 608–616. doi: 10.1111/gcb.13909
- Piao, S., Wang, X., Wang, K., Li, X., Bastos, A., Canadell, J. G., Ciais, P., Friedlingstein, P., and Sitch, S. (2020a). Interannual Variation of Terrestrial Carbon Cycle: Issues and Perspectives, *Global Change Biology*, **26**, 300–318. doi: 10.1111/gcb.14884
- Piao, S., Wang, X., Park, T., Chen, C., Lian, X., He, Y., Bjerke, J. W., Chen, A., Ciais, P., Tommervik, H., Nemani, R. R. and Myneni, R. B. (2020b). Characteristics, drivers and feedbacks of global greening. *Nature Reviews Earth & Environment*, **1**, 14–27. doi:10.1038/s43017-019-0001-x
- Pongratz, J., Reick, C. H., Houghton, R. A. and House, J. I. (2014). Terminology as a key uncertainty in net land use and land cover change carbon flux estimates. *Earth System Dynamics*, **5**, 177–195, 2014. doi: 10.5194/esd-5-177-2014



- Poulter, B., Frank, D., Ciais, P., Myneni, R. B., Andela, N., Bi, J., Broquet, G., Canadell, J. G., Chevallier, F., Liu, Y. Y., Running, S. W., Sitch, S. and van der Werf, G. R. (2014). Contribution of semi-arid ecosystems to interannual variability of the global carbon cycle. *Nature*, **509**, 600–603. doi:10.1038/nature13376
- Qin, Y. W. Xiao, X., Wigneron, J.-P., Ciais, P., Brandt, M., Fan, L., Li, X., Crowell, S., Wu, X., Doughty, R., Zhang, Y., Liu, F., Sitch, S., and Moore III, B. (2021). Carbon loss from forest degradation exceeds that from deforestation in the Brazilian Amazon, *Nature Climate Change*, **11**, 442–448. doi: 10.1038/s41558-021-01026-5, 2021.
- Qiu, B., Ge, J., Guo, W. D., Pittman, A. J. and Mu, M. Y. (2020). Responses of Australian dryland vegetation to the 2019 heat wave at a sub daily scale. *Geophysical Research Letters*, **47**, e2019GL086569. doi:10.1029/2019GL086569
- Quegan, S., Toan, L. T., Chave, J., Dall, J., Exbrayat, J. F., Minh, D. H. T., Lomas, M., D'Alessandro, M. M., Paillou, P., Papathanassiou, K., Rocca, F., Saatchi, S., Scipal, K., Shugart, H., Smallman, T. L., Soja, M. J., Tebaldini, S., Ulander, L., Villard, L. and Williams, M. (2019). The European Space Agency BIOMASS mission: measuring forest above-ground biomass from space. *Remote Sensing of the Environment*, **227**, 44–60. doi:10.1016/j.rse.2019.03.032
- Quilcaille, Y., Gasser, T., Ciais, P., Lecocq, F., Janssens-Maenhout, G., and Mohr, S. (2018). Uncertainty in projected climate change arising from uncertain fossil-fuel emission factors. *Environmental Research Letters*, **13**, 044017. doi: 10.1088/1748-9326/aab304#references
- Rabin, S. S., Melton, J. R., Lasslop, G., Bachelet, D., Forrest, M., Hantson, S., Kaplan, J. O., Li, F., Mangeon, S., Ward, D. S., Yue, C., Arora, V. K., Hickler, T., Kloster, S., Knorr, W., Nieradzik, L., Spessa, A., Folberth, G. A., Sheehan, T., Voulgarakis, A., Kelley, D. I., Prentice, I. C., Sitch, S., Harrison, S., and Arneth, A. (2017). The Fire Modeling Intercomparison Project (FireMIP), phase 1: experimental and analytical protocols with detailed model descriptions, *Geoscientific Model Development*, **10**, 1175–1197. doi: 10.5194/gmd-10-1175-2017.
- Ramankutty N., Gibbs, H. K., Achard, F., Defries, R., Foley, J. A. and Houghton, R. A. (2007). Challenges to estimating carbon emissions from tropical deforestation. *Global Change Biology*, **13**, 51–66. doi: 10.1111/j.1365-2486.2006.01272.x
- Randerson, J. T., Hoffman, F. M., Thornton, P. E., Mahowald, N. M., Lindsay, K., Lee, Y. H., Nevison, C. D. Doney, S. C., Bonan, G., Stöckli, R., Covey, C., Running, S. W. and Fung, I. Y. (2009). Systematic assessment of terrestrial biogeochemistry in coupled climate–carbon models. *Global Change Biology*, **15**, 2462–2484. doi: 10.1111/j.1365-2486.2009.01912.x
- Randerson, J. T., Lindsay, K., Munoz, E., Fu, W., Moore, J. K., Hoffman, F. M., Mahowald, N. M. and Doney, S. C. (2015). Multi-century changes in ocean and land contributions to the climate-carbon feedback. *Global Biogeochemical Cycles*, **29**, 744–759. doi:10.1002/2014GB005079
- Raupach, M. R., Canadell, J. G. and Le Quéré, C. (2008). Anthropogenic and biophysical contributions to increasing atmospheric CO<sub>2</sub> growth rate and airborne fraction. *Biogeosciences*, **5**, 1601–1613. doi:10.5194/bg-5-1601-2008
- Raupach, M. R., Gloor, M., Sarmiento, J. L., Canadell, J. G., Frölicher, T. L., Gasser, T., Houghton, R. A., Le Quéré, C. and Trudinger, C. M. (2014). The declining uptake rate of atmospheric CO<sub>2</sub> by land and ocean sinks. *Biogeosciences*, **11**, 3453–3475. doi:10.1007/s10584-009-9596-0

- Regnier, P., Friedlingstein, P., Ciais, P., Mackenzie, F. T., Gruber, N., Janssens, I. A., Laruelle, G., G., Lauerwald, R., Luyssaert, S., Andersson, A. J., Arndt, S., Arnosti, C., Borges, A. V., Dale, A. W., Gallego-Sala, A., Godd  ris, Y., Goossens, N., Hartmann, J., Heinze, C., Ilyina, T., Joos, F., LaRowe, D. E., Leifeld, J., Meysman, F. J. R., Munhoven, G., Raymond, P. A., Spahni, R., Suntharalingam, P. and Thullner, M. (2013). Anthropogenic perturbation of the carbon fluxes from land to ocean. *Nature Geosciences*, **6**, 597–607. doi:10.1038/ngeo1830
- Reichstein, M., Bahn, M., Ciais, P., Frank, D., Mahecha, M. D., Seneviratne, S. I., Zscheischler, J., Beer, C., Buchmann, N., Frank, D. C., Papale, D., Rammig, A., Smith, P., Thonicke, K., van der Velde, M., Vicca, S., Walz, A., and Wattenbach, M. (2013). Climate extremes and the carbon cycle, *Nature*, **500**, 287–295. doi: 10.1038/Nature12350, 2013
- Remaud, M., Chevallier, F., Maignan, F., Belviso, S., Berchet, A., Parouffe, A., Abadie, C., Bacour, C., Lennartz, S., and Peylin, P. (2022). Plant gross primary production, plant respiration and carbonyl sulfide emissions over the globe inferred by atmospheric inverse modelling, *Atmos. Chem. Physics*, **22**, 2525–2552. doi: 10.5194/acp-22-2525-2022
- Resplandy, L., Keeling, R. F., R  denbeck, C., Stephens, B. B., Khatiwala, S., Rodgers, K. B., Long, M. C., Bopp, L. and Tans, P. P. (2018). Revision of global carbon fluxes based on a reassessment of oceanic and riverine carbon transport. *Nature Geoscience*, **11**, 504–509. doi:10.1038/s41561-018-0151-3
- Reuter, M., Buchwitz, M., Hilker, M., Heymann, J., Schneising, O., Pillai, D., Bovensmann, H., Burrows, J. P., B  sch, H., Parker, R., Butz, A., Hasekamp, O., O'Dell, C. W., Yoshida, Y., Gerbig, C., Nehr Korn, T., Deutscher, N. M., Warneke, T., Notholt, J., Hase, F., Kivi, R., Sussmann, R., Machida, T., Matsueda, H. and Sawa, Y. (2014). Satellite-inferred European carbon sink larger than expected. *Atmospheric Chemistry and Physics*, **14**, 13739–13753. doi: 10.5194/acp-14-13739-2014
- Reuter, M., Buchwitz, M., Schneising, O., Krautwurst, S., O'Dell, C. W., Richter, A., Bovensmann, H. and Burrows, J. P. (2019). Towards monitoring localized CO<sub>2</sub> emissions from space: Co-located regional CO<sub>2</sub> and NO<sub>2</sub> enhancements observed by the OCO-2 and S5P satellites. *Atmospheric Chemistry and Physics*, **19**, 9371–9383. doi:10.5194/acp-19-9371-2019
- Ridge, S. M. and McKinley, G. A. (2020). Advective controls on the North Atlantic anthropogenic carbon sink. *Global Biogeochemical Cycles*, **34**, 1138. doi:10.1029/2019GB006457
- Ridge, S. M. and McKinley, G. A. (2021). Ocean carbon uptake under aggressive emission mitigation. *Biogeosciences* **18**, 2711–2725. doi: 10.5194/bg-18-2711-2021
- R  denbeck, C., Houweling, S., Gloor, M., and Heimann, M. (2003). CO<sub>2</sub> flux history 1982–2001 inferred from atmospheric data using a global inversion of atmospheric transport, *Atmospheric Chemistry and Physics*, **3**, 1919–1964. doi: 10.5194/acp-3-1919-2003, 2003.
- R  denbeck, C., Bakker, D. C. E., Metzl, N., Olsen, A., Sabine, C., Cassar, N., Reum, F., Keeling, R. F. and Heimann, M. (2014). Interannual sea-air CO<sub>2</sub> flux variability from an observation-driven ocean mixed-layer scheme. *Biogeosciences*, **11**, 4599–4613. doi:10.5194/bg-11-4599-2014
- R  denbeck, C., Bakker, D. C. E., Gruber, N., Iida, Y., Jacobson, A. R., Jones, S., Landsch  tzer, P., Metzl, N., Nakaoka, S., Olsen, A., Park, G.-H., Peylin, P., Rodgers, K. B., Sasse, T. P., Schuster, U., Shutler, J. D., Valsala, V., Wanninkhof, R. and Zeng, J. (2015). Data-based estimates of the ocean carbon sink variability – first results of the Surface Ocean pCO<sub>2</sub>

- Mapping intercomparison (SOCOM). *Biogeosciences*, **12**, 7251–7278. doi:10.5194/bg-12-7251-2015
- Rodgers, K. B., Schlunegger, S., Slater, R. D., Ishii, M., Frolicher, T. L., Toyama, K., Plancherel, Y., Aumont, O. and Fassbender, A. J. (2020). Reemergence of anthropogenic carbon into the ocean's mixed layer strongly amplifies transient climate sensitivity. *Geophysics Research Letters*, **47**, 130. doi:10.1002/2017GL073758
- Rosan, T. M., Goldewijk, K. K., Ganzenmüller, R., O'Sullivan, M., Pongratz, J., Mercado, L. M., Aragao, L. E. O. C., Heinrich, V., von Randow, C., Wiltshire, A., Tubiello, F. N., Bastos, A., Friedlingstein, P. and Sitch, S. (2021). A multi-data assessment of land use and land cover emissions from Brazil during 2000–2019. *Environmental Research Letters*, **16**, 074004. doi: 10.1088/1748-9326/ac08c3
- Rosen, P., Hensley, S., Shaffer, S., Edelstein, W., Kim, Y., Kumar, R., Misra, T., Bhan, R., Satish, R. and Sagi, R. (2016). An update on the NASA-ISRO dual-frequency dbf SAR (NISAR) mission. *2016 IEEE International Geoscience and Remote Sensing Symposium*. IEEE, New York, pp. 2106–2108. doi:10.1109/IGARSS.2016.7729543
- Rowland, L., da Costa, A. C., L., Galbraith, D. R., Oliveira, R. S., Binks, O. J., Oliveira, A. A. R., Pullen, A. M., Doughty, C. E., Metcalfe, D. B., Vsconcelos, S., S., Ferreira, L. V., Malhi, Y., Grace, J., Mencuccini, M., and Meir, P. (2015). Death from drought in tropical forests is triggered by hydraulics not carbon starvation. *Nature*, **528**, 119-122. doi: 10.1038/nature15539
- Rubino, M., Etheridge, D. M., Thornton, D. P., Howden, R., Allison, C. E., Francey, R. J., Langenfelds, R. L., Steele, L. P., Trudinger, C. M., Spencer, D. A., Curran, M. A. J., van Ommen, T. D., and Smith, A. M.(2019). Revised records of atmospheric trace gases CO<sub>2</sub>, CH<sub>4</sub>, N<sub>2</sub>O, and  $\delta^{13}\text{C}$ -CO<sub>2</sub> over the last 2000 years from Law Dome, Antarctica, *Earth System Science Data*, **11**, 473–492. doi:10.5194/essd-11-473-2019
- Rudnick, D. L. (2016). Ocean Research Enabled by Underwater Gliders. *Annual Review of Marine Science*, **8**, 519-541. doi:10.1146/annurev-marine-122414-033913
- Saatchi, S. S., Harris, N. L., Brown, S., Lefsky, M., Mitchard, E. T. A., Salas, W., Zutta, B. R., Buermann, W., Lewis, S. L., Hagen, S., Petrova, S., White, L., Silman, M. and Morel, A. (2011). Benchmark map of forest carbon stocks in tropical regions across three continents. *Proceedings of the National Academy of Sciences*, **108**, 9899-9904. doi: 10.1073/pnas.1019576108
- Sabine, C. L., Feely, R. A., Gruber, N., Key, R. M., Lee, K., Bullister, K. L., Wanninkhof, R., Wong, C. S., Wallace, D. W. R. Wallace, Tilbrook, B., Millero, F. J., Peng, T.-H., Kozyr, A., Ono, T. and Rois, A. F. (2004). The oceanic sink for anthropogenic CO<sub>2</sub>. *Science*, **305**, 367–371. doi:10.1126/science.1097403
- Sabine, C. L. and Tanhua, T. (2010). Estimation of anthropogenic CO<sub>2</sub> inventories in the ocean. *Annual Reviews of Marine Sciences*, **2**, 175-198. doi:10.1146/annurev-marine-120308-080947
- Sabine, C., Sutton, A., McCabe, K., Lawrence-Slavas, N., Alin, S., Feely, R., Jenkins, R., Maenner, S., Meinig, C., Thomas, J., van Ooijen, E., Passmore, A. and Tilbrook, B. (2020). Evaluation of a new carbon dioxide system for autonomous surface vehicles. *J. Atmos. Ocean. Technol.*, **37**, 1305-1317. doi:10.1175/JTECH-D-20-0010.1
- Sarmiento, J. L., and Sundquist E. T. (1992). Revised budget for the oceanic uptake of anthropogenic carbon dioxide, *Nature*, **356**, 589–593. doi:10.1038/356589a0

- 3950 Sarmiento, J. L. and Gruber, N. (2006). Ocean Biogeochemical Dynamics. Princeton University  
3951 Press. ISBN: 0-691-01707-7. doi:10.1017/S0016756807003755
- 3952 Sarmiento, J. L., Gloor, M., Gruber, N., Beaulieu, C., Jacobson, A. R., Mikaloff Fletcher, S. E.,  
3953 Pacala, S., and Rodgers, K. (2010). Trends and regional distributions of land and ocean  
3954 carbon sinks. *Biogeosciences*, **7**, 2351-2367. doi: 10.5194/bg-7-2351-2010
- 3955 Scharlemann, J. P. W., Tanner, E. V. J., Hiederer, R. and Kapos, V. (2014). Global soil carbon:  
3956 understanding and managing the largest terrestrial carbon pool. *Carbon Management*, **5**, 81-  
3957 91. doi:10.4155/cmt.13.77
- 3958 Schepaschenko, D., Moltchanova, E., Shvidenko, A., Blyshchyk, V., Dmitriev, E., Martynenko,  
3959 O., See, L. and Kraxner F. (2018). Improved estimates of biomass expansion factors for  
3960 Russian forests. *Forests*, **9**, 312. doi:10.3390/f9060312
- 3961 Schimel, D., Stephens, B. B., and Fisher, J. B. (2015). Effect of increasing CO<sub>2</sub> on the terrestrial  
3962 carbon cycle, *Proceeding of the National Academy of Sciences*, **112**, 436-441. doi:  
3963 10.1073/pnas.1407302112
- 3964 Scholze, M., Kaminski, T., Knorr, W., Voßbeck, M., Wu, M., Ferrazzoli, P., Kerr, Y., Mialon, A.,  
3965 Richaume, P., Rodríguez-Fernández, N., Vittucci, C., Wigneron, J. P., Mechlenburg, S. and  
3966 Drusch, M. (2019). Mean European carbon sink over 2010–2015 estimated by simultaneous  
3967 assimilation of atmospheric CO<sub>2</sub>, soil moisture, and vegetation optical depth. *Geophysical*  
3968 *Research Letters*, **46**. doi:10. 1029/2019GL085725
- 3969 Schourup-Kristensen, V., Sidorenko, D., Wolf-Gladrow, D. A. and Völker, C. (2014). A skill  
3970 assessment of the biogeochemical model REcoM2 coupled to the Finite Element Sea Ice–  
3971 Ocean Model (FESOM 1.3). *Geoscientific Model Development*, **7**, 2769–2802.  
3972 doi:10.5194/gmd-7-2769-2014
- 3973 Schuh, A., Jacobson, A. R., Basu, S., Weir, B., Baker, D., Bowman, K., Chevallier, F., Crowell,  
3974 S., Davis, K., Deng, F., Denning, S., Feng, L., Jones, D., Liu, J., and Palmer, P. (2019).  
3975 Quantifying the Impact of Atmospheric Transport Uncertainty on CO<sub>2</sub> Surface Flux  
3976 Estimates, *Global Biogeochemical Cycles*, **33**, 484–500. doi: 10.1029/2018GB006060
- 3977 Schulze, E.-D., and M. Heimann. 1998. Carbon and water exchange of terrestrial ecosystems.  
3978 Pages 145-161 in J. Galloway, and J. M. Melillo, editors. Asian change in the context of  
3979 global change. Cambridge University Press, Cambridge, UK.
- 3980 Schwinger, J., Tjiputra, J. F., Heinze, C., Bopp, L., Christian, J. R., Gehlen, M., Ilyina, T., Jones,  
3981 C. D., Salas-Méla, D., Segschneider, J., Séférian, R. and Totterdell, I. (2014). Nonlinearity  
3982 of ocean carbon cycle feedbacks in CMIP5 Earth system models. *Journal of Climate*, **27**,  
3983 3869–3888. doi:10.1175/JCLI-D-13-00452.1
- 3984 Schwinger, J., Goris, N., Tjiputra, J. F., Kriest, I., Bentsen, M., Bethke, I., Ilicak, M., Assmann,  
3985 K. M. and Heinze, C. (2016). Evaluation of NorESM-OC (versions 1 and 1.2), the ocean  
3986 carbon-cycle stand-alone configuration of the Norwegian Earth System Model (NorESM1).  
3987 *Geoscientific Model Development*, **9**, 2589–2622. doi:10.5194/gmd-9-2589-2016
- 3988 Schwinger, J. and Tjiputra, J. (2018). Ocean carbon cycle feedbacks under negative emissions.  
3989 *Geophysical Research Letters*, **26**, 5289. doi:10.1088/1748-9326/11/5/055006
- 3990 Seelmann, K., Aßmann, S. and Körtzinger, A. (2019). Characterization of a novel autonomous  
3991 analyzer for seawater total alkalinity: Results from laboratory and field tests. *Limnology and*  
3992 *Oceanography: Methods*, **17**, 515-532. doi:10.1002/lom3.10329
- 3993 Séférian, R., Berthet, S., Yool, A., Palmieri, J., Bopp, L., Tagliabue, A., Kwaitkowski, L.,  
3994 Aumont, O., Christian, J., Dunne, J., Gehlen, M., Ilyina, T., John, J. G., Li, H., Long, M. C.,

- 3995 Luo, J. Y., Nakano, H., Romanou, A., Schwinger, J., Stock, C., Santana-Falcon, Y., Takano,  
3996 Y., Tjiputra, J., Tsujino, H., Wantanabe, M., Wu, T., Wu, F. and Yamamoto, A. (2020).  
3997 Tracking Improvement in Simulated Marine Biogeochemistry Between CMIP5 and CMIP6.  
3998 *Curr. Clim. Change Rep.*, **6**, 95–119. doi: 10.1007/s40641-020-00160-0
- 3999 Sellers, P. J., Schimel, D. S., Moore III, B., Liu, J. and Eldering, A. (2018). Observing Carbon  
4000 Cycle-Climate Feedbacks from Space, *Proceedings of the National Academy of Sciences*,  
4001 **115**, 7860–7868. doi:10.1073/pnas.1716613115
- 4002 Sigman, D. M., Hain, M. P. and Haug, G. H. (2010). The polar ocean and glacial cycles in  
4003 atmospheric CO<sub>2</sub> concentration. *Nature*, **466**, 47–55. doi:10.1038/nature09149
- 4004 Sitch, S., Brovkin, V., von Bloh, W., van Vuuren, D., Eickhout, B. and Ganopolski, A. (2005).  
4005 Impacts of future land cover changes on atmospheric CO<sub>2</sub> and climate. *Global*  
4006 *Biogeochemical Cycles*, **19**, GB2013. doi: 10.1029/2004GB002311
- 4007 Sitch, S., Friedlingstein, P., Gruber, N., Jones, S. D., Murray-Tortarolo, G., Ahlström, A., Doney,  
4008 S. C., Graven, H., Heinze, C., Huntingford, C., Levis, S., Levy, P. E., Lomas, M., Poulter,  
4009 B., Viovy, N., Zaehle, S., Zeng, N., Arneeth, A., Bonan, G., Bopp, L., Canadell, J. G.,  
4010 Chevallier, F., Ciais, P., Ellis, R., Gloor, M., Peylin, P., Piao, S. L., Le Quéré, C., Smith, B.,  
4011 Zhu, Z. and Myneni, R. (2015). Recent trends and drivers of regional sources and sinks of  
4012 carbon dioxide. *Biogeosciences*, **12**, 653–679. doi:10.5194/bg-12-653-2015
- 4013 Sloyan, B. M., Wanninkhof, R., Kramp, M., Johnson, G. C., Talley, L. D., Tanhua, T.,  
4014 McDonagh, E., Cusack, C., O'Rourke, E., McGovern, E., Katsumata, K., Diggs, S.,  
4015 Hummon, J., Ishii, M., Azetsu-Scott, K., Boss, E., Ansorge, I., Perez, F. F., Mercier, H.,  
4016 Williams, M. J. M., Anderson, L., Lee, J. H., Murata, A., Kouketsu, S., Jeansson, E.,  
4017 Hoppema, M. & Campos, E. (2019). The Global Ocean Ship-Based Hydrographic  
4018 Investigations Program (GO-SHIP): A Platform for Integrated Multidisciplinary Ocean  
4019 Science. *Frontiers in Marine Science*, **6**, 445. doi: 10.3389/fmars.2019.00445
- 4020 Smith, B., Prentice, I. C., and Sykes, M. T. (2001). Representation of vegetation dynamics in the  
4021 modelling of terrestrial ecosystems comparing two contrasting approaches within European  
4022 climate space, *Global Ecol. Biogeogr.*, **10**, 621–637. doi: 10.1046/j.1466-822X.2001.t01-1-  
4023 00256.x
- 4024 Smith P., Bustamante, M., Ahammad, H., Clark, H., Dong, H., Elsiddig, E. A., Haberl, H.,  
4025 Harper, R., House, J., Jafari M., Masera, O., Mbow, C., Ravindranath N. H., Rice C. W.,  
4026 Robledo Abad, C., Romanovskaya, A., Sperling, F. and Tubiello F. (2014). Agriculture,  
4027 Forestry and Other Land Use (AFOLU). In: Climate Change 2014: Mitigation of Climate  
4028 Change. Contribution of Working Group III to the Fifth Assessment Report of the  
4029 Intergovernmental Panel on Climate Change [Edenhofer, O., R. Pichs-Madruga, Y. Sokona,  
4030 E. Farahani, S. Kadner, K. Seyboth, A. Adler, I. Baum, S. Brunner, P. Eickemeier, B.  
4031 Kriemann, J. Savolainen, S. Schlömer, C. von Stechow, T. Zwickel and J.C. Minx (eds.)].  
4032 Cambridge University Press, Cambridge, United Kingdom and New York, NY, USA.
- 4033 Smith, W. K., Reed, S. C., Cleveland, C. C. Ballantyne, A. P., Anderegg, W. R. L., Wieder, W. R.  
4034 Liu, Y. Y. and Running, S. (2015). Large divergence of satellite and Earth system model  
4035 estimates of global terrestrial CO<sub>2</sub> fertilization. *Nature Climate Change*, **6**, 306–310. doi:  
4036 Song, X.-P., Hansen, M. C., Stehman, S. V., Potapov, P. V., Tyukavina, A., Vermote, E. F. and  
4037 Townshend, J. R. (2018). Global land change from 1982 to 2016. *Nature*, **560**, 639–343.  
4038 doi:10.1038/s41586-018-0411-9

- Soong, J. L., Fuchslueger, L., Marañón-Jimenez, S., Torn, M. S., Janssens, I. A., Penuelas, J., and Richter, A. (2019). Microbial carbon limitation: The need for integrating microorganisms into our understanding of ecosystem carbon cycling. *Global Change Biology*, **26**, 1953–1961. doi:10.1111/gcb.14962
- Spawn, S. A., Sullivan, C. C., Lark, T. J. and Gibbs, H. K. (2020). Harmonized global maps of above and belowground biomass carbon density in the year 2010. *Scientific Data*, **7**, 112. doi:10.1038/s41597-020-0444-4
- Stamell, J., Rustagi, R. R., Gloege, L. and McKinley, G. A. (2020). Strengths and weaknesses of three Machine Learning methods for pCO<sub>2</sub> interpolation. *Geoscientific Model Development Discuss.* [preprint], doi:10.5194/gmd-2020-311, in review, 2020.
- Stock, C. A., Dunne, J. P., Fan, S., Ginoux, P., John, J., Krasting, J. P., Laufkötter, C., Paulot, F. and Zadeh, N. (2020). Ocean biogeochemistry in GFDL's Earth System Model 4.1 and its response to increasing atmospheric CO<sub>2</sub>. *J. Adv. Model. Earth Syst.*, **12**, e2019MS002043. doi:10.1029/2019MS002043
- Sun, Y., Frankenberg, C., Jung, J., Joiner, J., Guanter, L., Köhler, P. and Magney, T. (2018). Overview of solar-Induced chlorophyll fluorescence (SIF) from the Orbiting Carbon Observatory-2: Retrieval, cross-mission comparison, and global monitoring for GPP. *Remote Sensing of Environment*, **209**, 808–823. doi:10.1016/j.rse.2018.02.016
- Sundquist, E.T., (1993). The global carbon dioxide budget. *Science*, **259**, 934–941. doi:10.1126/science.259.5097.934
- Sutton, A. J., Sabine, C. L., Maenner-Jones, S., Lawrence-Slavas, N., Meinig, C., Feely, R. A., Mathis, J. T., Musielewicz, S., Bott, R., McLain, P. D., Fought, H. J. and Kozyr, A. (2014). A high-frequency atmospheric and seawater pCO<sub>2</sub> data set from 14 open-ocean sites using a moored autonomous system. *Earth System Science Data*, **6**, 353–366. doi:10.5194/essd-6-353-2014
- Sutton, A. J., Williams, N. L., & Tilbrook, B. (2021). Constraining Southern Ocean CO<sub>2</sub> Flux Uncertainty Using Uncrewed Surface Vehicle Observations. *Geophysical Research Letters*, **48**, e2020GL091748. doi:10.1029/2020gl091748
- Takahashi, T., Sutherland, S. C., Sweeney, C., Poisson, A., Metzl, N., Tilbrook, B., Bates, N., Wanninkhof, R., Feely, R. A., Sabine, C., Olafsson, J., Nojiri, Y. (2002). Global sea–air CO<sub>2</sub> flux based on climatological surface ocean pCO<sub>2</sub>, and seasonal biological and temperature effects. *Deep Sea Research Part II: Topical Studies in Oceanography*, **49**, 9–10, 1601–1622. doi:10.1016/S0967-0645(02)00003-6
- Takahashi, T., Sutherland, S. C., Wanninkhof, R., Sweeney, C., Feely, R. A., Chipman, D. W., Hales, B., Friederich, G., Chavez, F., Sabine, C., Watson, A., Bakker, D. C. E., Schuster, U., Metzl, N., Yoshikawa-Inoue, H., Ishii, M., Midorikawa, T., Nojiri, Y., Körtzinger, A., Steinhoff, T., Hoppema, M., Olafsson, J., Arnarson, T.S., Tilbrook, B., Johannessen, T., Olsen, A., Bellerby, R., Wong, C. S., Delille, B., Bates, N. R. and de Baar, H. J. W. (2009). Climatological mean and decadal change in surface ocean pCO<sub>2</sub>, and net sea–air CO<sub>2</sub> flux over the global oceans. *Deep Sea Research Part II: Topical Studies in Oceanography*, **56**, 554–577. doi:10.1016/j.dsr2.2008.12.009
- Takeshita, Y., Johnson, K. S., Martz, T. R., Plant, J. N. and Sarmiento, J. L. (2018). Assessment of autonomous pH measurements for determining surface seawater partial pressure of CO<sub>2</sub>. *Journal of Geophysical Research: Oceans*, **123**, 4003–4013. doi:10.1029/2017jc013387

- Takeshita, Y., Johnson, K. S., Coletti, L., J., Jannasch, H. W., Walz, P. M. and Warren, J. W. (2020). Assessment of pH dependent errors in spectrophotometric pH measurements of seawater. *Marine Chemistry*, **223**, 103801. doi: 10.1016/j.marchem.2020.103801
- Tanhua, T., van Heuven, S., Key, R. M., Velo, A., Olsen, A. and Schirnack, C. (2010). Quality control procedures and methods of the CARINA database. *Earth System Science Data* **2**, 35–49. doi:10.5194/essd-2-35-2010
- Tanhua, T. and Keeling, R. F. (2012). Changes in column inventories of carbon and oxygen in the Atlantic Ocean. *Biogeosciences*, **9**, 4819–4833. doi:10.5194/bg-9-4819-2012
- Tans, P. P., Fung, I. Y., and Takahashi, T. (1990). Observational constraints on the global atmospheric CO<sub>2</sub> budget, *Science*, **247**, 1431–1438. doi: 10.1126/science.247.4949.1431
- Teubner, I. E., Forkel, M., Jung, M., Liu, Y. Y., Miralles, D. G., Parinussa, R., van der Schalie, R., Vreugdenhil, M., Schwalm, C. R., Tramontana, G., Camps-Valls, G., and Dorigo, W. A. (2018). Assessing the relationship between microwave vegetation optical depth and gross primary production, *International Journal of Applied Earth Observation and Geoinformation*, **65**, 79–91. doi: 10.1016/j.jag.2017.10.006
- Thomas, R. T., Prentice, I. C., Graven, H., Ciais, P., Fisher, J. B., Hayes, D. J., Huang, M., Huntzinger, D. N., Ito, A., Jain, A., and Mao, J. (2016). Increased light-use efficiency in northern terrestrial ecosystems indicated by CO<sub>2</sub> and greening observations, *Geophysical Research Letters*, **43**, 11339–11349. doi: 10.1002/2016GL070710
- Tohjima, Y., Mukai, H., Machida, T., Hoshina, Y., and Nakaoka, S.-I. (2019). Global carbon budgets estimated from atmospheric O<sub>2</sub>/N<sub>2</sub> and CO<sub>2</sub> observations in the western Pacific region over a 15-year period, *Atmospheric Chemistry and Physics*, **19**, 9269–9285, doi: 10.5194/acp-19-9269-2019
- Torres, A. D., Keppel-Aleks, G., Doney, S. C., Fendrock, M., Luis, K., De Mazière, M., Hase, F., Petri, C., Pollard, D. F., Roehl, C. M., Sussmann, R., Velasco, V. A., Warneke, T. and Wunch, D. (2019). A geostatistical framework for quantifying the imprint of mesoscale atmospheric transport on satellite trace gas retrievals. *Journal of Geophysical Research: Atmospheres*, **124**. doi: 10.1029/2018JD029933
- Trenberth, K. E., and Smith, L. (2005). The mass of the atmosphere: A constraint on global analysis. *Journal of Climate*, **18**, 864–875. doi: 10.1175/JCLI-3299.1
- Umezawa, T., Matsueda, H., Sawa, Y., Niwa, Y., Machida, T., and Zhou, L. (2018). Seasonal evaluation of tropospheric CO<sub>2</sub> over the Asia-Pacific region observed by the CONTRAIL commercial airliner measurements. *Atmospheric Chemistry and Physics*, **18**, 14851–14866, doi: 10.5194/acp-18-14851-2018
- van der Laan-Luijkx, I. T., van der Velde, I. R., Krol, M. C., Gatti, L. V., Domingues, L. G., Correia, C. S. C., Miller, J. B., Gloor, M., van Leeuwen, T. T., Kaiser, J. W., Wiedinmyer, C., Basu, S., Clerbaux, C. and Peters, W. (2015). Response of the Amazon carbon balance to the 2010 drought derived with CarbonTracker South America, *Global Biogeochem. Cycles*, **29**, 1092–1108. doi: 10.1002/2014GB005082
- van der Velde, I. R., van der Werf, G. R., Houweling, S., Maasakkers, J. D., Borsdorff, T., Landgraf, J., Tol, P., van Kempen, T. A., van Hees, R., Hoogeveen, R., Veeffkind, P. J., and Aben, A. (2021). Vast CO<sub>2</sub> release from Australian fires in 2019–2020 constrained by satellite. *Nature*, **597**, 366–369. doi: 10.1038/s41586-021-03712-y
- van der Werf, G. R., Randerson, J. T., Giglio, L., van Leeuwen, T. T., Chen, Y., Rogers, B. M., Mu, M., van Marle, M. J. E., Morton, D. C., Collatz, G. J., Yokelson, R. J. and Kasibhatla,



- P. S. (2017). Global fire emissions estimates during 1997–2016. *Earth System Science Data*, **9**, 697–720. doi:10.5194/essd-9-697-2017
- Varon, D. J., Jacob, D. J., McKeever, J., Jervis, D., Durak, B. O. A., Xia, y., and Huang, Y. (2018). Quantifying methane point sources from fine-scale satellite observations of atmospheric methane plumes. *Atmospheric Measurement Technology*, **11**, 5673–5686. doi: 10.5194/amt-11-5673-2018
- Verdy, A. Mazloff, M. R. (2017). A data assimilating model for estimating Southern Ocean biogeochemistry. *Journal of Geophysical Research: Oceans*, **122**, 6968–6988. doi:10.1002/2016JC012650
- Vitousek, P. M., Porder, S., Houlton, B. Z., and Chadwick O. A. (2010). Terrestrial phosphorus limitation: mechanisms, implications, and nitrogen–phosphorus interactions. *Ecological Applications*, **20**, 5–15. doi: 10.1890/08-0127.1
- Walker, A. P., De Kauwe, M. G., Bastos, A., Belmecheri, S., Georgiou, K., Keeling, R. F., McMahon, S. M., Medlyn, B. E., Moore, D. J. P., Norby, R. J., Zaehle, S., Anderson-Teixeira, K. J., Battipaglia, G., Brienen, R. J. W., Cabugao, K. G., Cailleret, M., Campbell, E., Canadell, J. G., Ciais, P., Craig, M. E., Ellsworth, D. S., Farquhar, G. D., Fatichi, S., Fisher, J. B., Frank, D. C., Graven, H., Gu, L., Haverd, V., Heilman, K., Heimann, M., Hungate, B. A., Iversen, C. M., Joos, F., Jiang, M., Keenan, T. F., Knauer, J., Körner, C., Leshyk, V. O., Leuzinger, S., Liu, Y., MacBean, N., Malhi, Y., McVicar, T. R., Penuelas, J., Pongratz, J., Powell, A.S., Riutta, T., Sabot, M. E. B., Schleucher, J., Sitch, S., Smith, W. K., Sulman, B., Taylor, B., Terrer, C., Torn, M. S., Treseder, K. K., Trugman, A. T., Trumbore, S. E., van Mantgem, P. J., Voelker, S. L., Whelan, M. E. and Zuidema, P. A. (2021). Integrating the evidence for a terrestrial carbon sink caused by increasing atmospheric CO<sub>2</sub>. *New Phytol.*, **229**, 2413–2445. doi: 10.1111/nph.16866
- Wang, J., Wang, M., Kim, J.-S., Joiner, J., Zeng, N., Jiang, F., Wang, H., He, W., Wu, M., Chen, T., Ju, W. and Chen, J. M. (2021). Modulation of land photosynthesis by the Indian Ocean Dipole: Satellite-based observations and CMIP6 future projections. *Earth's Future*, **9**, e2020EF001942. doi: 10.1029/2020EF001942
- Wang, S., Zhang, Y., Hakkarainen, J., Ju, W., Liu, Y., Jiang, F. and He, W. (2018). Distinguishing anthropogenic CO<sub>2</sub> emissions from different energy intensive industrial sources using OCO-2 observations: A case study in northern China. *Journal of Geophysical Research: Atmospheres*, **123**, 9462–9473. doi:10.1029/2018JD029005
- Wanninkhof, R. (2014). Relationship between wind speed and gas exchange over the ocean revisited. *Limnology and Oceanography*, **12**, 351–362. doi: 10.4319/lom.2014.12.351
- Watson, A. J., Schuster, U., Shutler, J. D., Holding, T., Ashton, I. G. C., Landschützer, P., Woolf, D. K. and Goddijn-Murphy, L. (2020). Revised estimates of ocean-atmosphere CO<sub>2</sub> flux are consistent with ocean carbon inventory. *Nature Communications*, **11**, 4422. doi:10.1038/s41467-020-18203-3
- Waugh, D. W., Hall, T. M., McNeil, B. I., Key, R. and Matear, R. J. (2006). Anthropogenic CO<sub>2</sub> in the oceans estimated using transit-time distributions. *Tellus*, **58B**, 376–389. doi:10.1111/j.1600-0889.2006.00222.x
- Weir, B., Crisp, D., O'Dell, C. W., Basu, S., Chatterjee, A., Kolassa, J., Oda, T., Pawson, S., Poulter, B., Zhang, Z., Ciais, P., Davis, S. J., Liu, Z., and Ott, L. E. (2021). Regional impacts of COVID-19 on carbon dioxide detected worldwide from space. *Science Advances*, **7**, eabf9415. Doi: 10.1126/sciadv.abf9415

- Welp, L., Keeling, R. and Meijer, H. A. J. (2011). Interannual variability in the oxygen isotopes of atmospheric CO<sub>2</sub> driven by El Niño. *Nature*, **477**, 579–582. doi:10.1038/nature10421
- Wigneron, J.-P., Fan, L., Ciais, P., Bastos, A., Brandt, M., Chave, J., Saatchi, S., Baccini, A. and Fensholt, R. (2020). Tropical forests did not recover from the strong 2015–2016 El Niño event. *Science Advances*, **6**, eaay4603. doi:10.1126/sciadv.aay4603
- Williams, N. L., Juranek, L. W., Feely, R. A., Johnson, K. S., Sarmiento, J. L., Talley, L. D., Dickson, A. G., Gray, A. R., Wanninkhof, R., Russell, J. L., Riser, S. C. and Takeshita, Y. (2017). Calculating surface ocean pCO<sub>2</sub> from biogeochemical Argo floats equipped with pH: An uncertainty analysis. *Global Biogeochemical Cycles*, **31**, 591–604. doi:10.1002/2016GB005541
- Wohlfahrt, G., Gerdel, K., Migliavacca, M., Rotenberg, E., Tatarinov, F., Müller, J., Hammerle, A., Julitta, T., Spielmann, F. M., and Yakir, D. (2018). Sun-induced fluorescence and gross primary productivity during a heat wave. *Scientific Reports*, **8**, 14169. doi: 10.1038/s41598-018-32602-z
- Wolf, S., Keenan, T. F., Fisher, J. B., Baldocchi, D. D., Desai, A. R., Richardson, A. D., Scott, R. L., Law, B. E., Litvak, M. E., Brunzell, N. A., Peters, W., and van der Laan-Luijkx, I. T. (2016). Warm spring reduced carbon cycle impact of the 2012 US summer drought, *Proc Natl Acad Sci USA*, **113**, 5880. doi: 10.1073/pnas.1519620113
- Woolf, D. K., Shutler, J. D., Goddijn-Murphy, L., Watson, A. J., Chapron, B., Nightingale, P. D., Donlon, C. J., Piskozub, J., Yelland, M. J., Ashton, I., Holding, T., Schuster, U., Girard-Arduin, F., Grouazel, A., Piolle, J.-F., Warren, M., Wrobel-Niedzwiecka, I., Land, P. E., Torres, R., Prytherch, J., Moat, B., Hanafin, J., Arduin, F. and Paul, F. (2019). Key uncertainties in the recent air-sea flux of CO<sub>2</sub>. *Global Biogeochemical Cycles*, **33**, 1548–1563. doi:10.1029/2018GB006041
- Wu, D., Lin, J. C., Fasoli, B., Oda, T., Ye, X., Lauvaux, T., Yang, E. G. and Kort, E. A. (2018). A Lagrangian approach towards extracting signals of urban CO<sub>2</sub> emissions from satellite observations of atmospheric column CO<sub>2</sub> (XCO<sub>2</sub>): X-Stochastic Time-Inverted Lagrangian Transport model (“X-STILT v1”). *Geoscientific Model Development*, **11**: 4843–4871. doi:10.5194/gmd-11-4843-2018
- Wu, D. E., Lin, J. C., Oda, T. and Kort, E. A. (2020). Space-based quantification of per capita CO<sub>2</sub> emissions from cities, *Environmental Research Letters*, **15**, 035004. doi:10.1088/1748-9326/ab68eb
- Wunch, D., Toon, G. C., Blavier, J.-F. L., Washenfelder, R. A., Notholt, J., Connor, B. J., Griffith, D. W., Sherlock, V., and Wennberg, P. O. (2011). The total carbon column observing network, *Philosophical Transactions of the Royal. Society A*, **369**, 2087–2112, doi:10.1098/rsta.2010.0240.
- Wunch, D., Wennberg, P. O., Osterman, G., Fisher, B., Naylor, B., Roehl, C. M., O’Dell, C., Mandrake, L., Viatte, C., Griffith, D. W., Deutscher, N. M., Velazco, V. A., Notholt, J., Warneke, T., Petri, C., De Maziere, M., Sha, M. K., Sussmann, R., Rettinger, M., Pollard, D., Robinson, J., Morino, I., Uchino, O., Hase, F., Blumenstock, T., Kiel, M., Feist, D. G., Arnold, S. G., Strong, K., Mendonca, J., Kivi, R., Heikkinen, P., Iraci, L., Podolske, J., Hillyard, P. W., Kawakami, S., Dubey, M. K., Parker, H. A., Sepulveda, E., Rodriguez, O. E. G., Te, Y., Jeseck, P., Gunson, M. R., Crisp, D. and Eldering, A. (2017). Comparisons of the Orbiting Carbon Observatory-2 (OCO-2) XCO<sub>2</sub> measurements with TCCON, *Atmospheric Measurement Techniques*, **10**, 2209–2238. doi: 10.5194/amt-10-2209-2017

- Xiao, J., J. Chen, Davis, K. J. and Reichstein, M. (2012). Advances in upscaling of eddy covariance measurements of carbon and water fluxes. *Journal Geophysical Research: Biogeosciences*, **117**, G00J01. doi:10.1029/2011JG001889
- Xiao, J., Chevallier, F., Gomez, C., Guanter, L., Hicke, J. A., Huete, A. R., Ichii, K., Ni, W., Pang, Y., Rahman, A. F. Sun, G., Yuan, W., Zhang, L. and Zhang, X. (2019). Remote sensing of the terrestrial carbon cycle: A review of advances over 50 years. *Remote Sensing of Environment*, **233**, 111383. doi:10.1016/j.rse.2019.111383
- Xu, L., Saatchi, S. S., Yang, Y., Yu, Y., Pongratz, J., Bloom, A. A., Bowman, K., Worden, J., Liu, J., Yin, Y., Domke, G., McRoberts, R. E., Woodall, C., Nabuurs, G.-J., de-Miguel, S., Keller, M., Harris, N., Maxwell, S., and Schimel, D. (2021). Changes in global terrestrial live biomass over the 21st century. *Science Advances*, **7**, eabe9829. doi: 10.1126/sciadv.abe9829
- Xue, L., Cai, W.-J., Takahashi, T., Gao, L., Wanninkhof, R., Wei, M., Li, K., Feng, L., and Yu, W. (2018). Climatic modulation of surface acidification rates through summertime wind forcing in the Southern Ocean. *Nature Communications*, **9**, 3240. doi: 10.1038/s41467-018-05443-7
- Ye, X., Lauvaux, T., Kort, E.A., Oda, T., Feng, S., Lin, J. C., Yang, E. G., and Wu, D. (2020). Constraining fossil fuel CO<sub>2</sub> emissions from urban area using OCO-2 observations of total column CO<sub>2</sub>. *Journal of Geophysical Research, Atmospheres*, **125**, e2019JD030528. doi: 10.1029/2019JD030528.
- Yin, Y., Byrne, B., Liu, J., Wennberg, P., Davis, K. J., Magney, T., Koehler, P., He, L., Jeyaram, R., Humphrey, V., Gerken, T., Feng, S., Digangi, J. P. and Frankenberg, C. (2020). Cropland carbon uptake delayed and reduced by 2019 Midwest floods. *AGU Advances*, **1**, e2019AV000140. doi:10.1029/2019AV000140
- Yoshida, Y., Ota, Y., Eguchi, N., Kikuchi, N., Nobuta, K., Tran, H., Morino, I., and Yokota, T. (2011). Retrieval algorithm for CO<sub>2</sub> and CH<sub>4</sub> column abundances from short-wavelength infrared spectral observations by the Greenhouse Gases Observing Satellite, *Atmospheric Measurement Technology*, **4**, 717–734. doi:10.5194/amt-4-717-2011
- Yuan, W., Zheng, Y., Ciais, P., Lombardozzi, D., Wang, Y., Ryu, Y., Chen, G., Dong, W., Hu, Z., Jian, A. K., Jiang, C., Kato, E., Li, S., Lienert, S., Liu, S., Nabel, J. E. M. S., Qin, Z., Quine, T., Sitch, S., Smith, W. K., Wang, F., Wu, C., Xiao, Z., and Yang, S. (2019). Increased atmospheric vapor pressure deficit reduces global vegetation growth, *Science Advances*, **5**, eaax1396. doi: 10.1126/sciadv.aax1396
- Zavarsky, A. and Marandino, C. A. (2019). The influence of transformed Reynolds number suppression on gas transfer parameterizations and global DMS and CO<sub>2</sub> fluxes. *Atmospheric Chemistry and Physics*, **19**, 1819-1834. doi:10.5194/acp-19-1819-2019
- Zeebe, R. and Wolf-Gladrow, D. (2001). CO<sub>2</sub> in seawater: Equilibrium, kinetics, isotopes. *Elsevier Oceanogr. Ser.*, **65**, Elsevier, Amsterdam.
- Zeng, N., Zhao, F., Collatz, G. J., Kalnay, E., Salawitch, R., West, T. O. and Guanter, L. (2014). Agricultural Green Revolution as a driver of increasing atmospheric CO<sub>2</sub> seasonal amplitude. *Nature*, **515**, 394–397. doi: 10.1038/nature13893
- Zhang, Q., Li, M., Wang, M., Mizzi, A.P., Huang, Y., Wei, C., Jin, J., Gu, Q. (2021). CO<sub>2</sub> Flux over the Contiguous United States in 2016 Inverted by WRF-Chem/DART from OCO-2 XCO<sub>2</sub> Retrievals. *Remote Sens.*, **13**, 2996. doi: 10.3390/rs13152996
- Zhao, M., and Running, S. W. (2010). Drought-Induced Reduction in Global Terrestrial Net Primary Production from 2000 Through 2009. *Science*, **329**, 940-943. doi: 10.1126/science.1192666

- 4263 Zhu, Z., Bi, J., Pan, Y., Ganguly, S., Anav, A., Xu, L., Samanta, A., Piao, S., Nemani, R. R., and  
4264 Myneni, R. B. (2013). Global data sets of vegetation leaf area index (LAI)3g and fraction of  
4265 Photosynthetically active radiation (FPAR)3g derived from global inventory modeling and  
4266 mapping studies (GIMMS) normalized difference vegetation index (NDVI3g) for the period  
4267 1981 to 2011. *Remote Sensing*, **5**, 927–948. doi: 10.3390/rs5020927
- 4268 Zhu, Z., Piao, S., Myneni, R. B., Huang, M., Zeng, Z., Canadell, J. G., Ciais, P., Sitch, S.,  
4269 Friedlingstein, P., Arneth, A., Cao, C., Cheng, L., Kato, E., Koven, C., Li, Y., Sian, X., Liu,  
4270 Y., Liu, R., Mao, J., Pan, Y., Peng, S., Peñuelas, J., Poulter, B., Pugh, T. A. M., Stocker, B.  
4271 D., Vlovy, N., Wang, X., Wang, Y., Xiao, Z., Yang, H., Zaehle, S., and Zeng, N. (2016).  
4272 Greening of the Earth and its drivers. *Nature Climate Change*, **6**, 791–795. doi:  
4273 10.1038/NCLIMATE3004
- 4274 Zhu, Z., Piao, S., Xu, Y., Bastos, A., Ciais, P., Peng, S. (2017). The effects of teleconnections on  
4275 carbon fluxes of global terrestrial ecosystems. *Geophysical Research Letters*, **44**, 3209-  
4276 3218. doi: 10.1002/2016GL071743
- 4277 Zickfeld, K., MacDougall, A. H., and Matthews, H. D. (2016). On the proportionality between  
4278 global temperature change and cumulative CO<sub>2</sub> emissions during periods of net negative  
4279 CO<sub>2</sub> emissions. *Environmental Research Letters*, **11**, 055006, doi:10.1088/1748-  
4280 9326/11/5/055006
- 4281 Zscheischler, J., Michalak, A. M., Schwalm, C., Mahecha, M. D., Huntzinger, D. N., Reichstein,  
4282 M., Berthier, G., Ciais, P., Cook, R. B. El-Masri, B., Huang, M., Ito, A., Jain, A., King, A.,  
4283 Lei, H., Lu, C., Mao, J., Peng, S., Poulter, B., Ricciuto, D., Shi, X., Tao, B., Tian, H., Viovy,  
4284 N., Wang, W., Wei, X., Yang, J., and Zeng, N. (2014). Impact of large-scale climate  
4285 extremes on biospheric carbon fluxes: An inter-comparison based on MsTMIP data, *Global*  
4286 *Biogeochem. Cycles*, **28**, 585–600, doi: 10.1002/2014GB004826